TECHNOTRAIN
Enabling TECHNOlogies-driven chemistry: a tailored TRAINing research program for batch and flow synthesis of chiral amino derivatives
H2020-MSCA-ITN-2018, Grant Agreement n. 812944

UNIVERSITÀ DEGLI STUDI DI MILANO

In batch and in flow synthesis of quaternary amino acids/amino derivatives

Department of Chemistry
PhD in Industrial Chemistry, XXXIV Cycle

PhD candidate: Milena Krstić

Matricola: R12466

Coordinator of the Doctorate Course in Industrial Chemistry: Prof. Dominique Roberto

Tutor: Prof. Maurizio Benaglia

Co-Tutor: Dr. Miguel Sanz

Members of scientific committee:
Prof. Alessandra Puglisi, Dr. Sergio Rossi, Dr. David Bevk, Dr. Sumaira Umbreen

Table of Contents

Acknowledgement 6

Chapter 1. Introduction 8

1.1 Importance of amino acids bearing quaternary stereocenter 9

1.1.1 The aim and the scope of the project 10

1.2 Important strategies for the synthesis of quaternary amino acids 12

1.2.1 Stereoselective synthesis of acyclic quaternary amino acids promoted by phase-transfer catalysts 12

1.2.2 Enantioselective Strecker synthesis of acyclic α,α-disubstituted amino acids 22

1.3 Enantioselective Aza-Henry reaction - versatile approach for the synthesis of quaternary amino derivatives 26

Chapter 2. Continuous flow chemistry 30

2.1 Development (heretofore) of continuous flow processes 31

2.1.1 Flow parameters 32

2.1.2 General flow equipment 33

2.2 Biphasic systems in flow 34

2.2.1 *Solid-liquid* reactions 34

2.2.2 *Liquid-liquid* reactions 35

2.2.3. Phase transfer catalysis in flow 36

Chapter 3. Results and discussion 38

Phase transfer catalysis in continuous flow 38

3.1 Asymmetric phase transfer benzylation - Model reaction 39

3.2. Synthesis of starting material 40

3.2.1 Synthesis of starting L-alanine imine 40

3.2.2 Synthesis of phase transfer catalysts – derivatized cinchona alkaloids 41

3.3. Different continuous flow set up 41

3.3.1 *Liquid-liquid* asymmetric phase transfer benzylation 41

3.3.2 *Solid-liquid* asymmetric phase transfer benzylation 43

Conclusion – Liquid-liquid phase transfer benzylation in flow 48

Conclusion – Solid-liquid phase transfer benzylation in flow 53

Chapter 4. Chiral Organosuperbases 54

4.1 The history of the development of organosuperbases 55

4.1.1 Amidines 57

4.1.2 Guanidines 58

4.1.3 Cyclopropenimines 60

4.1.4 Iminophosphoranes 62

4.2 Synthesis of **Bi**functional **IM**ino**P**hosphoranes 63

4.3 Application of **Bi**functional **IM**ino**P**hosphoranes in enantioselective reactions 64

Chapter 5. Results and discussion 69

Synthesis of iminophosphorane catalysts and their use in asymmetric reactions 69

5.1 Synthesis of **B**ifunctional **IM**ino**P**hosphorane organocatalysts (**BIMP**) bearing one stereogenic center 71

5.1.1 Synthesis of BIMP derived from (*R*)-(−)-2-Phenylglycine 71

5.1.2 Synthesis of BIMP derived from L-*tert*-leucine possessing thiourea moiety 72

5.1.3 Synthesis of BIMP derived from L-*tert*-leucine possessing urea moiety 76

5.1.4 Synthesis of BIMP derived from L-*tert*-leucine and electron rich phosphines 78

5.2 Synthesis of **B**ifunctional **IM**ino**P**hosphorane organocatalysts (**BIMP**) bearing two stereogenic centers 80

5.2.1 Synthesis of BIMP bearing two stereogenic centers and thiourea moiety 80

5.2.2 Synthesis of BIMP bearing two stereogenic centers and urea moiety 81

5.3 Synthesis of **B**ifunctional **IM**ino**P**hosphorane organocatalysts (**BIMP**) bearing one stereocenter on organoazide scaffold and stereogenic phosphorus 82

5.4 Synthesis of starting ketimines for asymmetric syntheses 83

5.4.1 Synthesis of *N*-Boc aryl trifluoromethyl ketimines 83

5.4.2 Synthesis of *N*-Boc alkyl trifluoromethyl ketimines 86

5.4.3 Computational studies on *N*-Boc CF_3-Ketimines 87

5.5 Asymmetric Aza-Henry reaction of *N*-Boc CF_3 ketimines 88

5.6 Asymmetric Mannich reaction of malononitrile and oxidative decyanation 97

Conclusion – BIMP catalysts and their application 100

5.7 DFT calculations: Nitro-Mannich reaction of nitromethane with *N*-diphenyl-phosphinoyl ketimine 101

5.7.1 Density Functional Theory (DFT) optimization 102

5.7.2 Transition states search and optimization 103

5.7.3 Possible activation modes in aza-Henry reaction of *N*-Boc CF_3 ketimines promoted by iminophosphorane oranocatalysts 106

Chapter 6. Experimental part 107

6.1 General methods 108

6.2 Phase transfer catalysis in flow 109

6.2.1 Synthesis of starting imine for phase transfer catalysis in flow 109

6.2.2 Synthesis of cinchona alkaloids (phase transfer catalysis in flow) 110

6.2.3 *Liquid-liquid* phase transfer benzylation in flow 112

6.2.4 *Solid-liquid* phase transfer benzylation in flow 116

6.3 Synthesis of BIMP bearing one stereogenic center 125

6.3.1 Synthesis of BIMP derived from (*R*)-(−)-2-Phenylglycinol 125

6.3.2 Synthesis of BIMP derived from L-*tert*-leucine possessing thiourea moiety 127

6.3.3 Synthesis of BIMP derived from L-*tert*-leucine possessing urea moiety 133

6.3.4 Synthesis of BIMP derived from L-*tert*-leucine and electron rich phosphines 135

6.3.5 Synthesis of BIMP bearing two stereogenic centers and thiourea moiety 150

6.3.6 Synthesis of BIMP bearing two stereogenic centers and urea moiety 155

6.3.7 Synthesis of BIMP bearing one stereocenter on organoazide scaffold and stereogenic phosphorus 159

6.4 Synthesis of *N*-Boc aryl trifluoromethyl ketimines 166

6.5 Asymmetric Aza-Henry reaction of *N*-Boc CF_3 ketimines promoted by **B**ifunctional **IM**inophos**P**horan**e** organocatalysts 172

6.5.1 Asymmetric addition of nitromethane to *N*-Boc CF_3 ketimines promoted by catalyst **36a** 172

6.5.2 Screening of BIMPs in aza-Henry reaction with model ketimines **48** or **50** - general procedure: 212

6.6. Asymmetric Mannich reaction of malononitrile and oxidative decyanation 219

Chapter 7. References 224

Acknowledgement

This PhD thesis was accomplished through the training research program for batch and flow synthesis of chiral amino derivatives called **"Technotrain project**", coordinated by Prof. Maurizio Benaglia and supported by European Union as a part of the Marie Sklodowska-Curie innovative training network (ITN).

The experimental part was done in the Laboratory for Organic Chemistry (Department of Chemistry, University of Milan) and in the laboratories of a German high-tech company, Taros Chemicals GmbH & Co. KG, based in Dortmund.

I would like to use this opportunity to show the deepest gratitude to my mentor, Prof. Maurizio Benaglia and co-tutor Dr. Miguel Sanz, for their trust, professional help, and all the encouragement during my research.

Likewise, I would like to thank Prof. Alessandra Puglisi, Dr. Sergio Rossi, Dr. David Bevk, Dr. Sumaira Umbreen and Prof. Laura Maria Raimondi for their cooperation, guidance, valuable advice, and the helpful suggestions.

I also owe my thanks to the European Union as MSCA – ITN-EID project (Marie Sklodowska-Curie Actions Innovative Training Network European Industrial Doctorat), Università degli Studi di Milano and TAROS Chemicals for their financial, academic, and instrumental support.

This achievement would not have been possible without these significant contributions to my personal growth as well the expanding of science in the service of industry.

There is another part of my support which lies outside of the academia, namely, my family and friends, who have always been there for me through many years of devotion to science accompanied by lots of trials and tribulations.

I am especially grateful to my friend, Nikola Arsić for the lovely design of the cover page of my thesis.

Thank you, everyone!

"Nothing in life is to be feared. It is only to be understood."

- Maria Skłodowska-Curie-

Chapter 1. Introduction

1.1 Importance of amino acids bearing quaternary stereocenter

The asymmetric synthesis of α,α-disubstituted amino acids has been extensively explored in the last four decades. Due to the biochemical and medicinal importance of amino acids, the reproducible synthesis of non-proteinogenic amino acids as a research area has gained a lot of attention in the past period.[1,2] Unnatural α,α-dialkyl amino acids play a specific role in the design of peptides.[3,4] They can be potent enzyme inhibitors and significant fragments for the synthesis of different biologically active compounds. Conformationally constrained and stereochemically stable due to the presence of quaternary carbon atoms, unusual α,α-disubstituted amino acids may serve as useful tool in protein research. Inclusion of rigid amino acids into peptides can enhance their activity, bioavailability, and binding selectivity.[1,5] They represent relevant components of pharmaceuticals, agrochemicals, food additives and various natural products. [6,7]

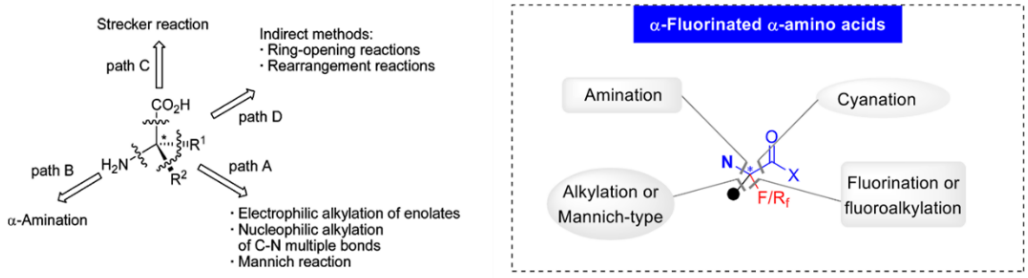

Figure 1. Selected synthetic paths for the construction of α,α-disubstituted α-amino acids (left)[25] and α-fluoro / α-fluoroalkyl quaternary amino acids (right)[40]

Besides, fluorinated α-amino acids are considered as a particular category of quaternary amino acids in modern synthetic/pharmaceutical chemistry.[26] Almost 20% of all approved pharmaceuticals bear at least one fluorine atom and many of them are already in phase II−III clinical trials.[38,39] The most common method for their preparation is the Strecker synthesis. Although they are not easy to synthesize, due to the low reactivity of ketimines[27], many research groups are still working on finding a safe, fast, and reproducible method for their formation. Non-proteinogenic amino acids containing fluorine showed very broad application in the development of antitumor and antibacterial drugs.[26,27]

Because of high fluorine electronegativity and lipophilicity, these types of molecules are possessing very specific properties.[28] The presence of fluorine atom/s may enhance metabolic stability of the drug, membrane permeability as well as *in vivo* absorption.[28] Important technology progress in this field is the usage of imaging technique (positron emission tomography), which gives the

possibility to recognize ^{18}F labelled peptides and therefore has a capacity to detect various human diseases.[28, 38]

1.1.1 The aim and the scope of the project

The main goal of this project is related to the development of general, reproducible and stereoselective, catalytic methods applicable for industrial production of enantiomerically pure, functionalized amino derivatives featuring a ***quaternary stereocenters***, since they are very interesting and valuable building blocks for the synthesis of novel active molecules. Target molecules are active pharmaceutical ingredients or immediate precursors and nonproteinogenic amino acids.

Accordingly, this PhD thesis covers the following topics that allowed us to achieve the scope of the project:

1) Development of an asymmetric phase transfer benzylation in **continuous flow** for the synthesis of **quaternary amino acids** (chapter 3, section 3.3):

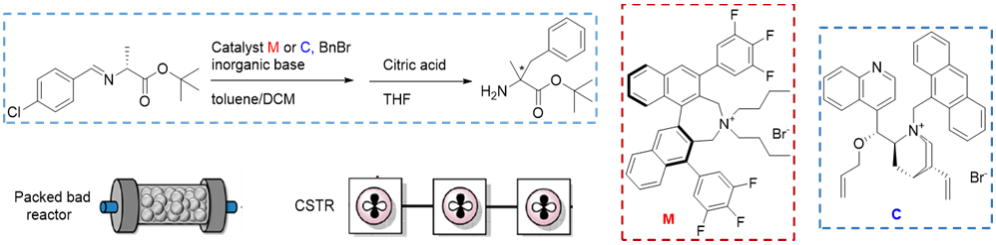

2) Synthesis of **novel thiourea / urea based organocatalysts** (***B**ifunctional **IM**ino**P**hosphorane superbases* - ***BIMP***) for the enantioselective organocatalytic addition of nucleophiles to differently functionalized ketimines (chapter 5, section 5.1-5.3):

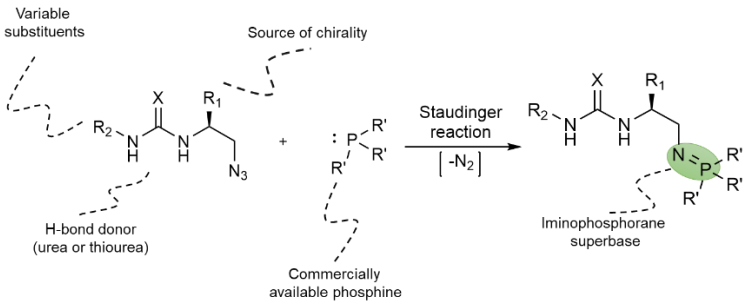

3) Synthesis of **different -CF_3 ketimines** (most of them are **new**) as a valuable precursor for the synthesis of quaternary amino derivatives (chapter 5, section 5.4):

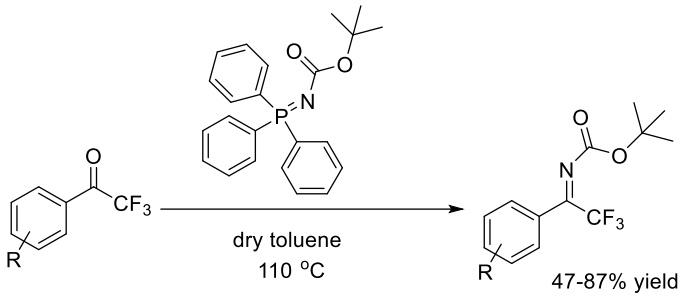

4) Enantioselective synthesis of a **new quaternary amino derivatives** applying different synthetic transformations, such as Aza-Henry or Mannich reaction of malononitrile to various -CF_3 ketimines, promoted by **new iminophosphorane organocatalysts** (chapter 5, section 5.5 and 5.6):

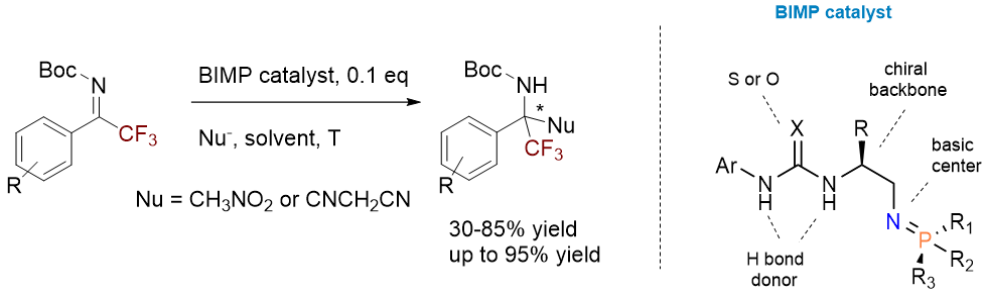

1.2 Important strategies for the synthesis of quaternary amino acids

1.2.1 Stereoselective synthesis of acyclic quaternary amino acids promoted by phase-transfer catalysts

Phase-transfer catalysis in batch, has been recognized as the most reliable method for the enantioselective synthesis of optically active α-amino acid derivatives using Schiff base esters.[8,9] This strategy was applied in the synthesis of nonproteinogenic amino acids bearing stable α-quaternary carbon center, a significant building blocks playing a vital role in biological systems.[10,11,12] Quaternary ammonium salts derived from the Cinchona alkaloids (such as O'Donnell, Corey, Lygo type catalyst) as well as Maruoka type catalysts were mainly used as a phase-transfer catalysts to perform asymmetric alkylation / benzylation of amino acid derivatives.[9,13]

How does phase transfer catalysis work?

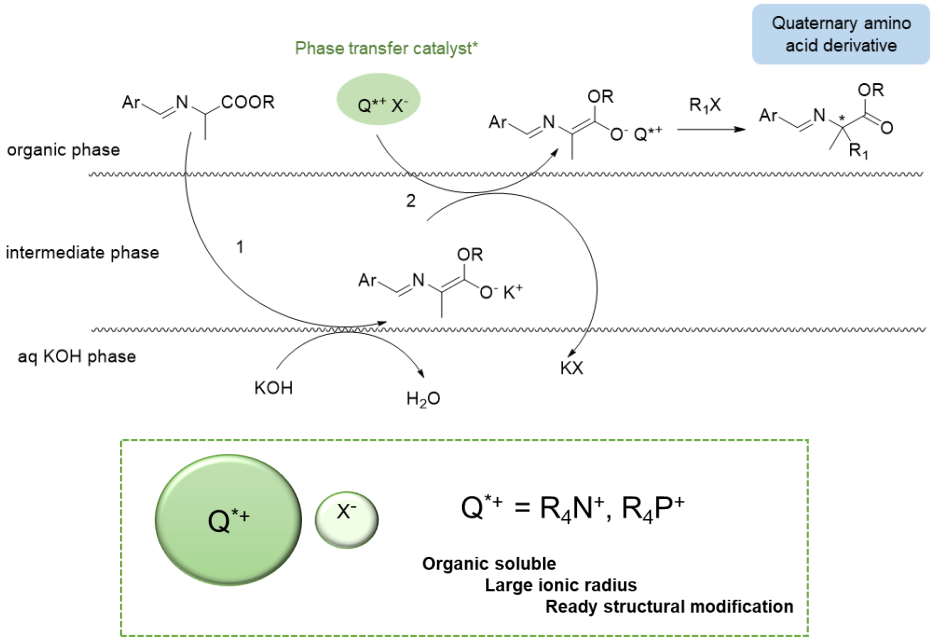

Figure 2. General mechanism of asymmetric phase transfer alkylation

Phase transfer catalysis depends on the nature the catalyst and two immiscible phases. Lygo and co-workers showed that initial deprotonation of the substrate by base occurs fast in the absence of a PTC, whereas for the alkylation step phase transfer catalyst is required. Therefore, the main role of the catalyst is to extract the enolate into the organic phase and facilitate further reaction with the alkyl halide.
As drawn in figure 2, the first step of the alkylation is the interfacial deprotonation of the *α*-proton of imine of alanine by inorganic base (in this case KOH) to give the corresponding enolate, which stays between the organic and water layers (intermediate phase).[9,14,15]

Ion-exchange of the anion with the phase transfer catalyst ($Q^{*+}X^-$) is forming a chiral enolate soluble in the organic phase where it reacts with an alkyl halide (R_1X) to yield the optically active dialkylation product.[14,15]

In 1992, O'Donnell and Wu described for the first-time phase-transfer alkylation of the *p*-chlorobenzaldehyde imine of alanine *tert*-butyl ester with *N*-benzyl cinchona quaternary ammonium salts (catalyst **8c**) and they succeeded in obtaining quaternary amino acid derivatives in good yields and modest enantioselectivity (scheme 1).[16]

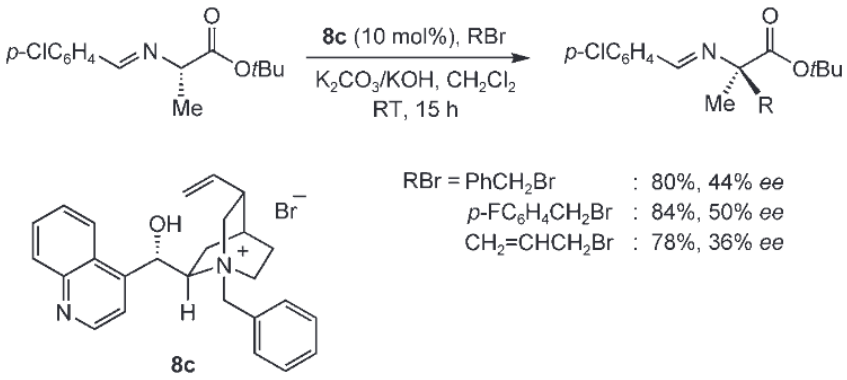

Scheme 1. The first example of α,α-dialkyl-α-amino acids synthesis by <u>*solid-liquid*</u> asymmetric phase-transfer catalysis using *N*-benzyl cinchoninium quaternary ammonium salt

In 1999, Lygo and co-workers have improved significantly the enantioselectivity of final quaternary amino esters (scheme 2), by modifying cinchona phase transfer catalyst, thus performing *N*-alkylation with 9-(chloromethyl)anthracene (catalyst **26l**). By using more electron-rich and more rigid phase transfer catalyst as well as freshly prepared base (solid K_2CO_3/KOH) in this transformation, they were able to isolate the products ((*S*)-enantiomer) with increased enantioselectivity.[17]

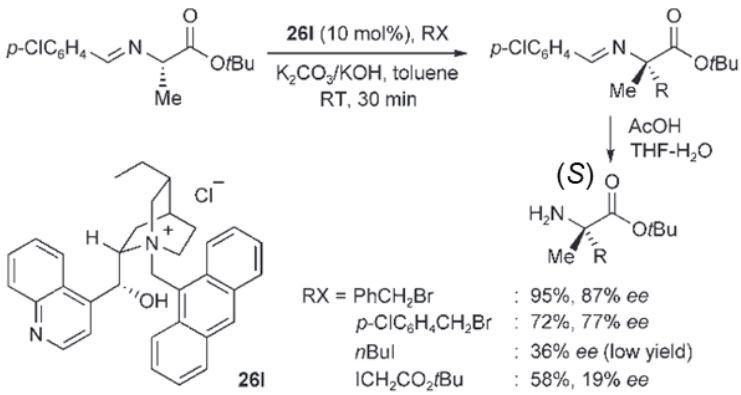

Scheme 2. Further progress in enantioselectivity in α,α-dialkyl-α-amino acids synthesis by *solid-liquid* asymmetric phase-transfer catalysis by introducing bulky *N*-anthracenylmethyl moiety

In 2012, Cook et al. reported quantum mechanical transition-state analysis for the precise explanation of the O'Donnell *tert*-butyl glycinate-benzophenone Schiff base stereoselectivity in chiral quaternary cinchonidinium phase-transfer catalyzed enolate allylation (figure 3).[81]

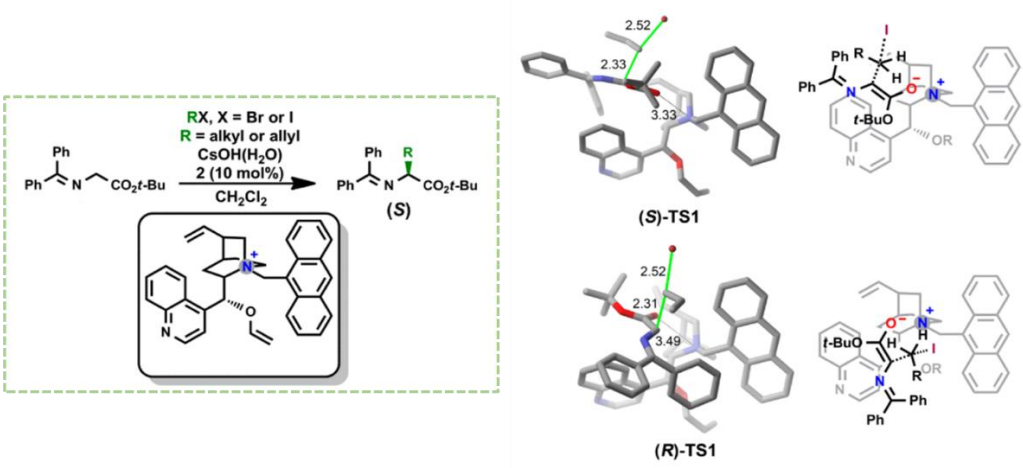

Figure 3. Transition state study in asymmetric phase transfer allylation of imine of glycine catalyzed by cinchona catalyst[81]

The preference for electrophilic attack of the allyl bromide on the enolate *Re* face in (*S*)-TS1 versus attack of the enolate *Si* face in (*R*)-TS1 can be justified by oxy-anion-quaternary ammonium interaction. In (*S*)-TS1 the distance between the enolate O anion and the quaternary nitrogen is 3.33 Å while in (*R*)-TS1 this same distance is 3.49 Å. Also, in (*S*)-TS1 the O anion is on average 0.1 Å closer to the quaternary ammonium N-CH bonds. These shorter interaction distances imply that the enolate-electrophile transition state geometry fits better into the pocket of catalyst due to more favorable CH-π and π-π interactions in (*S*)-TS1 compared to when the enolate-electrophile is flipped in (*R*)-TS1.[81]

In 2000, Maruoka et al. designed one of the most selective phase transfer catalyst for the synthesis of amino acids bearing quaternary stereocenter in α position (scheme 3, catalyst **(*S,S*)-20e**).

Further evolution of phase transfer catalysts has shown that *N*-spiro quaternary ammonium salts are the most effective in this type of synthesis, with very low catalyst loading (1 mol%). This powerful method enabled obtaining the products as *R*-enantiomer with excellent enantioselectivity (up to 98% ee).[18]

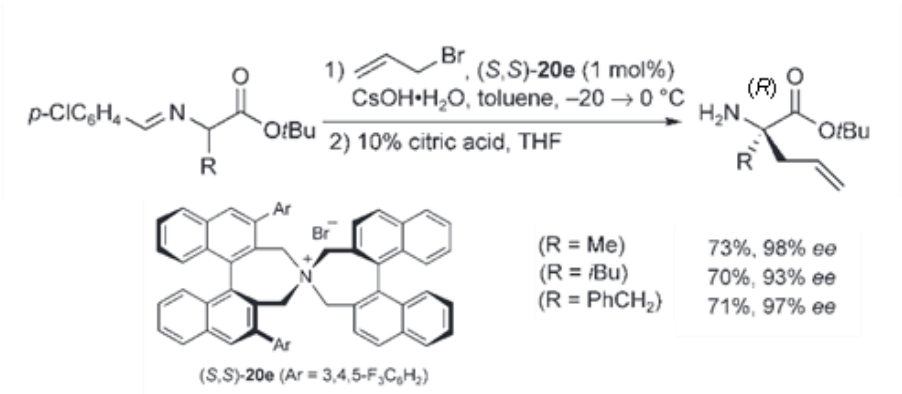

Scheme 3. *Solid-liquid* asymmetric phase-transfer catalysis for the synthesis of quaternary amino acid derivatives by employing *N*-spiroammonium bromide (Maruoka type catalyst)

According to Kamachi and Yoshizawa phase transfer benzylation of glycine imine occurs via the nucleophilic attack of the *Re*-face of the enolate ion in the vicinity of the cationic ammonium center (Maruoka catalyst), leading to the *R*-benzylated product, figure 4.[82]

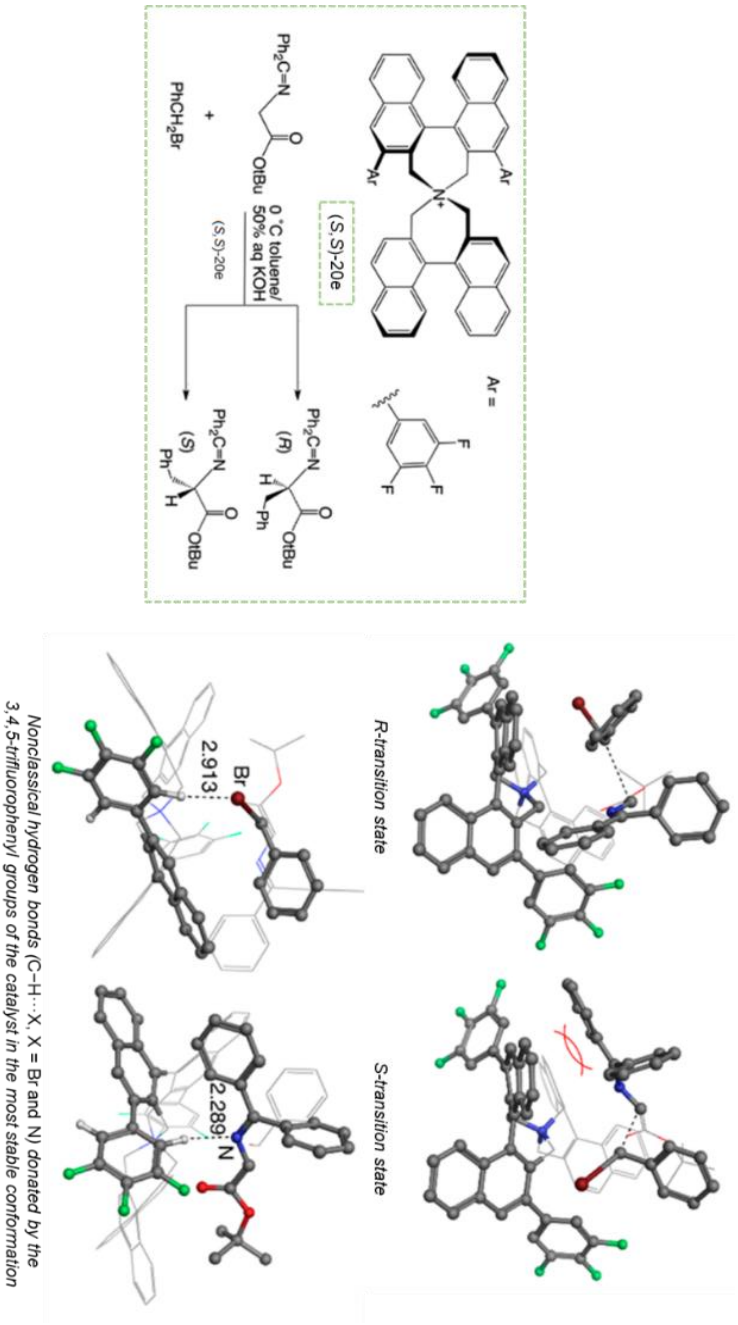

Figure 4. DFT-based conformational analysis of asymmetric phase transfer benzylation of imine of glycine catalyzed by binaphthyl Maruoka catalyst, **(*S,S*)-20e** [82]

In the most stable conformation, the 3,4,5-trifluorophenyl groups of the catalyst form nonclassical hydrogen bonds to the leaving Br atom and to the N atom of

the enolate ion. The fluorine atoms at the 3,4,5-postions of the substituent play an important role in the enantioselectivity due to the higher acidity of the protons at the 2,6-positions of the substituent caused by the presence of fluorine atoms which reinforces the hydrogen-bonding interactions.[82] A phenyl group of the enolate ion experiences a significant steric interaction with the binaphthyl subunit of the catalyst in the transition state for the *S*-enantiomer, whereas the repulsion is not observed in the case of the *R*-enantiomer due to the asymmetric geometry of the binaphthyl subunit. To avoid the steric interaction, the enolate ion rotates in the conformation for the *S*-production, leading to the loss of some key interactions between the reactants and the catalyst (figure 4).[82] Maruoka and his colleagues have shown it is also possible to perform one-pot double alkylation from achiral Schiff base of glycine, and generate α,α-disubstituted-α-amino acids by using Maruoka type phase transfer catalyst (**(*S,S*)-20e**), figure 5.[18]

The alkylation of glycine or alanine enolates is the most established method under phase transfer conditions. Predominantly, monoalkylation of glycine systems requires the use of ketone imines, whereas aldehyde imines are the appropriate derivatives in dialkylation step due to steric reasons and different pKa values (figure 6 and 7).[6,19, 22]

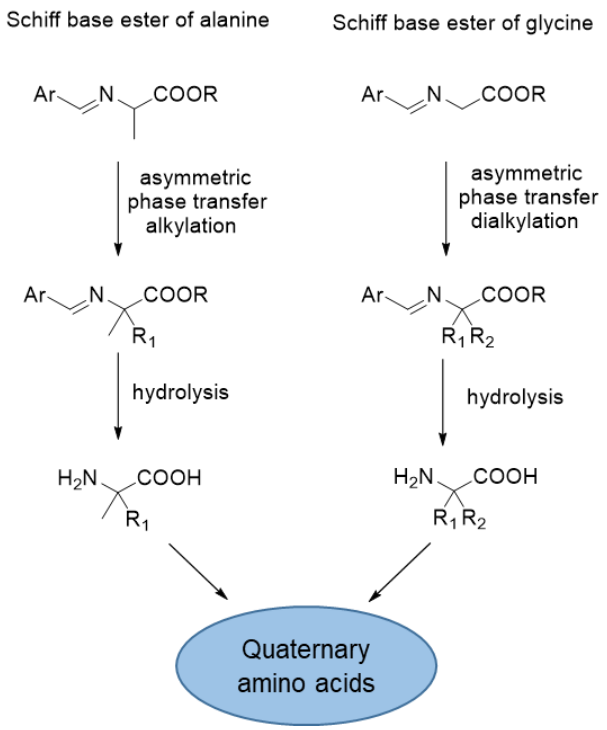

Figure 5. General asymmetric transformation of imine of glycine/alanine with PTC catalyst.[3,18,20,21]

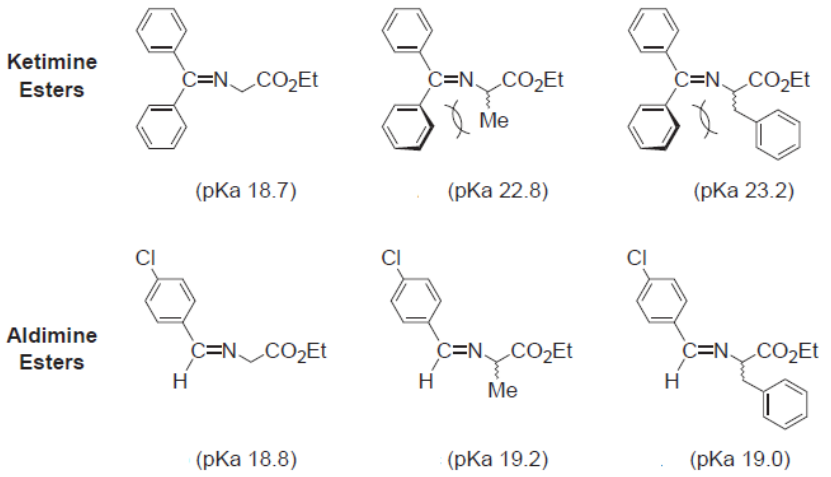

Figure 6. Acidities (pKa, DMSO) of benzophenone- and 4-chlorobenzaldehyde imines of glycine ethyl ester and monoalkylated amino acid esters.[22]

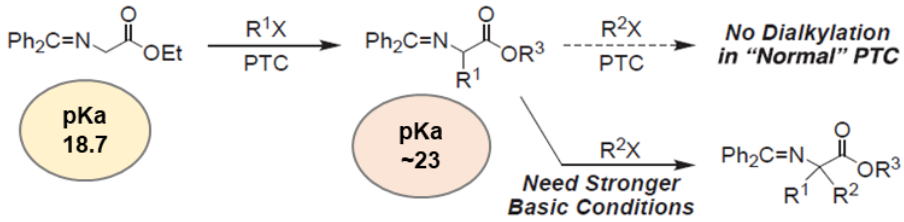

Figure 7. Selective monoalkylation of the benzophenone imines of glycine ethyl ester.[19]

The most common phase transfer catalysts used in for asymmetric synthesis of unnatural amino acids are shown in figure 8.[10,14,18,19]

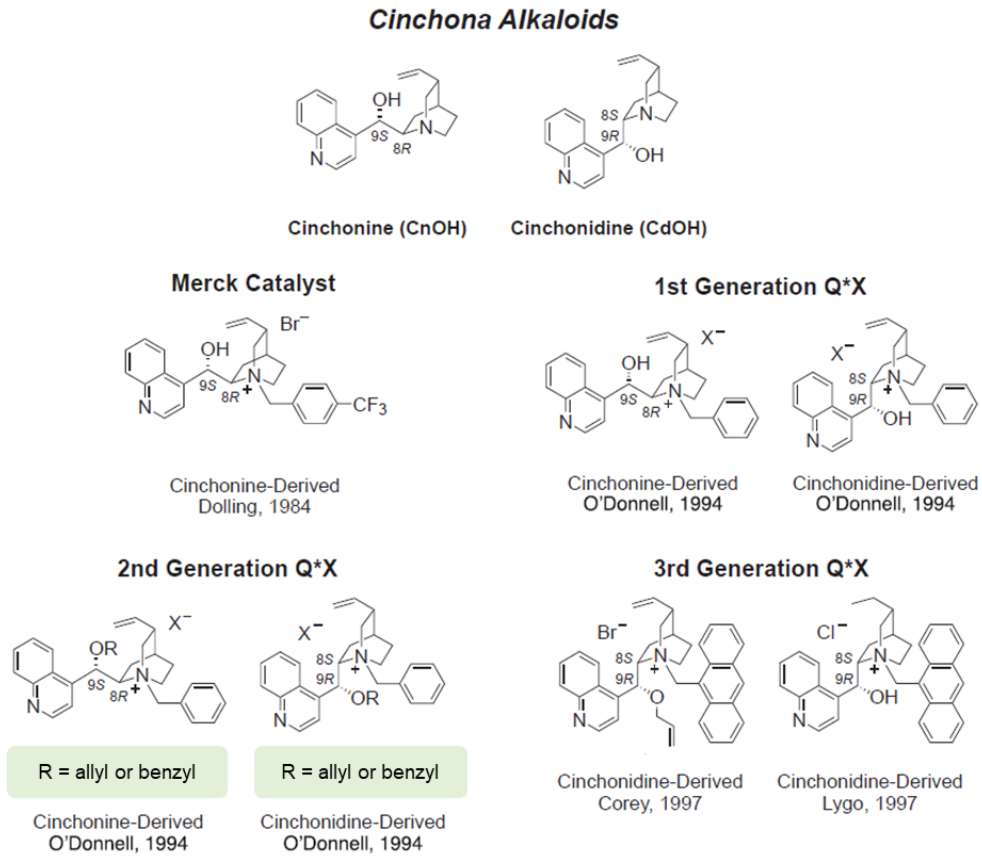

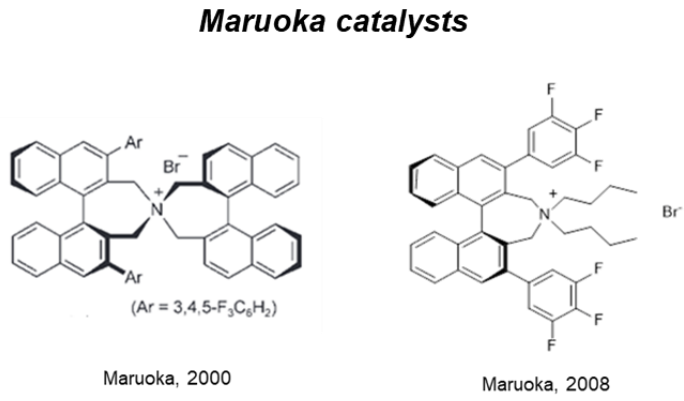

Figure 8. Phase-transfer catalysts development retrospective (since 1984)

In the last 20 years, Maruoka has made a great contribution to the design of new and efficient catalysts in phase transfer synthesis.

Thus, in 2012 Maruoka and collaborators have described successful asymmetric synthesis of α,α-dialkyl amino acids under *liquid-liquid* phase transfer conditions, using aqueous 50% KOH and conformationally fixed biphenyl quaternary ammonium salt (**(*S*)-21c**) at room temperature. This reaction was performed in excellent yields and enantioselectivities, even with very low catalyst loading (scheme 4).[8,23]

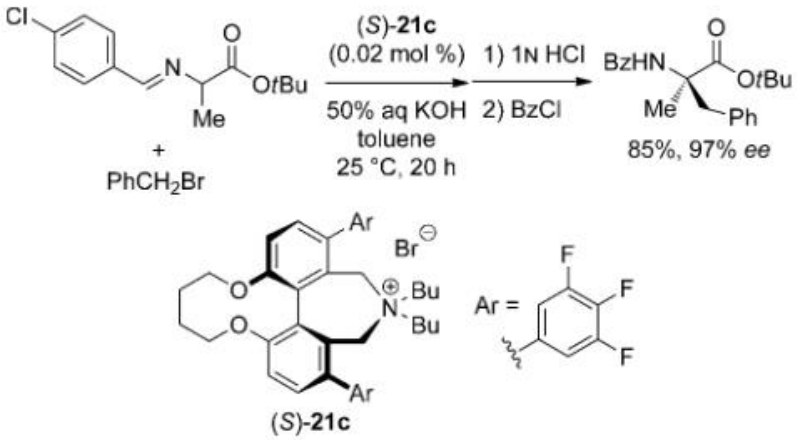

Scheme 4. Practical *liquid-liquid* asymmetric phase-transfer catalysis for the synthesis of quaternary amino acid derivatives, under mild conditions and low catalyst loading (biphenyl core of the catalyst)

Chinchilla et al. performed *liquid-liquid* phase transfer benzylation in the presence of Lygo type catalyst **2a,** by affording the products in good yields and enantioselectivity. In comparison with Maruoka catalyst, higher catalyst loading was required in this case (scheme 5).[12]

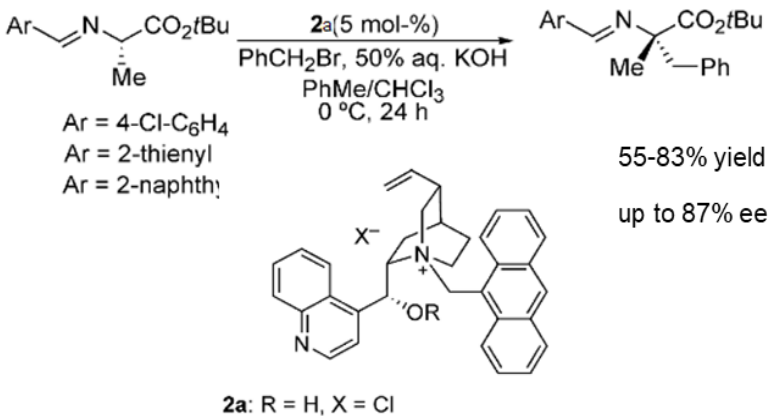

Scheme 5. *Liquid-liquid* asymmetric phase-transfer benzylation of alanine imine derivatives catalysed by cinchona catalyst **2a**

In 1999, Belokon and co-workers propose the use of chiral bases (**TADDOL** or **NOBIN**) as phase transfer catalysts. These catalysts chelate the sodium cation and makes the resulting ion pair soluble in toluene which keep a rigid complex between the chiral ligand and the substrate in the transition state for the alkylation. This type of catalysis showed lower enantioselectivity of the final quaternary amino acids (scheme 6).[13,25]

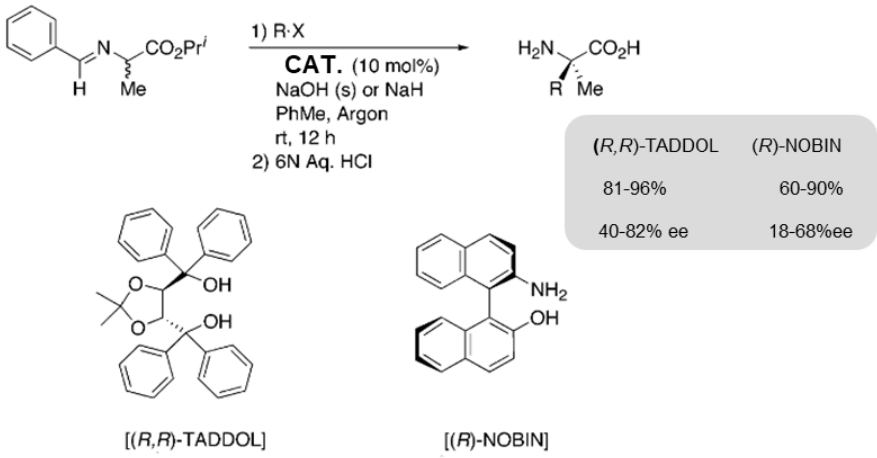

Scheme 6. Enantioselective synthesis of quaternary amino acid derivatives promoted by (***R,R*)-TADDOL** or **(*R*)-NOBIN**

1.2.2 Enantioselective Strecker synthesis of acyclic α,α-disubstituted amino acids

The Strecker reaction is well-known and one of the most straightforward methods for amino acids synthesis.[29] So far, many chiral catalysts (metal-based or metal-free) have been developed for the asymmetric cyanation of different ketimines / α-iminoesters.[29,30,40]

Jacobsen and co-workers have made a breakthrough in the development of organocatalytic Strecker synthesis.[30] The first generation of chiral urea **Jacobsen catalyst** promoted enantioselective addition of HCN to ketimines and yielded quaternary α-aminonitriles in excellent enantioselectivity (scheme 7).[31]

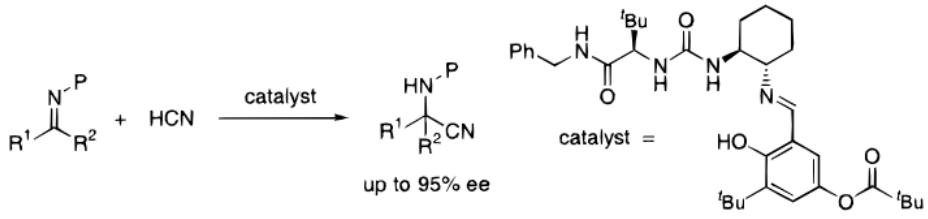

Scheme 7. The first organocatalytic Strecker synthesis of quaternary α-aminonitriles (amino acids) developed by Jacobsen and his group

Jacobsen et al. also reported the transition state of thiourea-catalyzed asymmetric Strecker synthesis of unnatural α-amino acids (figure 9).[83]

The mechanism of the hydrocyanation reaction involve initial amido-thiourea-induced imine protonation by HCN to generate a catalyst-bound iminium/cyanide ion pair. Disintegration of this ion pair and C–C bond formation to form the α-aminonitrile occurs in a post–rate-limiting step.[83]

Calculation of intermediate in imine hydrocyanation mechanism were done using the Gaussian 03 program at the B3LYP/6-31G(d) level of density functional theory. The structure shown below (figure 9) is an intermediate on the potential energy surface leading to (*R*)-product that directly precedes the C–C bond forming step.[83]

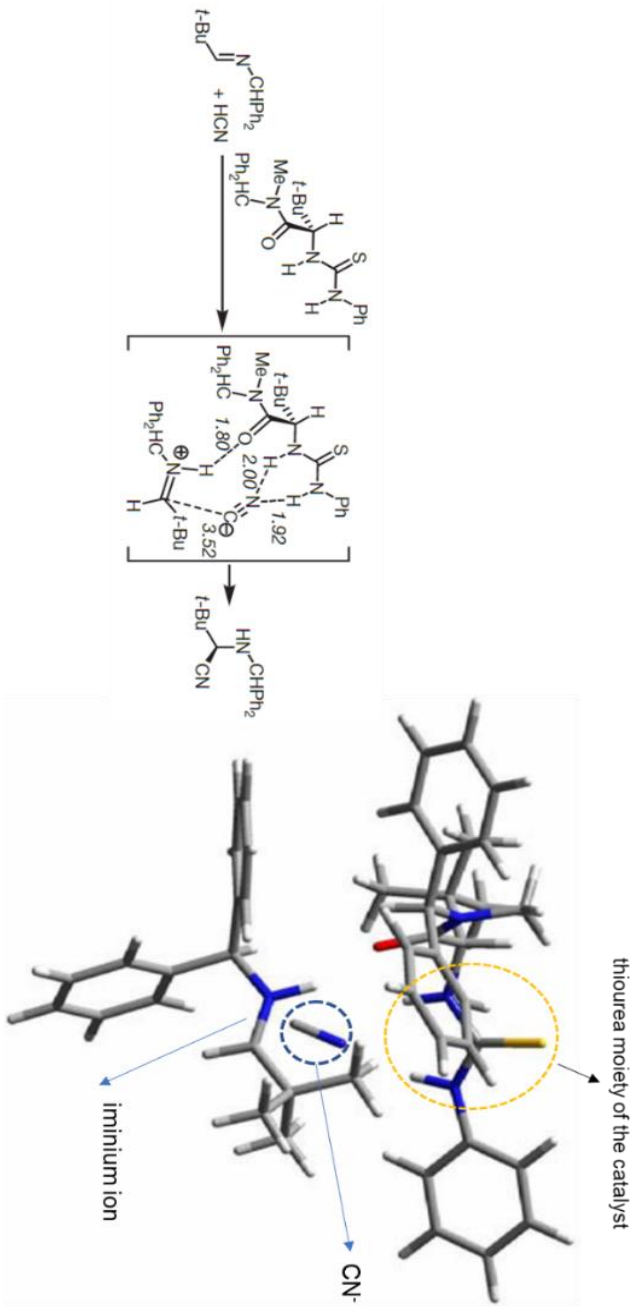

Figure 9. Jacobsen's transition state for the asymmetric synthesis of α-aminonitrile

In 2007, Rueping et al. reported BINOL phosphate-catalyzed Strecker reaction providing the quaternary α-aminonitriles in very good yields and moderate enantioselectivities (scheme 8).[32]

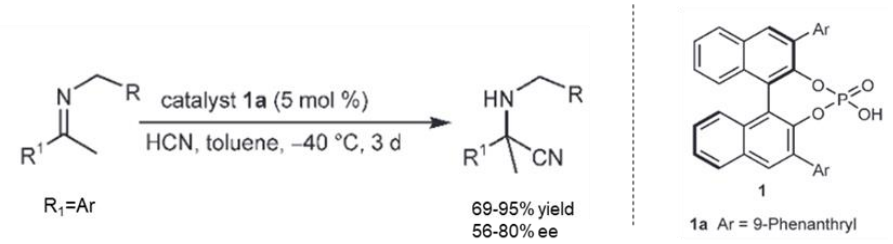

Scheme 8. Brønsted acid-catalyzed enantioselective hydrocyanation of ketimines

The first organocatalytic Strecker reaction of quaternary α-trifluoromethyl amino acids was described by Enders and his group twelve years ago, by using Takemoto catalyst, **C47** (scheme 9). Although the reaction time was very long (up to 27 days), the final products were isolated in high enantioselectivities.[33]

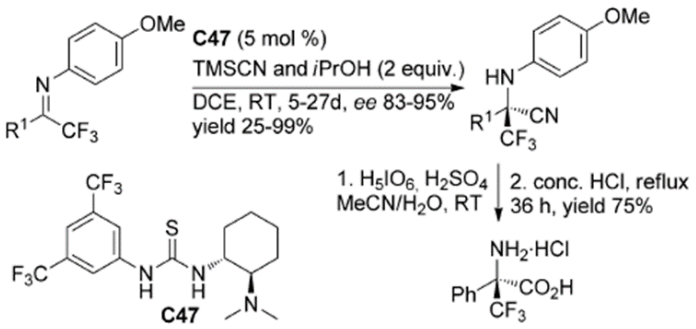

Scheme 9. Asymmetric Strecker reaction of α-trifluoromethylated ketimines catalyzed by cyclohexyl diamine-derived thiourea

Thereafter, Zhou et al. contributed to the development of Strecker synthesis of acyclic trifluoromethylated amino acids.[34,35,36]

In one of the most recent works, published in 2020, the use of dual organophosphine catalyst and methyl acrylate as an additive, has been described (scheme 10).[37] The first step of the reaction is a conjugate addition of the phosphine moiety to methyl acrylate, which generates an enolate anion and activates trimethylsilyl cyanide toward the nucleophilic addition.[37] The selectivity of the reaction is controlled by the steric hindrance of the C=N bond. It was determined that *para*-methoxyphenyl imine could link to the catalyst via the N–H and F–H bonding, while the *N*-Boc imine may interact with the catalyst via O–H and N–H bonding, thereby affording the products in reverse configuration (scheme 10).[37]

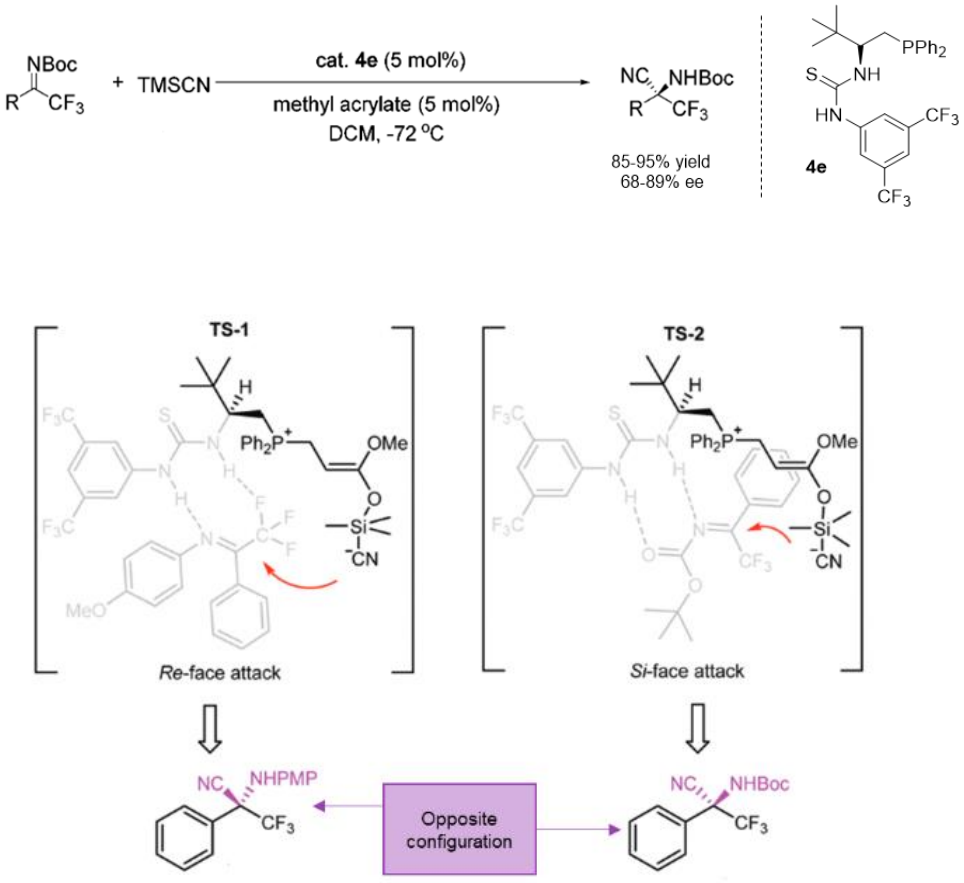

Scheme 10. Asymmetric Strecker reaction of *N*-Boc-α-trifluoromethyl ketimines promoted by organophosphine catalyst

1.3 Enantioselective Aza-Henry reaction - versatile approach for the synthesis of quaternary amino derivatives

Principally, asymmetric addition of various nucleophiles to ketimines is one of the most important strategies for the preparation of enantiopure quaternary amino derivatives (scheme 11).[41]

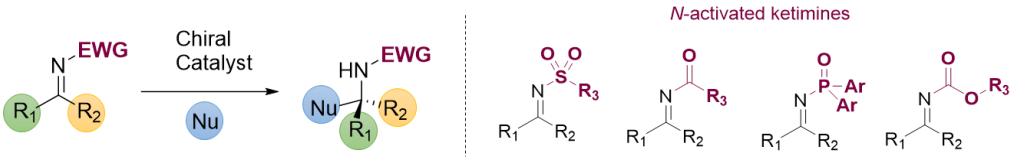

Scheme 11. Enantioselective catalyzed synthesis of amino derivatives using *N*-activated ketimines as starting material

The generation of quaternary amino derivatives using this approach is known to be very demanding work and it is required a lot of time and energy for their synthesis.[41] Therefore, the type of protecting group attached to the nitrogen of ketimine play an important role.[41] Ketimines are less reactive than aldimines, so by adjusting the nature of a starting ketimine, it is possible to increase their electrophilicity.[41]

In this PhD thesis, most of the attention will be focused on the development of nitro-Mannich reaction, with novel organocatalysts.

Approximately, more than 80% of molecules containing nitrogen are present in pharmaceuticals, thus many biologically active compounds (anticancer, antiviral drugs, enzyme inhibitors) containing C-N bond have been synthetized by asymmetric nitro-Mannich reaction.[42] This method is very useful, since nitro group can be easily converted to other functional groups.[42]

The first catalytic enantioselective aza-Henry reaction was developed by Feng and his group in 2008, using a chiral *N*,*N'*-dioxide copper complex (scheme 12, left).[43] In 2011, Wang et al. reported the first asymmetric nitro-Mannich variety using cyclic trifluoromethyl ketimines, promoted by quinine thiourea catalyst (scheme 12, right).[44] In 2013, Dixon and co-workers designed powerful organo-superbases (**B**ifunctional **IM**ino**P**hosphorane organocatalysts (**BIMP**)), and used them successfully in asymmetric addition of nitromethane to unactivated ketimines (scheme 13).[45]

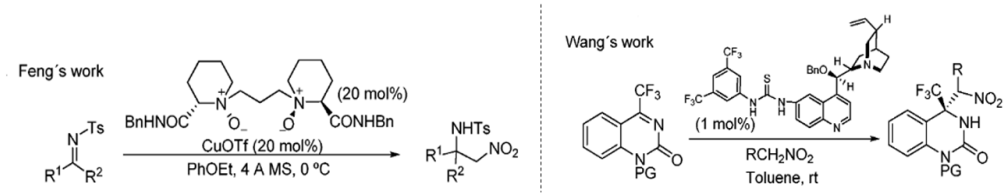

Scheme 12. The first asymmetric addition of nitro compounds to acyclic and cyclic ketimines to generate quaternary amino derivatives described by Feng and Wang

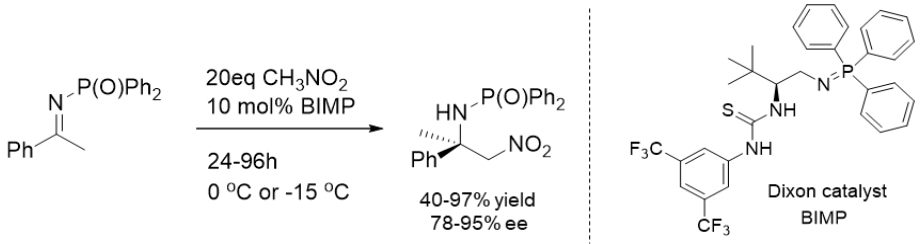

Scheme 13. Enantioselective aza-Henry reaction on less active ketimines developed by Dixon

In 2014, Zhou et al. showed an efficient organocatalytic addition of $MeNO_2$ to activated *N*-tosyl aryl α-ketiminoesters and isatin derived *N-tert*-butyloxycarbonyl (*N*-Boc) ketimines catalyzed by bifunctional Brønsted base/hydrogen-bond donor chiral catalysts (scheme 14).[46]

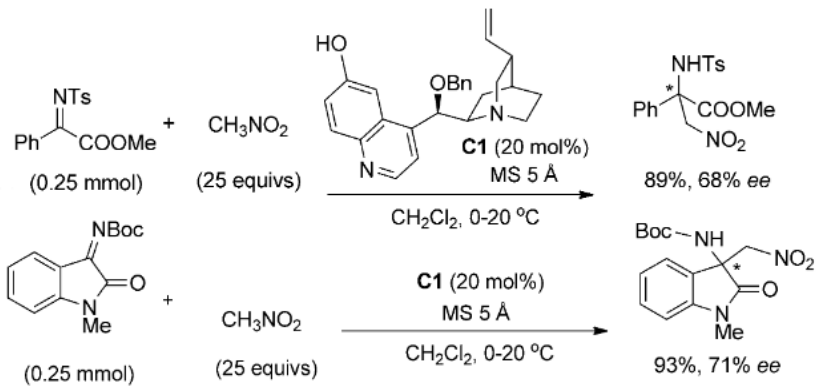

Scheme 14. Asymmetric nitro-Mannich reaction on more active ketimines developed by Zhou and co-workers

Afterwards, in 2018 Fang et al. reported very similar stereoselective addition of nitromethane to *N*-tosyl aryl α-ketiminoesters, by employing bifunctional thiourea-tertiary amine catalyst derived from quinine. Corresponding products were obtained in very good yields, and enantioselectivities (scheme 15).[47] The proposed transition state model include multiple hydrogen bonding interaction between the catalyst and ketimines or nitromethane, (usually thiourea hydrogen bonding to the nitrogen of imine and oxygen of Boc protecting group, scheme 15). In this transition state nitromethane attack from the *Re*-face and forms the corresponding product.[47]

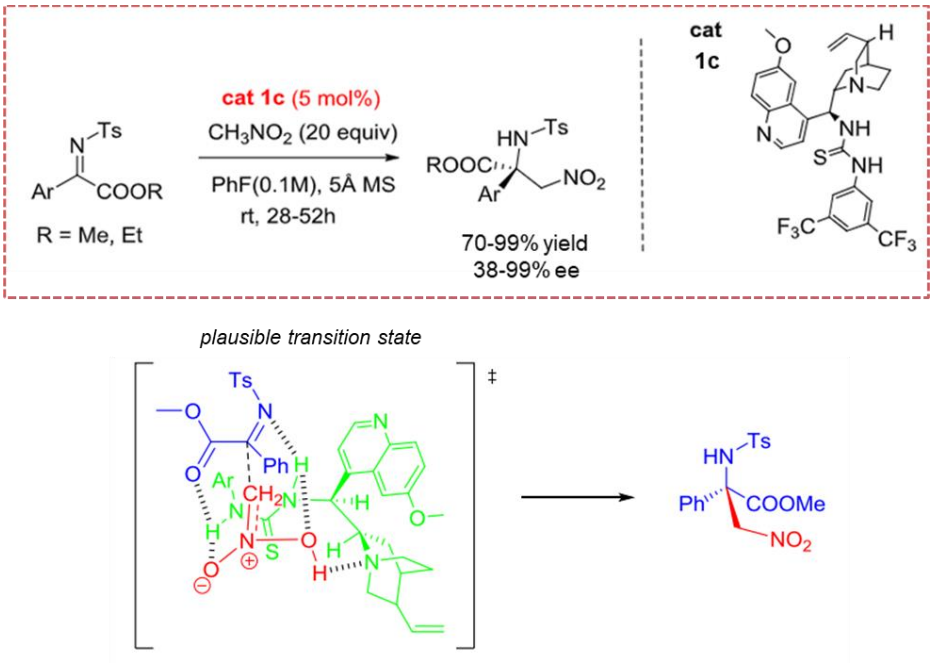

Scheme 15. Asymmetric addition of nitromethane to active ketimines promoted by chiral bifunctional catalyst **1c**

As already stated above (section 1.1), fluorine containing molecules represents an important component of pharmaceuticals, agrochemical products and materials.[48] Nevertheless, synthesis of stable quaternary amino derivatives bearing fluorine atom or trifluoromethyl group remains a big challenge.[48] Accordingly, the development of efficient and reliable methods for the construction of quaternary-CF_3 organic molecules is still on-going.[48] Thus, Duan

et al. recently published an article for the asymmetric aza-Henry reaction of acyclic aryl trifluoromethyl ketimines with nitromethane, catalyzed by a bifunctional phase-transfer catalyst containing multiple hydrogen bonding donors (scheme 16).[48]

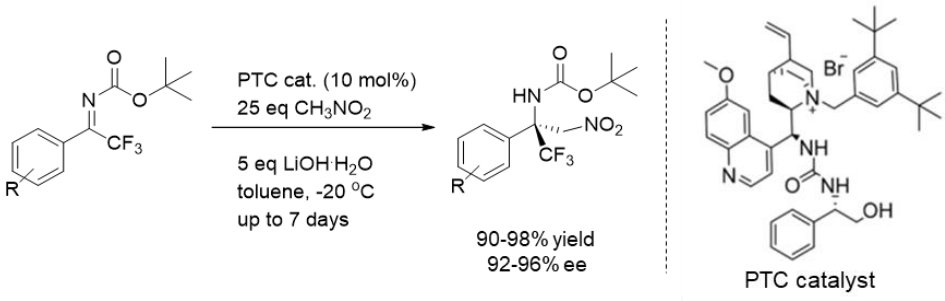

Scheme 16. Asymmetric addition of nitromethane to open-chain trifluoromethylated ketimines promoted by phase-transfer catalyst

Although it takes a long time for the reaction to complete, this is the first example of asymmetric nitro-Mannich reaction to acyclic aryl trifluoromethyl ketimines.

All the examples shown above represent the most important synthetic pathways on this topic.

Chapter 2. Continuous flow chemistry

2.1 Development (heretofore) of continuous flow processes

In the last two decades, numerous studies illustrated utility of continuous flow processes in the field of synthetic chemistry.[50] In many cases, continuous flow technology has shown an advantage over traditional batch conditions, since it may offer less hazardous process operating conditions, higher efficiency, better stirring, heat and mass transfer, easier scale-up.[49,50] Flow reactors have a high surface/volume ratio, which provides a very accurate temperature control (fast heating and cooling).[51,54] This technique can be especially important for industries because it provides higher safety (possibility of running the reactions at high/low temperature and high pressure, reducing manual handling), possibility of automation, in-line purification techniques and reaction telescoping.[51]

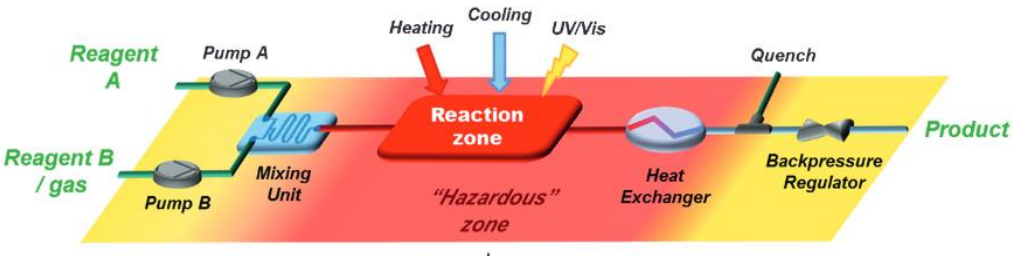

Figure 10. General concept of flow chemistry using microreactors[52]

In figure 10 is shown the example of flow process using microreactors which exclude the manual handling/storing of toxic, reactive, or explosive chemicals. Reagents can be mixed at specified points along the reactor, heated, cooled, and quenched minimizing safety concerns.[52]

In order to develop efficient continuous flow synthesis, it is necessary to know how to use flow parameters (such as residence time, flow rate, reactor volume, space-time yield, productivity, process mass intensity). All these parameters depend on the reactor type, specific flow set-up and it usually requires a different "mindset" compared to standard batch conditions.

2.1.1 Flow parameters

Many parameters in a continuous flow processes are dependent on each other.[53] The most important flow parameters are shown below.

- **Residence time (RT)** for a homogeneous liquid system can be calculated according to equation 1:

RT = $\mathbf{V_r}$ (internal reactor volume) / $\mathbf{Q_t}$ (flow rate of the feeds flowing into the reactor) [eq. 1][53]

For a packed-bed system, the residence time represents the length of time that a reactant solution is in contact with a catalyst, solid-supported reagent, or scavenger resin (eq. 2):

RT = Void volume of packed bed reactor / Flow rate [eq. 2][53]

- **Flow rate (Q_t)** is proportional to the internal reactor volume and can be calculated based on equation 3:

$\mathbf{Q_t}$ (mL/min) = $\mathbf{V_r}$ (internal reactor volume) / **RT** (residence time) [eq. 3][53]

Performance Metrics. The fundamental metrics in flow chemistry are conversion of starting material, product selectivity (product ratio), product yield, throughput, and space-time yield.

- **Throughput** can be described according to equation 4:

Throughput = *amount of product / operation time* [eq. 4][53]

- **Space-time yield (STY)** can be defined according to equation 5:

STY = *product mol / reactor volume x operation time* [eq. 5][53]

- **Process mass intensity (PMI)** can be defined according to equation 6:

PMI = *total mass used in process / mass of the product* [eq. 6][53]

Process mass intensity is considered as primary mass-related green chemistry metric in batch as well in flow.[53]

- **Productivity:**

P = $n_{prod} * \%Y / t_{collection} * 100\%$

(n_{prod} = quantitative yield of product, %Y = isolated yield; $t_{collection}$ = collection time of the product)

2.1.2 General flow equipment

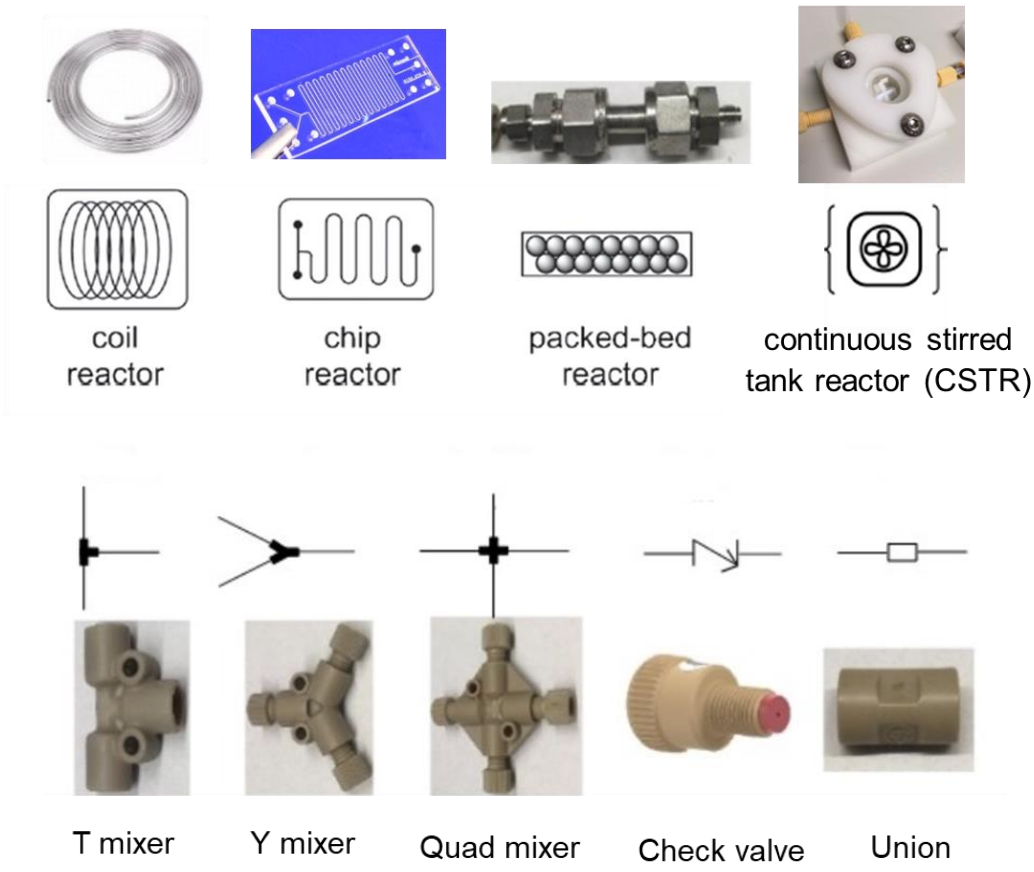

Figure 11. The common parts used in the assembly of continuous flow systems[50,52,53]

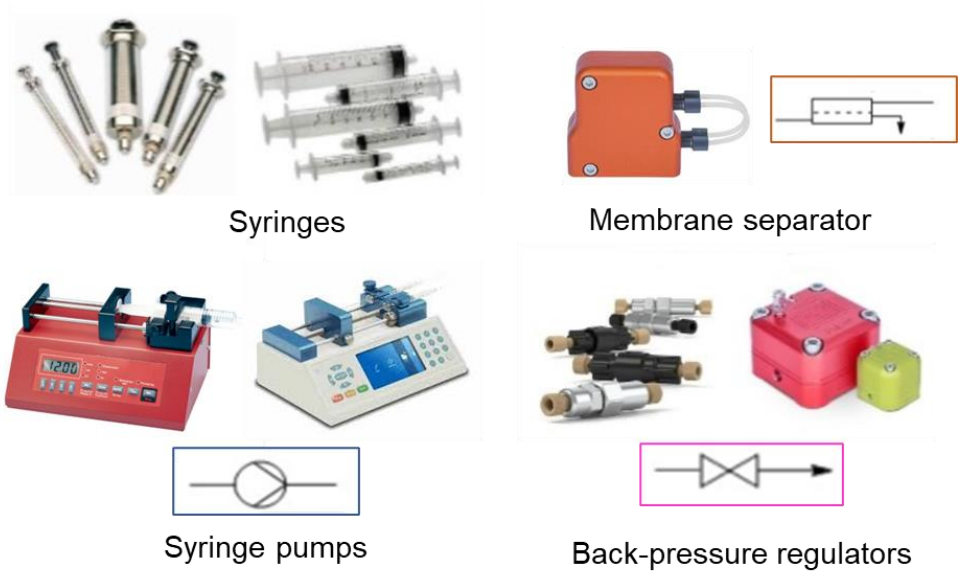

Figure 12. Additional regular components for the continuous flow setup[50,52,53]

2.2 Biphasic systems in flow

Biphasic reactions have shown broad application in organic syntheses, in batch as well as in continuous flow mode.[50,51,55] One of the most common biphasic systems used are *liquid-liquid* and *liquid-solid*, where the reactants have different solubility between the two phases. Therefore, to ensure good selectivity and high conversion to the product, interfacial efficient mixing is very important parameter in this type of reactions.[50,55] In flow, micro- and milli-scale flow reactors have proven to be very good for biphasic systems due to the small dimensions/high surface of the reactor, providing homogeneous heating and mass transfer.[56]

2.2.1 *Solid-liquid* reactions

In the continuous flow regime, *solid-liquid* reactions generally take place in packed bed reactors.[50] Generally, to build packed-bed reactor, it is possible to use glass or stainless-steel column (such as standard HPLC column) filled with inert solid material, like resistant beads.[51]

The mostly used reactor beds are shown on figure 13 (left picture).[50] Packed beds and mixed beds are the most convenient to use, due to their simple assembly and usage.[50] Depending on the strength of the flow, this type of set up can provide very efficient stirring inside the reactor. In particular, these reactors have found significant application in heterogeneous catalysis, as a consequence of easy separation and isolation of the product without performing complex work up.[50]

2.2.2 *Liquid-liquid* reactions

Different flow regimes can be found in liquid−liquid mixtures.[50] Nonetheless, laminar and slug flow most often occur in reactions performed in microchips and tube reactors (figure 13, right picture).[50] Low flow rates, viscous liquids and large channels generally produce laminar flow (there is no disruption of phase 1 and phase 2).[50] Slug flow can be generated when the crosswise phase 2 enter the tube, causing a pressure increase in contact with phase 1. Thus, high pressure makes breakage of droplets. Iteration of this process leads to the creation of slug regime.[50]

In biphasic flow reactions it is very important to consider the diameter of the tubes and the length-to diameter ratio of the flow reactor, which determines the number of slugs generated and therefore the interfacial area.[51]

Principally, *liquid-liquid* reactions in flow can be divided in two groups: reactions promoted by phase transfer catalysts and without phase transfer catalysts.[55]

In this doctoral thesis, special attention will be devoted to the *asymmetric phase-transfer catalysis in flow.*

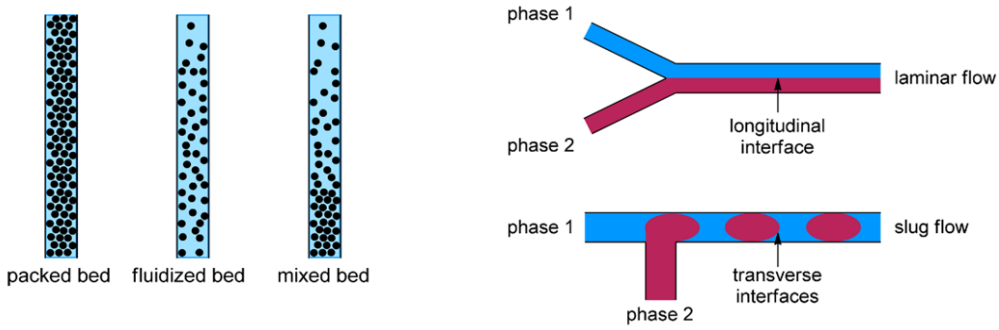

Figure 13. The most used bed reactors (left) in *solid-liquid* continuous flow and different flow regimes in *liquid-liquid* flow reactions (right)[50]

2.2.3. Phase transfer catalysis in flow

Scaling up of phase transfer catalysis reactions in a batch can be a challenging process due to various factors: reactor size and shape, stirring rate, which directly affects the heat and mass transfer performances, influencing the overall reaction rate and temperature distribution in batch reactor.[56] The phase-transfer catalysis system is a complex system in which the catalyst constantly moves from one phase to another and therefore it makes the measurement of mass transfer problematic.[59] Microreactors/packed-bed reactors and continuous flow technologies have shown certain advantages compared to batch conditions in phase transfer catalysis, in terms of better control over the process, faster mass and heat transfer, and shorter reaction times.[59-66] The challenge in phase transfer catalysis is the control of drop size distribution between two phases, the size of the interfacial surface area, the rate of catalyst transfer, and selectivity.[59] Thus, for the development of efficient phase-transfer catalysis in flow, many parameters are important, such as reactor design, aqueous and organic flow rates, the slug length, the diameter of the channels, residence time.[59]

So far, many phase transfer reactions were described in continuous flow mode; nevertheless, not in a stereoselective manner. For example, in 2003 Kobayashi et al. illustrated very efficient phase transfer alkylation of β-keto esters in a microchip reactor using tetrabutylammonium bromide.[60] In 2006, Okamoto studied the influence of microchannel flow process on the reaction yield in alkylation of malonic ester with a phase transfer catalyst (tetrabutylammonium hydrogen sulfate).[61] Schouten et al. demonstrated prosperous solvent-free continuous phase-transfer alkylation of phenylacetonitrile in a microchannel reactor.[59]

In 2010, Buchwald and co-workers developed the usage of packed-bed reactors for continuous flow palladium-catalyzed C-N cross-coupling under phase transfer conditions (use of aqueous KOH, toluene as a reaction solvent, and tetrabutylammonium bromide as a phase-transfer catalyst).[62] The year after, Šinkovec and Krajnc described phase transfer Wittig reaction in continuous flow using microtube reactor, carried out in slug flow regime.[63] The overall reaction rate in microtube reactor was much higher compared to the batch reactor due to the higher-surface-to volume ration and faster mass transport.[63]

In 2012, De Zani and Colombo reported an efficient continuous flow conditions for the ***liquid-liquid*** phase transfer O-alkylation of substituted phenols with alkyl halides, by using T-junction inlet before the reactor, to form the segmented flow. The target phenyl ethers were obtained in very good yields, in very short reaction times.[64] Afterwards, Reichart, Kappe and Glasnov investigated continuous-flow technology for the biphasic phase transfer O- and S-alkylation of phenols and thiphenols.[65] They tested different flow set up: a stainless-steel coil reactor, a packed bed reactor (filled with stainless steel beads) and a glass chip

microreactor. All of them showed excellent performances, showing more than 93% conversion.[65] A continuous flow process for the *N*-alkylation of different substrates based on the PTC approach has been developed by Garcia-Losada and colleagues.[56]

However, following the aim of our project, our interest in phase transfer catalysis in flow is related to the *asymmetric synthesis of quaternary amino acids in flow.*

As far as we know, there are scarce data in the literature about phase-transfer catalysis in flow for the synthesis of chiral amino acid derivatives. The only reported example on this topic was done by Jensen and co-workers. They have conducted *liquid-liquid* asymmetric benzylation of N-(diphenylmethylene) glycine *tert*-butyl ester by cinchonidine-derived phase-transfer catalyst in continuous stirred-tank reactor (CSTR), using various residence times and agitation intensities, to form tertiary amino acid derivatives (figure 14).[57] Kobayashi et al. have demonstrated the use of heterogenous solid base catalyst (CsF on alumina) for the stereoselective continuous-flow synthesis of glutamic acid derivatives, however this synthesis was performed without using phase-transfer catalyst.[58]

To the best of our knowledge**, there is no published study for the asymmetric phase transfer preparation of amino acid derivatives containing a quaternary stereocenter under continuous flow regime.**

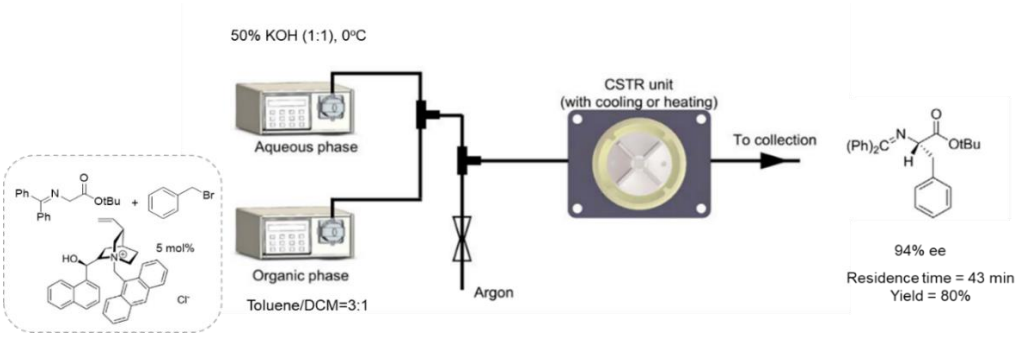

Figure 14. The first asymmetric phase transfer benzylation of glycine imine in continuous flow mode for the formation of chiral amino acid derivative

Chapter 3. Results and discussion

Phase transfer catalysis in continuous flow

3.1 Asymmetric phase transfer benzylation - Model reaction

As already stated in the section 2.2.3 various continuous flow technologies were used for the phase transfer catalysis. Many of them were tested to compare productivity regard to the batch conditions and syntheses were mostly performed without using a chiral catalyst. One of the well-known methodologies for the asymmetric synthesis of enantiopure amino acids featuring quaternary stereocenter is phase transfer catalysis (section 1.2.1).

The use of quaternary ammonium salts (such as Corey-Lygo or Maruoka catalyst) for the enantioselective benzylation/allylation/Michael addition of alanine/glycine imine under *solid-liquid* or *liquid-liquid* phase-transfer conditions to get tertiary or quaternary non-proteinogenic amino acids has been developed in batch to a great extent in the last 3 decades (section 1.2.1). Up to know, enantioselective phase transfer catalysis for the synthesis of unnatural amino acids is poorly described. Thus, our idea was to explore this area thoroughly.

Liquid-liquid asymmetric PT benzylation of *N*-(diphenylmethylene) glycine *t*-butyl ester by cinchonidine-derived phase-transfer catalyst in continuous stirred-tank reactor (CSTR) to obtain tertiary amino acid derivative was tested by Yiming Mo[57] and co-workers (figure 14). The same experiment was performed in our lab as well, to prove reproducibility. This experiment showed complete repeatability as it is described. In fact, following the objective of our project, *we were particularly engaged in the development of flow processes for the synthesis of quaternary amino acid derivatives*, using imine of alanine as model starting material (figure 15). Herein, we are reporting two different *in continuo* methodologies to generate quaternary amino acids:

1) *Liquid-liquid* phase transfer catalysis using continuous-stirred tank reactor (CSTR), figure 16,
2) *Solid-liquid* phase transfer catalysis using CSTR (figure 17) or packed-bed reactor figure 18**.**

The most relevant experiments are presented in table 1 and 2.

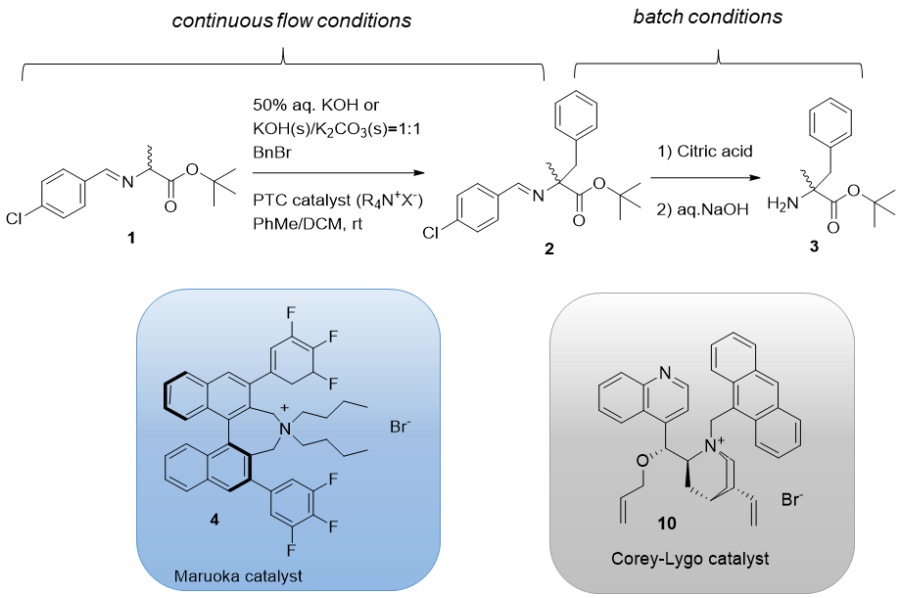

Figure 15. Model reaction - asymmetric phase transfer benzylation of alanine imine in *continuous flow mode* for the formation of quaternary amino acid derivative

3.2. Synthesis of starting material

3.2.1 Synthesis of starting L-alanine imine

The starting Schiff base of alanine (**1**) was prepared according to the procedure.[94]

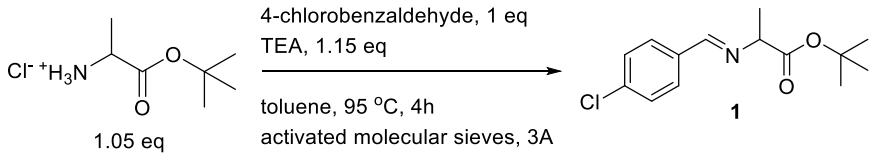

Scheme 17: Synthesis of 2-[(4-Chlorobenzyliden)amino]propanoic acid *tert*-butyl ester

3.2.2 Synthesis of phase transfer catalysts – derivatized cinchona alkaloids

Phase-transfer cinchona catalysts (quaternary ammonium salts, **5-10**) were synthetized according to the following procedure, starting from cinchonidine.[90]

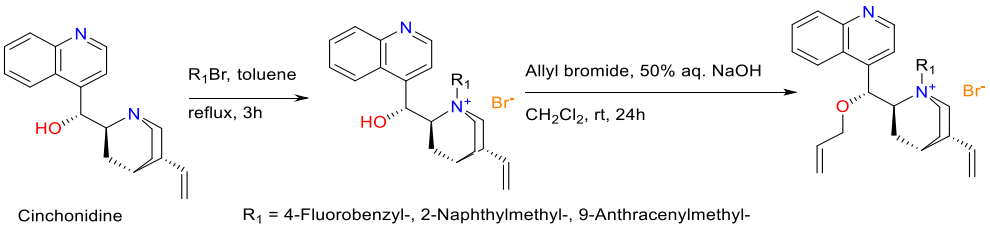

Scheme 18: Synthesis of different cinchonidine derived phase transfer catalysts

3.3. Different continuous flow set up

3.3.1 *Liquid-liquid* asymmetric phase transfer benzylation

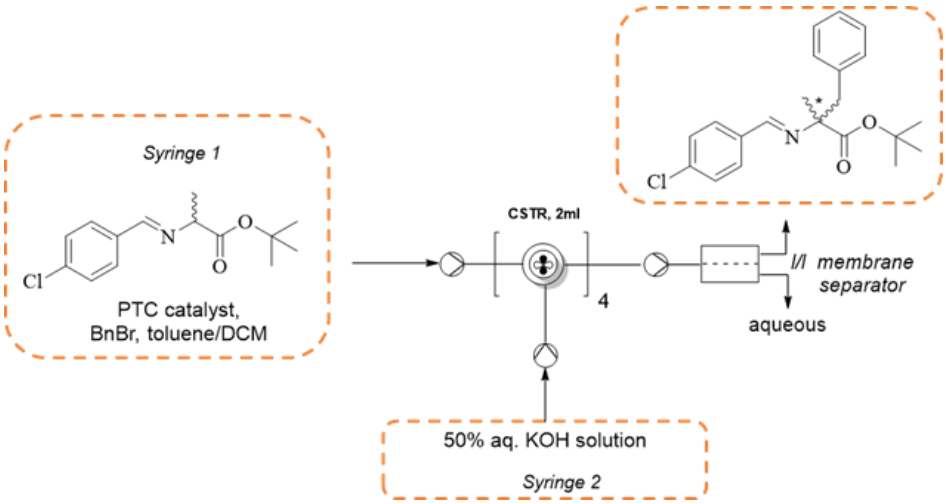

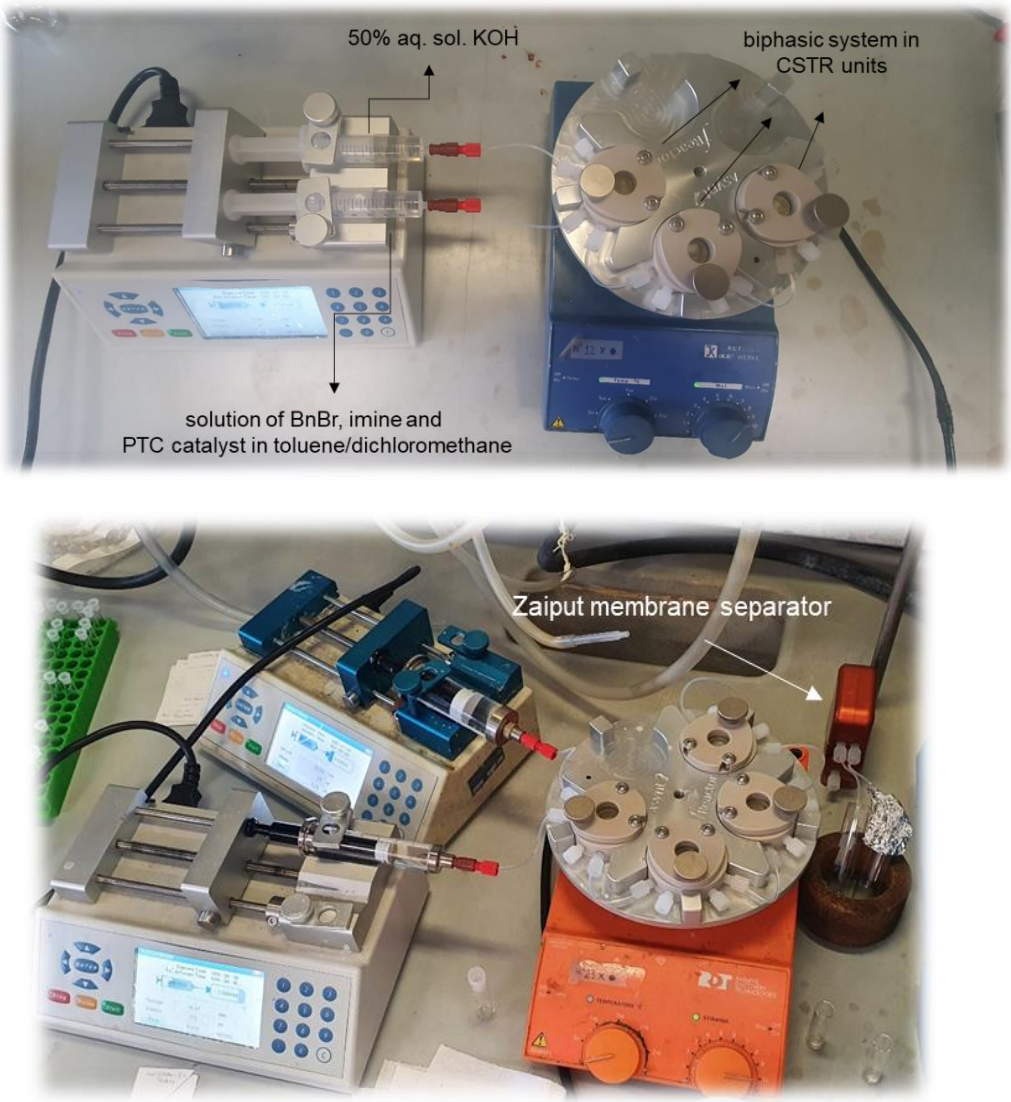

Figure 16. ***Liquid-liquid*** asymmetric phase transfer benzylation of L-alanine imine using continuous-stirred tank reactor (with the same flow rates (above) or different flow rates (below))

3.3.2 *Solid-liquid* asymmetric phase transfer benzylation

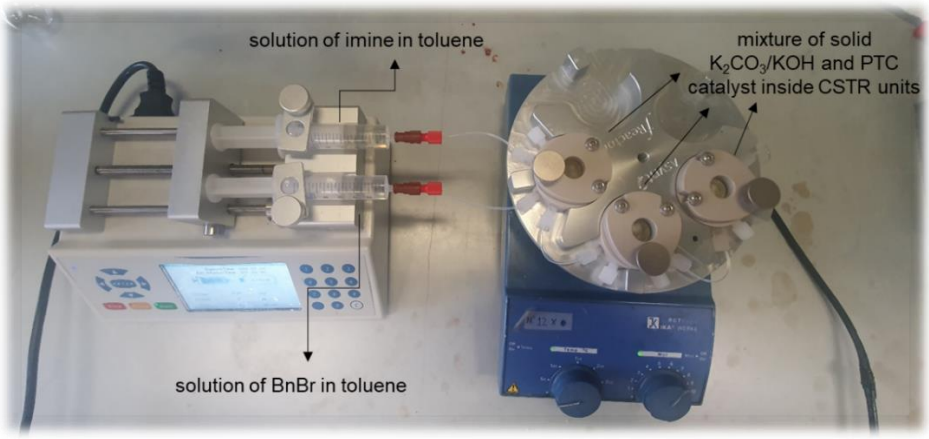

Figure 17. ***Solid-liquid*** asymmetric phase transfer benzylation of L-alanine imine using continuous stirred tank reactor

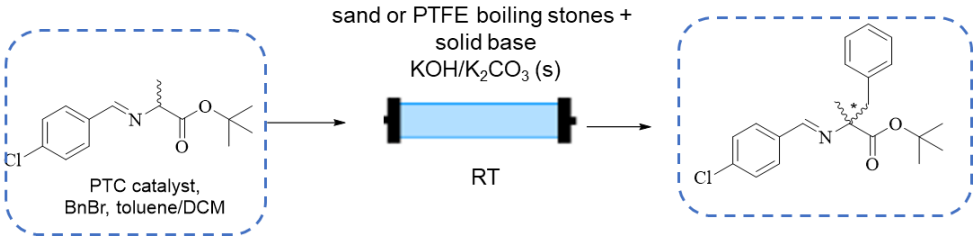

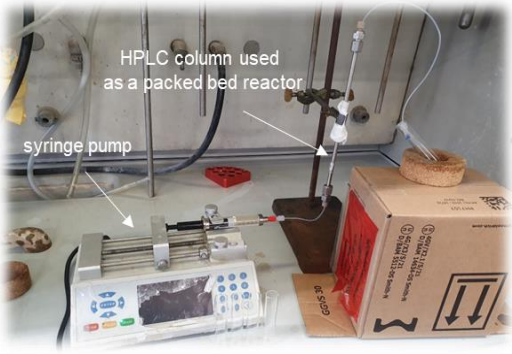

Figure 18. ***Solid-liquid*** asymmetric phase transfer benzylation of L-alanine imine in packed-bed reactors (streams delivered by a syringe pump (left) or by Vapourtec flow system (right))

Miniature continuously stirred tank reactors (CSTRs) are agitated vessels with inlets and outlets providing intensive agitation inside the sealed miniaturized chamber.[57,95] They are very convenient for multiphasic reactions, but also designed to handle reactions that involve solid precipitates.[57] As already described, phase transfer catalysis are usually biphasic systems (*liquid-liquid* or *solid-liquid*), so we decided to test continuous stirred tank reactors for this purpose. Specially, *f*Reactor[96] (cascaded continuous stirred tank reactor) which contains 5 CSTR units in line, located onto a metal baseplate and placed on conventional laboratory hotplate-stirrer, was used for our experiments (figure 19).

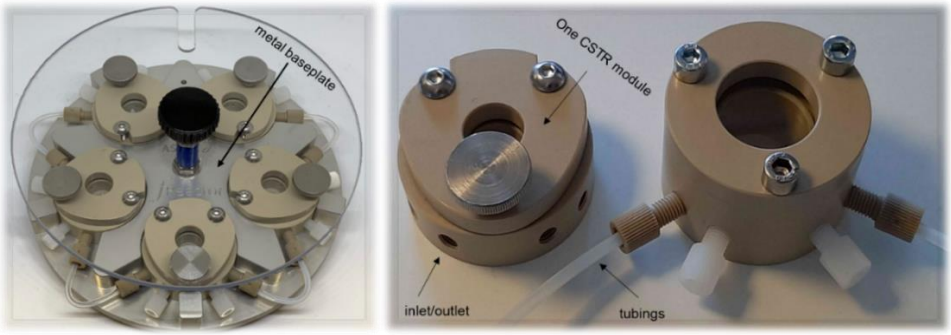

Figure 19. Cascaded continuous stirred tank reactor – ***f*Reactor**

CSTR modules are made of heat and chemical resistant materials, such as high-performance engineering plastic PEEK (polyether ether ketone) and borosilicate glass cover. The total volume of the reactor is 8 mL (1.6 mL per each CSTR unit). To ensure efficient stirring inside the CSTR units, special PTFE cross stirrer bar is designed. Standard PTFE tubing (1/8" OD (outer diameter), 1/16 ID (inner diameter)) are used to connect CSTR modules.

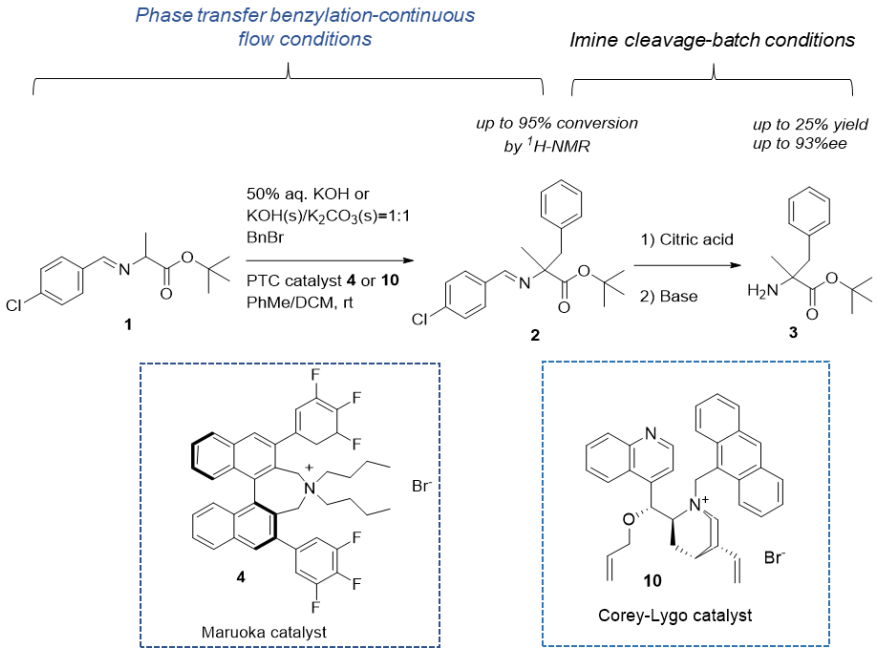

Figure 15 (section 3.1). Model reaction - asymmetric phase transfer benzylation of alanine imine in *continuous flow mode* for the formation of quaternary amino acid derivative

Asymmetric phase transfer benzylation of L-alanine imine in continuous flow for the formation of quaternary amino acid derivative was used as a model reaction (figure 15).

The first step was performed under different reaction conditions, *liquid-liquid* (table 1), by using liquid base (50% aqueous solution of KOH) or *solid-liquid* (table 2), by using solid bases such as solid KOH/K_2CO_3 or CsOH·H_2O. In both cases phase transfer catalyst **4** or **10** was used to catalyze the reaction. The second step (figure 15), deprotection of benzylated imine to get quaternary amino ester **3** was conducted under batch conditions.

The reactions were monitored by ^{1}H NMR in $CDCl_3$, and the conversion of the starting material **1** into a product **2** is expressed as ^{1}H NMR conversion.

In the case of *liquid-liquid* phase transfer benzylation of L-alanine imine (figure 16, table 1), all experiments were conducted in continuous stirred tank reactor at room temperature and two phases were usually separated by membrane separator (zaiput separation device) at the end of the process (figure 16). The first two volumes were usually discarded in order to achieve steady state. Due to the high viscosity of 50% aq. KOH solution, the suitable membrane to separate two immiscible phases was PTFE hydrophilic membrane (p/n: IL-2000-S10). After

the separation, solvents were removed, and the residue was analyzed by ^{1}H NMR. In table 1, only selected number of experiments were presented, and different continuous flow conditions were explored (variation of residence time, phase transfer catalysts, flow rate of organic or water phase, ratio of solvents etc.). In most of the cases (entry 1-3 and 6-8, table 1), it was enough to use 1mol% of Maruoka catalyst **4** to promote the reaction. Application of 2 mol% Maruoka catalyst (entry 5, table 1) did not greatly improve the conversion to the product **2**, but it was necessary to use bigger volume of dichloromethane to dissolve the catalysts, reducing the enantioselectivity of the final product **3**. Due to the low solubility in toluene, Corey-Lygo catalyst **10** was dissolved in 4:1 mixture of toluene/dichloromethane (entry 4, table 1), to achieve a certain conversion to the product **2**. Very long residence time (entry 2 and 3, table 1) showed very low formation of benzylated product **2,** which could be explained by decomposition of starting imine **1** while staying in long contact with a strong base. It was observed that the optimal number of continuous stirred tank reactors are 3 in a row (entry 5 or 6, table 1) or 4 in line (entry 7, table 1). Due to the instability of the product **2**, acidic hydrolysis of imine was done under batch conditions, to afford the stable amino ester **3** after basification (figure 15). In case of ***liquid-liquid*** phase transfer benzylation, determination of enantioselectivity of the final amino ester **3** was done for the best result obtained (entry 6, table 1).

Comparison of productivity and space-time yield for *liquid-liquid* phase transfer benzylation in continuous stirred tank reactor or batch conditions (see section 2.1.1):

Entry	Conversion to the product 2 (% by ^{1}H-NMR)	Reactor volume [mL]	Residence time [min]	Productivity [mmol/h] [a]	Space-time yield [mmol/ml*h] [b]
Batch*	Quant.	5.43	1680	0.027	0.05
Table **1**/entry **6**	40	25	333	0.053	0.002

*In-batch process was performed with 50% aq. sol. KOH to get 0.75 mmol of the product **2** (reaction completed in 28h)

[a] Productivity: moles of product **2** (calculated by ^{1}H NMR conversion, average value) divided by the collection time required to collect 0.75 mmol of benzylated product **2**

[b] Space-time yield: productivity divided by reactor volume

Based on the calculation reported above, the productivity of continuous flow phase transfer benzylation (table 1, entry 6) was slightly better than batch process. However, there was no improvement in space-time yield compared to batch procedure due to the incomplete conversion to the product **2** (max. 40% conversion), as well as higher reactor volume.

Table 1 (section 3.3.1). The most relevant experiments in ***liquid-liquid*** asymmetric phase transfer benzylation of L-alanine imine using **continuous-stirred tank reactor**

Entry	Catalyst	Base	BnBr (eq)	Ratio of solvents (toluene:DCM)	Concentration in mol/dm^3 (op)	Flow rate of op[a] (ml/min)	Flow rate of wp[b] (ml/min)	CSTR units (number)	Residence time (min)	Conversion to the product 2 (% by ^{1}H-NMR)
1	4 (1mol%)	50% aq. KOH	1.4	14:1	0.024	0.01	0.02	1	60	13
2	4 (1mol%)	50% aq. KOH	1.5	14:1	0.024	0.0025	0.0025	1	6h 36 min	15
3	4 (1mol%)	50% aq. KOH	2.5	14:1	0.024	0.01	0.01	2	3h 40 min	20
4	10 (10 mol%)	50% aq. KOH	1.4	4:1	0.025	0.1	0.2	3	20	10
5	4 (2mol%)	50% aq. KOH	1.4	4:1	0.025	0.1	0.2	3	20	37
6[c]	4 (1mol%)	50% aq. KOH	1.4	14:1	0.025	0.025	0.05	3	80	40
7	4 (1mol%)	50% aq. KOH	1.4	14:1	0.025	0.025	0.05	4	106	38
8	4 (1mol%)	50% aq. KOH	3	3.6:1	0.2	0.03	0.03	2	64	23

[a] flow rate of organic phase (first syringe - solution of imine, benzyl bromide and the corresponding phase transfer catalyst in toluene/dichloromethane)

[b] flow rate of water phase (second syringe – 50% aqueous solution of KOH)

[c] determination of ee% was done on target amino ester (**3**) after cleavage of imine in batch with citric acid and basification with aq. sol. of NaOH, entry 6 (**20% yield**, **91% ee**)

The experiments in table 1 are performed at ambient temperature and agitation ~1100 RPM; for the ^{1}H NMR conversion average values of collected volumes (except first two to achieve steady state) are presented in table 1

Conclusion – Liquid-liquid phase transfer benzylation in flow

In summary, liquid-liquid phase transfer benzylation of L-alanine imine in flow, using continuous stirred-tank reactor has been performed successfully, to get quaternary amino acid derivative **2,** in 80 min of residence time and 40% NMR yield (entry 6, table 1).

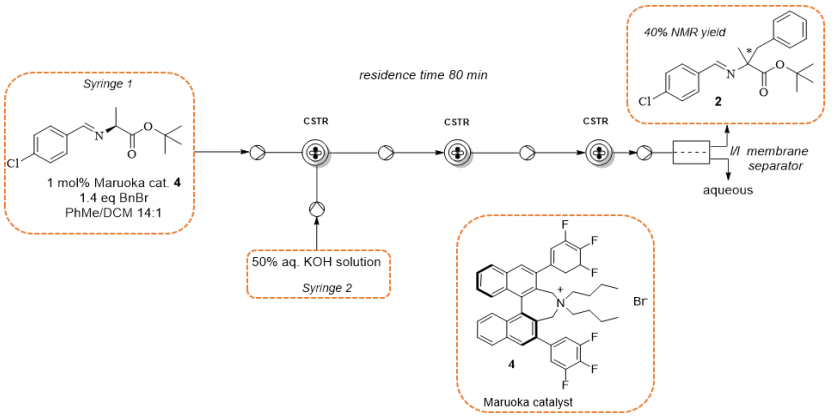

In the direction of liquid-liquid flow process optimization, various flow conditions were applied. Herein, we summarize general observations about this continuous flow method:

-As under batch conditions, low catalyst loading (1 mol% of Maruoka catalyst) was sufficient to run liquid-liquid phase transfer experiments in flow.

-Higher catalyst loading (> 5 mol%) of phase transfer catalysts requires larger volume of dichloromethane compared to the essential solvent (toluene), leading to enantioselectivity decrease of target quaternary amino acid derivative **3**.

-Higher solution concentration may trigger precipitation of a catalyst and therefore uneven flow of organic phase through the system.

-Longer residence time (extended up to 6h) did not improve the conversion of starting imine of alanine to the benzylated imine **2**.

-Liquid-liquid phase transfer process in flow showed slightly better productivity than batch process. Although the complete conversion of the starting material into the product has not been achieved (40% NMR yield), the phase transfer benzylation in flow was accomplished in 80 min, while in batch it was necessary much longer time (28h).

-Likewise in batch syntheses, Maruoka catalyst **4** showed the best performances in enantioselectivity. High ee% values of the final product **3** were observed in flow (entry 6, table 1, 91% ee), which is in accordance with batch experiments described in section 1.2.1.

Solid-liquid phase transfer conditions imply the use of a solid base to do deprotonation of alanine imine. We applied two different ways:

1) use of HPLC column to pack to solid base inside with auxiliary mixer such as glass beads, sand, or PTFE boiling stones (table 2),
2) use of continuous stirred tank reactor which serves as a reactor, but also as a mixer.

In the first case, standard stainless steel HPLC columns (different dimensions depending on the reaction scale) equipped with frit and endcaps from both sides are filled with solid base (grounded mixture of KOH and K_2CO_3 or $CsOH \cdot H_2O$ as a solid) and additional inert solids (sand, PTFE boiling stones or glass beads). Glass beads, sand or PTFE boiling stones have dual role. This inert material may enhance mixing inside the reactor, but also decrease the pressure inside the column. Without those fillers a huge pressure can be generated inside the reactor due to the very small particles of solid base and it can stop the flow of the reaction. The organic phase (solution of imine, benzyl bromide and phase transfer catalyst in toluene/dichloromethane) is delivered by syringe pump (figure 18, left) or Vapourtec pump (figure 18, right) through the reactor (HPLC column), with certain flow rates. For example, from entry 9 to 15 (HPLC column, L15 cm x OD 6 mm x ID 4.6 mm), organic phase was delivered to the reactor by syringe pump, while in entry 16 and 17 (HPLC column, L 25 cm x OD 6 mm x ID 4.6 mm), as well entry 18 (HPLC column 30 cm x 7.8 mm), organic phase was delivered to the reactor by Vapourtec flow system. The ^{1}H NMR conversion to the product **2** of the experiments in table 2, is expressed as an average value of collected volumes (except first two to achieve steady state).

The reaction occurs inside the reactor and the residence time is calculated based on the time contact between the solid base and the liquid organic phase. In table 2, various packed-bed continuous flow conditions are reported (using Maruoka or Corey-Lygo catalyst, applying different residence times and flow rates, concentrations of organic phase, ratio of solvents, solid bases as well as auxiliary mixers). As inert solid, which can serve as a stirrer inside the packed-bed reactor were used PTFE boiling stones, sand, or glass beads. In some cases, additional devices such as ultrasonic bath (entry 11, table 2) or orbital shaker (entry 12, table 2) were tested with the aim to enhance mixing. Unfortunately, under these conditions, conversion to the product **2** was very low (up to 22%). Only using PTFE boiling stones gave better results in conversion (entry 13, table 2), but still not satisfactory considering higher amount of Maruoka catalyst (5 mol%). Interestingly, when using Corey-Lygo catalyst higher volume of dichloromethane is required due to the low solubility of the catalyst in toluene (entry 14 and 15, table 2). Comparable conversion to the product **2** was observed with 40 min and 66 min of residence time. As expected, lower enantioselectivity of the target amino ester **3** was obtained, after cleavage of benzylated imine in batch (figure 15). 1 mol% of Maruoka catalyst is enough to be dissolved by toluene. In combination with very strong solid base $CsOH \cdot H_2O$, relatively good conversion to

the benzylated imine **2** was obtained, 47% in 10 min of residence time (entry 16, table 2). $CsOH{\cdot}H_2O$ is highly hygroscopic, thus reactor packing must be done very fast. As described in batch conditions, for this type of the reaction toluene is a solvent of choice which provide very high enantioselectivity, 93% ee. Glass beads proved to be much better mixers inside the packed-bed reactor than PTFE boiling stones (table 2). Interesting results were observed with lower amount of the solid base (entry 17, table 2) and very concentrated solution of reagents. 15 min of residence time was enough to achieve 60% conversion. Lower reaction temperature (-15 ^oC, entry 17, table 2) noticeable increased the enantioselectivity of amino ester **3** (72% ee). Huge excess of the solid base and very concentrated organic solution led almost to the complete conversion in 30 min of residence time (entry 18, table 2). As already stated before, for such concentrated solutions more polar solvent must be used to dissolve reagents and the catalyst. Therefore, low enantioselectivity was detected (56% ee). Phase transfer reactions performed in packed bed reactor showed that the more concentrated solutions give better conversion to the product. Nevertheless, this can cause solidification of the catalyst, especially the Corey-Lygo catalyst **10**. To achieve good efficiency, catalyst **10** usually required higher loading (up to 10 mol%). Thus, higher amount of the catalyst leads to precipitation of the catalyst in toluene. Addition of dichloromethane can overcome this problem; however, decrease in enantioselectivity was detected at room temperature (entry 15 and 18, table 2).

In the second case (figure 17), solid base and phase transfer catalyst were placed in three CSTR units uniformly. The same syringe pump was used to pump the solution of benzyl bromide in toluene (the first syringe) as well as the solution of starting imine (the second syringe) into the CSTR units filled with the solid. During the reaction, a lot of gas has been generated in the tube (CO_2 bubbles). The solid inside the CSTR has blocked the holes in the reactor, so collected fractions were not representative. One of the accompanying problems was also emersion of solid outside of the tubes and CSTR units. To prevent clogging of a solid in the reactor, the holes in each CSTR were secured with Millipore membrane filters. To inhibit the formation of bubbles in the tubes, in another experiment, the mixture of solid base KOH/K_2CO_3 was replaced just with solid KOH. Unfortunately, these modifications did not reduce the pressure generation and solid output. Nevertheless, strong mixing of solid base and the catalyst also leads to the creation of a very fine solid and therefore causes blocking of syringe pump, clogging and overpressure formation. Accordingly, use of packed bed reactor was the right choice to deal with solids (*solid-liquid* phase transfer benzylation) and the flow set up for *liquid-liquid* phase transfer catalysis was more convenient in continuous stirred tank reactors.

Comparison of productivity and space-time yield for *solid-liquid* phase transfer benzylation in packed-bed reactor or batch conditions (see section 2.1.1):

Entry	Conversion to the product 2 (% by ^{1}H-NMR)	Reactor volume [mL]	Residence time [min]	Productivity [mmol/h] [a]	Space-time yield [mmol/ml*h] [b]
Batch*	Quant.	4	180	0.248	0.062
Table **2**/entry **15**	65	1.05	66	0.436	0.415
Table **2**/entry **16**	47	0.35	5	4.2	12
Table **2**/entry **17**	60	0.23	4.33	6.23	27
Table **2**/entry **18**	95	1	30	1.4	1.4

*In-batch process was performed with solid base 5.0 equiv. K_2CO_3 / 5.0 equiv. KOH to get 0.75 mmol of the product **2** (reaction completed in 3h)

[a] Productivity: moles of product **2** (calculated by ^{1}H NMR conversion, average value) divided by the collection time required to collect 0.75 mmol of benzylated product **2**

[b] Space-time yield: productivity divided by reactor volume

Compared to batch process, *solid-liquid* phase transfer benzylation reveals much higher advantage in terms of productivity and space-time yield. Apparently, entry 17, table 2 has shown substantial increase of productivity (x25) and space-time yield. Although showing lower conversion, even in case of entry 16 table 2, a significant increment of productivity was observed (x17) in comparison to batch *solid-liquid* phase transfer benzylation. In entry 15, slight improvement in productivity was measured while entry 18 showed up to 6x higher productivity compared to the batch conditions.

Table 2 (section 3.3.2). The most relevant experiments in ***solid-liquid*** asymmetric phase transfer benzylation of L-alanine imine using packed-bed reactor

Entry	Catalyst	Solid base (eq)[b]	BnBr (eq)	Ratio of solvents (toluene:DCM)	Auxiliary mixer	Concentration in mol/dm^3 (op)	Flow rate of op[a] (ml/min)	Residence time (min)	Conversion to the product 2 (% by ^{1}H-NMR)
9	4 (1mol%)	KOH/K_2CO_3 (15/15)	2	8.5:1	sand	0.1	0.025	40	19
10	4 (1mol%)	KOH/K_2CO_3 (10/10)	2	8.5:1	PTFE boiling stones	0.1	0.025	40	35
11	4 (1mol%)	KOH/K_2CO_3 (10/10)	2	8.5:1	PTFE boiling stones + ultrasonic bath	0.1	0.025	40	10
12	4 (1mol%)	KOH/K_2CO_3 (10/10)	2	8.5:1	PTFE boiling stones + orbital shaker	0.1	0.025	40	22
13	4 (5mol%)	KOH/K_2CO_3 (10/10)	2	5.2:1	PTFE boiling stones	0.1	0.025	40	28
14	10 (10mol%)	KOH/K_2CO_3 (10/10)	2	1:2.4	sand	0.1	0.025	40	63
15[c]	10 (10mol%)	KOH/K_2CO_3 (10/10)	2	1:2.4	sand	0.1	0.015	66	65
16[c,d]	4 (1mol%)	CsOH·H_2O (10)	1.5	toluene	glass beads	0.2	0.1	10	47
17[c,d]	10 (5mol%)	KOH/K_2CO_3 (6/6)	1.2	1.6:1	glass beads	0.3	0.1	15	60
18[c]	10 (10mol%)	KOH/K_2CO_3 (45/45)	1.2	DCM	glass beads	0.35	0.1	30	>95

[a] flow rate of organic phase (solution of imine, benzyl bromide and the corresponding phase transfer catalyst in toluene/dichloromethane)

[b] solid base (the same equivalents of KOH and K_2CO_3) are finely grounded and packed inside the HPLC column, which serves as packed-bed reactor

[c] determination of ee% was done on target amino ester (**3**) after cleavage of imine in batch with citric acid and basification with aq. sol. of NaOH, entry 15 (**23% yield**, **52% ee**), entry 16 (**<20% yield, 93% ee**), entry 17 (**<15% yield, ~72% ee**), entry 18 (**<30% yield, 56% ee**)

[d] Entry 16 – reaction temperature 0 °C (the HPLC column was placed vertically in the ice bath); Entry 17 – reaction temperature -15 °C (the HPLC column was placed vertically in the cooling bath ice/NaCl). The other experiments were performed at ambient temperature.

Conclusion – Solid-liquid phase transfer benzylation in flow

Solid-liquid continuous flow experiments are summarized in table 2. Different reaction conditions were tested in flow, using various reactors to perform phase transfer benzylation.

Here are reported main conclusions:

-Solid-liquid phase transfer benzylation showed the same trend in terms of enantioselectivity (much better enantioselectivity was observed with Maruoka catalyst, entry 16, table 2). This result showed comparable enantioselectivity with described experiments in batch (section 1.2.1.).

-Regarding the conversion of imine **1** to benzylated imine **2** (figure 15)**,** much faster transformation was achieved under solid-liquid flow conditions, up to 47% NMR conversion with Maruoka catalyst **4** in 10 min of residence time (entry 16, table 2).

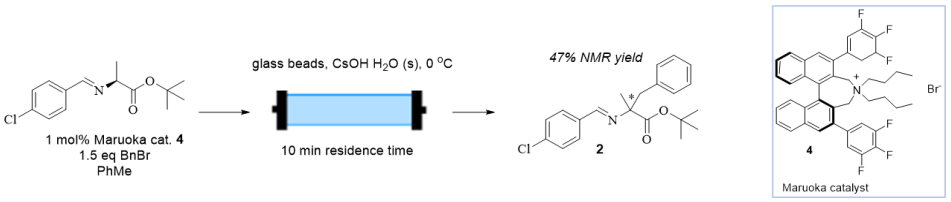

-Solid-liquid phase transfer benzylation tested in continuous stirred-tank reactor resulted in unsuccessful outcome, due to the clogging and overpressure generation inside CSTR units.

-Operating at lower temperatures (-15 °C, table 2, entry 17) can enhance enantioselectivity of the product, even when using a larger volume of DCM as a solvent.

-As a mixer, glass beads exhibit the best mixing properties inside packed-bed reactor.

-Significantly higher concentration of solution (up to 0.35 M), boost the conversion to the target quaternary amino acid derivative **2**.

-In the case of cinchona phase transfer catalyst **10**, higher catalyst loading is required (up to 10 mol%), and therefore larger volume of DCM to dissolve the total amount of the catalyst. These experiments demonstrate the influence of the selected solvents on the enantioselectivity of the target product.

Solid-liquid phase transfer benzylation in packed-bed reactor on a model reaction (figure 15), showed much higher productivity compared to batch synthesis (up to 17 times more, table 2, entry 16), while preserving the high ee% of the target quaternary amino ester **3**. There is no significant loss in ee% values of the final product **3**.

Chapter 4. Chiral Organosuperbases

4.1 The history of the development of organosuperbases

Chiral organosuperbases are defined as a chiral organic molecular entity capable of abstracting protons. In the first step, they can capture a proton from acidic pronucleophiles and generate a carbanion. Consequently, the corresponding protonated catalysts can interact strongly with the carbanion through hydrogen bonding or electrostatic interaction. Furthermore, chiral organobase catalysts bearing another functional group besides base site may demonstrate dual functionalization, activating the pronucleophiles and electrophiles simultaneously.[66]

The use of a chiral Brønsted base to mediate the enantioselective reactions has a long history. In early 1912, Bredig and Fiske reported the first example of the hydrocyanation to aldehydes with quinine or quinidine, although generating the desired products in less than 10% ee.[68] At that time, it was possible to deprotonate substrates with a low pKa. As time passed, it becomes more challenging for the direct deprotonation of pronucleophiles bearing a less acidic proton.[68] Immense efforts by different research groups led to various interesting modifications of the cinchona alkaloid scaffold (figure 20).[67] The major changes in the structure of the chiral catalysts occurred due to the inability to activate pronucleophiles with high pKa values by using conventional chiral tertiary amines (among them cinchona alkaloids).[68] To overcome this great challenge, a novel chiral Brønsted superbases, including **amidines**, **guanidines**, **cyclopropenimines**, and **iminophosphoranes** have been developed in the last two decades.[67] The advantage of these powerful superbases opens new opportunities for developing more demanding asymmetric transformations of weakly acidic pronucleophiles.[67,68]

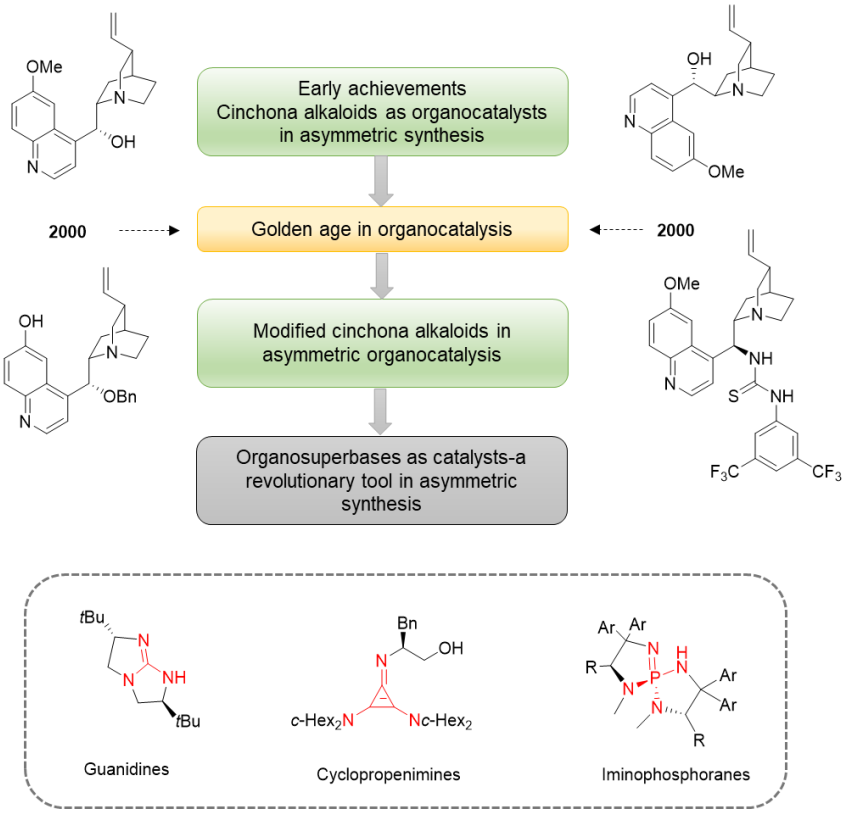

Figure 20. The development of the design of chiral Brønsted bases in the last decades[67]

The use of chiral organosuperbases have shown many advantages, such as: good solubility in organic solvents, good resistance to moisture, the possibility of expanding the scope of substrates with higher pKa values, decreasing the catalyst loading and reaction time, great chance to perform C−C and C−X (X = O, N, P, S, Br) bond formation reactions with high levels of stereocontrol, promotion of enantioselective reactions without using co-catalyst or metal ions.[68]

As illustrated in figure 21, the basicity increases with the number of substituted nitrogen functions at the same carbon, due to the growing number of isoelectronic forms of the corresponding conjugate acids.[68] For example, phenyl groups on the imino nitrogen have a big effect to the basicity of triaryliminophosphorane. The incorporation of electron-donating group (such as *p*-OMe) into the benzene ring leads to a significant increase in basicity.[68]

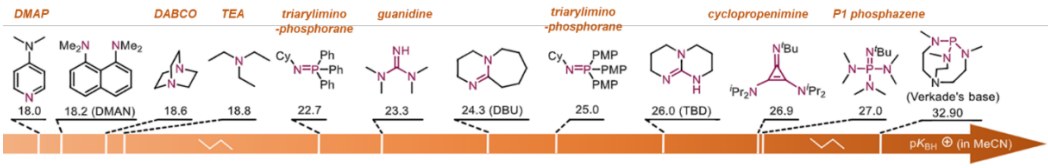

Figure 21. The basicity of organobases (pK_{BH+} values in CH_3CN)[68]

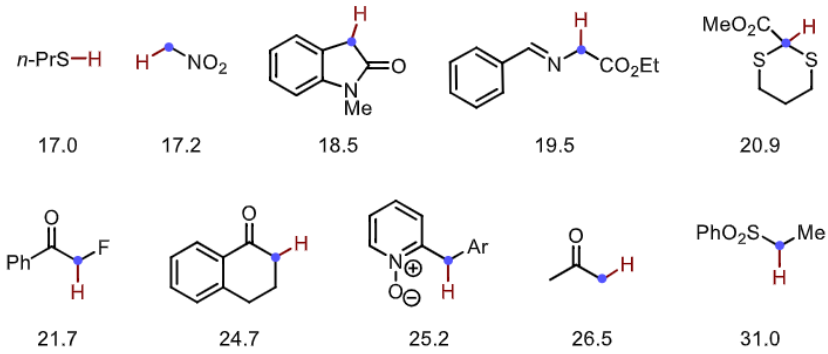

Figure 22. Selected examples of pronucleophiles with high p*K*a values. (p*K*a values in DMSO)[68]

4.1.1 Amidines

Amidine superbase can be formed by introducing an imine function group to the α-carbon of amine, and guanidine carries one more nitrogen atom based on amidine. In 2005, Tsogoeva and co-workers synthetized a novel bifunctional chiral Brønsted base **S1** bearing an imidazole and a thiourea group. Amidine type superbase showed high efficiency in promoting the Michael addition of acetone to *trans*-*β*-nitrostyrene with enantioselectivity up to 87% ee (figure 23).[68]

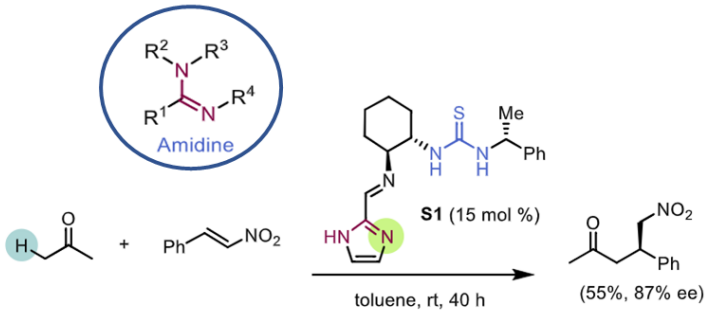

Figure 23. Enantioselective Michael addition of acetone to *trans*-1-nitro-2-phenylethylene promoted by amidine superbase

4.1.2 Guanidines

Guanidines are a class of organosuperbases which have been screened in different research areas of chemistry, such as auxiliaries, organocatalysts in organic synthesis, ligands in coordination chemistry and homogeneous catalysis.[70] The peculiar property of guanidine is the strong basicity coming from the formation of a conjugated planar guanidinium system after protonation, in which the positive charge could be delocalized over the three nitrogen atoms.[70]

Guanidine [$(NH_2)_2C=NH$] was isolated for the first time by Strecker via the oxidative degradation of guanine in 1861, and pioneering studies for the development of guanidines and derivatives was done by Nájera and Davis groups in the 1990's.[69,70] From 1996 to 1999, Corey and Grogan as well as the Lipton's group have contributed to the development of structurally diverse chiral guanidines and their use as effective chiral organocatalysts.[69]

Figure 24 represents a selection of chiral guanidine organocatalysts which can be classified as bicyclic, monocyclic, and acyclic molecules.[69] Many groups reported wide applications of chiral guanidines. For example, in 2001 Ishikawa and co-workers showed the use of monocyclic type guanidine to deprotonate glycine imine and catalyze asymmetric Michael addition to ethyl acrylate under solvent-free condition.[68] It was not possible to perform this reaction by using only quinine, which can be explained by its low basicity. Kobayashi et al. used the same type of the catalysts for the catalytic asymmetric imine−imine cross-coupling reaction based on an umpolung strategy.[68] Feng, Lui and their group implemented bifunctional C1-symmetric guanidine organocatalyst in an asymmetric vinylogous Michael reaction.[68] Many other applications were reported but it is also documented that it is not easy to introduce chiral groups around the guanidine, so these compounds appear to be very difficult to isolate.[69]

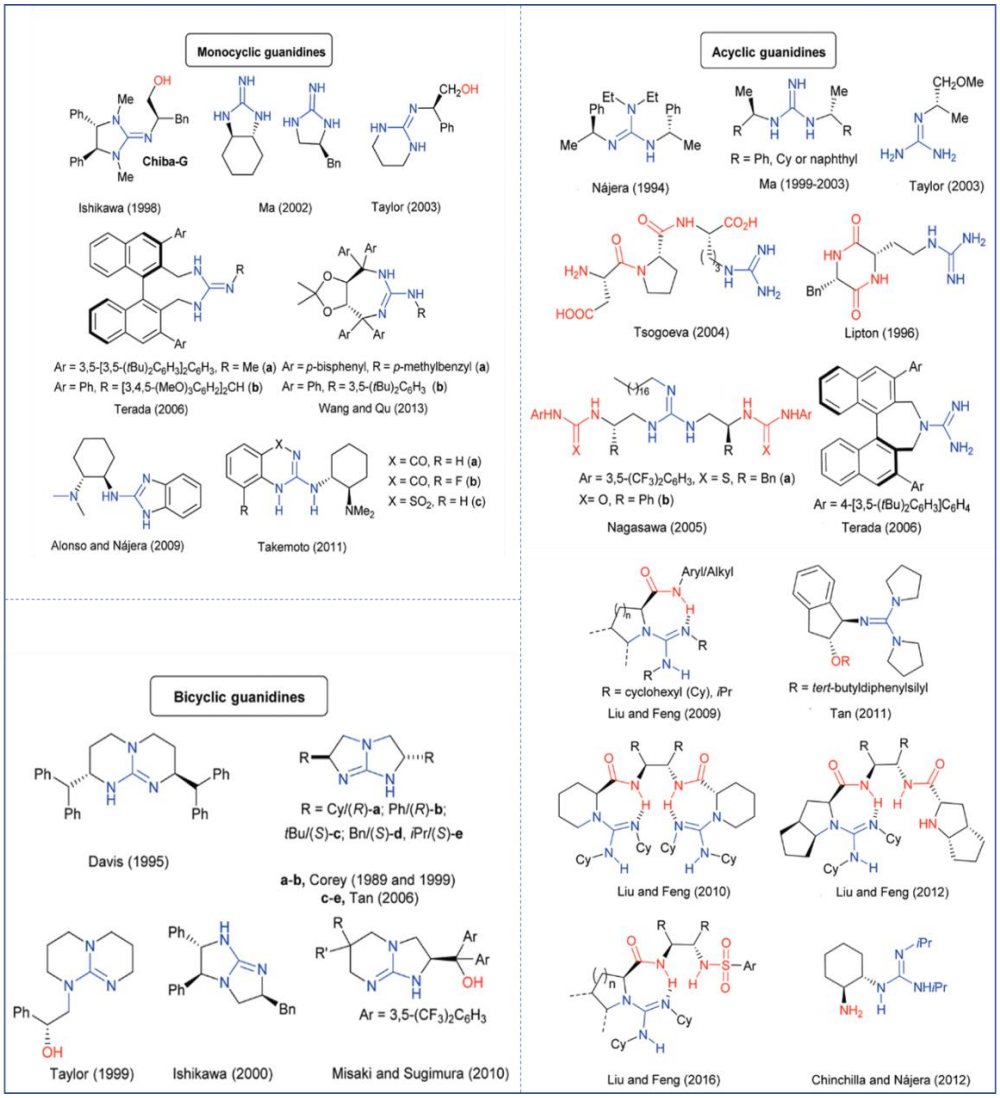

Figure 24. Classification of guanidines based on their difference in the structure

4.1.3 Cyclopropenimines

Cyclopropenimine organosuperbases possess one imino group and two amino groups. Based on experimentally measured pK_{BH+} values of superbases (figure 21), it can be stated that cyclopropenimines have stronger basicity than amidine and guanidine, because its conjugated acid could be stabilized by three nitrogen ione pairs and aromatic cyclopropenium cation (figure 25, left).[66,68]

In 2012, Bandar and Lambert reported experimental confirmation indicating that the basicity of cyclopropenimine is almost equal to the P1-phosphazene (pK_{BH+} (in MeCN) ~ 27).[68]

A few applications of cyclopropenimines in asymmetric catalysis were published.[66,68] Lambert and his co-authors designed chiral cyclopropenimines (figure 25, right) by using (*S*)-2-amino-3-phenylpropan-1-ol or alternative chiral primary amines to introduce chirality within the molecule. Afterwards, his group described the application of chiral cyclopropenimines bearing additional hydroxyl group and *N*-cyclohexyl groups in asymmetric Michael reaction of glycine imine with methyl acrylate (figure 26, above).[66,68] Deprotonation of glycine imine with cyclopropenimine gives an ion pairing species while the hydroxyl group of the catalyst activates methyl acrylate via hydrogen bonding (figure 27).[66] In 2016, Jørgensen and co-workers applied for the first time the chiral cyclopropenimine to the asymmetric [3+2] cycloaddition of 2-acyl cycloheptatrienes with azomethine ylides (figure 26, right). They proved as well that cinchona alkaloids were not effective enough to promote this asymmetric transformation.

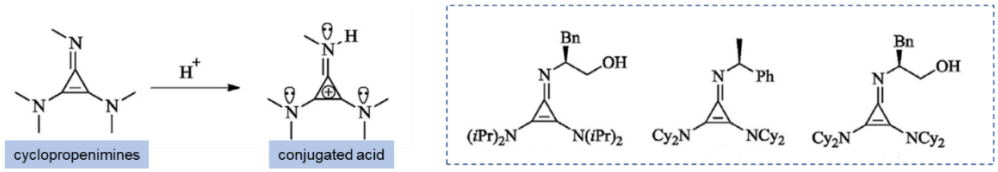

Figure 25. Selected chiral cyclopropenimines

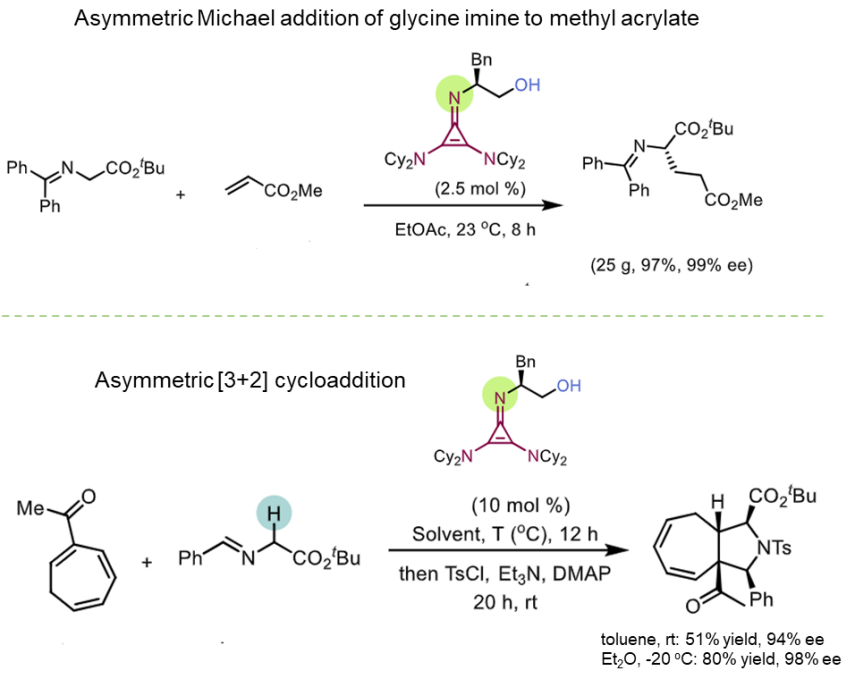

Figure 26. Selected asymmetric organocatalytic reactions promoted by cyclopropenimines

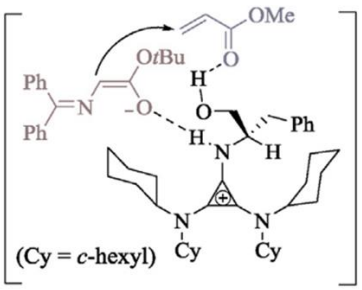

Figure 27. Transition state of cyclopropenimine catalyzed enantioselective Michael reaction of glycine imine with methyl acrylate

4.1.4 Iminophosphoranes

Iminophosphoranes are part of organosuperbases family and they can be divided in three main groups (figure 28).[67] Type **1** (chiral spiro cyclic system) and type **3** (chiral open chain system) superbases belong to phosphazene bases which are characterized by the presence of P (V) atom bonded to three amines and one imine group.[68] Schwesinger's phosphazenes are well-established and commercially available *N*-superbases and are among the most active steric hindered superbases.[72] Initial structure was first proposed by Schwesinger in 1985 and the chiral phosphazenes were prepared in 2007 by Ooi and co-workers.[68] So far, type **1** organosuperbase found application in different asymmetric reactions such as: Henry reaction, Pudovik reaction, asymmetric oxidation of *N*-sulfonyl imines, direct aldolization of α-benzyl-α-hydroxyphosphonoacetate, Michael reaction of nitroalkanes with olefinic 2-phenyl-1*H*-tetrazol-5-yl sulfones, asymmetric conjugate addition of azlactones to methyl propiolate etc.[67] The type **3** superbases possess a source of chirality within amide moieties of the catalysts (P-N single bonds). The basicity of these systems was predicted to be approximately pK_{BH+}=35–37.

Type **2** organosuperbases were developed in 2013 by Dixon and his group.[45] They designed novel, bifunctional iminophosphorane organocatalysts which have dual role. They act as a Brønsted base (basic nitrogen of -N=P functional group), but also as a hydrogen bond donor (thiourea or urea moiety). By constructing such a catalyst, it is possible to perform double activation of both pronucleophile (via deprotonation) and electrophile (via H-bonding interactions).[67]

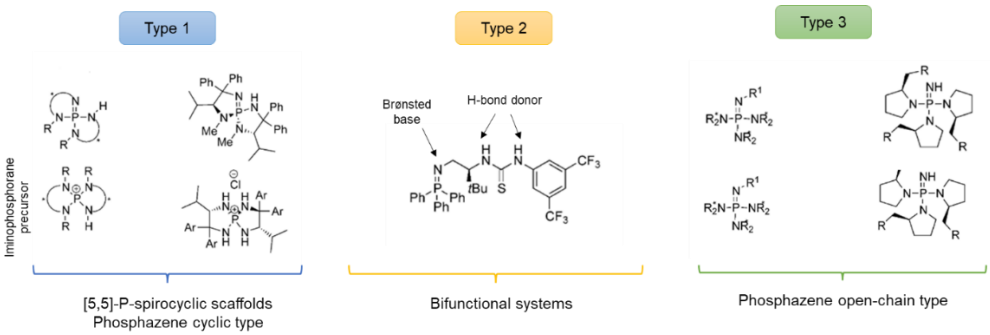

Figure 28. Classification of iminophosphorane organocatalysts

4.2 Synthesis of **Bi**functional **IM**ino**P**hosphoranes

The great demand for new and efficient organocatalysts led the scientific community to search for a solution to perform challenging asymmetric syntheses. Thus, in 2013 Dixon and his group designed and developed novel acyclic amino acid derived bifunctional iminophosphorane organocatalyst, which showed great potential for the synthesis of many chiral compounds that were previously very difficult to achieve.[45] That was a key stage for the further development of similar catalysts with enhanced properties, depending on the performed asymmetric synthesis. Commonly, all iminophosphorane organocatalysts developed by Dixon et al. are derived from the corresponding chiral natural or unnatural amino acids (D or L-*tert*-leucine, D or L-valine, D or L-phenyl glycine, D or L-phenyl alanine).

Subsequent synthetic steps include: 1) reduction of carboxylic group to the corresponding alcohol; 2) protection of amino group (Boc or Fmoc); 3) conversion of hydroxy group to a leaving group; 4) formation of azide; 5) construction of thio(urea) azide from the isothiocyanate or isocyanate. The synthesis of the final iminophosphorane organocatalyst is performed via Staudinger reactions between chiral organoazide and commercially available phosphine, releasing nitrogen as the only byproduct (figure 29).[45,73,74]

The Staudinger reaction was discovered in 1919[112], and it is described as a two-step process. The first step involves nucleophilic attack of phosphorus atom coming from the corresponding phosphine to the terminal nitrogen of an azide[113], generating phosphazide intermediate. The consecutive extrusion of a nitrogen molecule yields the iminophosphorane (figure 29).

In order to apply this type of bifunctional organocatalysts in different enantioselective reactions, the authors (Dixon and co-workers) were enforced to design different catalyst structures, due to the diverse activation modes in individual asymmetric reactions. Thus, bifunctional iminophosphorane catalyst can be divided in two groups: 1) catalysts bearing one stereocenter (scheme 19 and 20)[45,76,79] and 2) catalysts bearing two stereocenters (scheme 21 and 22).[74,77,78]

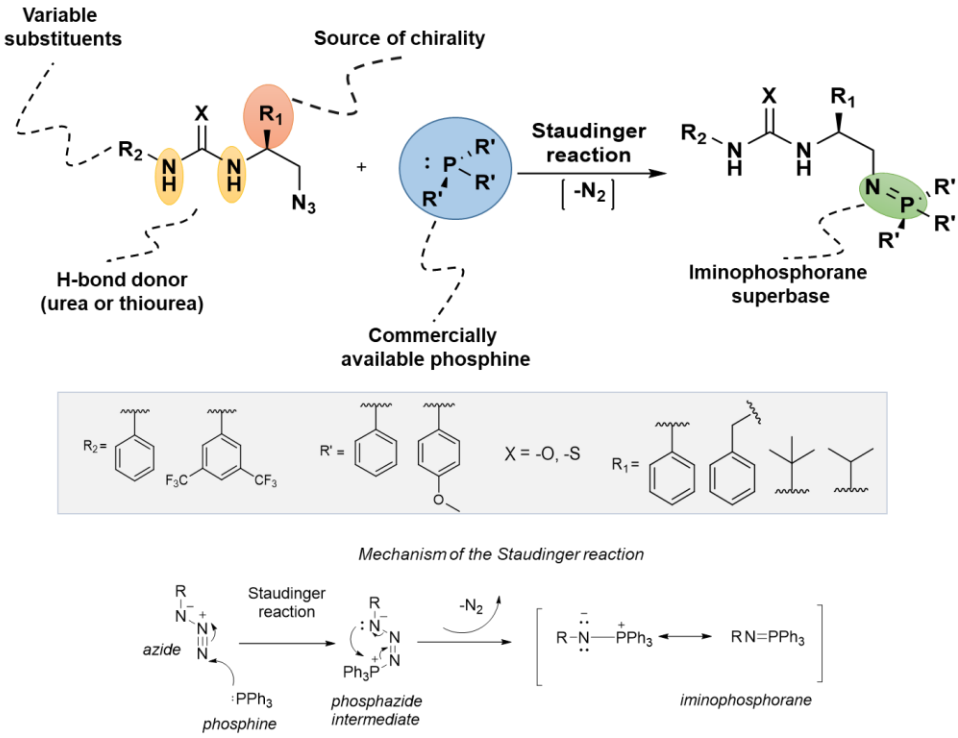

Figure 29. Standard Staudinger reaction for the formation of bifunctional iminophosphorane organocatalysts

4.3 Application of **Bi**functional **IM**ino**P**hosphoranes in enantioselective reactions

Many bifunctional Brønsted base catalysts were reported by the groups of Takemoto, Deng, Chen, Soós, Connon, Rawal, Hiemstra, Pedrosa, Berkessel, Jacobsen, and used in enantioselective addition reactions.[73] Their unique features lie in the fact that they possess basic moiety (Brønsted base part of the molecule) but also H-bond donor group which is crucial for reactivity and stereocontrol (via transition structure stabilization).[73]

However, Dixon and his co-authors pointed out some limitations of certain bifunctional organocatalysts. For instance, cinchona based, and Takemoto type bifunctional tertiary amine catalysts have proven to be air stable and easy to handle but the accessible pronucleophile range is quite limited.[73] On the other

hand, guanidine and phosphazene superbases enable access to high pK_a pronucleophiles; nevertheless, their synthesis is complex, they are difficult to isolate, store and handle.[73] Therefore, Dixon and co-workers made a great progress on this topic. They designed bifunctional iminophosphorane catalysts (**BIMP**), that cover all the limitations listed above. The key properties of BIMP that should be emphasized are high tunability and stability, access to high pK_a pronucleophiles, easy handling and synthesis, resistance to air and moisture.[73] The high activity of the BIMP catalysts was demonstrated in the **1,2-addition reactions** (Mannich reaction of nitromethane to low electrophilicity *N*-diphenylphosphinoyl-protected ketimines (scheme **13)**[45], Michael addition of malonates to nitro-styrene by employing catalyst immobilization on polystyrene support (scheme 19)[79], direct aldol addition of aryl ketones to α-fluorinated ketones (scheme 20)[76]), **1,4-addition reactions** (enantioselective sulfa-Michael to α-substituted acrylate esters (scheme 21)[77]), **enantioselective prototropic shift reactions** (1,3-prototropic shift of γ,β-unsaturated cyclohexenones (schemes 22a/b)[78]), and even in the total synthesis of (-)-nakadomarin A.[80]

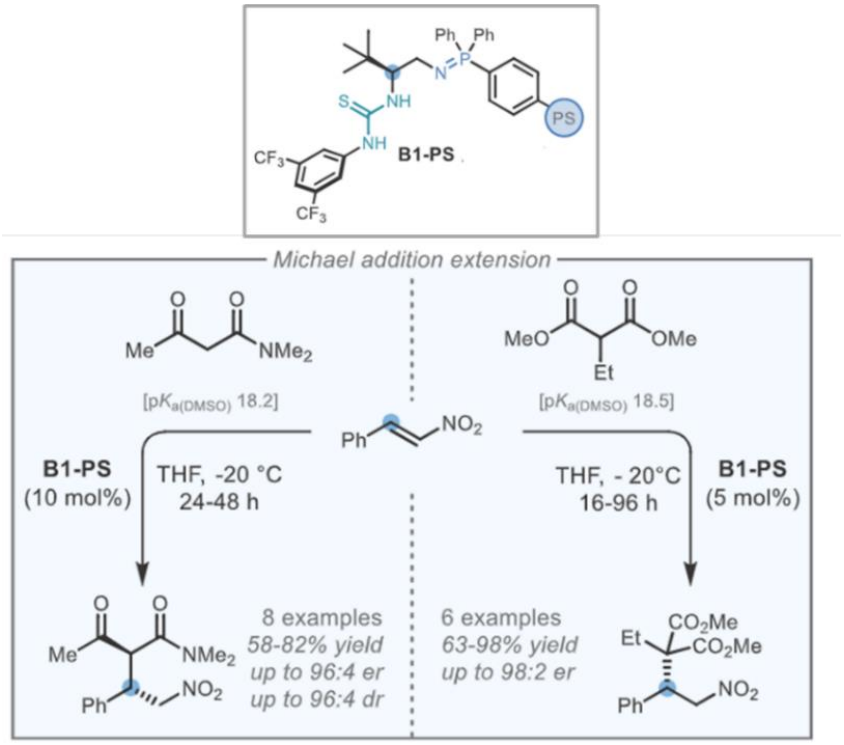

Scheme 19. ***1,2 addition*** **-** enantioselective Michael addition of malonates to nitro-styrene promoted by BIMP bearing one stereocenter

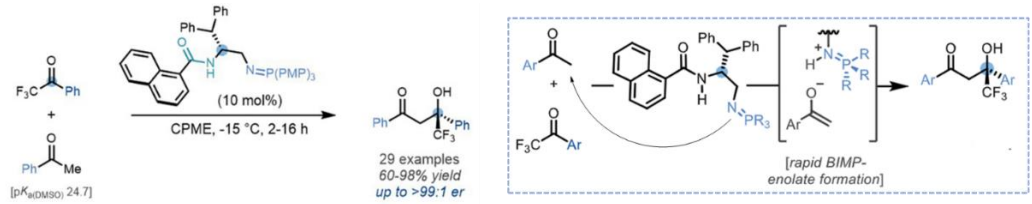

Scheme 20. *1,2 addition* - enantioselective aldol addition of aryl ketones to *α*-fluorinated ketones catalyzed by BIMP bearing one stereocenter

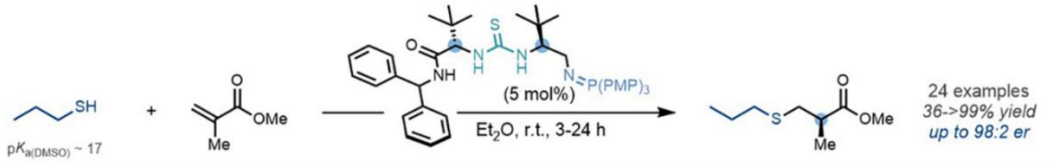

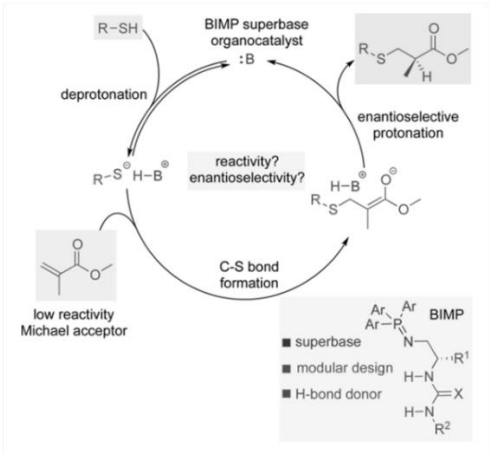

Scheme 21. *1,4 addition* - enantioselective sulfa-Michael reaction to α-substituted acrylate esters promoted by BIMP bearing two stereocenters

Dixon and co-workers investigated the mechanistic pathway of prototropic shift reactions (scheme 22a), corroborated by computational analysis. Transition structures of γ,β-unsaturated cyclohexenones undergo successive α-deprotonation and γ-reprotonation by BIMP catalyst (see Gibbs energy profile shown in scheme 22b). The reprotonation is the rate- and enantio-determining step due to the higher energy. Likewise, the bifunctional catalyst engages the

substrate oxygen with a dual H-bonding interaction from both thiourea N-H protons and the iminophosphorane, which participates as proton acceptor/donor. It was found that the preferred transition state is *S* (it has less torsional strain and less 1,3-allylic strain), which was consistent with experimental data.

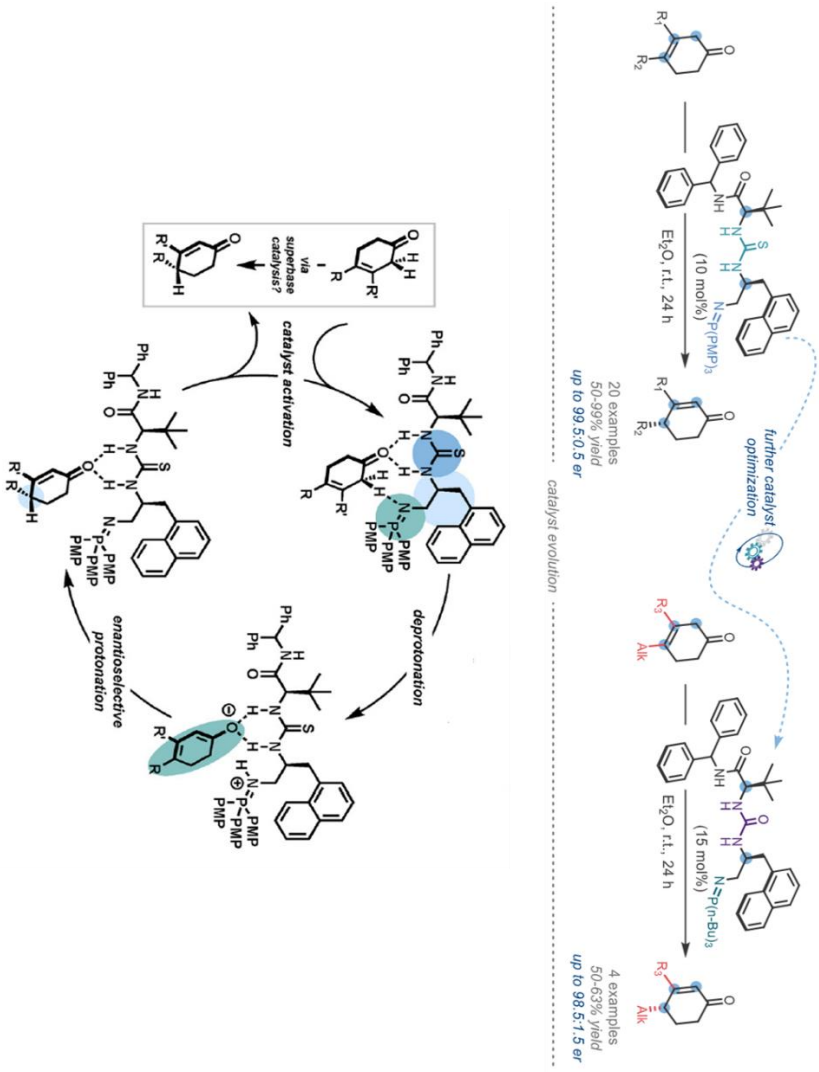

Scheme 22a. ***Prototropic shift reactions*** - 1,3-prototropic shift of γ,β-unsaturated cyclohexenones catalyzed by BIMP bearing two stereocenters

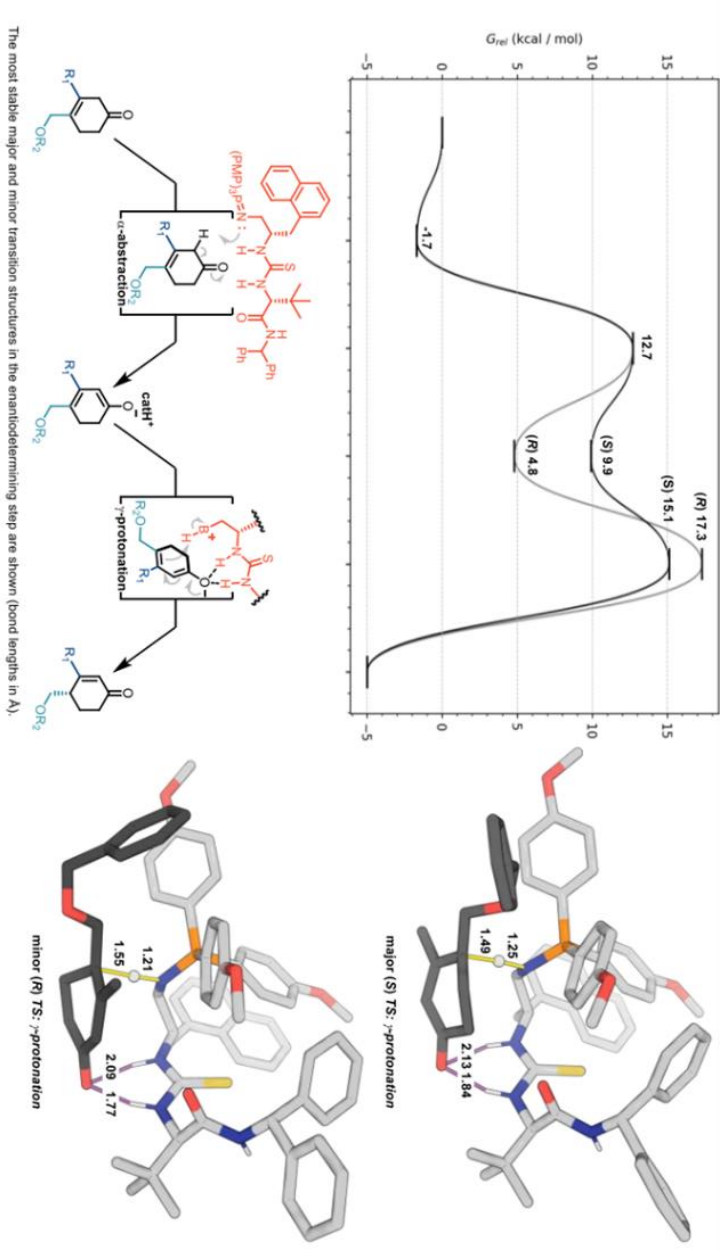

Scheme 22b. ***Prototropic shift reaction*** - Gibbs energy profile (kcal mol-1) showing deprotonation and reprotonation steps (M06-2X+D3/def2-TZVP)

Chapter 5. Results and discussion

Synthesis of iminophosphorane catalysts and their use in asymmetric reactions

Guided by the excellent work of scientists in the field of organocatalysts development directed us to continue our research in that sequence and contribute to the field of green chemistry. The synthesis of efficient, metal-free organocatalysts able to promote more challenging asymmetric reactions is still one of the relevant issues in synthetic organic chemistry. In the last 20 years, great movement has been made in that area, especially in terms of stability and isolation of organocatalysts, as well as their applications in enantioselective reactions. In particular, bifunctional iminophosphorane organocatalysts have shown great potential in their basicity, modular design and tunability. The synthesis of this relatively new class of superbases was introduced by Dixon and his group.[45,73-80] The dominance of these catalysts is reflected, among other things, in their easy modifications, by using available and environmentally friendly chiral amino acids as starting material.

Here, in this PhD thesis we reveal a new design within the iminophosphorane scaffold by employing more electron-rich achiral or chiral phosphines and chiral amino acids (L-*tert*-leucine, L-phenylglycine, D-phenylglycine) for the synthesis of chiral organoazide moiety.

Various iminophosphorane organocatalysts will be described, with modified parts of the molecule such as hydrogen bond donor moiety (urea or thiourea) or phosphine unit. Changing the nature of the catalyst may help to understand the interaction between the catalyst and the substrate in asymmetric reactions. We also investigated the role of electron withdrawing groups on thiourea or urea phenyl ring as well as the influence of very electron rich phosphines used to synthetize the final, target iminophosphorane organocatalysts.

Moreover, the application of new iminophosphorane organocatalysts in enantioselective aza-Henry reaction and Mannich reaction of malononitrile to ketimines to construct quaternary amino or amino acid derivatives will be depicted.

5.1 Synthesis of **B**ifunctional **IM**ino**P**hosphorane organocatalysts (**BIMP**) bearing one stereogenic center

5.1.1 Synthesis of BIMP derived from (*R*)-(−)-2-Phenylglycine

Synthesis of the bifunctional iminophosphorane organocatalysts **17** and **25** (section 5.1.2) were prepared for the first time in 2013 by Dixon and co-workers.[45] This type of catalysts, bearing one stereocenter, belong to the first class of iminophosphoranes and they are successfully used in asymmetric nitro-Mannich reaction of nitromethane with low active *N*-diphenyl-phosphinoyl ketimines.[45]

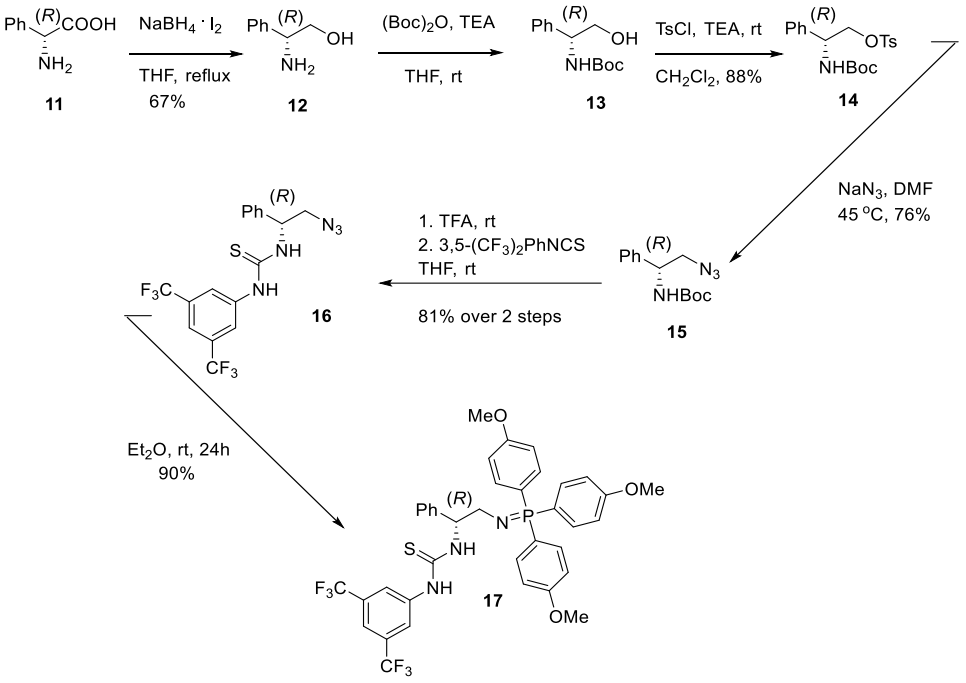

Scheme 23. Synthesis of BIMP bearing one stereocenter derived from D-2-Phenylglycine (**11**) proposed by Dixon[45]

The synthesis of the iminophosphorane catalyst **17** or **25** is initiated using the corresponding chiral amino acids (**11** or **18**, respectively), which introduce a stereogenic center into the molecule. In their case (scheme 23), sodium borohydride/iodine reduction was used to generate the amino alcohol **12**.[97] In order to convert hydroxy group to the target azide **15**, they had to perform

protection of amino group by using di-*tert*-butyl decarbonate ($(Boc)_2O$) and triethylamine in tetrahydrofuran (THF) at room temperature, which is straightforward procedure for Boc protection of primary amines.[98] *N*-Boc protected amino alcohol **13** was transformed into leaving group (tosylate **14**), which facilitated the preparation of azide **15**. The isolated azide **15**, after Boc deprotection with trifluoroacetic acid (TFA) was coupled with 3,5-bis(trifluoromethyl)phenyl isothiocyanate under mild conditions to get thioureazide **16**, a stable and important intermediate for the synthesis of the final iminophosphorane organocatalyst.[45] The formation of the target catalyst **17** was achieved via Staudinger reaction between compound **16** and tris(4-methoxyphenyl) phosphine by stirring in diethyl ether at room temperature.[45]

We applied the same synthetic pathway to synthetize catalyst **17**, starting from corresponding alcohol (**12**). For the formation of better leaving group, we synthetized mesylate (**14a**) instead of tosylate (**14**) proposed by Dixon. A small modification was done in the synthesis of Boc-protected aminoazide (**15**). This step was performed at higher temperature (65 °C) in dimethylformamide (DMF), and the intermediate **15** was isolated in higher yield (86%) after 16h.

5.1.2 Synthesis of BIMP derived from L-*tert*-leucine possessing thiourea moiety

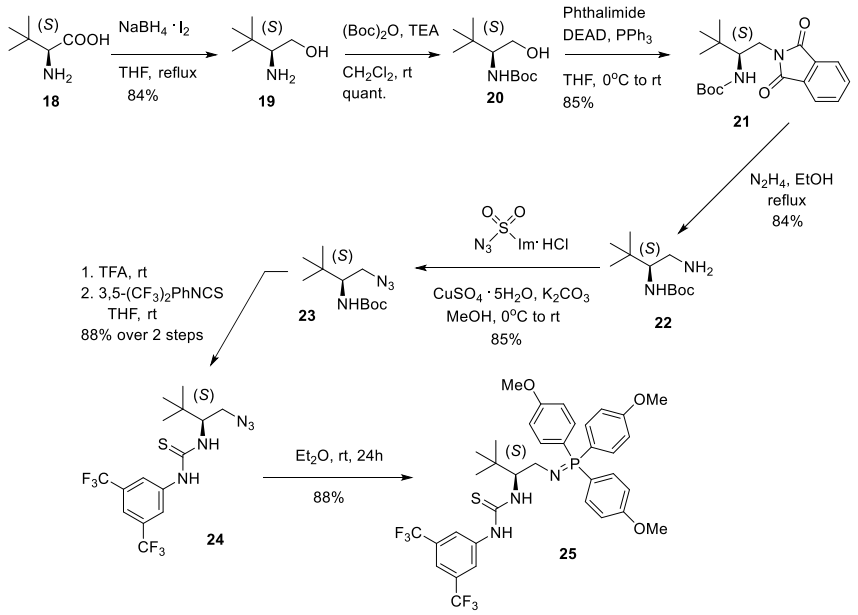

Scheme 24. Synthesis of BIMP **25** bearing one stereocenter derived from L-*tert*-leucine (**18**) proposed by Dixon[45]

As in the scheme 23, the same strategy of the first two synthetic steps was applied to obtain *N*-Boc protected L-*tert*-leucinol **20**. Nevertheless, different approach was designed for the synthesis of azide **23**. Mitsunobu amination of alcohol **20** with phthalimide yielded phthalimidocarbamate **21** in 85% yield. Hydrazinolysis of the phthalimide completed the synthesis of the *N*-Boc protected diamine **22**.[45] In the last step of azide **23** synthesis, diazotransfer reagent, imidazole-1-sulfonyl azide hydrochloride was applied to introduce azide group.[45] The last two steps to get thiourea-azide **24** and catalyst **25** were performed under the same conditions, as previously described in scheme 23.

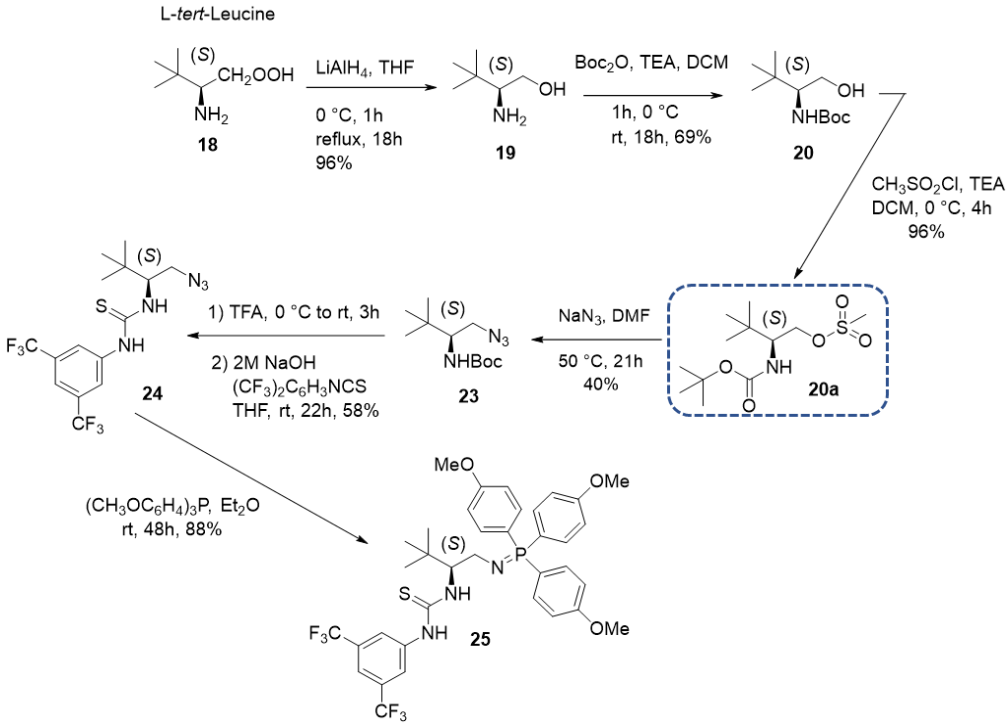

Scheme 25. Proposed redesign of the synthetic pathway of catalyst **25**

In order to reduce the number of synthetic steps, chemical waste and the cost of the process, the synthesis of the iminophosphorane catalyst **25** was revised. According to our experience, the reduction of L-*tert*-leucine with lithium aluminum hydride provided better yield of amino alcohol **19** and cleaner reaction.[98] Synthesis of phthalimide **21**, hydrazinolysis and conversion of diamine **22** to

N-Boc azide **23** by employing diazotransfer reagent (scheme **24**) proposed by Dixon has been replaced by the formation of mesylate **20a** followed by nucleophilic attack of NaN_3 to obtain compound **23** (scheme 25).

In such manner, we avoided the use of phthalimide, diethyl azodicarboxylate (DEAD, toxic and shock sensitive chemical), hydrazine (the National Institute for Occupational Safety and Health (NIOSH) lists it as a "potential occupational carcinogen") and imidazole-1-sulfonyl azide hydrochloride, potentially explosive and sensitive reagent. Several safety issues regarding the preparation, storage and use of imidazole-1-sulfonyl azide hydrochloride have been indicated by Goddard-Borger and Stick.[101]

Anyhow, synthesis of organic azides can be very risky, depending on the ratio between carbon, oxygen, and nitrogen atoms within the molecule. Therefore, they should be considered and handled as explosive materials, regardless of the synthetic route used. Thus, following the rule (C+O)/N<3, it is possible to predict whether there is a risk of decomposition for azido compounds.[99] In case of azides **15** (scheme 23) and **23** (scheme 24 and 25), this ratio is higher than 3, which tells us there is less chance to cause an explosion.

When the synthesis of azide **23** (scheme 25) was carried out from the corresponding mesylate **20a**, all safety measures were applied. This step was first tested in milligram scale, to determine the sensitivity of the reaction outcome. During the experimental setup, the screen of the fume hood was always kept closed and used additional blast-shield. Plastic spatulas were used instead of metal ones because they transfer stronger mechanical stress to the material.[99] All acid sources were eliminated before setting up the reaction due to the possibility of hydrazoic acid formation. During the work up, excess of sodium azide was deposited as basic solution (pH=8 or 9) due to the reasons mentioned above. In order to decrease the mechanical stress, the final product, azide **23**, was isolated as a solid with smaller particle sizes. The last two steps of the synthesis (access to the molecule **24** and **25**) were completed according to Dixon's procedure.[45]

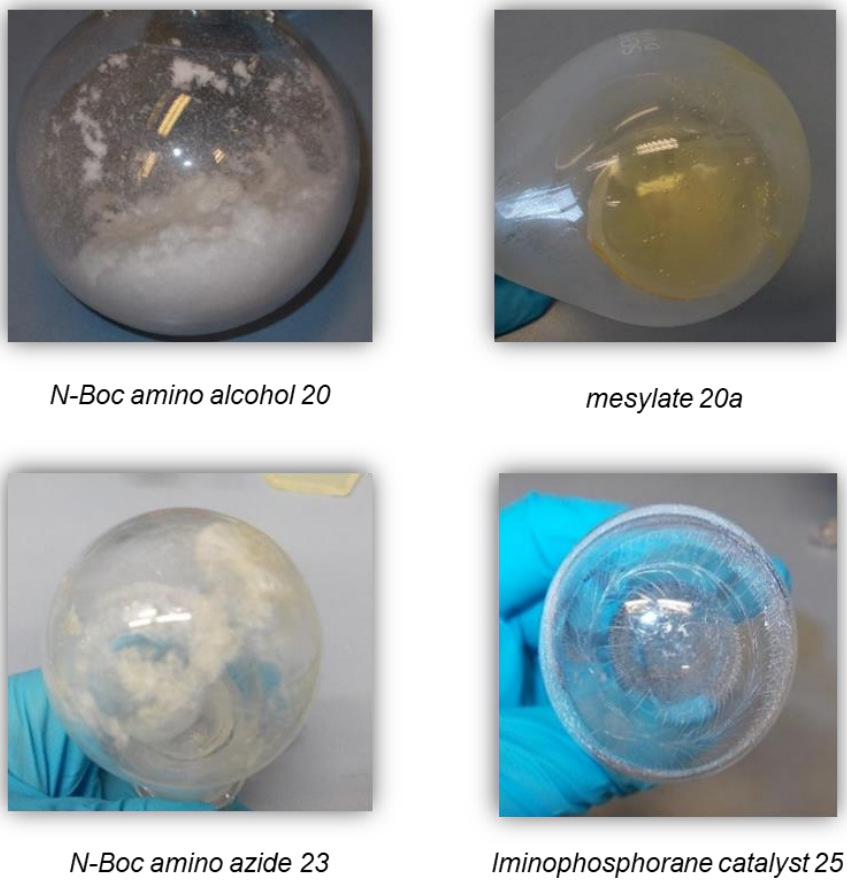

Figure 30. Physical appearance of certain intermediates in catalyst **25** synthesis

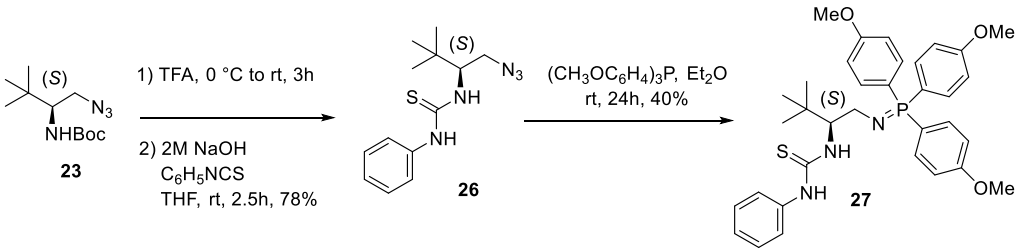

Scheme 26. Synthesis of the catalyst **27** bearing thiourea phenyl ring without electron withdrawing groups

The synthesis of bifunctional iminophosphorane catalyst **27** was done in order to understand the effect of a different phenyl rings on thiourea hydrogen bond donor part of the molecule. The first catalyst synthetized by Dixon (**25**, scheme 24) contains trifluoromethyl groups in 3,5 positions of thiourea phenyl ring. The catalyst **27** was prepared in similar way by using phenyl isothiocyanate as electrophile in the reaction with previously synthetized *N*-Boc aminoazide **23.** The last step was performed between thiourea azide **26** and tris(4-methoxyphenyl) phosphine to afford catalyst **27,** which doesn't have electron withdrawing groups on the phenyl part.

5.1.3 Synthesis of BIMP derived from L-*tert*-leucine possessing urea moiety

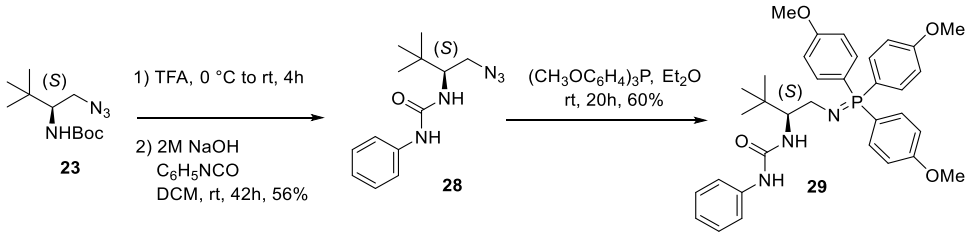

Scheme 27. Synthesis of the catalyst **29** bearing urea moiety without electron withdrawing groups on phenyl ring

The catalyst **29** was obtained by nucleophilic attack of aminoazide **32** (after Boc deprotection of **23** with trifluoroacetic acid) to phenyl isocyanate to get first urea-azide **28,** which is further coupled with tris(4-methoxyphenyl) phosphine. The final catalyst **29** was isolated in 60% yield (scheme 27).

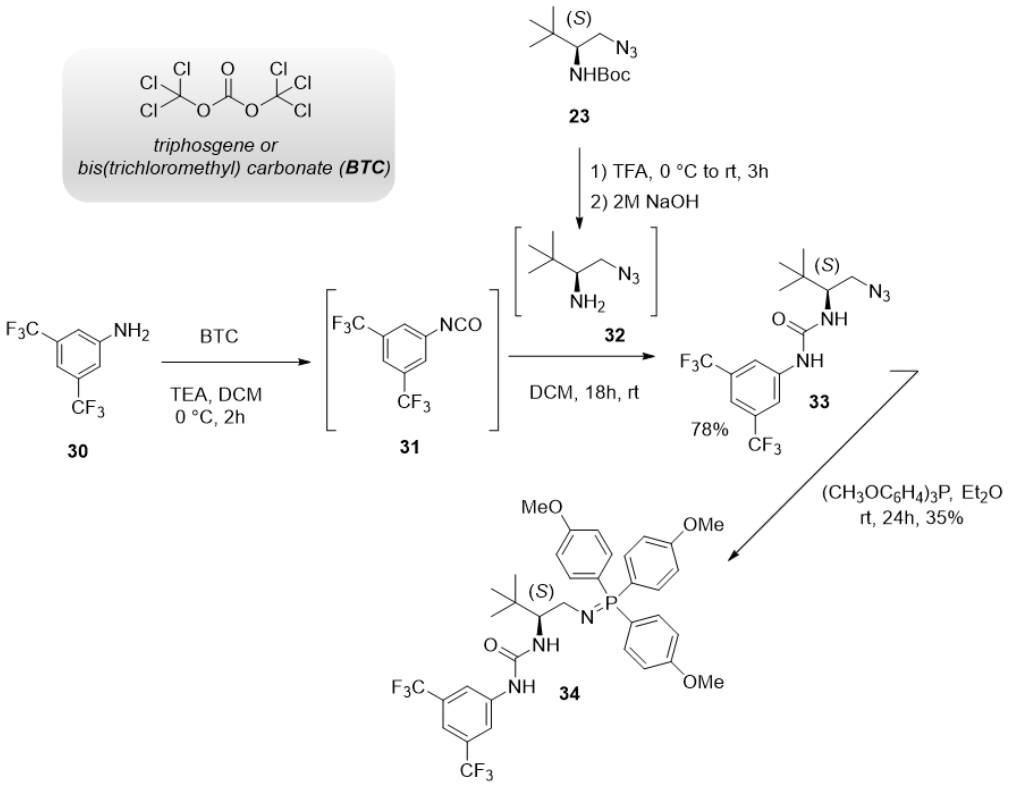

Scheme 28. Synthesis of the catalyst **34** bearing urea moiety with electron withdrawing groups on phenyl ring

The synthesis of iminophosphorane catalyst **34** was accomplished in small scale due to the toxicity of triphosgene. The synthetic route started from commercially available 3,5-bis(trifluoromethyl)aniline **30**, which was reacted with bis(trichloromethyl) carbonate (BTC) to form reactive 3,5-bis(trifluoromethyl) isocyanate **31** *in situ*. Without isolation, intermediates **31** and **32** were mixed and stirred for 18h to afford urea-azide **78** in good yield. Like in the scheme 26**,** the last step was performed with the same phosphine and the catalyst **34** was isolated after 24h stirring in diethyl ether, at room temperature. The yield of the target compound was quite lower (35%) compared to the other catalysts, due to the very small-scale reaction (scheme 28).

5.1.4 Synthesis of BIMP derived from L-*tert*-leucine and electron rich phosphines

Up to now, Dixon and co-workers have mainly modified and redesigned organozide scaffold (for example **16**, **24**, **26**, **28**), while in the last step of the catalyst synthesis (Staudinger reaction) they predominantly used triphenylphosphine or tris(4-methoxyphenyl) phosphine. According to the literature research, no data has been published on the use of more electron rich and steric hindered phosphines to generate iminophosphorane organocatalysts.

Correspondingly, our hypothesis of using different series of monophosphorus ligands such as oxaphosphole-based phosphine (BIDIME) or acyclic biphenyl phosphine (SPhos) to generate novel iminophosphoranes has resulted in obtaining the ***new catalysts*** **35** and **36,** respectively (scheme 29).

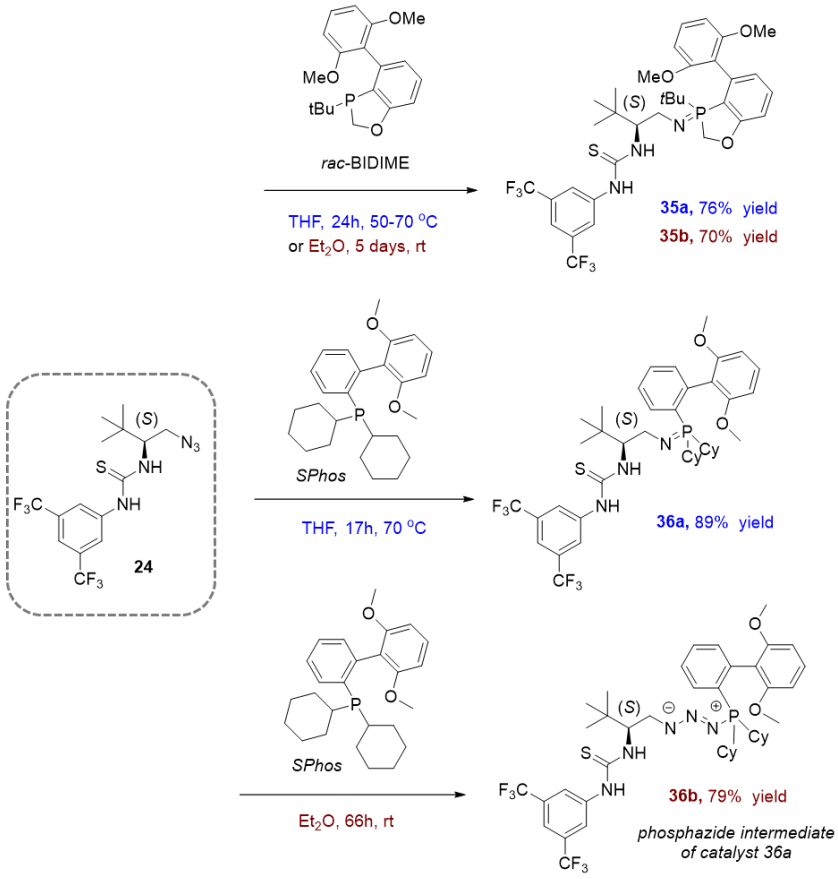

Scheme 29. Synthesis of the catalysts **35a/b** and **36a** derived from L-*tert*-leucine organoazide and more electron rich phosphines (BIDIME and SPhos)

Initially, the first attempt to synthetize these two catalysts (scheme 29) was done under standard Dixon's conditions (stirring of organoazide and the corresponding phosphine in diethyl ether at room temperature). It is important to emphasize that the synthesis of the catalyst **36** shown peculiar performance, depending on the solvent and temperature used for their synthesis. According to the published calculations done by Rzepa et al.[113] as well our analysis (see experimental part), we found out that experiment performed at room temperature led to the formation of phosphazide intermediate **36b**. Although these species usually are not stable, due to the very fast conversion to iminophosphoranes, some phosphazide have been isolated. The stability of the phosphazide depends on their nature. Accordingly, the presence of electron donating and bulky substituents on phosphorus atom as well possible hydrogen bonding within the molecule makes them more stable.[113,114] For the formation of N=P bond via nitrogen loss, based on the reported X-ray data, s-*cis* configuration of phosphazide central N-N bond is required (figure 29). These structural data explain easier ring closure to 4-membered transition state necessary for nitrogen elimination, which is difficult to perform in s-*trans* configuration.[114] Our analysis also confirmed the same behavior of SPhos (more electron rich and steric hindered phosphine) in the reaction with organoazide **24**. It is assumed that the phosphazide intermediate **36b** exists in s-*trans* configuration, which can be additionally stabilized by thiourea hydrogen bonding. Phosphazide intermediate **36b** has been isolated and characterized by HMR and HR-MS. Also, it was tested in asymmetric Aza-Henry reaction (see section 5.5) and, as expected, very low reactivity of this intermediate was observed. As well, the solubility in nitromethane, diethyl ether or even methanol was very poor.

Unlike, preparing the catalyst **36a** at 70 ^{o}C in tetrahydrofuran (scheme 29) allowed the formation of "active iminophosphorane catalyst form" which was confirmed by NMR and high-resolution mass spectra analysis (see experimental part). The activity of the catalysts **36a** in asymmetric Aza-Henry reaction synthetized in this way was much higher. Likewise, the solubility of this catalyst (scheme 29) in nitromethane and methanol was much better.

The catalyst **35a** or **35b** (scheme 29) showed comparable enantioselectivity results in asymmetric aza-Henry reaction (table 4, entry 29 and 30) regardless of the method of preparation. However, significant difference in yield was observed.

5.2 Synthesis of **B**ifunctional **IM**ino**P**hosphorane organocatalysts (**BIMP**) bearing two stereogenic centers

5.2.1 Synthesis of BIMP bearing two stereogenic centers and thiourea moiety

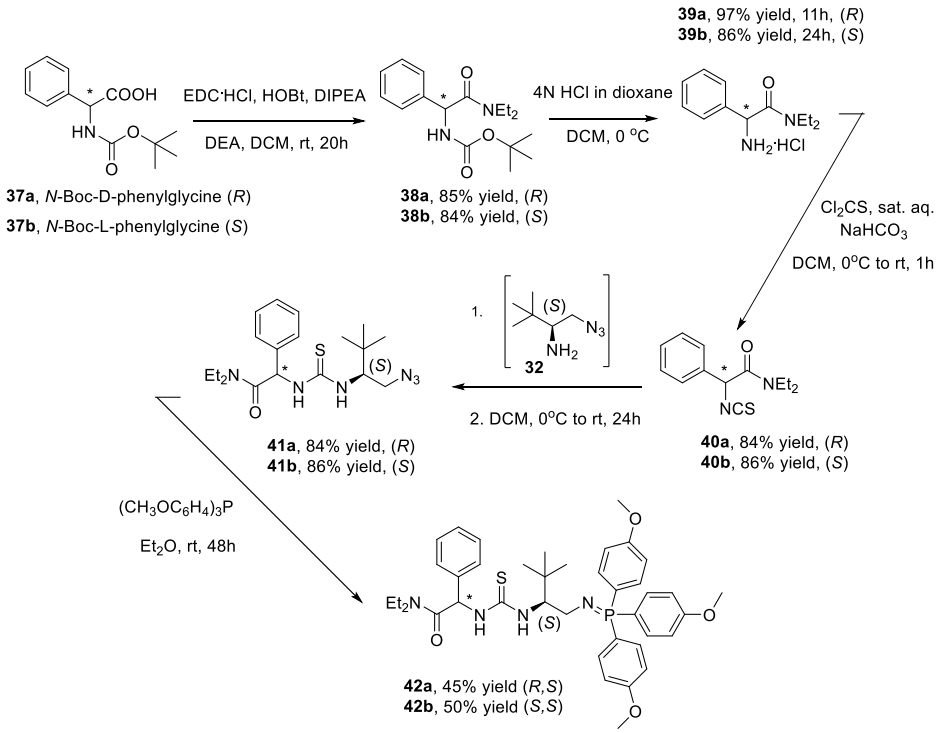

Scheme 30. Synthesis of two iminophosphorane diastereomers **42a** and **42b**

Introduction of two stereocenters within iminophosphorane molecules is well-known concept previously explored by Dixon and his group.[74] The same pattern was used to obtain two new diastereomers **42a** and **42b** (scheme 30). The synthesis was initiated by standard amide coupling of commercially available *R* or *S* phenylglycine isomer and diethylamine. The corresponding diethylamide **38a/38b** was converted to hydrochloride salt **39a/39b**, which reacted further with thiophosgene to get the correlative isothiocyanate **40a/40b.** The second stereogenic center was inserted from typical aminoazide **32** (used in aforementioned syntheses) by formation of thiourea azide **41a/41b.** Staudinger reaction yielded two different iminophosphorane organocatalysts as *R,S* and *S,S* diastereomers, **42a/42b**. These ***new catalysts*** (**42a/42b**) were tested in asymmetric aza-Henry reaction (section 5.5).

5.2.2 Synthesis of BIMP bearing two stereogenic centers and urea moiety

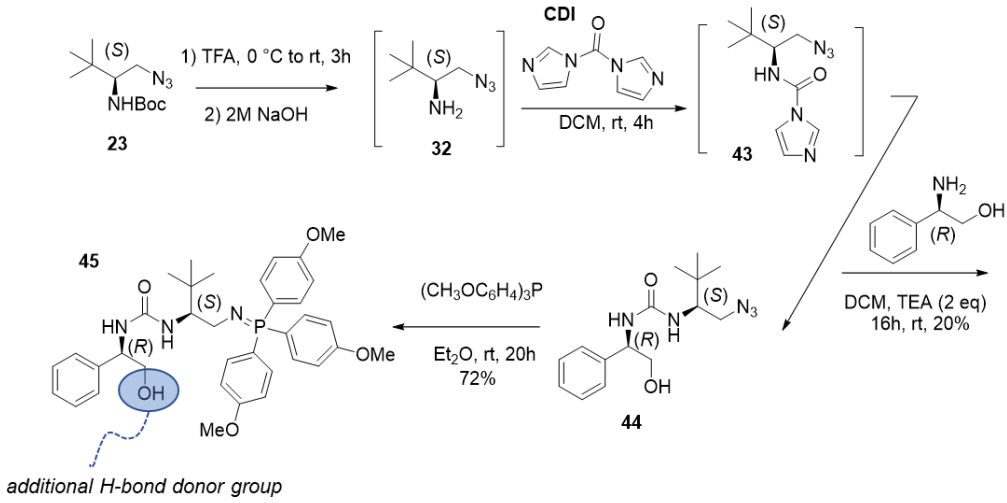

Scheme 31. Synthesis of the iminophosphorane catalyst **45** with -OH hydrogen bond donor group

The role of hydrogen bond donor groups in asymmetric organocatalytic reactions is well described in many articles. Knowing that hydrogen bonding of iminophosphorane catalysts with the substrates has an important outcome in enantioselectivity, we came up with an idea to introduce additional hydrogen bond donor. This proposition was implemented using different approach. Condensation of well-established aminoazide **32** with 1,1′-carbonyldiimidazole (CDI) enabled the formation of intermediate **43**, followed by second nucleophilic attack with (*R*)-2-phenylglycinol (scheme 31). The organoazide **44** was isolated in low yield (20%) due to the competition reaction (self-condensation of starting aminoazide **32** to form symmetric urea). The new target catalyst **45,** possessing urea and hydroxy hydrogen bond donor groups was collected as 70% pure solid by NMR analysis. The main impurities are coming from the starting phosphine (used to generate iminophosphorane in the last step). Purification of the catalyst **45** was very difficult due to instability on silica gel chromatography. The ***new catalyst 45*** was tested in asymmetric nitro-Mannich reaction (section 5.5).

5.3 Synthesis of **B**ifunctional **IM**ino**P**hosphorane organocatalysts (**BIMP**) bearing one stereocenter on organoazide scaffold and stereogenic phosphorus

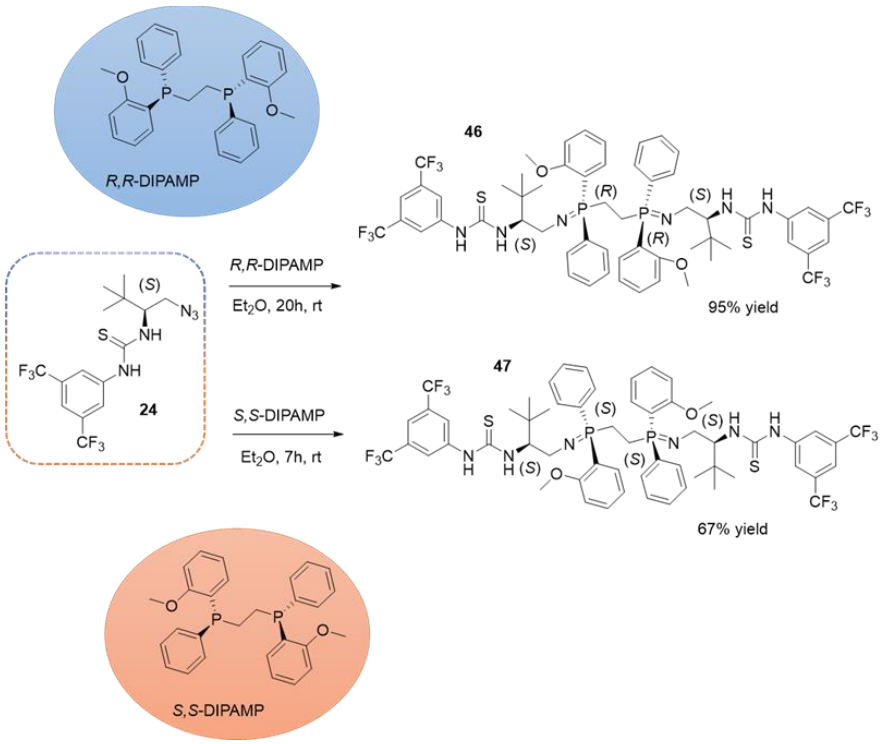

Scheme 32. Synthesis of the iminophosphorane catalysts bearing P-stereogenic center

Application of chiral phosphines (bis-phosphines) in the synthesis of iminophosphoranes represents a novel system to obtain these types of catalysts with stereogenic phosphorus incorporated. To our knowledge, there is no published study on this specific topic. Nowadays, broad array of chiral phosphines can be found on the market, so this led us to link them with suitable organoazide. In our case, we decided to use C_2-symmetric diphosphines such as enantiomers (*R,R*) or (*S,S*)-DIPAMP (catalyst **46** and **47**, respectively). The standard Staudinger reaction was done between thiourea-azide **24** and diphosphines (scheme 32). Notably, (*S,S)* enantiomer has reacted much faster. In both cases, ***new diiminophosphoranes*** **46** and **47** were isolated in a satisfactory yield.

All iminophosphoranes described in section 5.1, 5.2 and 5.3 were applied in asymmetric Aza-Henry reaction (see section 5.5) and Mannich reaction of malononitrile (see section 5.6) to *N*-Boc CF_3 ketimines (see the synthesis if imines

in section 5.4.1). The ***new iminophosphorane organocatalysts*** (cat. **35** and **36a**, section 5.1.4; cat. **46** and **47**, section 5.3) are of special importance showing high ee% value for aza-Henry product (section 5.5, table 4).

5.4 Synthesis of starting ketimines for asymmetric syntheses

5.4.1 Synthesis of *N*-Boc aryl trifluoromethyl ketimines

With the aim of introducing the CF_3 group within the quaternary stereocenter, one of the convenient approaches is the synthesis of ketimines bearing trifluoromethyl group. Up to this point, many different ketimines were described as a starting material (electrophiles) suitable for enantioselective transformations. For the synthesis of ketimines applicable in asymmetric aza-Henry reaction or Mannich reaction, two criteria were taken into consideration: 1) to contain a protective group that can potentially be coordinated by the iminophosphorane organocatalyst and 2) to remove easily protecting group of imines, without using extreme reaction conditions. Therefore, the construction of *N*-Boc trifluoromethyl ketimines was the synthesis of choices, having CF_3 group and C=O bond which could be coordinated by urea/thiourea group of iminophosphoranes.

N-Boc aryl trifluoromethyl ketimines **48-60** (scheme 33 / figure 32) were synthesized according to procedure.[37]

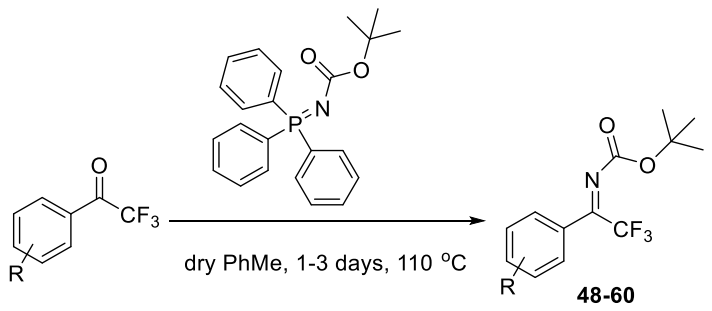

Scheme 33. General procedure for the synthesis of *N*-Boc trifluoromethyl ketimines

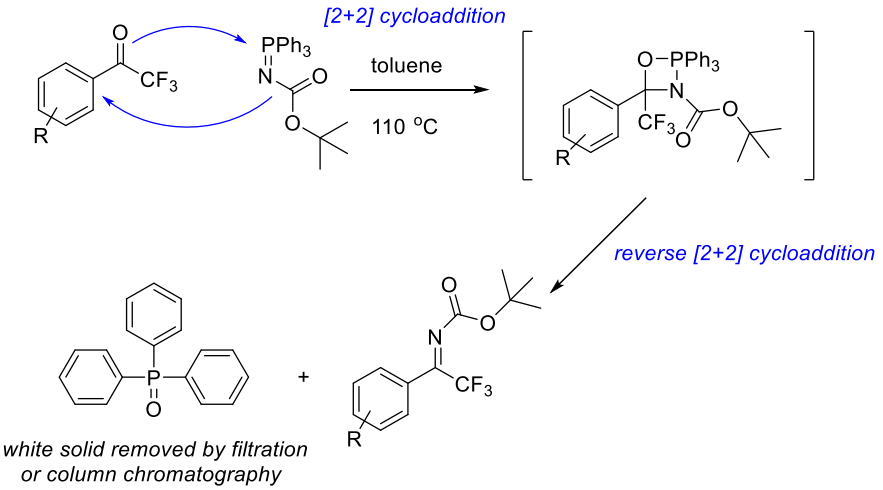

Figure 31. Proposed mechanism for the formation of *N*-Boc trifluoromethyl ketimines

The creation of *N*-Boc trifluoromethyl ketimines primarily occurs through [2+2] cycloaddition of iminophosphorane reagent (*N*-Boc-imino-(triphenyl)-phosphorane) and trifluoromethyl ketones, forming four membered heterocyclic intermediate which easily undergoes reverse [2+2] cycloaddition to afford the target ketimine and triphenylphosphine oxide as byproduct (figure 31). It is easy to separate triphenylphosphine oxide from the imine just by trituration and filtration in *n*-hexane/ethyl acetate 9:1, due to the different solubility in this eluent. The reaction time depends on the nature of ketone (having electron donating groups on phenyl ring prolongs the reaction time).

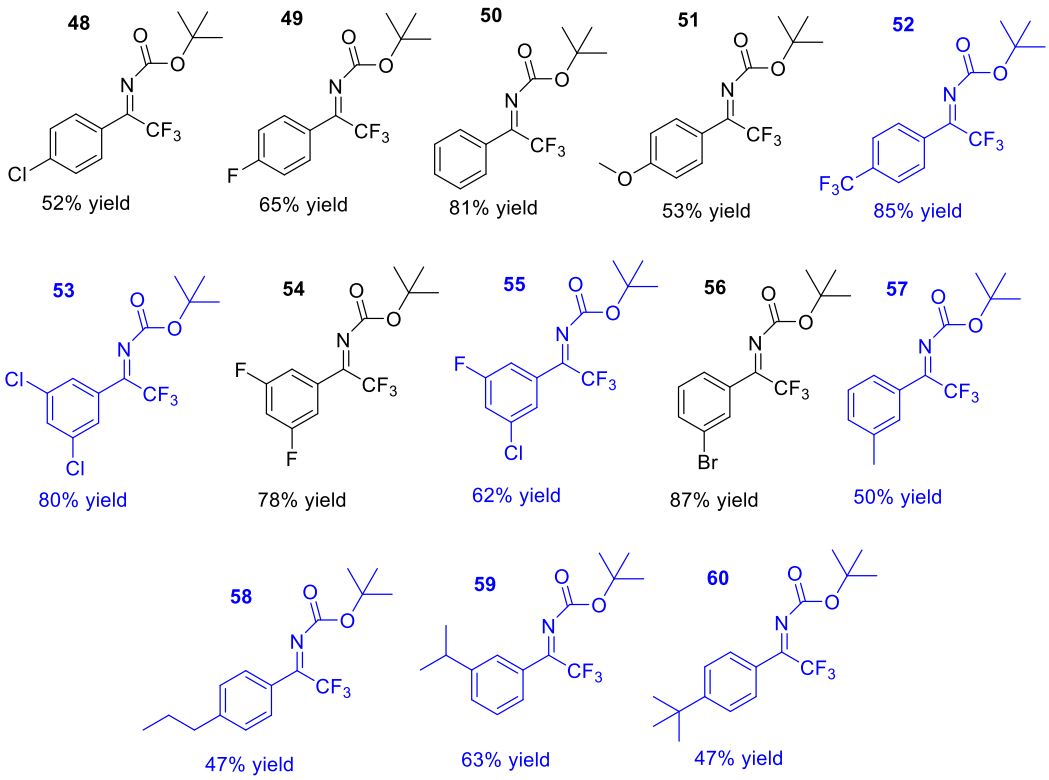

Figure 32. Small library of various *N*-Boc trifluoromethyl ketimines (*the ketimines marked in blue color are new compounds*)

The attempts to synthetize ketimines **61** and **62** under the same reaction conditions[37] were unsuccessful. Even after 4 days running the reaction at 115 °C, only traces of target ketimines were formed (figure 33).

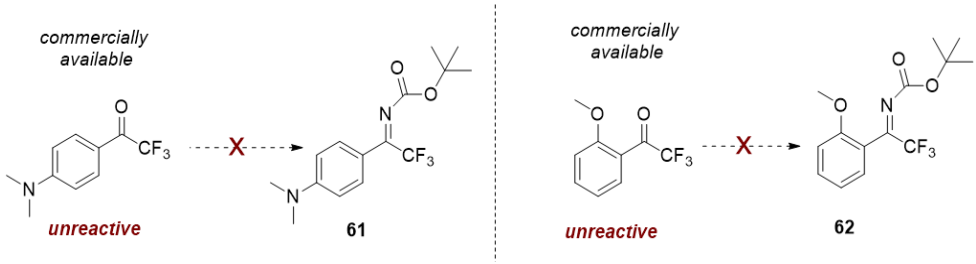

Figure 33. The attempts to synthesize ketimines **61** and **62** from 4-(dimethylamino)-2,2,2-trifluoroacetophenone and 2-OMe-2,2,2-trifluoroacetophenone

5.4.2 Synthesis of *N*-Boc alkyl trifluoromethyl ketimines

One of the ideas to expand the scope of *N*-Boc CF_3 ketimines was to introduce an alkyl group instead of aryl group. The same reaction conditions were applied.[37] Interestingly, employing alkyl trifluoromethyl ketones to synthetize *N*-Boc CF_3 ketimines led to the formation of the corresponding enamine **63**, as a more stable species (figure 34). The enamine **63** was isolated by silica gel column chromatography with eluent *n*-hexane/ethyl acetate 95:5, as a white solid in 82% yield, as a byproduct of the reaction.

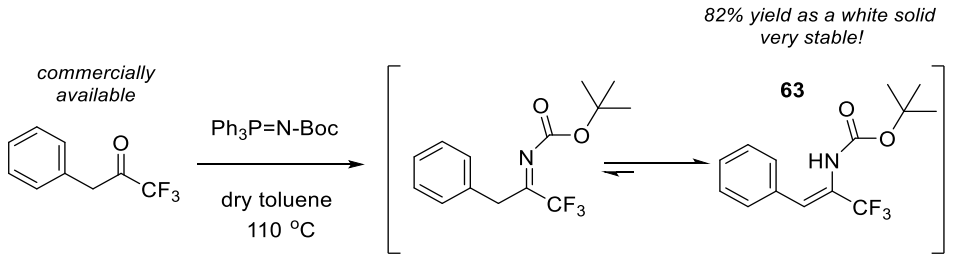

Figure 34. The attempt to synthesize alkyl CF_3 ketimine from 1,1,1-trifluoro-3-phenyl-propanone

tert-butyl-(3,3,3-trifluoro-1-phenylprop-1-en-2-yl) carbamate (**63**)[89] is known in the literature and experimental data are in accordance with this article.

Mass (ESI+) for the compound 25: m/z = calc. for $C_{14}H_{16}F_3NO_2$ = 287.28, found 310.4 [M + Na].

5.4.3 Computational studies on *N*-Boc CF_3-Ketimines

CYLview visualization and analysis software for computational chemistry was used to determine the minimum of energy of the most stable ketimine isomers, using the level of theory M062X-631G (d,p), figure 35.

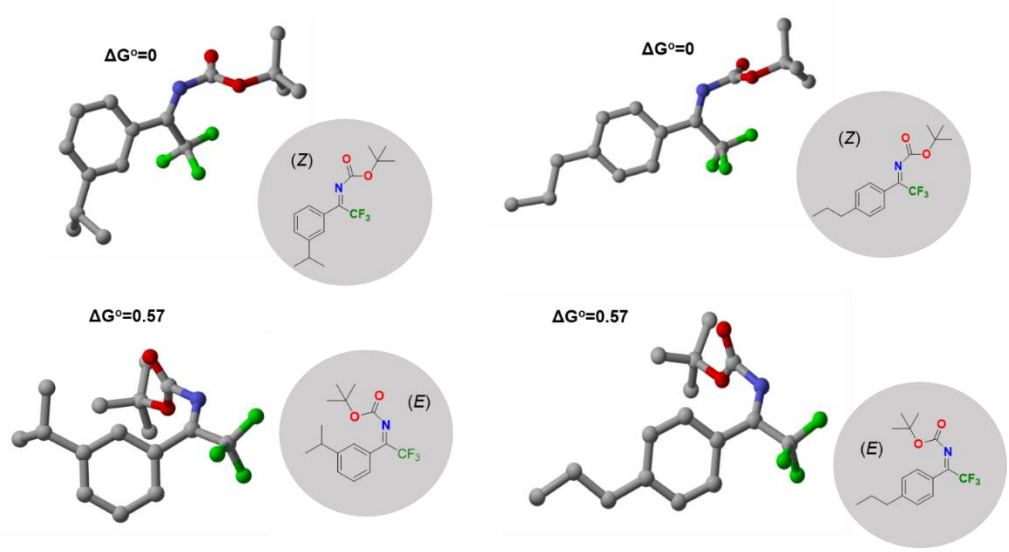

Figure 35. Computational calculations of minimum energy for the ketimines **58** and **59**

Calculations were done for the *N*-Boc CF_3-ketimines **58** and **59**. In both cases it was observed that the most stable configuration of C=N double bond was *(Z)* isomer ($\Delta G^o=0$).

According to the 3D models, (*E*)-configuration is not favorable due to the steric hindrance caused by Boc (*tert*-butoxycarbonyl) protection group.

Based on these calculations, it can be stated that other *N*-Boc CF_3-ketimines would have the same configuration.

As well, these data are in agreement with ^{1}H NMR spectra (only one major isomer was observed).

5.5 Asymmetric Aza-Henry reaction of *N*-Boc CF_3 ketimines

Enantioenriched β-nitroamines synthetized by aza-Henry or nitro-Mannich reaction are one of the most significant molecules in asymmetric synthesis. Enantioselective addition of nitromethane to aldimines or ketimines has been described by different groups.[44,46,47,48,102,103] An easy accessibility to different functional groups in a few steps makes these molecular units perfect as a building blocks or chiral auxiliaries. In particular, we were interested in asymmetric synthesis of quaternary amino derivatives containing CF_3 group. The relevance of organofluorine molecules in pharmaceutical and agrochemical industry is well recognized.[104] To our knowledge, asymmetric addition of nitromethane to acyclic *N*-Boc protected trifluoromethylated ketimines was described only using phase transfer catalyst as a source of chirality.[48] Wang et al. performed this reaction by using excess of strong inorganic base, more specifically $LiOH{\cdot}H_2O$, with the reaction time up to 7 days (scheme 16). Our goal was to find simpler and milder synthetic method applicable for industrial production. It also involves careful selection of the ketimine protecting group, which can be easily removed to give the final amines. So far, this type of transformation is not described by iminophosphoranes. In 2013, Dixon et al. demonstrated the use of BIMP in nitro-Mannich reaction of nitromethane with *N*-diphenyl-phosphinoyl ketimines[45] and that gave us the impetus to continue exploring molecules bearing CF_3 group.

Application of new bifunctional iminophosphorane organocatalysts in asymmetric aza-Henry reaction of *N*-Boc CF_3 ketimines will be described in this section.

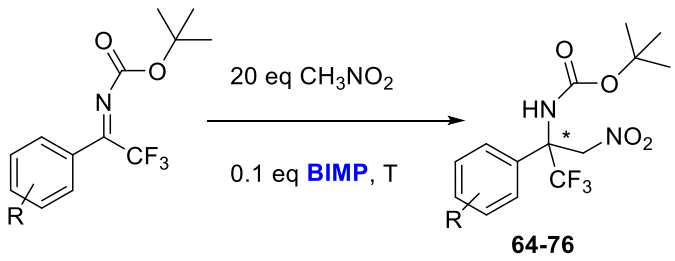

Scheme 34. General synthesis of trifluoromethylated quaternary *N*-Boc protected β-nitroamines catalyzed by **B**ifunctional **IM**ino**P**hosphorane organocatalysts

Unless otherwise indicated, it was used 0.1 equiv. of selected iminophosphorane organocatalyst, 20 equiv. of nitromethane (which serves as a pronucleophile and solvent) and 1.0 equiv. of the corresponding ketimine at specified temperature.

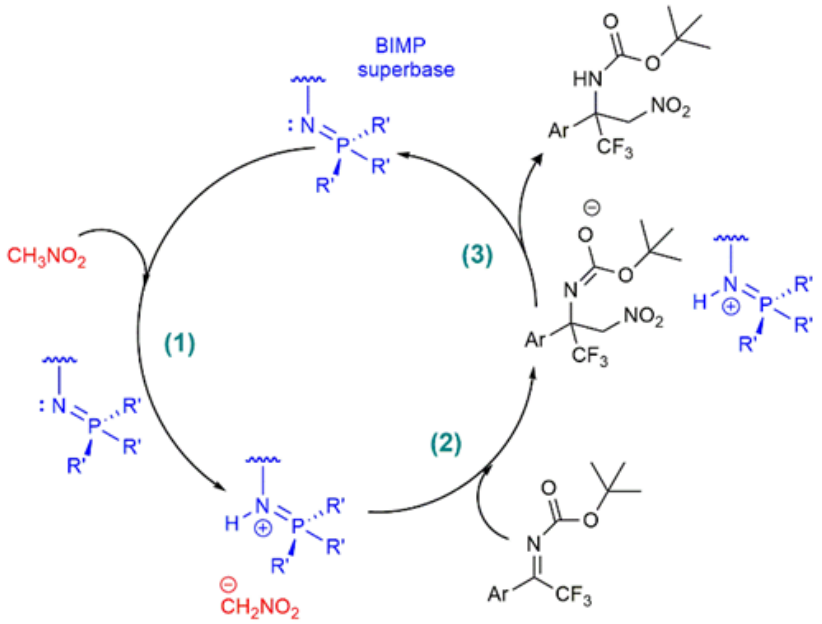

Figure 36. Proposed mechanism for enantioselective aza-Henry reaction catalyzed by **B**ifunctional **IM**ino**P**hosphorane organocatalysts

The design of this mechanism (figure 36) was inspired by Dixon's previous work.[77] In the first step the deprotonation of nitromethane occurs and simultaneously protonation of iminophosphorane organocatalyst. The second step is related to nucleophilic attack of nitromethane anion to CF_3 ketimine. In the third step comes to the protonation and recovering of the catalyst that can be further used.

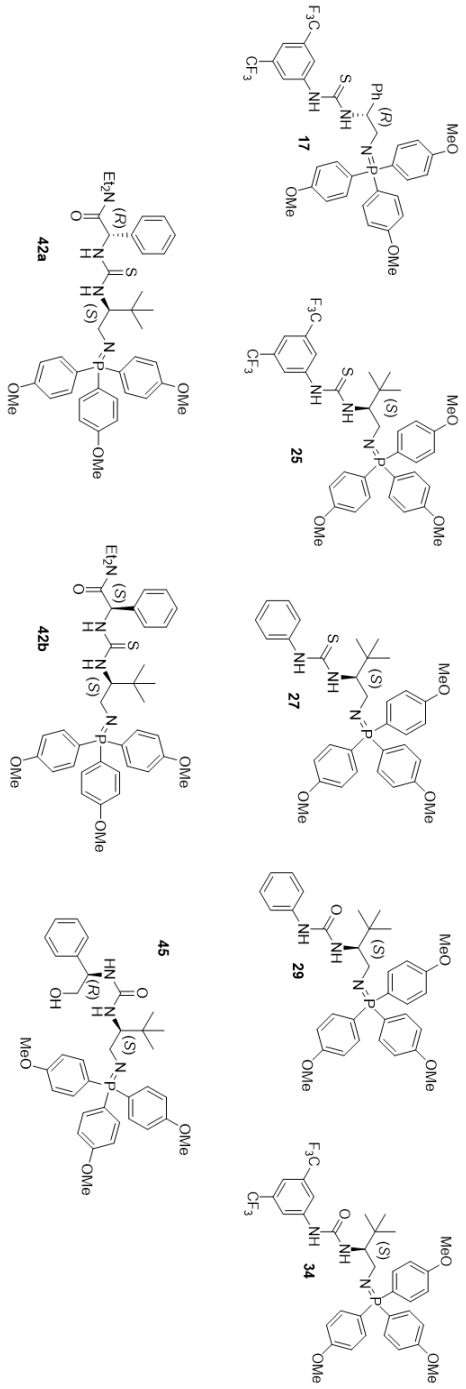

Figure 37. List of the **B**ifunctional **IM**ino**P**hosphorane organocatalysts which showed lower enantioselectivity in asymmetric aza-Henry reaction (**table 3**)

Table 3. Asymmetric aza-Henry experiments (**scheme 34**) promoted by BIMP shown in **figure 37**

Entry	Ketimine	Catalyst	Reaction time (h)	Temperature (°C)	Yield (%)	ee%
1	**50** (C_6H_5)	**25**	5	25	80	64
2	**50** (C_6H_5)	**25**	11	0	86	72
3[a]	**50** (C_6H_5)	**25**	53	-30	37	68
4	**48** (*p*-ClC_6H_4)	**25**	20	-20	69	61
5	**57** (*m*-MeC_6H_4)	**25**	24	-20	<10	70
6	**51** (*p*-$MeOC_6H_4$)	**25**	24	-20	61	71
7	**49** (*p*-FC_6H_4)	**25**	24	-20	87	71
8	**56** (*m*-BrC_6H_4)	**25**	24	-20	69	68
9	**53** (3,5-$Cl_2C_6H_4$)	**25**	24	-20	52	58
10	**57** (*m*-MeC_6H_4)	**17**	92	25	55	48
11	**51** (*p*-$MeOC_6H_4$)	**17**	92	25	31	59
12	**49** (*p*-FC_6H_4)	**17**	92	25	72	54
13	**50** (C_6H_5)	**17**	92	25	77	56
14	**48** (*p*-ClC_6H_4)	**17**	92	25	36	56
15	**50** (C_6H_5)	**42a**	21	25	75	<5
16	**50** (C_6H_5)	**42b**	21	25	75	<5
17	**50** (C_6H_5)	**34**	16	25	72	54
18	**50** (C_6H_5)	**29**	46	0	52	<5
19	**50** (C_6H_5)	**27**	23	0	30	20
20[b]	**50** (C_6H_5)	**45**[b]	24	-20	30	<5

Unless otherwise noted, all experiments were performed with 1.0 equiv. of ketimine, 0.1 equiv. of BIMP catalyst and 20 equiv. of CH_3NO_2

[a] Entry 3 - experiment done with 10 equiv. of nitromethane and toluene as the second solvent (0.2 M)

[b] Entry 20 - experiment done with 0.2 equiv. of BIMP catalyst

The first catalytic trials in enantioselective aza-Henry reaction of *N*-Boc trifluoromethyl ketimines were done with the Dixon catalyst **25** (figure 37), for which he already proved it can be successfully used in nitro-Mannich reaction of nitromethane with N-diphenyl-phosphinoyl ketimines.[45]

Trifluoromethyl β-nitroamines were obtained in good yields but lower enantioselectivity, up to 72% ee (entry 1-9, table 3). Even at lower temperatures (-20 ^{o}C or -30 ^{o}C), the enantioselectivity has not been improved. Only in one case mixture of toluene (0.2 M) and nitromethane was used as a solvent (entry 3, table 3). Unfortunately, the reaction time was too long, the yield was low without improving the enantioselectivity. In order to improve the outcome of aza-Henry reaction, a library of diverse bifunctional iminophosphorane organocatalysts were synthetized (section 5.1-5.3) and tested. In table 3 are shown aza-Henry experiments done with the catalysts which contain the same phosphine moiety (tris(4-methoxyphenyl) phosphine) with modified properties of organozides (figure 37). The BIMP catalysts with two stereogenic centers (cat. **42a**, **42b** and **45,** figure 37) and L-*tert*-leucine derived catalyst bearing urea moiety with no electron withdrawing groups on phenyl ring (cat. **29,** figure 37) showed complete absence of enantioselectivity in aza-Henry reaction (scheme 34, entry 15, 16, 18 and 20, table 3). Moving from urea (cat. **29**) to thiourea structure of the catalyst **27**, a slight progress in enantioselectivity was observed (entry 19, table 3). All catalysts containing thiourea hydrogen bond donor with CF_3 groups in 3,5-positions on the phenyl ring exhibit dominance in enantioselectivity compared to the urea based iminophosphoranes (with or without electron withdrawing groups on phenyl ring). This is giving clear evidence that the thiourea is a stronger H-bond donor, with the possibility to enhance these properties if the phenyl ring has attached electron-withdrawing groups, such as CF_3 (catalyst **17** and **25**). Due to the higher acidity of thiourea -NH protons, superior hydrogen bonding preferences to the substrate can be expected. After examining the selectivity of the catalysts having different nature of organoazide scaffold, we understood which characteristics of the organoazide moiety are crucial for the substrate coordination. The second part of BIMP study is related to the evaluation of phosphine part used in the last step synthesis. Application of electron rich phosphines such as BIDIME (cat. **35a** and **35b**, figure 38) or SPhos (cat. **36a**, figure 38) in the synthesis of iminophosphoranes showed much better results in enantioselectivity of nitro-Mannich reaction (up to 95% ee in case of the catalyst **36a**, table 4, entry 21). The bifunctional iminophosphorane organocatalysts bearing stereogenic phosphorus (cat. **46** and **47**, figure 38) showed as well quite good ee% (entry 31-34, table 4).

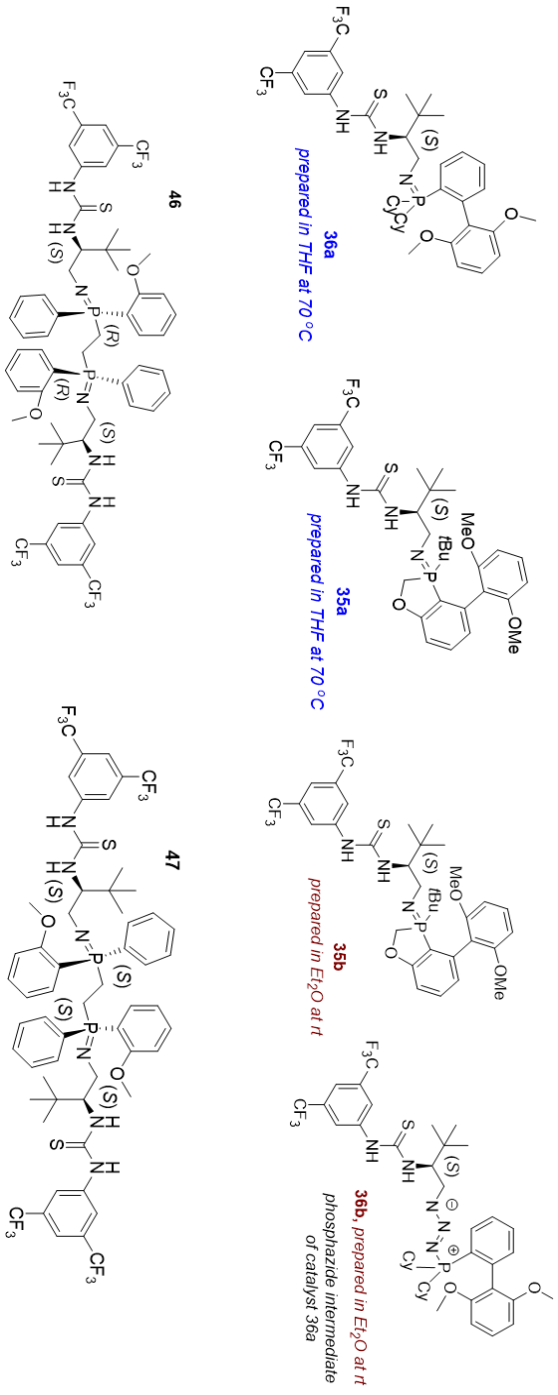

Figure 38. List of the **B**ifunctional **IM**ino**P**hosphorane organocatalysts which showed higher enantioselectivity in asymmetric aza-Henry reaction (**table 4**)

Table 4. Asymmetric aza-Henry experiments (**scheme 34**) promoted by BIMP shown in **figure 38**

Entry	Ketimine	Catalyst	Reaction time (h)	Temperature (°C)	Yield (%)	ee%
21	**50** (C_6H_5)	**36a**	26	0	82	95
22	**48** (*p*-ClC_6H_4)	**36a**	24	0	78	91
23	**52** (*p*-$CF_3C_6H_5$)	**36a**	48	0	35	86
24	**57** (*m*-MeC_6H_4)	**36a**	48	0	30	90
25[a]	**52** (*p*-$CF_3C_6H_5$)	**36b**	48	0	<60	67
26[a]	**48** (*p*-ClC_6H_4)	**36b**	48	0	60	74
27	**56** (*m*-BrC_6H_4)	**36a**	48	0	<50	88
28	**49** (*p*-FC_6H_4)	**36a**	48	0	<85	82
29	**50** (C_6H_5)	**35a**	24	0	<30	88
30	**50** (C_6H_5)	**35b**	24	0	<95	92
31	**50** (C_6H_5)	**47**	11	0	42	88
32	**56** (*m*-BrC_6H_4)	**47**	26	0	53	86
33	**49** (*p*-FC_6H_4)	**47**	26	0	50	87
34	**50** (C_6H_5)	**46**	26	0	51	84
35	**50** (C_6H_5)	**46**	11	0	58	73

All experiments in table 4 were performed with 1.0 equiv. of ketimine, 0.1 equiv. of BIMP catalyst and 20 equiv. of CH_3NO_2

[a] Entry 25 and 26 – in these trials phosphazide intermediate was used to promote the aza-Henry reaction

After the catalysts screening, our next goal was to extend the scope of the asymmetric aza-Henry reaction with the most effective iminophosphorane organocatalyst **36a**. To our surprise, most of the *N*-Boc CF_3 ketimines demonstrated excellent enantioselectivity under mild reaction conditions (0 °C, 10 mol% of the catalyst **36a** and 20 equiv. of nitromethane). However, it is known that electron donating groups on aromatic ring increase the electron density in the molecule of ketimines, which makes them more prone to be coordinated by acidic protons of thiourea group (higher values of ee% were recorded, figure 39).

The imines possessing electron-withdrawing groups on aromatic ring expressed destabilization effect and therefore lower enantioselectivity (compounds **68**, **69** and **70**, figure 39). Absolute configuration of the compounds **66** (α_D^{25} = -15.9 (C=0.052 g/mL, $CHCl_3$)) and **72** (α_D^{25} = -7.7 (C=0.038 g/mL, $CHCl_3$)) in figure 39, was determined by polarimeter, in a glass polarimeter cell with a length of 1 dm (S enantiomer). Based on these values, the other β-nitroamines shown in figure 39 are considered to have the same absolute configuration.

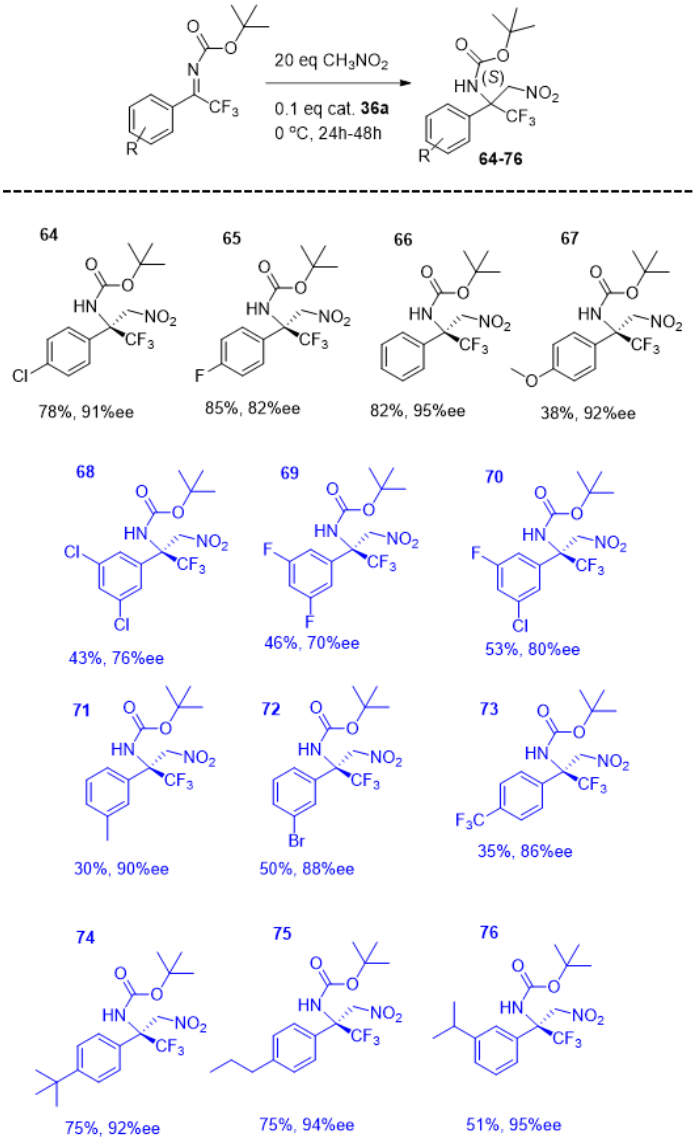

Figure 39. The scope of the asymmetric aza-Henry reaction performed with catalyst **36a** (*blue color-new compounds*)

In conclusion, this study aims to clarify interaction between the catalysts and substrate as well as to identify the factors which control enantioselectivity.

The iminophosphorane organocatalyst derived from L-*tert*-leucine, bearing thiourea moiety with electron-withdrawing groups (CF_3) on phenyl ring and electron rich, steric hindered phosphine (**36a**) proved to be a privileged catalyst for the asymmetric aza-Henry reaction of *N*-Boc CF_3 ketimines. Based on performed experiments and available information, the outcome of this reaction can be explained by simultaneous activation of both the nucleophile and the electrophile. Iminophosphorane organocatalysts most likely activate electrophile (imine) and nucleophile (nitromethane) by keeping nitromethane close to the reactive center of the catalyst pocket, as well close to the imine to ensure facile nucleophilic attack. Strong and specific coordination of the catalyst **36a** to the substrates yielded new β-nitroamines (**68-76**, figure 39) in excellent enantioselectivity.

The control experiment of aza-Henry reaction carried out without the iminophosphorane organocatalyst (CF_3 ketimines dissolved in 20 equiv. of nitromethane) did not yield the target CF_3 β-nitroamines. This is additional proof of the essentiality of BIMP catalysts in the synthesis of quaternary amino derivatives.

Scaling up of nitro-Mannich reaction described in this section with the catalyst **36a** (up to 1g) at 0 ^oC, afforded the product **66** in 65% yield and 92% ee. Increasing the scale of the reaction did not diminish the outcome of the reaction. An attempt to recover the catalyst **36a** by column chromatography on silica gel, unfortunately did not gave any results. The decomposition of the catalyst occurred on silica gel, which gives us clear evidence about iminophosphoranes instability in the presence of acidic materials.

Reduction of Aza-Henry product

β-diamines are important subunits of building blocks in organic chemistry.[105.106,107] This class of compounds shown broad utility in various fields of organic chemistry (pharmaceutical compounds, natural products, ligands in stereoselective organic synthesis). [105.106,107]

Therefore, we demonstrated conversion of trifluoromethyl β-nitroamine to trifluoromethyl *β*-diamine following the known procedure.[48] The product **78** (scheme 35) was isolated in 80% yield using mild reduction agent, sodium borohydride.

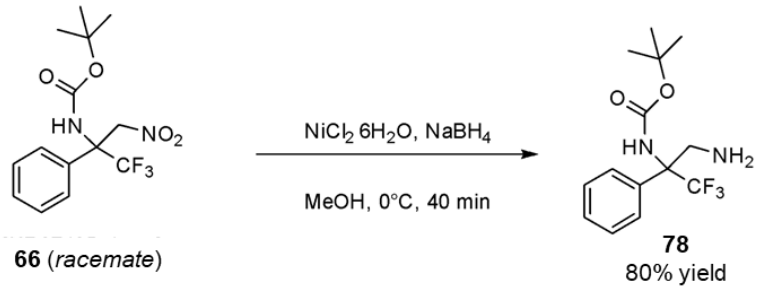

66 (*racemate*)

78
80% yield

Scheme 35. General synthesis of trifluoromethylated quaternary diamine

5.6 Asymmetric Mannich reaction of malononitrile and oxidative decyanation

Another asymmetric reaction explored with bifunctional iminophosphorane organocatalysts is nitro-Mannich reaction of malononitrile to *N*-Boc aryl trifluoromethyl ketimines followed by oxidative decyanation, which is particularly interesting as a source of CF_3 quaternary amino acids. One of the straightforward methods for the synthesis of quaternary amino acids is Strecker synthesis. Usually, generation of quaternary stereocenter is quite challenging and it requires long reaction times (days). The catalytic asymmetric Mannich-type reaction of malononitrile with *N*-Boc α-ketiminoesters for the synthesis of α,α-disubstituted α-amino esters was described by Kuwano.[108] Our strategy relies on use of malononitrile as pronucleophile which can be easily deprotonated by strong base iminophosphorane. So far, nucleophilic addition of malononitrile to *N*-Boc protected trifluoromethyl ketimines to get quaternary trifluoromethyl amino acid derivatives has not been described. In this specific case, addition of malononitrile

to *N*-Boc ketimines has been successfully promoted by iminophosphoranes, significantly reducing the reaction time. The intermediate **79** was isolated as white solid in very good yield (table 5). Using higher excess of malononitrile shortens the effective reaction time (table 5, entry 3). However, formation of dicyanomethyl compound **79** is feasible even with 2.0 equiv. of malononitrile. With the aim of obtaining an amino acid derivative in the form of an ester (compound **81**, scheme 36), oxidative decyanation with magnesium monoperoxyphthalate hexahydrate as oxidant was carried out. Proposed oxidative decyanation starts with deprotonation of intermediate **79** by lithium carbonate forming nitrile carbanion (scheme 37).[109] Peroxyanion is easily generated between nitrile carbanion and oxidative reagent (magnesium monoperoxyphthalate hexahydrate), which further undergoes cyclization and generate 4-membered peroxide. By decomposition of peroxide 1.0 equiv. of cyanate is liberated. In the last step, methanol enables formation of final compound, amino ester **81** (scheme 36).

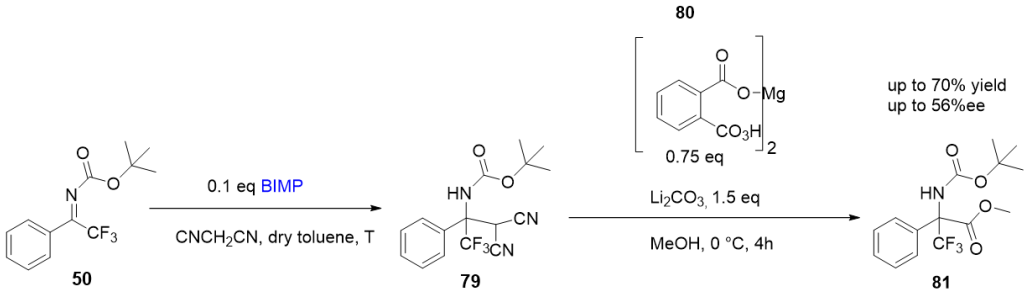

Scheme 36. Synthesis of trifluoromethylated amino ester promoted by selected iminophosphoranes

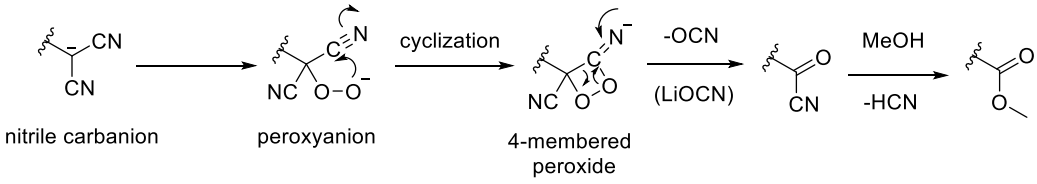

Scheme 37. Plausible mechanism of oxidative decyanation[109]

Based on the bifunctional iminophosphorane (BIMP) catalyst performance, some of them were selected (cat. **35b** and **36a**, section 5.1.4; cat. **25**, section 5.1.2) and used in asymmetric Mannich reaction of malononitrile (table 5). Changing of iminophosphorane organocatalysts nature did not improve drastically the enantioselectivity of the final product **81** (table 5).

Table 5. Catalyst screening in asymmetric Mannich reaction promoted by BIMP followed by oxidative decyanation (**scheme 36**)

Entry	Ketimine	Catalyst	Reaction time, 1st step (h)	Temperature, 1st step (°C)	$CNCH_2CN$ (eq)	Yield, 1st step (%)	Yield, 2nd step (%)	ee%, 2nd step
1	**50** (C_6H_5)	**36a**	15	0	2	72	60	50
2	**50** (C_6H_5)	**35b**	15	0	2	76	65	56
3	**50** (C_6H_5)	**25**	7	-20	10	77	70	54

Considering that the change of phosphine part of iminophosphoranes did not have any influence in enantioselectivity of Mannich reaction, this clarifies the role of thiourea organoazide moiety in substrates coordination. Finally, using bifunctional iminophosphoranes in similar asymmetric reactions can manifest different outcome of the reaction. Even changing one parameter, such as catalyst structure change, imine modification and nucleophile/solvent variation can remarkably diminish enantioselectivity of the target compound. By comparing asymmetric aza-Henry reaction (section 5.5) with asymmetric Mannich reaction of malononitrile of *N*-Boc CF_3 ketimines (section 5.6) using the same catalyst **36a**, much lower enantioselectivity was observed when malononitrile was used as a nucleophile.

In these two cases, this is a clear indication of different nucleophile activation by iminophosphorane organocatalyst **36a**.

Conclusion – BIMP catalysts and their application

Chapter 5 of this dissertation reveals the most important results achieved in the synthesis of bifunctional iminophosphorane organocatalysts and their use in asymmetric synthesis of amino derivatives. This study helped us to better understand the properties of new iminophosphoranes and their role in the synthesis of quaternary amino derivatives.

Herein, we briefly describe the key results:

-Synthesis of **new** iminophosphorane organocatalysts derived from L-*tert*-leucine organoazide scaffold and **diphosphines bearing stereogenic phosphorus** (catalyst **46** and **47**), as well the catalysts synthetized from more electron-rich phosphines (**SPhos**, catalyst **36a**) or (**BIDIME**, catalyst **35b**) has been achieved.

-Synthesis of **new** diastereomeric iminophosphoranes derived from L-*tert*-leucine and *R* or *S*-phenylglycine possessing **aliphatic amide group** (catalyst **42a** and **42b**) and BIMP catalyst having additional **-OH hydrogen bond donor group** with two stereocenters (catalyst **45**) has been accomplished.

-All BIMP catalysts reported in the sections 5.1-5.3 have been successfully used in predominantly in asymmetric aza-Henry reaction (and some of them in asymmetric Mannich reaction of malononitrile), which gave us valuable information about catalyst mode of action and coordination.

-Several **new** CF_3 *N*-Boc ketimines (with electron-withdrawing and electron-donating groups on aromatic ring) have been synthetized, as a precious precursor for the synthesis of quaternary CF_3 amino derivatives / amino acids.

-BIMP catalysts **35b**, **36a**, **46** and **47**, isolated for the first time, showed great performances in asymmetric nitro-Mannich reaction, giving remarkable yields and enantioselectivities of aza-Henry products.

-The scope of the asymmetric aza-Henry reaction (section 5.5) has been extended with the best BIMP catalyst **36a**, affording **new quaternary amino derivatives** in very good yields and excellent ee%.

-Some of the new BIMP catalysts have been applied in asymmetric Mannich reaction of malononitrile to *N*-Boc aryl trifluoromethyl ketimines followed by oxidative decyanation, to get quaternary amino acid **81** in good yields and moderate ee%.

Noteworthy results were obtained with chiral iminophosphorane organocatalysts in the synthesis of enantioenriched amino derivatives, providing a new perspective in the development of future asymmetric syntheses.

5.7 DFT calculations: Nitro-Mannich reaction of nitromethane with *N*-diphenyl-phosphinoyl ketimine

So far, many asymmetric reactions promoted by very complex bifunctional thiourea based organocatalysts are published. This involves various interactions between the organocatalysts and the substrates, which is usually not easy to predict. Therefore, nowadays computational studies are inevitable tool to clarify non-covalent interactions in enantioselective organocatalysis. The identification of reaction's transition states has several important advantages, such as easier comprehension of the reaction mechanism, confirmation of obtained experimental results or prediction of possible catalysts applications.

Herein, as a starting point in computational studies, developing a computational model for enantioselective addition of nitromethane to acetophenone-derived *N*-diphenyphosphinoyl (DPP) ketimines published by Dixon and co-workers[45] in 2013 (scheme 38), will be explained. The aim of density functional theory (DFT) is to understand which is the iminophosphorane catalyst (scheme 25, catalyst **25**, section 5.1.2) mode of operation in nitro-Mannich reaction.

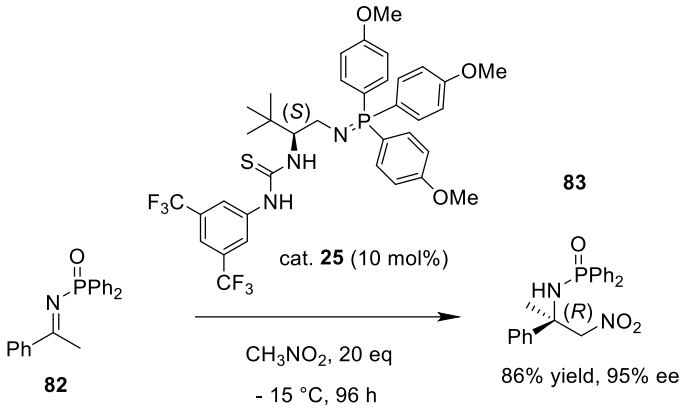

Scheme 38. Nitro-Mannich addition to *N*-DPP ketimines promoted by catalyst **25**

5.7.1 Density Functional Theory (DFT) optimization

The optimizations were performed all in vacuum with level of theory M062X and with basis set 6-31G (d,p). The choice of this function was dictated by the fact that is the top performer in the study of non-covalent interactions, which are the interactions principally involved in BIMPs' catalysis. Two interesting results emerged from this DFT-optimization. Primarily, the energy of the complex between the catalyst **25** and the imine **82** was lower (figure 40, left) than the energy of the complex between catalyst **25** and the pronucleophile nitromethane (figure 40, right). This is important evidence that the coordination of the acetophenone derived *N*-DPP-ketimine to the iminophosphorane is favored.

Level of theory **M062X/6-31G (d,p)**, *in vacuum*

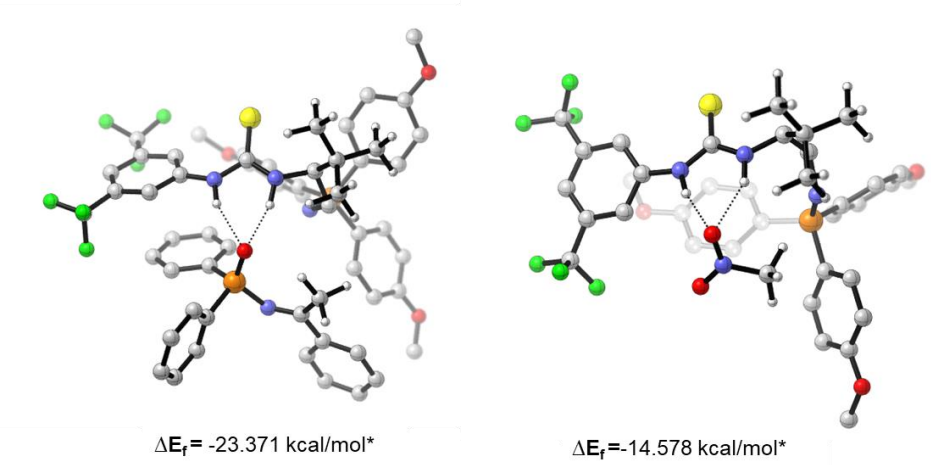

Figure 40. Optimized BIMP **25**-imine **82** complex (left) and BIMP **25**-nitromethane complex (right) *Compared to the free species

Secondly, the DFT optimization of the complexes between catalyst **25** and both the (*R*) and (*S*) enantiomers of product **83** highlighted how these complexes' energies are identical (table 6). If there is no energy difference in the two optimized complexes, it means that the reaction of choice is not under *thermodynamic control*, thus the two possible enantiomeric products have the same stability. Therefore, this is confirmation that the cause of the enantiomeric excess observed in product **83** must be found in the *kinetic control* exerted by the iminophosphorane catalyst **25**.

Table 6. Energy difference of complexes between BIMP **25** and products **(*R*)**- and **(*S*)-83**

*Compared to the free species

Complex with cat. 25	Product 83	ΔE_f /(kcal/mol)*
1	(*R*)	-32.845
2	(*S*)	-32.845

5.7.2 Transition states search and optimization

The final aim of the computational studies was the identification of the transition states involved in the asymmetric aza-Henry reaction described by Dixon. Transition states were obtained starting from already optimized structures of the imine **82**, the nitromethane and the catalyst **25**. In a first moment, DFT optimizations were completed considering three different dual activation modes approaches to find the optimal TSs: the Takemoto-like[110], the Papai-like[110] and the Benaglia-Rossi-like approach (figure 41). In all of them it was supposed a coordination of the imine **82** with the P=O moiety, and of the nitromethane molecule with the two oxygens atoms. However, these approaches completely failed to assemble the correct transition states.

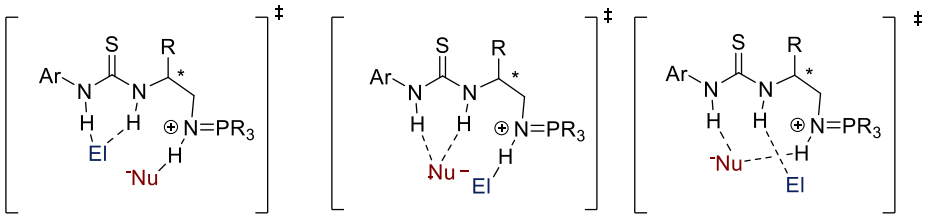

Figure 41. Possible dual activation modes of bifunctional iminophosphorane organocatalysts

So, it was decided to change the hypothetical coordination of the reaction substrates. In particular, it was considered a Takemoto-like approach were the imine **82** was kept coordinated to the thiourea's hydrogens with its P=O moiety, while the nitromethane coordination was completely inverted considering a non-bonding interaction between the deprotonated CH_2^- moiety of CH_3NO_2 and the protonated nitrogen atom of the iminophosphorane functional group.

The new substrate's coordination mode enabled to run new DFT optimizations *in vacuum* at M062X/3-21G level of theory, finally achieving the two different transition states leading to the opposite product's enantiomers, the (*R*-major) and the (*S*-minor). The transition state energies found are reported in table 7.

Table 7. Transition state energies at M062X/3-21G level of theory, *in vacuum*

Transition state	E_{rel} **/(kcal/mol)**
TS-R_{major}	0
TS-S_{minor}	+9.70

It can be seen how the favored TS is the one leading to the *R*-product, confirming what was experimentally observed by Dixon.[45] However, the energy barrier between the two transition states is way too high to be a plausible one. Because of this, the level of theory of the DFT optimizations was increased to M062X/6-31G (d,p) and the transition state energies obtained are reported in table 8.

Table 8. Transition state energies at M062X/6-31G (d,p) level level of theory, *in vacuum*

Transition state	E_{rel} **/(kcal/mol)**	***ee (%)***
TS-R_{major}	0	**> 99%**
TS-S_{minor}	+3.35	

Improving the level of theory to M062X/6-31G (d,p) has led to significantly more reliable results. In this case, it is noticed how the favored enantiomer is still the (*R*)-product observed by Dixon, but the TSs energy difference is reduced to 3.35 kcal/mol. This energy barrier should determine > 99% enantiomeric excess in the studied reaction, still higher with respect to the 95% ee achieved by Dixon's group. Nevertheless, it is important to emphasize that all the optimizations were

done *in vacuum*, while the experimental reaction was performed in neat nitromethane.

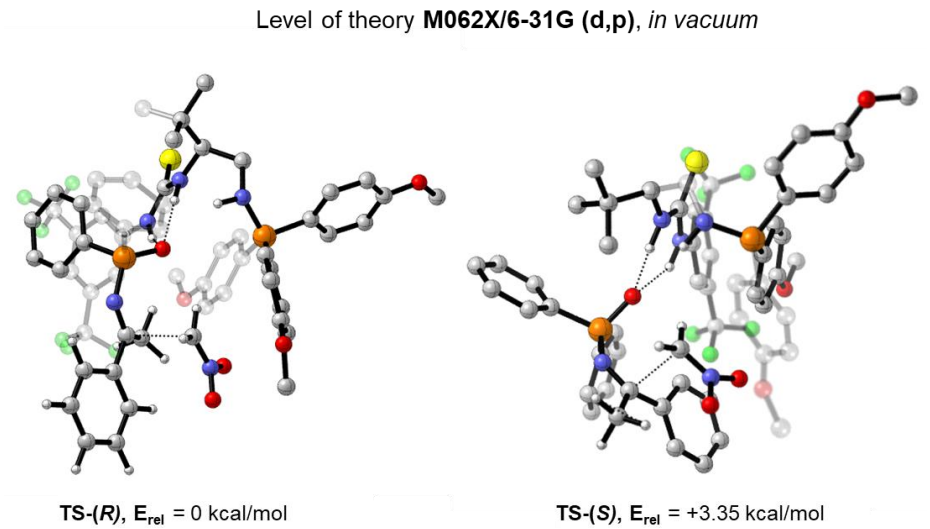

Figure 42. Asymmetric aza-Henry reaction transition states using higher level of theory

Observing the achieved transition states (figure 42), some hypotheses could be done on the reaction mechanism. Probably, the first species that is formed, is the complex between the catalyst **25** and the *N*-diphenyphosphinoyl (DPP) ketimine **82**, which underlined the lower energy of this complex with respect to the one between the BIMP and nitromethane.

The CH_3NO_2 molecule arrives at the reaction site only in a second moment, pointing it's CH_3 group towards the superbasic N=P functionality of the catalyst. Upon the deprotonation, the nitromethane immediately attacks the exposed imine face while leaving the catalyst's chiral pocket, affording the desired product **83**. Considering the enantiomeric excess, this can be justified analyzing the different geometries of the two TSs. In the Pro-R transition state, the imine directs its methyl group toward the catalyst while the phenyl ring is away from it. On the contrary, in the Pro-*S* transition state the situation is the opposite, with the phenyl ring which is directed to the already steric hindered part of the catalyst.

Moreover, in the Pro-*R* transition state is also present π-stacking interaction between one phenyl ring of imine's phosphorus atom and the CF_3-substituted phenyl ring of the catalyst. This interaction is completely absent in the Pro-*S* transition state, and thus further destabilizes it.

5.7.3 Possible activation modes in aza-Henry reaction of *N*-Boc CF_3 ketimines promoted by iminophosphorane oranocatalysts

Based on literature search, asymmetric aza-Henry reaction of *N*-Boc CF_3 ketimines (section 5.4.1, figure 32) catalyzed by iminophosphorane type organocatalysts has not been described yet. Before we started detailed research on *N*-Boc CF_3 ketimines, we used Dixon catalyst **25** (section 5.1.2, scheme 25) as a model iminophosphorane catalyst to promote asymmetric addition of nitromethane to CF_3 ketimines. As it is already reported in section 5.5 (table 3, entry 1-9), the catalyst **25** may provide up to 70% ee of aza-Henry product in case of *N*-Boc CF_3 ketimines. Apparently, lower enantioselectivities were observed compared to *N*-diphenyphosphinoyl (DPP) ketimines used in Dixon's experiments (section 5.7.2, scheme 38).

This can be explained by the different ketimine nature. *N*-Boc CF_3 ketimines are less basic in comparison with *N*-diphenyphosphinoyl ketimines due to the presence of electron-withdrawing CF_3 group within the imine, thus more coordination patterns are possible. In case of *N*-diphenyphosphinoyl ketimines, P=O moiety is strongly bonded by thiourea H-bonds of the catalyst **25**, indicating that this complex is stronger than the one with nitromethane (section 5.7.1). *N*-Boc CF_3 ketimines showed peculiar behavior, expressing difficulties to locate a transition structure leading to the products, due to the flat potential energy surface.

By modifying the structures of the BIMP catalyst we found out that iminophosphorane organocatalyst derived from L-*tert*-leucine, bearing thiourea moiety with electron-withdrawing groups (CF_3) on phenyl ring and electron rich, steric hindered phosphine (catalyst **36a,** table 4**,** entry 21) proved to be a privileged catalyst for the asymmetric aza-Henry reaction of *N*-Boc CF_3 ketimines. Based on performed experiments and available information, the outcome of this reaction can be explained by simultaneous activation of both the nucleophile and the electrophile. Iminophosphorane organocatalysts most likely activate electrophile (imine) and nucleophile (nitromethane) by keeping nitromethane close to the reactive center of the catalyst pocket, as well close to the imine to ensure facile nucleophilic attack. Strong and specific coordination of the catalyst **36a** to the substrates yielded new β-nitroamines (**68-76**, figure 39) in excellent enantioselectivity.

Chapter 6. Experimental part

6.1 General methods

Dry solvents were purchased and stored under nitrogen over molecular sieves (bottles with crown caps). Reactions were monitored by analytical thin-layer chromatography (TLC) using silica gel glass plates (0.25 mm thickness) and visualized using UV light. Flash chromatography was carried out on silica gel (230-400 mesh). Proton NMR spectra were recorded on spectrometers operating at 300 MHz (Bruker Avance 300). Proton chemical shifts are reported in ppm (δ) with the solvent reference relative to tetramethylsilane (TMS) employed as the internal standard ($CDCl_3$ δ = 7.26 ppm). ^{13}C NMR spectra were recorded on 300 MHz spectrometers (Bruker Avance 300) operating at 75 MHz, with complete proton decoupling. Carbon chemical shifts are reported in ppm (δ) relative to TMS with the respective solvent resonance as the internal standard ($CDCl_3$, δ = 77.0 ppm).

^{19}F NMR spectra were recorded on 300 MHz spectrometers (Bruker Avance 300) operating at 282.1 MHz; fluorine chemical shifts are reported in ppm (δ) relative to $CFCl_3$ with the respective solvent resonance as the internal standard ($CFCl_3$: δ = 77.0 ppm). ^{31}P NMR spectra were recorded on a 300 MHz spectrometer (Bruker Avance 300) operating at 121.2 MHz, with complete proton decoupling. Phosphorous chemical shifts are reported in ppm (δ) relative to H_3PO_4 as internal standard. ^{1}H NMR, ^{31}P NMR and ^{19}F NMR of iminophosphorane organocatalysts were recorded in $CDCl_3$, toluene_d_8 or acetone_d_6 as solvents at room temperature and 50 ^{o}C. The following abbreviations are used to indicate the multiplicity in NMR spectra: s - singlet; d - doublet; t - triplet; q - quartet; pq – pseudo quartet; dd - double doublet; tt – triplet of triplets, sext – sextuplet; sept – septuplet; bs - broad signal; m - multiplet. Enantiomeric excess determinations were performed under the conditions reported below with Agilent 1100 series HPLC. The corresponding chiral stationary phase is indicated in the experimental part.

High-resolution mass spectrometry analysis was performed on a Q-TOF Synapt G2-Si instrument available at the MS facility of the Unitech COSPECT at the University of Milan.

Preparative HPLC-MS was conducted on a Agilent 1260 Infinity Series (Autosampler, Fraction Collector, DAD, Pumps, Check valves, all while coupled to a Agilent 6120 LC-MS Quadrupole mass-spectrometer.

Gas chromatography-mass spectrometry (GC-MS) was performed on GC Agilent 6890N, inlet: EPC split-splitless; column: Agilent 19091S-433 HP-5MS 5% phenyl methyl siloxane; MS: quadrupole G2589A EI; Autosampler: Agilent 7683; gas carrier: helium.

CYLview visualization and analysis software for computational chemistry was used to determine the minimum of energy of CF_3 ketimines, using the level of theory M062X-631G(d,p).

For the reagents pumping in continuous flow, it was used Vapourtec's E-Series systems with two reactor positions, up to three pumps, using the revolutionary V-3 pump, in Taros Chemicals, Dortmund. At the University of Milan for this purpose it was used syringe pump by Chemyx, the Fusion 200 dual syringe infusion and withdrawal pump.

(11b*S*) - 4,4-Dibutyl-2,6-bis (3,4,5-trifluorophenyl) - 4,5-dihydro-3H-dinaphtho [2,1-c:1',2'-e] azepinium bromide or Maruoka catalyst (**4**) was purchased from Strem Chemicals and was used without further purification.

Compounds marked with an asterisk (*) refer to new compounds.

6.2 Phase transfer catalysis in flow

6.2.1 Synthesis of starting imine for phase transfer catalysis in flow

Compound **1** was synthesized according to a literature procedure[94], and its spectroscopic data are in agreement to this report.[94]

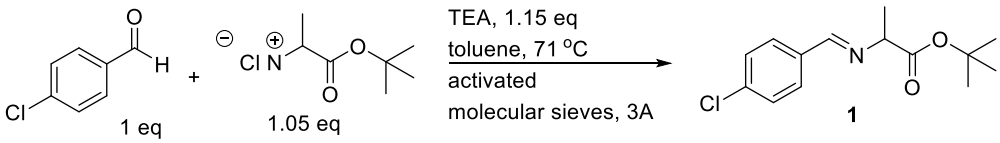

Scheme 38. General procedure for the synthesis of L-alanine imine **1**[94]

6.2.2 Synthesis of cinchona alkaloids (phase transfer catalysis in flow)

Phase-transfer cinchona catalysts (quaternary ammonium salts, **5-10**) were synthetized according to the following procedure, starting from cinchonidine.[90]

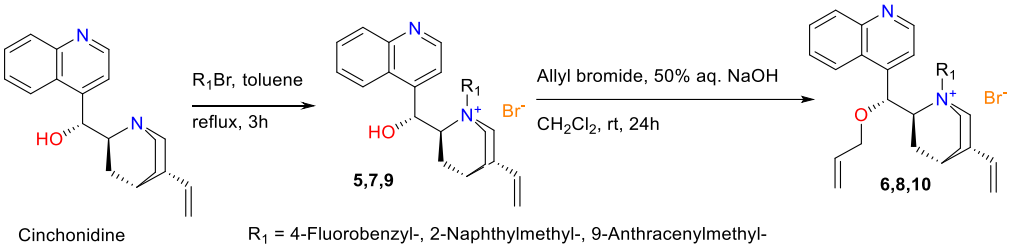

Scheme 39. General procedure for the synthesis of cinchonidine derived phase transfer catalysts[90]

N-(4-Fluorobenzyl)cinchonidinium bromide (**5**)[92,93]:

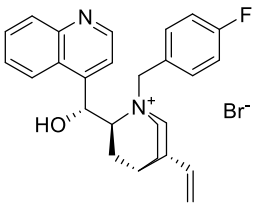

The synthesis was performed according to the procedure (first step)[90]. The product was isolated as light rose solid, 90% yield.

Mass (LC-MS): m/z = calc. for $C_{26}H_{28}FN_2O^+$ = 403.52, found 404.4 [M + H].

O-Allyl-*N*-(4-Fluorobenzyl)cinchonidinium bromide (**6***):

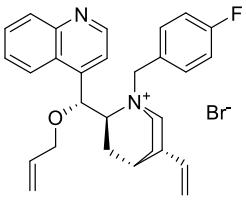

The synthesis was performed according to the procedure (second step)[90]. The product was isolated as brown solid, 94% yield.

Mass (LC-MS): m/z = calc. for $C_{29}H_{32}FN_2O^+$ = 443.59, found 444 [M + H].

N-(2-Naphthylmethyl)cinchonidinium bromide (**7**):

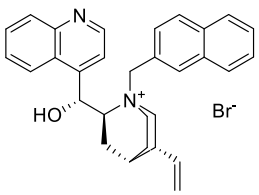

The synthesis was performed according to the procedure (first step)[90]. The product was isolated as white solid, 94% yield.

Spectral data are in agreement with the protocol.[91]

O-Allyl-*N*-(2-Naphthylmethyl)cinchonidinium bromide (**8**):

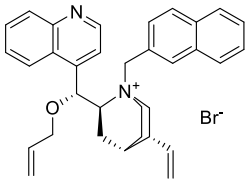

The synthesis was performed according to the procedure (second step)[90]. The product was isolated as brown solid, 89% yield.

Spectral data are in agreement with the protocol.[91]

N-(9-Anthracenylmethyl)cinchonidinium bromide (**9**):

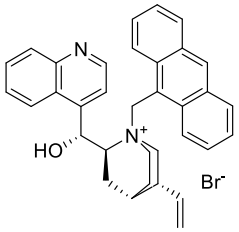

The synthesis was performed according to the procedure (first step)[90]. The product was isolated as light-yellow solid, 89% yield.

Spectral data are in agreement with the protocol.[90]

O-Allyl-*N*-(9-Anthracenylmethyl)cinchonidinium bromide (**10**):

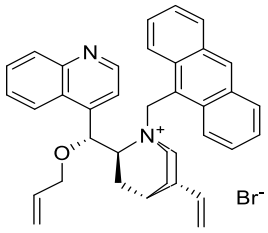

The synthesis was performed according to the procedure (first step)[90]. The product was isolated as light brown solid, 57% yield.

Spectral data are in agreement with the protocol.[90]

6.2.3 *Liquid-liquid* phase transfer benzylation in flow

Experimental procedure for entry 6, table 1, section 3.3.1: 0.18 mmol (1.0 equiv., 50 mg) of the starting imine **1**, 0.25 mmol (1.4 equiv., 44.5 mg, 0.03 mL) of benzyl bromide and 1.35 mg (1 mol%) of the Maruoka catalyst **4** (figure 15, section 3.1) were dissolved in 7.5 mL of toluene/dichloromethane 14:1 and placed in a 10 mL SGA gas tight syringe. 50% aq. sol. of KOH (15 mL) was placed in another SGA gas tight syringe (25 mL). Both syringes are connected to the different syringe pumps. The flowrate of the 50% aq. sol. of KOH was 0.05 mL/min and the flow rate of the organic phase was 0.025 mL/min.

Three CSTR units were used in line. The residence time was calculated for 3 CSTR units + tubing between them and between the third CSTR and membrane separator. Calculated residence time is 80 min. Zaiput membrane separator was connected to the last CSTR unit. The organic and water phase were directly separated inside the membrane separator using PTFE hydrophobic membrane (pore size 0.5 µm).

The volume of 3 CSTR units is 5.4 mL. The volume of the tube which connects 3 CSTRs is 2x0.2 mL (7.5 cm length, od=1.58 mm, r=0.58 mm). The volume of the tube at the output is 0.2 mL (the same length like between two CSTR units).

After separation of water/organic phases inside membrane separator, organic phase was collected, solvent was removed under reduced pressure and conversion to the benzylated product **2** was analyzed by ^{1}H NMR in $CDCl_3$ (figure 40), showing ~35-41% conversion to the product **2** (figure 42).

Collected volumes (average value showing ~40% conversion to the product **2**) were dissolved in 2 mL of THF and 4 mL of 0.5 M aq. sol. of citric acid was added to the solution. The reaction mixture was stirred at room temperature 8h. After 8h, the reaction was stopped and THF was removed under reduced pressure. The water phase was washed with cyclohexane (2x10 mL). Phases were separated in separatory funnel and water phase was basified using solid K_2CO_3 until pH=10. Basified water layer was extracted with Et_2O (3x15 mL). Organic phases were combined, washed with brine (30 mL), dried over Na_2SO_4, filtered, and removed on rotary evaporator. Compound **3** (figure 41) was isolated in 20% yield as a pale-yellow oil.

Compounds **2** and **3** are known and spectral data are in accordance with the literature.[11,94] Absolute configuration of the amino acid derivative **3** is also known.[94]

(11b*S*) - 4,4-Dibutyl-2,6-bis (3,4,5-trifluorophenyl) - 4,5-dihydro-3H-dinaphtho [2,1-c:1',2'-e] azepinium bromide or Maruoka catalyst (**4**) was purchased from Strem Chemicals and was used without further purification.

The enantioselectivity of the compound **3** was determined by chiral HPLC (Chiralpak AD column, eluent: *n*-hexane/isopropanol 95:5, flow rate 1 mL/min, t(major)=6.06 min, t(minor)= 8.7 min, 91% ee), figure 44.

The other peaks visible are residues of catalyst or benzyl bromide.

Other experiments in table 1 were performed in the same manner, with specified parameters (solvent, concentration, flow rate, residence time, number of CSTR units, equivalents of benzyl bromide).

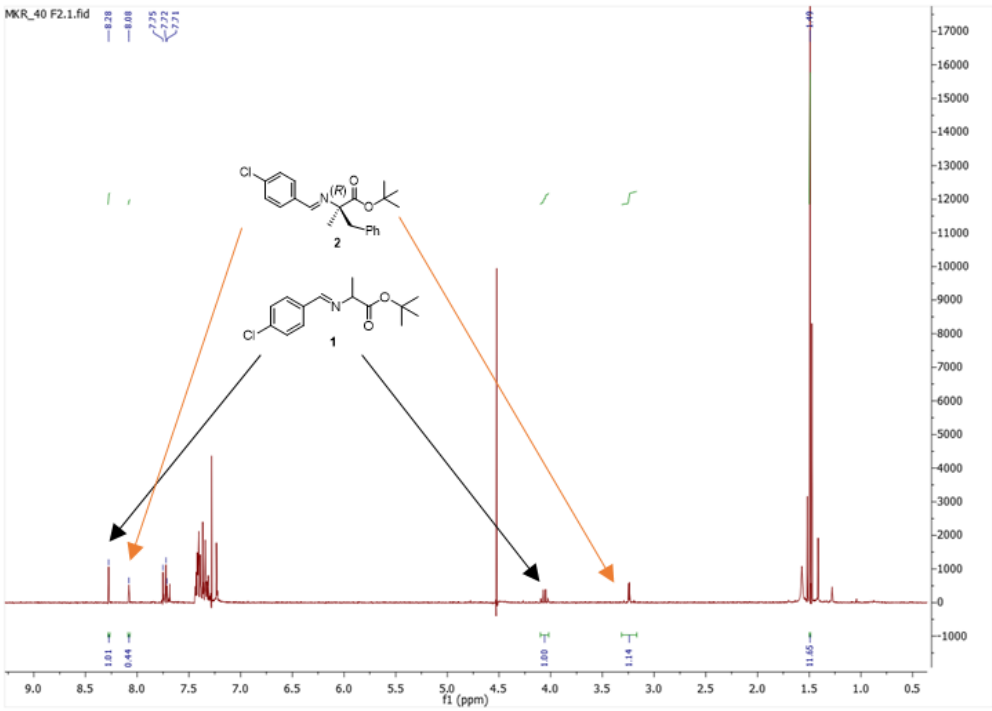

Figure 40. ^{1}H NMR in $CDCl_3$ of *liquid-liquid* phase transfer benzylation *in continuo* (**entry 6, table 1**)

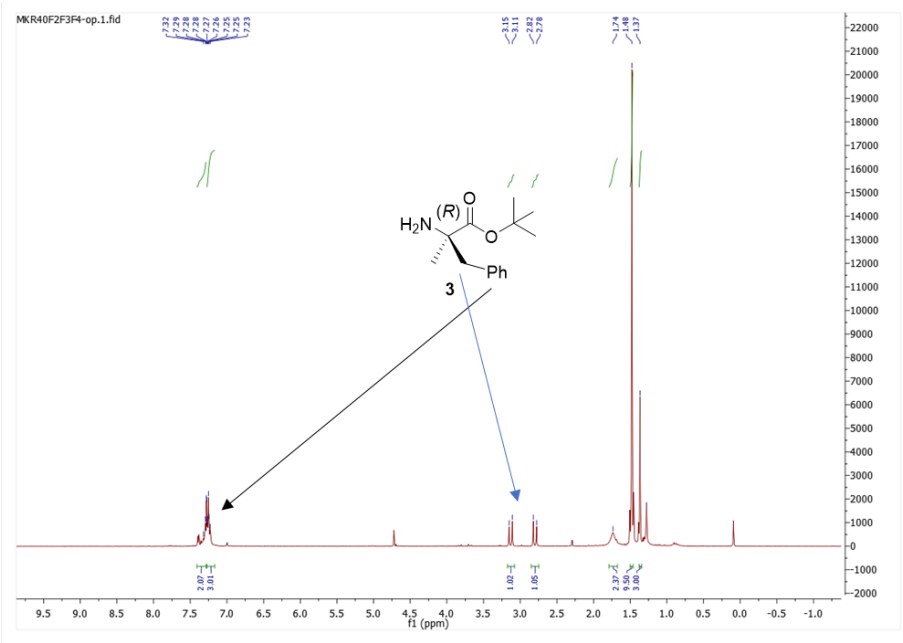

Figure 41. ^{1}H NMR in $CDCl_3$ of deprotected compound **2** done in batch (**entry 6, table 1**)

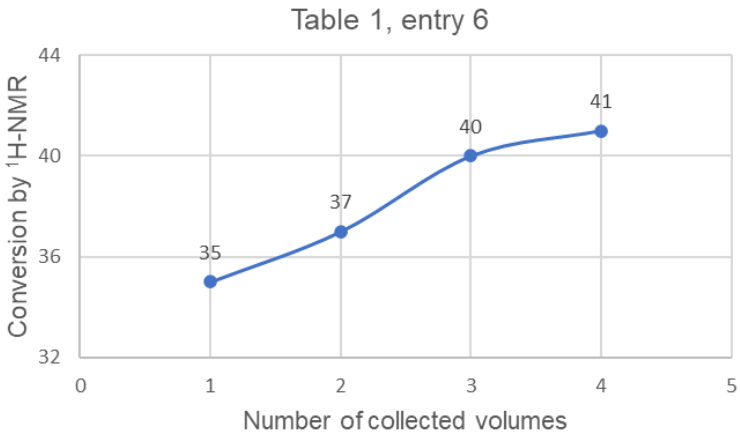

Figure 42. Conversion of the alanine imine **1** to the benzylated product **2** under *liquid-liquid* phase transfer continuous flow conditions**,** after each 80 min (**entry 6, table 1, section 3.3.1**)

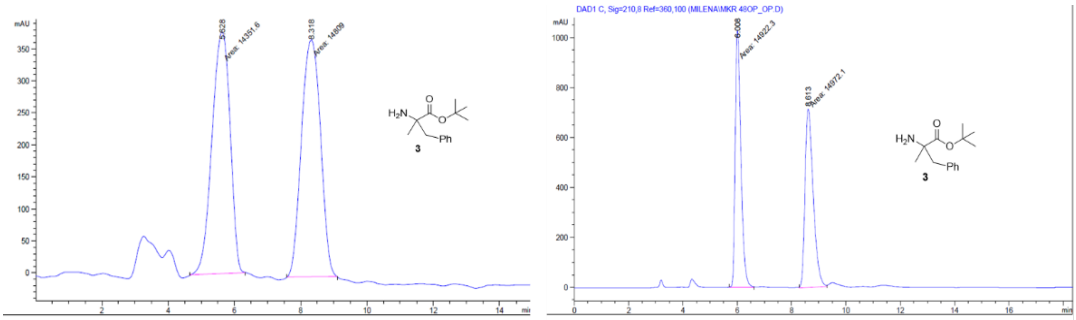

Figure 43. Racemic aminoester **3** (Chiralpak IA, *n*-hexane/isopropanol 95:5, left chromatogram) and (Chiralpak AD, *n*-hexane/isopropanol 95:5, right chromatogram)

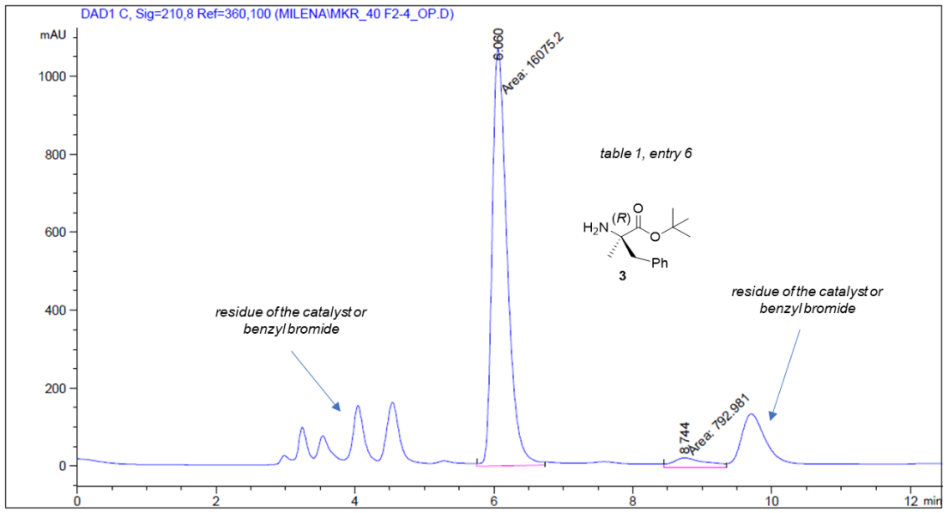

Peak #	RetTime [min]	Type	Width [min]	Area [mAU*s]	Height [mAU]	Area %
1	6.060	MM	0.2503	1.60752e4	1070.56421	95.2990
2	8.744	MM	0.5559	792.98090	23.77531	4.7010

Figure 44. Determination of enantioselectivity of aminoester **3** (**entry 6, table 1**)

6.2.4 *Solid-liquid* phase transfer benzylation in flow

Experimental procedure for entry 15, table 2, section 3.3.2:

In a 25 mL round bottom flask, 0.746 mmol (1.0 equiv., 200 mg) of the starting alanine imine **1**, 1.5 mmol (2.0 equiv., 0.18 mL) of benzyl bromide and 45 mg (10 mol%) of the cinchona catalyst **10** was dissolved in 6.8 mL of toluene/dichloromethane 1:2.4. The reaction mixture was stirred for 15 min at room temperature, and it was placed in the glass SGA syringe (10 mL).

The empty HPLC metal column equipped with endcaps and porous metal frits (L 15 cm x OD 6 mm x ID 4.6 mm) was filled with the mixture of solid bases (420 mg of KOH (10 equiv.), 1g of K_2CO_3 (10 equiv.) and 2 g of sand (~3.4 g of solid inside the column). The reaction mixture inside SGA syringe was delivered by syringe pump into the reactor (HPLC column filled with solid base and sand).

The total volume of the packed-bed reactor was 1.05 mL and the corresponding residence time for the flow rate of 0.015 mL/min was 66 min. The column was positioned vertically, and the solution goes from the bottom up through the column. Each volume of the reaction mixture was collected at the reactor output, solvent was removed under reduced pressure and conversion to the benzylated product **2** was analyzed by ^{1}H NMR in $CDCl_3$ (figure 45), showing ~83-64% conversion to the product **2** (figure 46). The cleavage of benzylated imine **2** was performed according to the section 6.2.3. Additional purification on silica gel column chromatography (eluent *n*-hexane/ethyl acetate 1:1) was necessary to afford aminoester **3** in 23% yield. The enantioselectivity of the compound **3** was determined by chiral HPLC (Chiralpak AD column, eluent: *n*-hexane/isopropanol 95:5, flow rate 1 mL/min, t(major)=8.15 min, t(minor)= 5.84 min, 52% ee, figure 47).

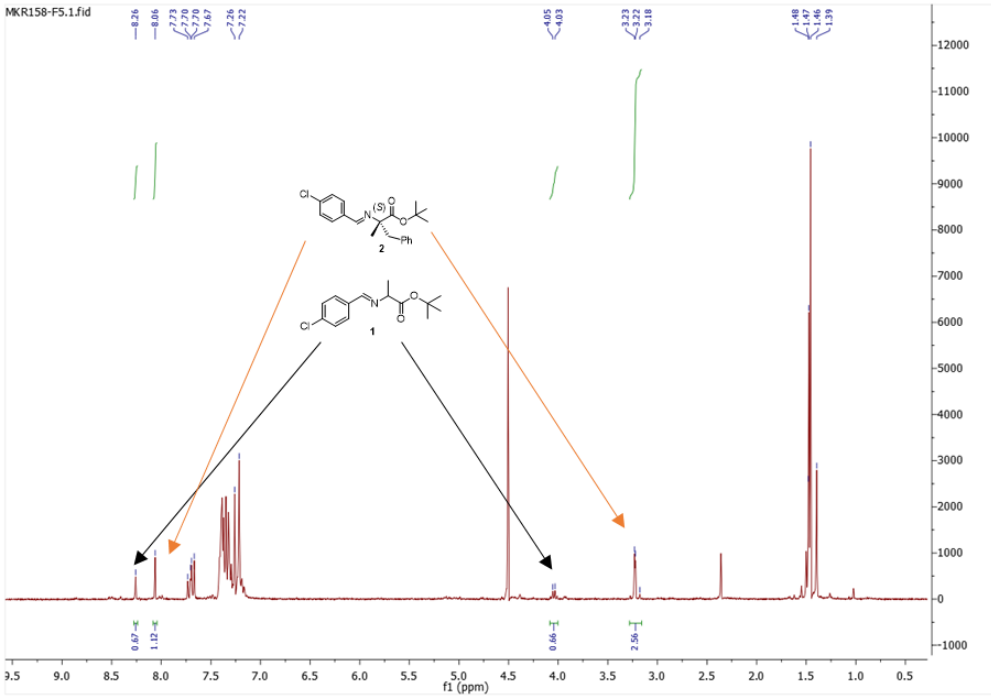

Figure 45. ^{1}H NMR in $CDCl_3$ of *solid-liquid* phase transfer benzylation *in continuo* (**entry 15, table 2, section 3.3.2**)

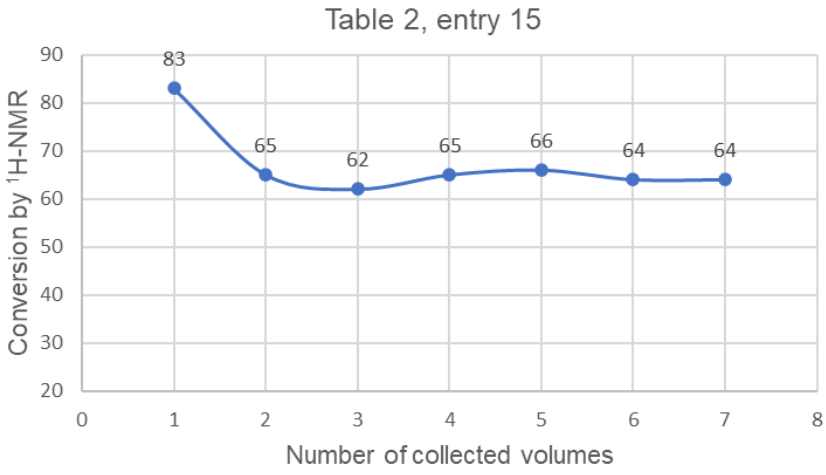

Figure 46. Conversion of the alanine imine **1** to the benzylated product **2** under *solid-liquid* phase transfer continuous flow conditions**,** after each 66 min (**entry 15, table 2, section 3.3.2**)

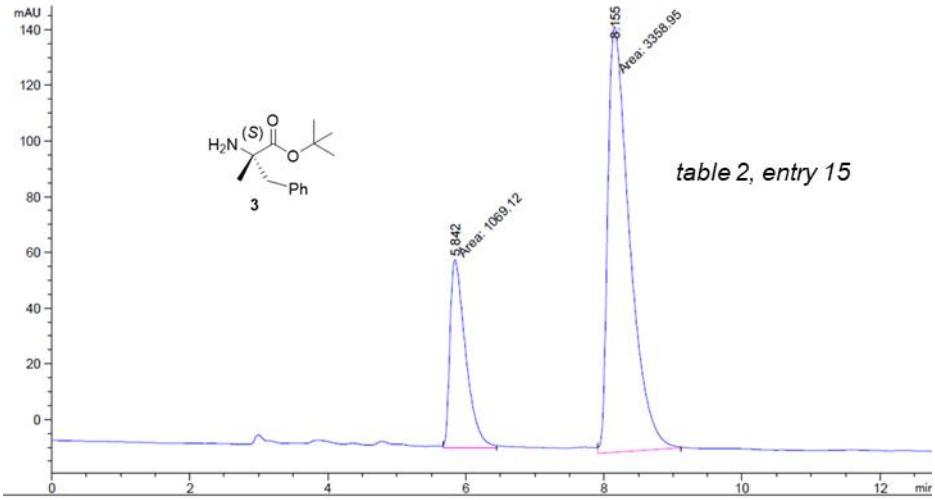

Peak #	RetTime [min]	Type	Width [min]	Area [mAU*s]	Height [mAU]	Area %
1	5.842	MM	0.2638	1069.11768	67.55331	24.1441
2	8.155	MM	0.3662	3358.95386	152.87383	75.8559
Totals :				4428.07153	220.42713	

Figure 47. Determination of enantioselectivity of aminoester **3** (**entry 15, table 2, section 3.3.2**)

Experimental procedure for entry 16, table 2, section 3.3.2:

25 mL flask with a nitrogen inlet, was charged with 400 mg (1.5 mmol, 1.0 equiv.) of imine **1**, 10 mg (0.015 mmol, 0.01 equiv.) of Maruoka catalyst **4** and 383 mg (2.2 mmol, 1.5 equiv.) of benzyl bromide dissolved in 7.5 mL of toluene dried over molecular sieves (0.2 M).

Stainless steel HPLC column (packed-bed reactor) with endcaps and frits (L 25 cm x OD 6 mm x ID 4.6 mm) was filled with the solid base $CsOH{\cdot}H_2O$ (2.5-2.6 g, ~0.015 mol, ~10 equiv.) and glass (soda-lime) beads (4.5 g). Glass beads were used to reduce high pressure in the system.

HPLC metal column was placed vertically in plastic graduated cylinder and cooled down to 0 °C in ice/water cooling bath. The reaction mixture from the flask was delivered into packed-bed reactor by pump A of Vapourtec flow system through

PTFE tubing. The volume of the PTFE tubes was not considered because the reaction occurs inside the packed-bed reactor.

All fractions were collected after every 10 min (one volume 0.7 mL) with the flow rate of reaction mixture 0.1 mL/min. The reaction was monitored by ^{1}H NMR in $CDCl_3$. Toluene was removed from each fraction; residue was dissolved in $CDCl_3$ and analyzed by ^{1}H NMR.

After the completion of the flow process, the last fraction showing the best conversion (volume 9, see figure 48) was used for the acidic cleavage of imine **2** in batch conditions to afford aminoester **3.**

90 mg of the last volume 9 residue (after toluene removal) was dissolved in 2 mL of THF and 4 mL of 15% sol. of citric acid monohydrate (pH=2). Reaction mixture was stirred at room temperature for 5h. The reaction mixture was stopped, THF was removed, and the residue was washed with cyclohexane (15 mL). Phases were separated in separatory funnel and after that water phase was basified using solid of Na_2CO_3 until pH=9. After that basic water layer was extracted with dichloromethane (3x15 mL). Organic phases were combined, washed with brine (30 mL), dried over $MgSO_4$, filtered, and removed on rotary evaporator. 40 mg of aminoester **3** was isolated as a light-yellow oil (<20% yield).

The enantioselectivity of the compound **3** was determined by chiral HPLC (Chiralpak AD column, eluent: *n*-hexane/isopropanol 95:5, flow rate 1 mL/min, t(major)=6.03 min, t(minor)= 8.7 min, 93% ee), figure 49.

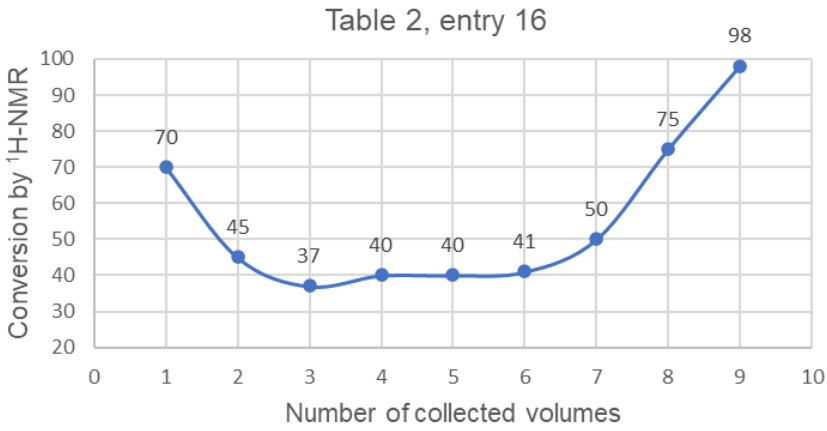

Figure 48. Conversion of the alanine imine **1** to the benzylated product **2** under *solid-liquid* phase transfer continuous flow conditions**,** after each 10 min (**entry 16, table 2, section 3.3.2**)

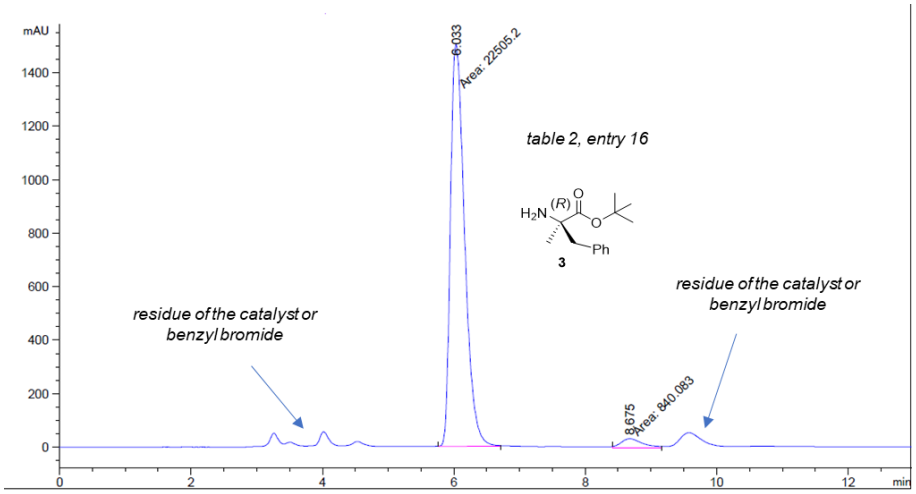

Peak #	RetTime [min]	Type	Width [min]	Area [mAU*s]	Height [mAU]	Area %
1	6.033	MM	0.2494	2.25052e4	1503.77368	96.4015
2	8.675	MM	0.3955	840.08264	35.40022	3.5985
Totals :				2.33452e4	1539.17390	

Figure 49. Determination of enantioselectivity of aminoester **3** (**entry 16, table 2, section 3.3.2**)

Experimental procedure for entry 17, table 2, section 3.3.2:

25 mL round bottom flask with a nitrogen inlet, was charged with 700 mg (2.6 mmol, 1.0 equiv.) of alanine imine **1**, 79 mg (0.13 mmol, 0.05 equiv.) of cinchona catalyst **10** and 537 mg (0.89 mmol, 0.37 mL, 1.2 equiv.) of benzyl bromide dissolved in 5.2 mL of toluene and 3.3 mL of dichloromethane (toluene/dichloromethane 1.6:1). The flask with reaction mixture was cooled down in the cooling bath ice/NaCl (-15 °C) and connected to the Vapourtec continuous flow system.

HPLC metal column (250 mm x 4.6 mm) was filled with the mixture of base KOH/K_2CO_3 1:1 (2.9 g in total (2.06 g of K_2CO_3 and 0.84 g of KOH), ~6 equiv. each) and glass (soda-lime) beads (3.77 g). HPLC metal column was cooled down in the cooling bath ice/NaCl (0 °C up to -15 °C) and attached through PTFE tube (0.8mm x 1.6 mm) and corresponding fittings with the pump A of Vapourtec machine. Fractions were collected after each 15 min (residence time for flow rate 0.1 mL/min) and the total volume of the reactor is 0.8 mL.

The reaction was monitored by ^{1}H NMR in $CDCl_3$, showing 48-76% conversion to the product **2** (figure 50). Toluene was removed from each fraction; residue was dissolved in $CDCl_3$ and analyzed by ^{1}H NMR. After the completion of the flow process, the last fraction (volume 9, see figure 50) was used for the acidic cleavage of imine **2** in batch conditions to afford amino ester **3.**

80 mg of the last volume **9** residue (after toluene removal) was dissolved in 1 mL of THF and 3 mL of 15% sol. of citric acid monohydrate (pH=3). Reaction mixture was stirred at room temperature for 5h. The reaction mixture was stopped, THF was removed, and the residue was washed with cyclohexane (15 mL). Phases were separated in separatory funnel and after that water phase was basified with saturated solution of K_2CO_3 until pH=9, followed by stirring for 1h. After that basic water layer was extracted with diethyl ether (3x15 mL). Organic phases were combined, washed with brine, dried over $MgSO_4$, filtered, and removed on rotary evaporator. 25 mg of the aminoester **3** was isolated as dark orange oil (<15% yield). The enantioselectivity of the compound **3** was determined by chiral HPLC (Chiralpack IA column, eluent: *n*-hexane/isopropanol 9:1, flow rate 1 mL/min, t(major)=8.33 min, t(minor)= 5.63 min, 72% ee), figure 51.

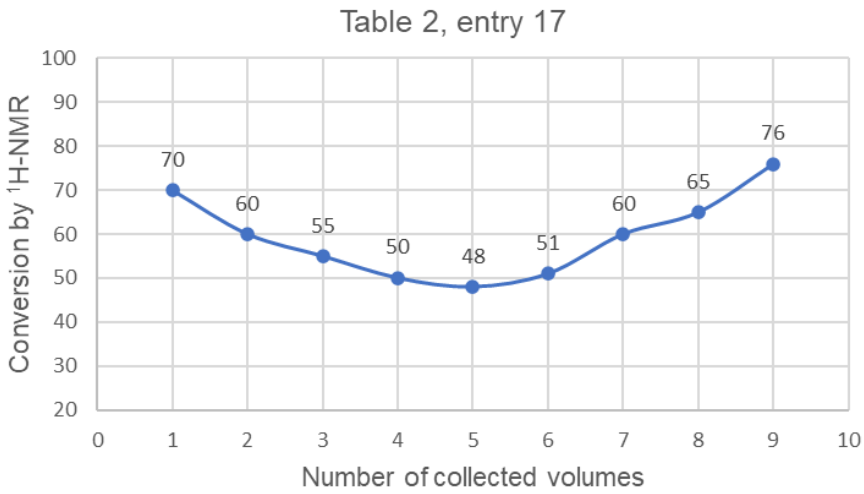

Figure 50. Conversion of the alanine imine **1** to the benzylated product **2** under *solid-liquid* phase transfer continuous flow conditions**,** after each 15 min (**entry 17, table 2, section 3.3.2**)

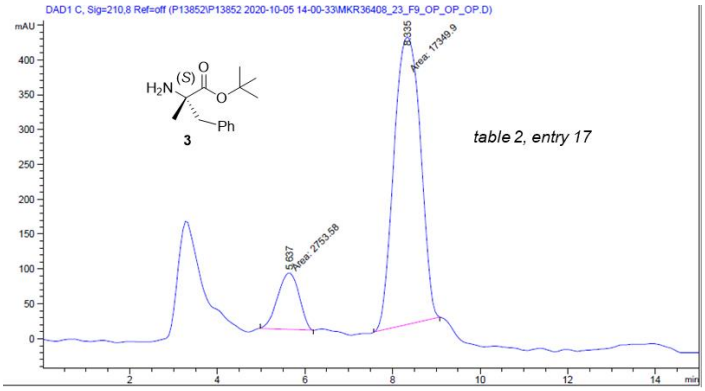

Peak #	RetTime [min]	Type	Width [min]	Area [mAU*s]	Height [mAU]	Area %
1	5.637	MM	0.5645	2753.57593	81.29742	13.6970
2	8.335	MM	0.6994	1.73499e4	413.47247	86.3030
Totals :				2.01035e4	494.76990	

Figure 51. Determination of enantioselectivity of aminoester **3** (**entry 17, table 2, section 3.3.2**)

Experimental procedure for entry 18, table 2, section 3.3.2:

50 mL round bottom flask with a nitrogen inlet, was charged with 200 mg (0.7 mmol, 1.0 equiv.) of alanine imine **1**, 45 mg (0.07 mmol, 0.1 equiv.) of *O*-Allyl-*N*-(9-anthracenylmethyl) cinchonidinium bromide PTC catalyst **10**, 153 mg (0.89 mmol, 0.1 mL, 1.2 equiv.) of benzyl bromide and 2 mL of dichloromethane (DCM). The flask with reaction mixture was connected to the continuous flow Vapourtec system.

HPLC metal column (L 30 cm x 7.8 mm) was filled with the mixture of base KOH/K_2CO_3 1:1 (6.55 g in total, 45 equiv. each) and glass (soda-lime) beads (13 g). HPLC metal column was attached through PTFE tube (0.8mm x 1.6 mm), 1m and corresponding fittings with the pump A of Vapourtec machine. Fractions were collected after each 30 min (residence time for flow rate 0.1 mL/min, reactor volume 1mL). The reaction was monitored by benchtop ^{1}H NMR (Spinsolve 60 ultra-carbon NMR spectrometer) in reaction solvent, dichloromethane. Four volumes were collected and all of them showed complete conversion of alanine imine **1** to the product **2** (see figure 52)**.** All four fractions were collected, solvent was evaporated, and 94 mg of yellow oil was isolated (product **2**). 94 mg was dissolved in 1 mL of THF and 1 mL of 5% citric acid was added. Reaction mixture was stirred at room temperature for 4h. Solution was diluted with diethyl ether (10 mL) and extracted with water (10 mL). The acid extract (pH=4) was than basified

(sat. aq. sol. K_2CO_3) and extracted with ethyl acetate (3x20 mL). The ethyl acetate extracts were then washed with brine, dried over $MgSO_4$, and concentrated under reduced pressure. 34 mg of aminoester **3** was isolated as a pink oil (<30% yield). The enantioselectivity of the compound **3** was determined by chiral HPLC (RegisPack 25 cm X 4.6 mm 5 Micron column, eluent: *n*-hexane/isopropanol 9:1, flow rate 1 mL/min, t(major)=4.7 min, t(minor)= 4.09 min, 56% ee), figure 53. Peaks at rt=3-3.6 min originate from impurities (aromatic compounds).

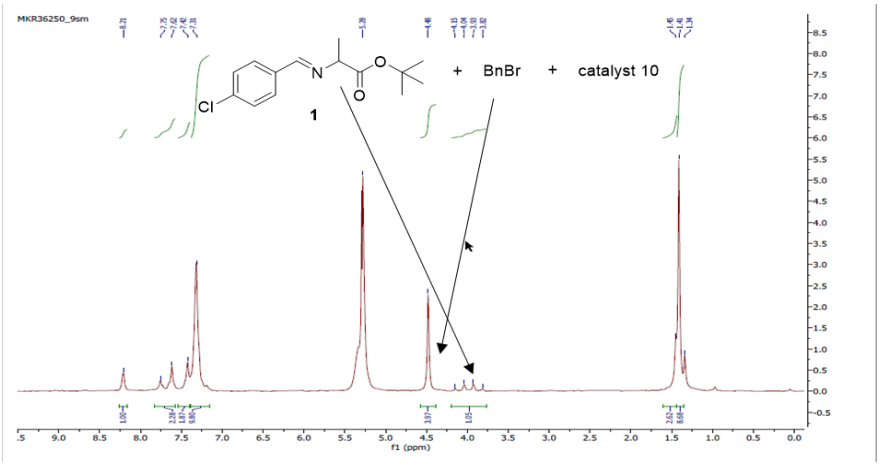

^{1}H-NMR in DCM (60 MHz): Mixture of benzyl bromide, starting imine and the catalyst (before starting the reaction)

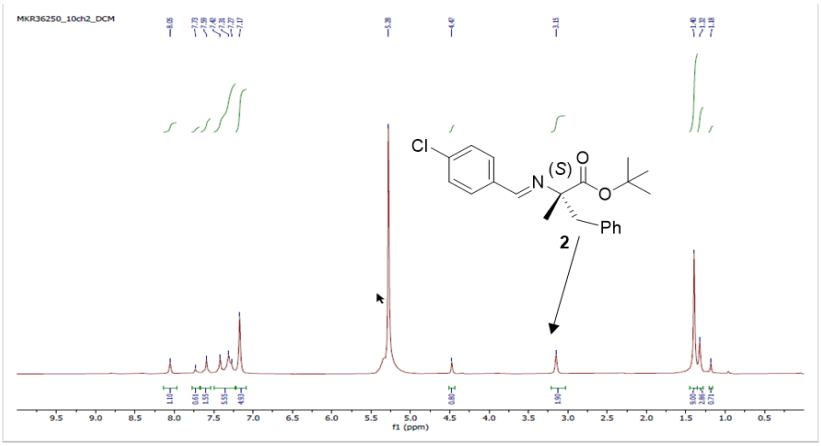

^{1}H-NMR in DCM (60 MHz): Second reaction check after 1h (flow rate 0.1 mL/min)

Figure 52. Comparison of the *solid-liquid* phase transfer benzylation of alanine imine **1** after 1h of reaction in packed-bed reactor with the reaction mixture before starting the reaction (**entry 18, table 2, section 3.3.2**)

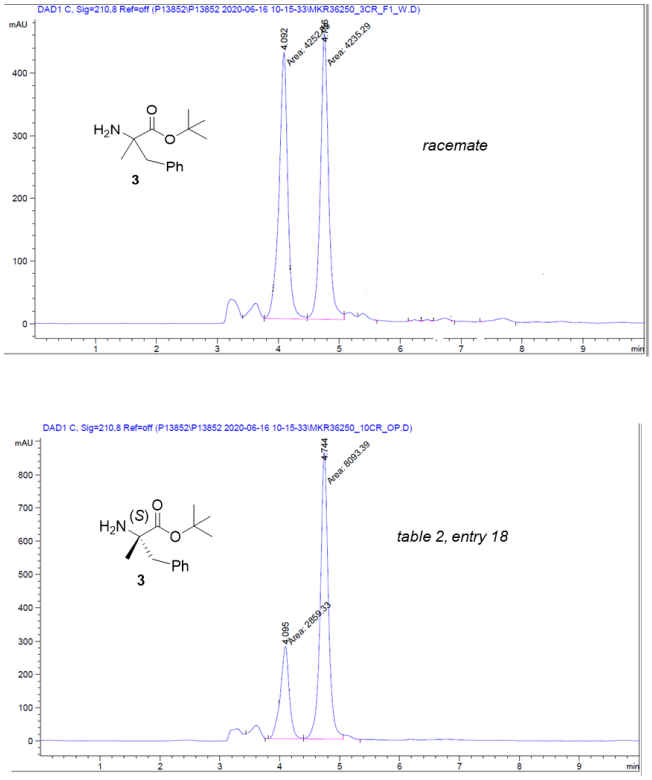

Figure 53. Determination of enantioselectivity of aminoester **3** (**entry 18, table 2, section 3.3.2**)

Calculation of productivity and space-time yield (see section 3.3):

Entry	Conversion to the product 2 (% by ^{1}H-NMR)	Reactor volume [mL]	Residence time [min]	Productivity [mmol/h] [a]	Space-time yield [mmol/ml*h] [b]
Liquid-liquid phase transfer benzylation in continuous stirred tank reactor					
Batch	Quant.	5.43	1680	0.027	0.05
Table **1**/entry **6**	40	25	333	0.053	0.002
Solid-liquid phase transfer benzylation in packed-bed reactor					
Batch	Quant.	4	180	0.248	0.062
Table **2**/entry **15**	65	1.05	66	0.436	0.415
Table **2**/entry **16**	47	0.35	5	4.2	12
Table **2**/entry **17**	60	0.23	4.33	6.23	27
Table **2**/entry **18**	95	1	30	1.4	1.4

[a] Productivity: moles of product **2** (calculated by ^{1}H NMR conversion, average value) divided by the collection time required to collect 0.75 mmol of benzylated product **2**

[b] Space-time yield: productivity divided by reactor volume

6.3 Synthesis of BIMP bearing one stereogenic center

6.3.1 Synthesis of BIMP derived from (*R*)-(−)-2-Phenylglycinol

N-Boc protected amino alcohol **13** was prepared following the procedure[98] and all spectral date are in accordance with the published article.

Mesylate **14a** was synthetized according to the following procedure[111] and NMR spectra agreed with this article.

General procedure for the synthesis of mesylate 14a:

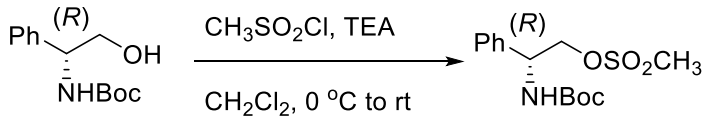

13 **14a**

An oven-dried, two-necked, round-bottomed flask is equipped with a nitrogen inlet adapter, a rubber septum, a pressure equalizing dropping funnel fitted with a rubber septum and magnetic stirring bar. The flask is flushed with nitrogen and charged with *N*-Boc protected amino alcohol **13** (700 mg, 2.94 mmol, 1.0 equiv.), 7 mL of dry dichloromethane and triethylamine (0.62 mL, 4.41 mmol, 1.5 equiv.), then is cooled in an ice bath at 0 °C. The solution of methanesulfonyl chloride (0.24 mL, 3.08 mmol, 1.05 equiv.) in 3.5 mL of dry dichloromethane is then added to the flask dropwise over 10 min. The reaction mixture was stirred at 0 °C for 4h and until the reaction completion at room temperature. The reaction mixture was monitored by TLC (eluent *n*-hexane/ethyl acetate 1:1) and ^{1}H NMR in $CDCl_3$.

After 11h, the reaction was stopped and in the mixture was added 7 mL of saturated solution $NaHCO_3$ followed by stirring for 20 min. The reaction mixture was transferred to the separatory funnel and extracted with DCM (3 x 15 mL). Combined organic phases were washed with brine (2x15 mL), dried over Na_2SO_4, filtered, and concentrated in vacuo to afford 822 mg crude product **14a** as a light beige solid, with 88% yield.

^{1}H-NMR of mesylate 14a (300 MHz, $CDCl_3$) δ ppm: 1.44 (s, 9H), 2.88 (s, 3H), 4.37-4.50 (m, 2H), 5.01 (bs, 1H), 5.12 (bs, 1H), 7.29-7.41 (m, 5H)

General procedure for the synthesis of *N*-Boc protected aminoazide 15:

The azide **15** was prepared according to Dixon's procedure[45], with modification of reaction temperature. Spectral data are in agreement with the literature.[45]

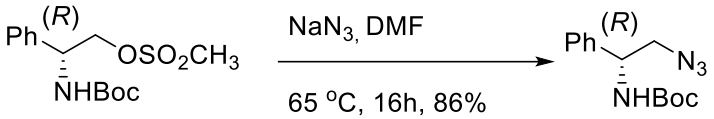

14a **15**

In a two-necked round bottom flask (50 mL) equipped with magnetic stirrer, reflux condenser and nitrogen line, 790 mg (2.5 mmol, 1.0 equiv.) of **14a** was dissolved in 8 mL of dimethylformamide dried over molecular sieves (DMF), (0.3 M solution) and 814 mg (12.5 mmol, 5.0 equiv.) of sodium azide (NaN_3) was added in the flask. After that, reaction mixture was heated at 65 °C, overnight. The reaction mixture was monitored by TLC (eluent *n*-hexane/ethyl acetate 1:1) and ^{1}H NMR in $CDCl_3$.

After 16h, the reaction mixture was diluted with 100 mL of water and 30 mL of diethyl ether (Et_2O). Aqueous layer was extracted three times more with 30 mL of Et_2O. Organic layers were combined and washed 3 times more with 50 mL of brine. Organic phase was then dried over Na_2SO_4, filtered and solvent was removed under reduced pressure. The azide **15** was isolated as light-yellow solid, with the yield of 86%, 565 mg.

^{1}H NMR of *N*-Boc protected aminoazide 15 (300 MHz, $CDCl_3$) δ ppm: 1.44 (s, 9H), 3.63-3.64 (m, 2H), 4.87-5.03 (2 x bs, 2H), 7.29-7.40 (m, 5H)

The thioureazide **16** and the final iminophosphorane organocatalyst **17** were also synthetized following the Dixon' procedure[45]. All relevant spectra can be found in this article.[45]

6.3.2 Synthesis of BIMP derived from L-*tert*-leucine possessing thiourea moiety

Compounds **19** and **20** were prepared according to the following article.[98]

General procedure for the synthesis of L-*tert*-leucinol 19:

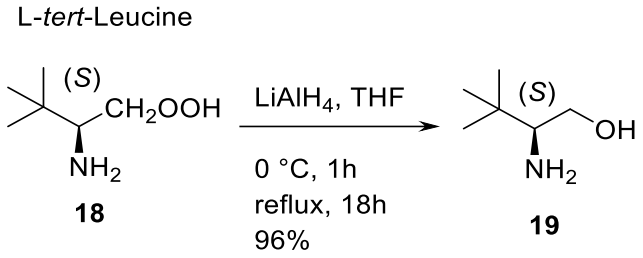

Three-necked round bottom flask (500 mL) under the flow of nitrogen was charged with 5.71 g (150 mmol, 2.0 equiv.) of lithium aluminum hydride ($LiAlH_4$), and 230 mL of dry tetrahydrofuran (THF), at 0 °C. After that, 10 g (76 mmol, 1.0 equiv.) of commercially available L-*tert*-Leucine **18** was added slowly portionwise in an ice cooled solution of $LiAlH_4$ in dry THF. The mixture was allowed to react at 0 ° for 1h followed by reflux overnight (around 70 °C).

The reaction mixture was checked by ^1H NMR in $CDCl_3$ (aliquot was taken, $LiAlH_4$ was quenched with 2 M aq. NaOH and the suspension was filtered through pad of cotton; THF was removed under reduced pressure and residue was dissolved in $CDCl_3$) and TLC (eluent dichloromethane/methanol 19:1, stained by ninhydrin). After the reaction is complete, the solution was cooled to 0 °C, and diluted with 100 mL of Et_2O. The excess of $LiAlH_4$ was quenched with 2 M aq. solution of NaOH (50 mL). After quenching, the reaction mixture was stirred for 15 min, $MgSO_4$ was added, solid was filtered and washed 6 times with 50 mL of THF.

THF was concentrated affording 8.57 g of L-*tert*-leucinol **19** as a light-yellow oil (96% yield).

^{1}H NMR of L-*tert*-leucinol 19 (300 MHz, $CDCl_3$) δ ppm: 0.88 (s, 9H), 1.9 (3H, broad singlet (protons from NH_2 and OH group)), 2.47-2.51 (dd, 1H), 3.16-3.22 (t, 1H), 3.67-3.72 (dd, 1H).

General procedure for the synthesis of *N*-Boc protected L-*tert*-leucinol 20:

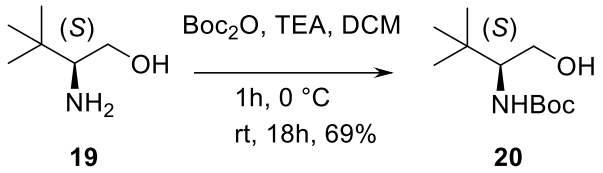

19 **20**

8.5 g (0.0725 mol, 1.0 equiv.) of L-*tert*-leucinol **19** and 8.67 g (0.0857 mol, 1.2 equiv., 11.94 mL) of triethylamine (TEA) in 200 mL of dichloromethane (DCM) was added in the three-necked round bottom flask (500 mL). The flask was cooled down to 0 °C in ice bath, and after that in the mixture was added 18.7 g (0.0857 mol, 1.2 equiv.) of di-*tert*-butyl decarbonate (Boc_2O) dissolved in 55 mL of DCM. Reaction mixture was stirred at 0 °C for 1h, and overnight at room temperature. The reaction mixture was checked by ^1H NMR in $CDCl_3$. After 18h, the reaction mixture was washed with brine 2x250 mL, organic phase was dried over $MgSO_4$, filtered and concentrated. White to light yellow solid was obtained. Trituration of this solid was done with 120 mL of *n*-pentane, 30 min.
After that, solid was filtered (filtrate was light yellow from impurities) on Büchner funnel, washed with *n*-pentane (70 mL) and dried under vacuo at 45 °C. After trituration, 10.8 g of the product **20** was obtained as a white solid (69% yield).

^1H NMR of compound 20 (300 MHz, $CDCl_3$) δ ppm: 0.93 (s, 9H), 1.45 (s, 9H), 1.80 (bs, 2H), 3.45-3.52 (dd, 2H), 3.80-3.88 (dd, 1H), 4.62 (bs, 1H)

General procedure for the synthesis of mesylate 20a:

For the preparation of mesylate **20a**, the same synthesis of mesylate **14a** was applied.[111]

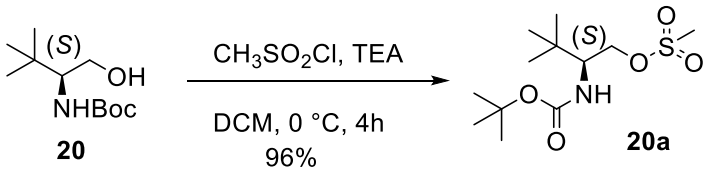

20 **20a**

In a two-necked round bottom flask (250 mL), to a stirred solution of 10.8 g (0.049 mol, 1.0 equiv.) of amino alcohol **20** in 125 mL of DCM at 0 °C was added 10 g (0.099 mol, 2.0 equiv., 13.8 mL) of triethylamine, under the flow of nitrogen. After 10 min of stirring, 6.26 g (0.055 mmol, 1.2 equiv., 4.2 mL) methanesulfonyl chloride was added dropwise. After addition of the first 2.5 mL of methanesulfonyl chloride colorless reaction mixture became white suspension, and after addition the whole amount of methanesulfonyl chloride, white suspension changed color

to yellow suspension. Stirring was maintained at 0 °C. Starting material was consumed after 4h and it was confirmed by ^{1}H NMR. Reaction mixture was stopped and diluted with 120 mL of brine and was washed 2 times (2x120 mL). In order to remove excess of methanesulfonic acid, organic phase was washed 2x120 mL with sat. aq. sol. $NaHCO_3$, dried over $MgSO_4$, filtered, and concentrated on rotary evaporator. 14.03 g of mesylate **20a** was obtained as a thick orange oil with 96% yield (figure 30).

^{1}H NMR of mesylate 20a (300 MHz, $CDCl_3$) δ ppm: 0.97 (s, 9H), 1.44 (s, 9H), 3 (s, 3H), 3.03 (s, 1H), 3.68-3.75 (m, 1H), 4.15-4.21 (dd, 1H), 4.35-4.40 (dd, 1H), 4.62-4.65 (d, 1H)

General procedure for the synthesis of *N*-Boc protected aminoazide 23:

The azide **23** was prepared according to the following procedure[100] and spectral characterization can be found in Dixon's article.[45]

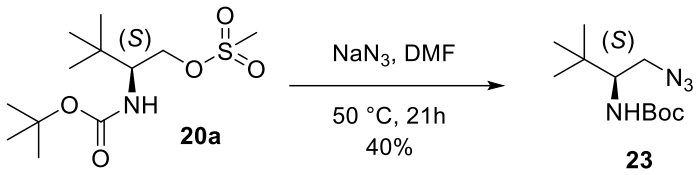

5.82 g (89.5 mmol, 5.0 equiv.) of sodium azide and 20 mL of dry DMF was added in the two-necked round bottom flask (250 mL) under the flow of nitrogen. The suspension was stirred at room temperature. 5.309 g (17.9 mol, 1.0 equiv.) of mesylate **20a** was dissolved in another 35 mL of DMF dried over molecular sieves and added slowly in the suspension of NaN_3 in DMF at room temperature. The reaction mixture was heated at 50 °C overnight. The reaction mixture was checked by TLC in *n*-hexane/ethyl acetate 1:1, staining by ninhydrin. After the consumption of starting mesylate, the reaction mixture was diluted with 50 mL of water and 50 mL of Et_2O. Water layer was extracted two times more with 100 mL of Et_2O. Organic layers were combined and washed 2 times more with 250 mL of brine. Organic phase was then dried over Na_2SO_4, filtered and solvent was removed under reduced pressure. The residue was purified by silica gel column chromatography using eluent *n*-hexane/ethyl acetate 9:1. In total, 1.73 g of the product **23** was isolated as a white solid, 40% yield.

General procedure for the synthesis of thiourea-azide 24:

The synthesis and spectral characterization of compound **24** can be found in Dixon's article.[45]

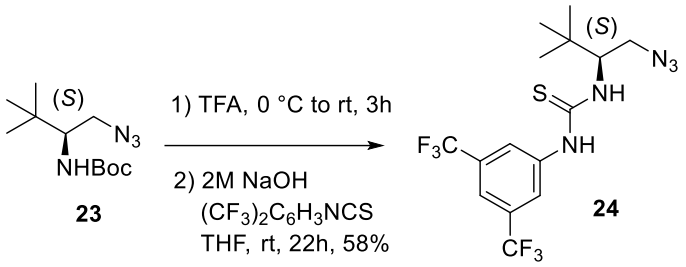

An ice-cooled two-necked round bottom flask containing 1.98 g (0.0082 mol, 1.02 equiv.) of azide **23** under nitrogen was added dropwise 11.78 g (0.103 mol, 12.6 equiv., 7.9 mL) of trifluoroacetic acid (TFA) behind a blast-shield. The resulting solution was stirred at room temperature for 3h. TFA was concentrated under reduced pressure carefully (behind a blast-shield!), the residue was diluted with Et_2O (30 mL) and washed with 2 M NaOH (20 mL). The aqueous layer was extracted with Et_2O (20 mL), and the combined organic layers were washed with brine (10 mL) with some drops of 2 M NaOH, dried over $MgSO_4$ and concentrated to dryness under reduced pressure. The intermediate **32** (for the structure see scheme 28 or 31) was isolated as light-yellow oil in 77% yield.

PRECAUTION: at high vacuum the deprotected aminoazide **32** distills out!

The obtained amine **32** (0.9 g, 6.3 mmol) was dissolved in 20 mL THF and 1.7 g (6.3 mmol) 3,5-bis(trifluoromethyl)phenyl isothiocyanate was added dropwise. The mixture was stirred at room temperature overnight. After the reaction completion (check by TLC (cyclohexane/ethyl acetate 9:1), THF was removed and in the residue was added 10 mL of *n*-pentane in order the remove excess of 3,5-bis(trifluoromethyl)phenyl isothiocyanate. The residue was stirred 1h at room temperature. After 1h, solid was filtered and washed with 20 mL of *n*-pentane. The second wash was done with mixture of solvents *n*-pentane/diethyl ether 5:1. Solid was collected and dried on rotary evaporator for 2h.

1.96 g of product **24** was isolated as white solid, 58% yield.

General procedure for the synthesis of iminophosphorane catalyst 25:

The synthesis and spectral characterization of the catalyst **25** can be found in Dixon's article.[45]

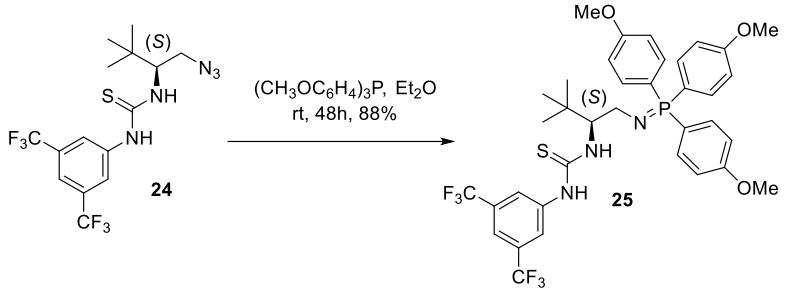

In the three-necked flask was added 300 mg (0.72 mmol, 1.0 equiv.) of thiourea-azide **24** and 255 mg 0.72 mmol, 1.0 equiv. of tris(4-methoxyphenyl) phosphine in 2 mL of dry Et_2O. The reaction mixture was stirred at room temperature, under the flow of nitrogen. After 2 days reaction running, the reaction mixture was left one day more under the flow of nitrogen to remove the solvent completely. The third day, white solid was checked by TLC and ^{1}H NMR/^{31}P NMR/^{19}F NMR in $CDCl_3$. All analytics showed complete conversion of starting material to the product, without washing, without any purification. 470 mg of the catalyst **25** was isolated as a white solid (88% yield).

^{1}H NMR of BIMP catalyst 25 (300 MHz, $CDCl_3$) δ ppm: 0.95 (s, 9H), 2.85-2.95 (pq, 1H), 3.19-3.25 (m, 1H), 3.84 (s, 9H), 4.07 (bs, 1H), 6.96-7 (dd, 6H), 7.24 (1H) and 7.27 (2H (overlapped with $CDCl_3$), 7.48-7.55 (m, 7H)

^{19}F NMR of BIMP catalyst 25 (282.1 MHz, $CDCl_3$) δ ppm: -62.65

^{31}P NMR of BIMP catalyst 25 (121.2 MHz, $CDCl_3$) δ ppm: 27

Synthesis of thiourea-azide 26:

The synthesis and spectral characterization of the precursor **26** can be found in Dixon's article.[45]

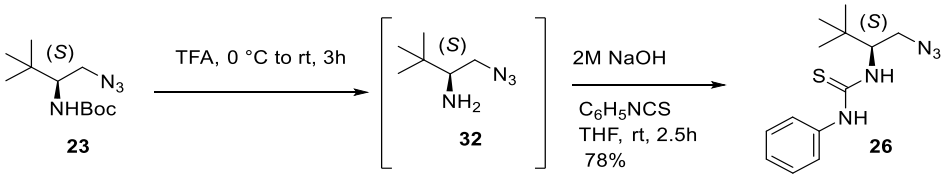

Boc deprotection of azide **23** (200 mg) to get intermediate **32** was done in the same manner like for the synthesis of thiourea-azide **24**.

In a two-necked flask 86 mg (0.604 mmol, 1.0 equiv. of intermediate **32**) was dissolved in 2 mL of dry THF. Further, 90 mg (0.66 mmol, 1.1 equiv.) of phenyl isothiocyanate was dissolved in 2 mL of dry THF and was added to a solution of azide **32** under a nitrogen flow. The reaction mixture was stirred at 800 rpm for 2.5 h at room temperature (TLC check in *n*-hexane/ethyl acetate 1:1).

After evaporation of the volatiles, the crude reaction mixture was purified by flash column chromatography (*n*- hexane/ethyl acetate 95:5 to 9:1) to obtain **26** (130 mg, 78%) as a yellow solid.

Synthesis of iminophosphorane organocatalyst 27:

The synthesis and spectral characterization of the catalyst **27** can be found in Dixon's article.[45]

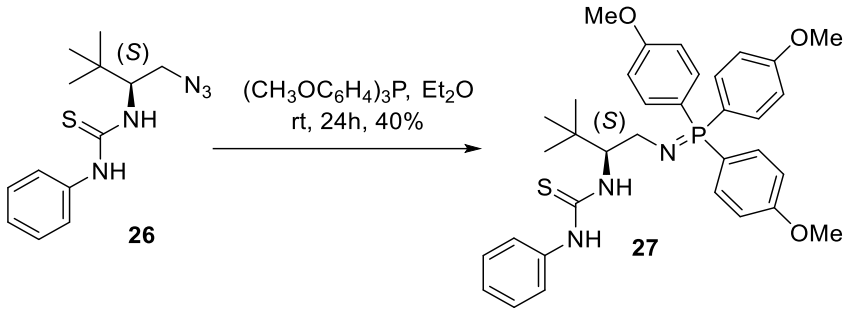

In the 10 mL two-necked flask was added 128 mg (0.461 mmol, 1.0 equiv.) of thiourea-azide **26** and 163 mg (0.461 mmol, 1.0 equiv.) of tris(4-methoxyphenyl) phosphine in 2.5 mL of dry Et_2O. The reaction mixture was stirred at room temperature for 24 h, under the flow of nitrogen. After reaction completion, the solvent was removed under N_2 flow, and the residue was washed with a mixture *n*-pentane/diethyl ether 4:1 (2x10 mL) to remove the traces of unreacted tris(4-methoxyphenyl) phosphine. 136 mg of the product **27** was obtained as a white solid (85% pure, ~40% yield) and it was used as such in asymmetric aza-Henry reaction (section 5.5).

6.3.3 Synthesis of BIMP derived from L-*tert*-leucine possessing urea moiety

Synthesis of the iminophosphorane catalyst 29*:

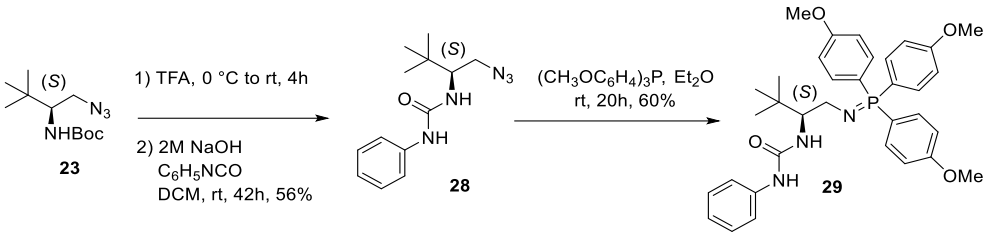

Synthesis of urea-azide **28** was performed according to the previously described procedure (like thiourea-azide **24** or thiourea-azide **26**).

In a two-necked flask cooled to 0 °C was added 28 mg (0.19 mmol, 1.2 equiv.) of intermediate **32** (after Boc deprotection) and 19 mg (1.0 equiv.) phenyl isocyanate dissolved in 1.5 mL of dry DCM. The reaction mixture was then warmed to room temperature and stirred overnight. After the starting material consumption (TLC check in *n*-hexane/ethyl acetate 1:1), DCM was removed, and the crude was purified by silica gel column chromatography using eluent *n*- hexane/ethyl acetate 85:15.

23 mg of the urea-azide **28** was obtained as a white solid, 56% yield.

In the 5 mL glass vial with the septum was added 22 mg (0.084 mmol, 1.0 equiv.) of urea-azide **28** and 30 mg (0.084 mmol, 1.0 equiv.) of tris(4-methoxyphenyl) phosphine in 1 mL of dry Et_2O. The reaction mixture was stirred at room temperature overnight. After 20h, the reaction was stopped, and the solvent was removed under high vacuum. Further manipulation/trituration was not possible to perform due to a very small reaction scale. 30 mg of the catalyst **29** was obtained as a pale-yellow solid (~90% pure, 60% yield) and it was used as such in asymmetric aza-Henry reaction (section 5.5).

^{1}H NMR of urea-azide 28 (300 MHz, $CDCl_3$) δ ppm: 0.95 (s, 9H), 3.25-3.33 (dd, 1H), 3.54-3.60 (dd, 1H), 3.88 (bs, 1H), 4.67 (bs, 1H), 6.27 (bs,1H), 7.14-7.35 (m, 5H)

^{1}H NMR of BIMP catalyst 29* (300 MHz, $(CD_3)_2CO$) δ ppm: 0.91(s, 9H), 2.41 (dd, 1H), 2.84 (dd, 1H), 3.15 (q, 1H), 3.25 (dd, 1H), 3.52 (m, 1H), 3.86 (s, 9H), 6.85 (m, 2H), 7.06 (m, 6H), 7.43 (m, 3H), 7.60 (m, 6H)

^{31}P NMR of BIMP catalyst 29* (121.2 MHz, $(CD_3)_2CO$) δ ppm: 25.77

Synthesis of the urea-azide 33:

Spectral characterization of the precursor **33** can be found in Dixon's article.[45]

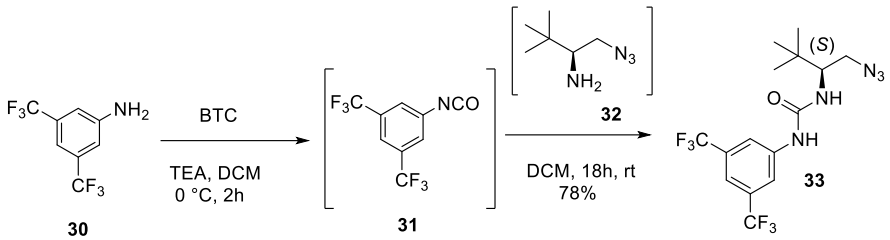

A 5 mL glass vial connected with nitrogen inlet, was charged with 3,5-Bis(trifluoromethyl)aniline (50 mg, 0.22 mmol, 1.0 equiv.) and TEA (2.0 equiv., 0.44 mmol, 0.06 mL) dissolved in 1.5 mL of DCM. The solution of triphosgene (BTC) (78 mg, 0.26 mmol, 1.2 equiv.) in 1.5 mL was added to a solution at 0 °C. The mixture was then stirred at 0 °C for 2 h. Afterwards, free aminoazide **32** (1.1 equiv., 35 mg) was dissolved in 1.5 mL of dry DCM and added to the reaction mixture. Stirring was continued at room temperature overnight. After the consumption of starting material (TLC check in *n*-hexane/ethyl acetate 5:1), the reaction was stopped, and column chromatography was done. The crude was purified by silica gel column chromatography using eluent *n*-hexane/ethyl acetate 8:2. The product **33** was obtained as white solid (67 mg, 78% yield).

^{1}H NMR of urea-azide 33 (300 MHz, $CDCl_3$) δ ppm: 1.02 (s, 9H), 3.39 (dd, 1H), 3.66 (dd, 1H), 3.87 (m, 1H), 4.75 (d, 1H), 6.80 (s, 1H), 7.54 (s, 1H), 7.91 (s, 2H)

^{19}F NMR of urea-azide 33 (282.1 MHz, $CDCl_3$) δ ppm: -63.07

Synthesis of the BIMP catalyst 34:

The synthesis of the catalyst **34** was prepared according to the previous synthesis (for example catalyst **27**), following Dixon's article.[45]

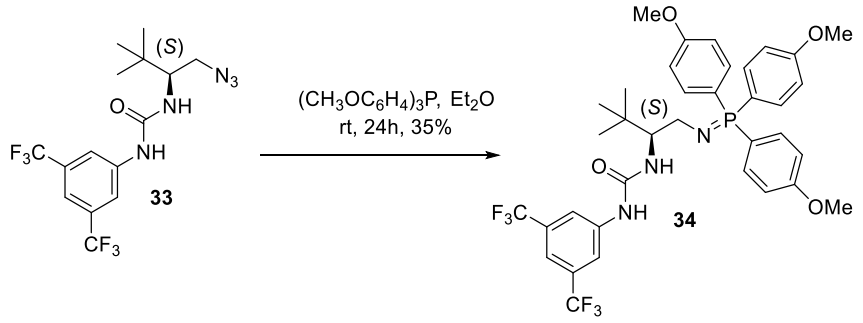

In the 5 mL glass vial with the septum was added 65 mg (0.16 mmol, 1.0 equiv.) of urea-azide **33** and 56.3 mg (0.16 mmol, 1.0 equiv.) of tris(4-methoxyphenyl) phosphine in 1 mL of dry Et_2O. After the reaction completion, the solvent was removed under the flow of nitrogen. The residue was triturated with *n*-pentane/diethyl ether 5:1 (2x1 mL) and filtered off. The residual solid was washed the second time with 10 mL *n*-pentane/diethyl ether 4:1 on fritted Büchner filter funnel, the solid was collected and dried on high vacuum. The catalyst **34** was isolated as a white solid (40 mg, 35% yield).

^{1}H NMR of BIMP catalyst 34 (300 MHz, $CDCl_3$) δ ppm: 0.88 (s, 9H), 3.10 (bs, 1H), 3.49 (bs, 2H), 3.79 (s, 9H), 6.88-6.93 (m, 7H), 7.24-7.27 (dd, 2H), 7.49-7.56 (dd, 6H)

^{19}F NMR of BIMP catalyst 34 (282.1 MHz, $CDCl_3$) δ ppm: -62.92

^{31}P NMR of BIMP catalyst 34 (121.2 MHz, $CDCl_3$) δ ppm: 25.75

6.3.4 Synthesis of BIMP derived from L-*tert*-leucine and electron rich phosphines

The catalysts **35** and **36** are ***new compounds*** and the synthesis was performed between previously synthetized thiourea-azide **24** and electron rich phosphines (*rac*-BIDIME or SPhos).

Synthesis of the BIMP catalysts 35a* and 35b*:

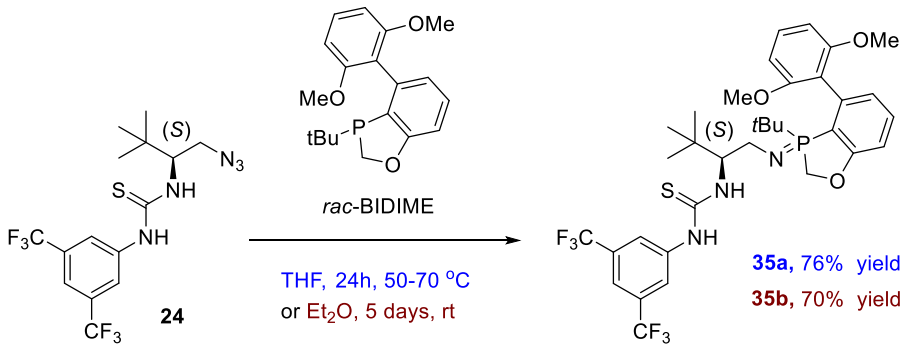

Synthesis of the BIMP catalyst 35a* (50-70 ^{o}C in THF):

In a high-pressure vial (10 mL) was added 50 mg (0.12 mmol, 1.0 equiv.) of thiourea-azide **24** and 39.6 mg (0.12 mmol, 1.0 equiv.) of ***rac*-BIDIME** in 2 mL of dry THF. The reaction mixture was stirred at 50 °C overnight, under N_2 conditions. The reaction was checked the day after by TLC in *n*-hexane/ethyl acetate 1:1 (the starting material was still visible). The reaction mixture was further heated at 70 ^{o}C for 5h and checked by NMR. By ^{19}F NMR and ^{31}P NMR starting azide and phosphine were consumed, so the reaction was stopped and THF was removed under the flow of nitrogen. The crude (residue after removing the solvent) was triturated with 1 mL of dry *n*-pentane for 15 min. Solvent was filtered off and the sample was dried under the flow of nitrogen. 66 mg of the catalyst **35a** was isolated as yellow solid (~76% yield).

By ESI positive, molecular ion of the catalyst is visible, while ^{1}H NMR is showing more complex spectra, indicating that the molecule probably exists as a mixture of rotamers (*t*-Bu groups (0.85-1 ppm), -OMe groups (3.62-3.79 ppm)). Due to the complexity of the signals by ^{19}F NMR and ^{31}P NMR, further analysis is required for elucidation.

^{1}H NMR of BIMP catalyst 35a* (300 MHz, $CDCl_3$)

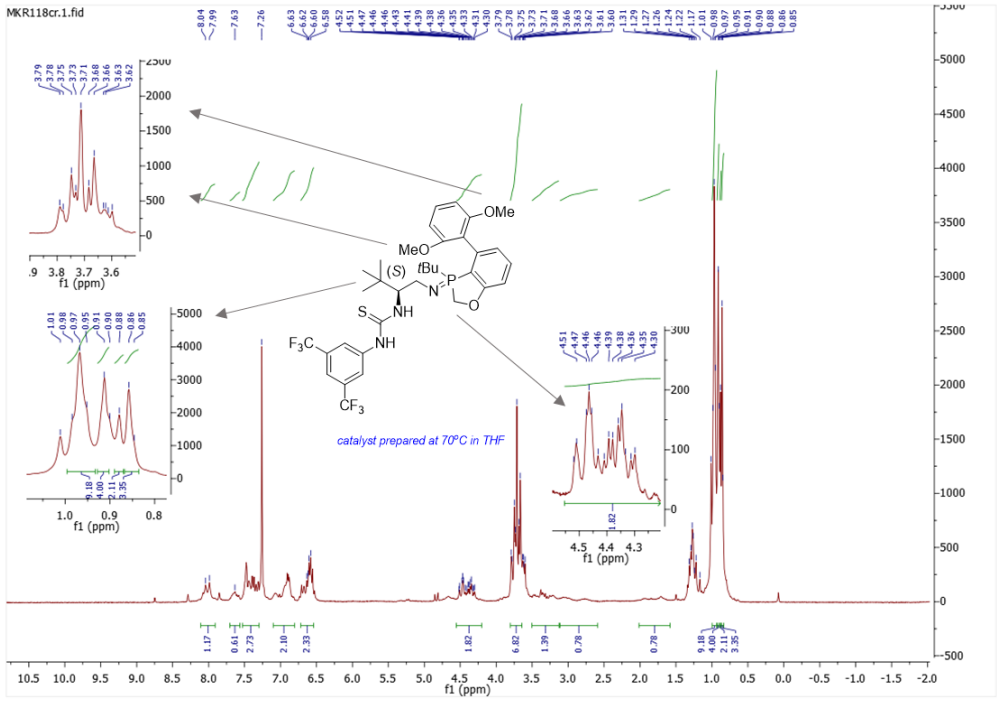

^{31}P NMR of BIMP catalyst 35a* (121.2 MHz, $CDCl_3$)

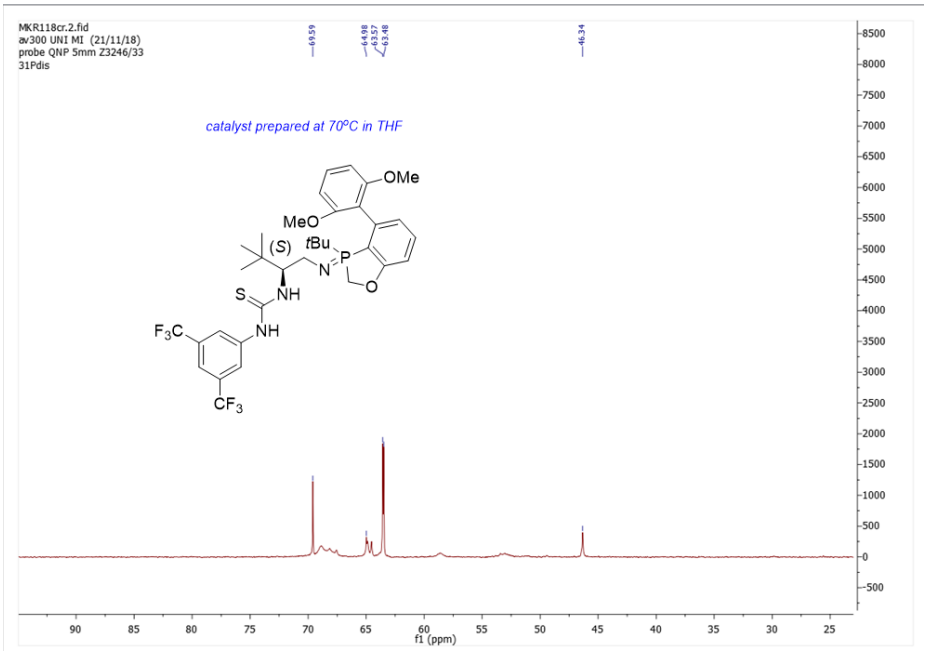

^{19}F NMR of BIMP catalyst 35a* (282.1 MHz, $CDCl_3$)

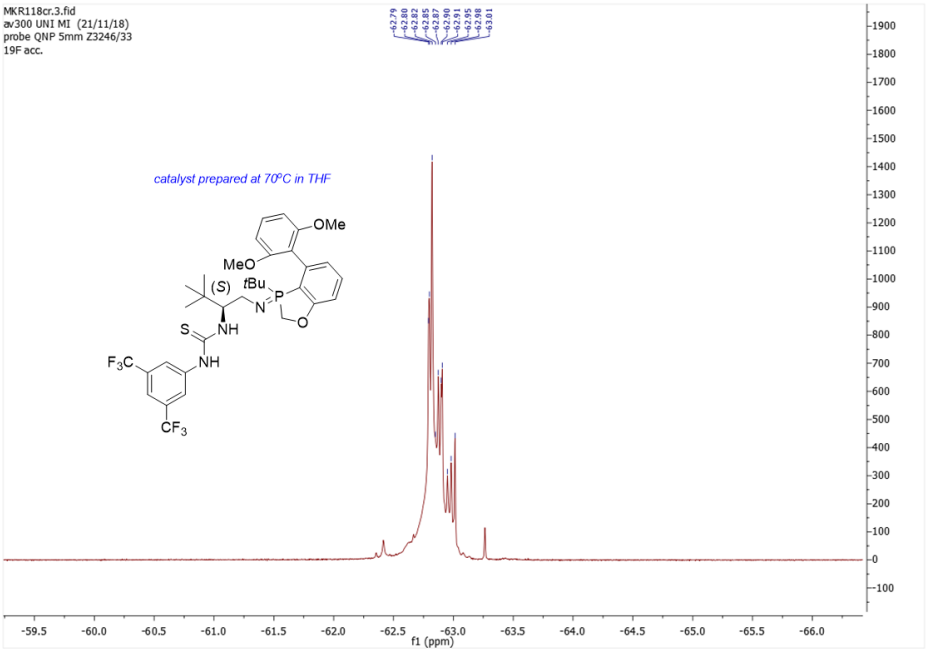

ESI positive of BIMP catalyst 35a*

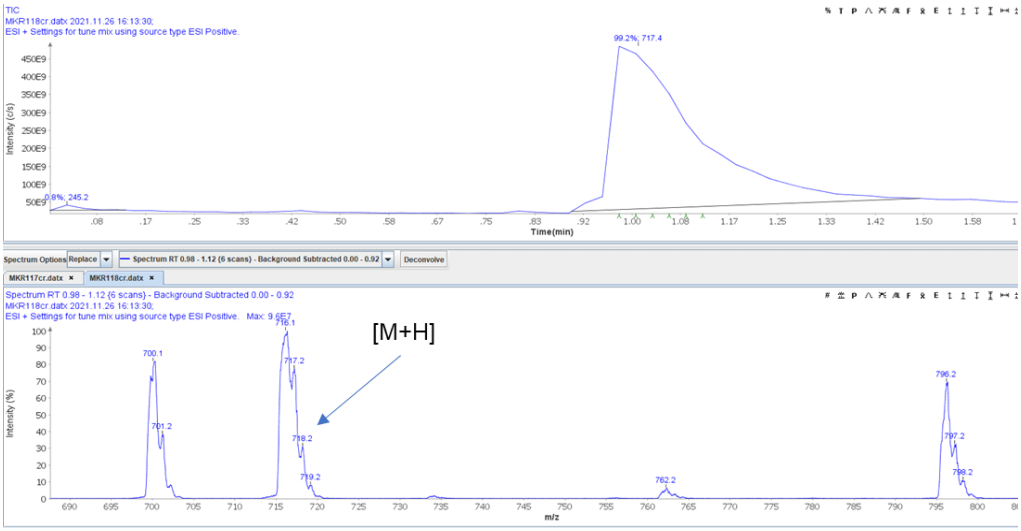

Synthesis of BIMP catalyst 35b* (room temperature in Et_2O):

In the two-necked flask was added 50 mg (0.12 mmol, 1.0 equiv.) of thiourea-azide **24** and 39.6 mg (0.12 mmol, 1.0 equiv.) of ***rac*-BIDIME** in 2 mL of dry Et_2O. The reaction mixture was stirred at room temperature for 5 days. The reaction was monitored by TLC and ^{1}H NMR, ^{19}F NMR and ^{31}P NMR. After 5 days, solvent was removed under the flow of nitrogen. 60 mg of the residue (catalyst **35b**) was obtained as a pale-yellow solid (~70% yield).

By ESI positive, molecular ion of the catalyst is the most intensive, showing cleaner mass spectra compared to the catalyst prepared on higher temperature. Nevertheless, ^{31}P NMR showed the presence of unreacted phosphine, while ^{19}F NMR unreacted organoazide.

^{1}H NMR of BIMP catalyst 35b* (300 MHz, $CDCl_3$)

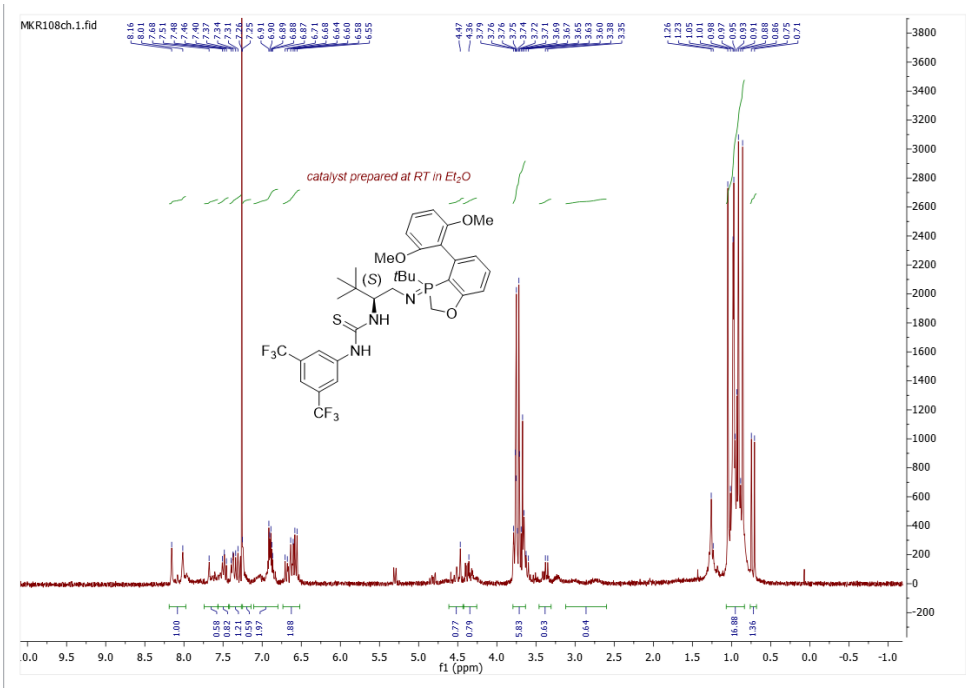

^{31}P NMR of BIMP catalyst 35b* (121.2 MHz, $CDCl_3$)

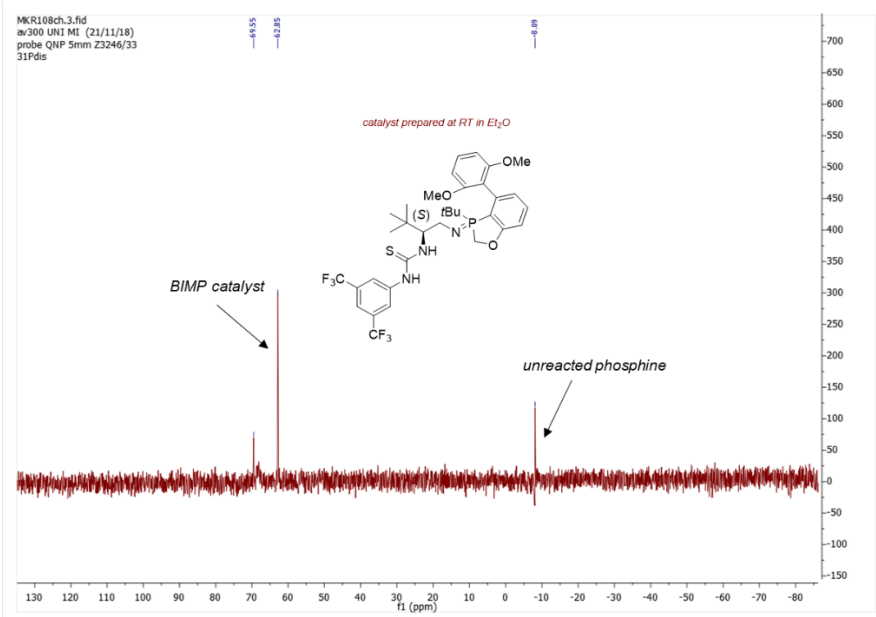

^{19}F NMR of BIMP catalyst 35b* (282.1 MHz, $CDCl_3$)

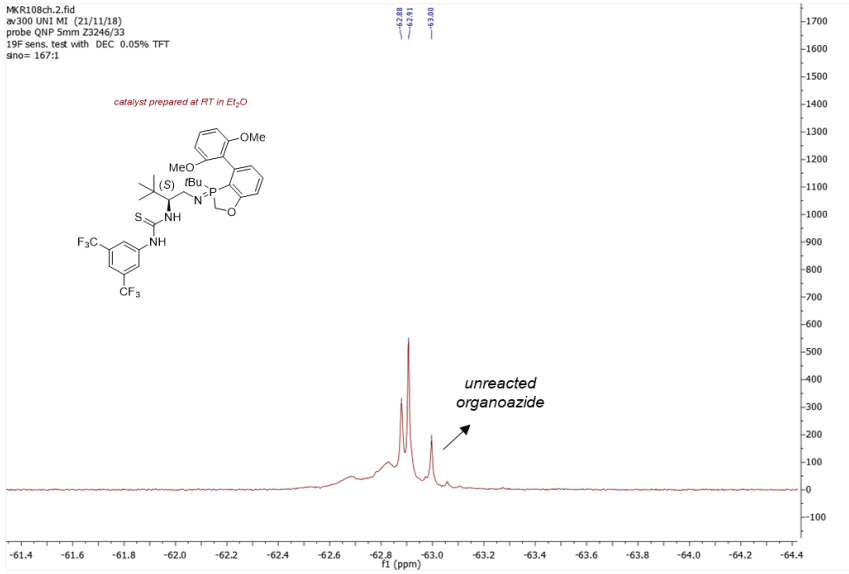

ESI positive of BIMP catalyst 35b*

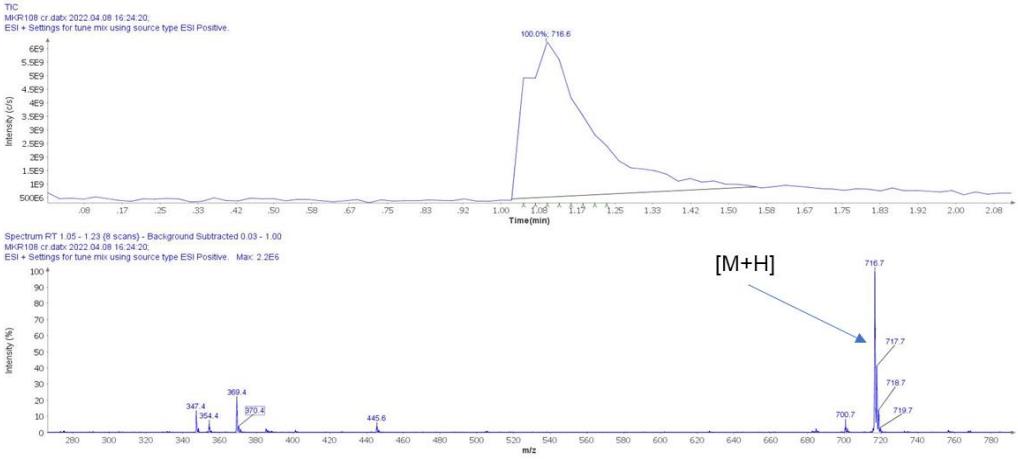

Synthesis of the BIMP catalysts 36a* or intermediate 36b*:

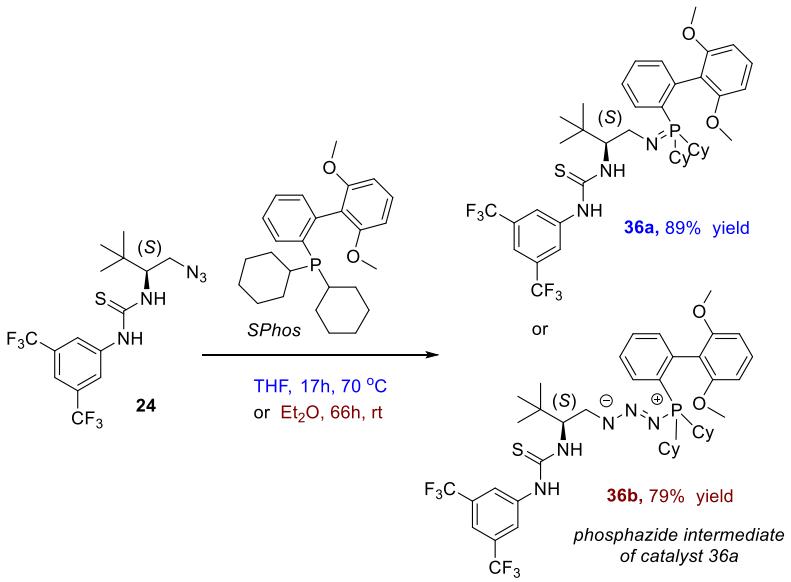

Synthesis of the BIMP catalyst 36a* (70 ºC in THF):

In a high-pressure vial (10 mL) was added 100 mg (0.24 mmol, 1.0 equiv.) of azide **24** and 98.5 mg (0.24 mmol, 1.0 equiv.) of phosphine **SPhos** in 4 mL of dry THF. The reaction mixture was stirred at 70 °C overnight, under N_2 conditions. After 17h, the reaction mixture was checked by ^{31}P NMR (providing the best indication about conversion to the product). The starting material was consumed, THF was removed under the flow of nitrogen and dried additionally on high-vacuum pump. 170 mg of the catalyst **36a** was obtained, as a shiny light-yellow solid (~89% yield).

^{1}H NMR of BIMP catalyst 36a* (300 MHz, $C_6D_5CD_3$)

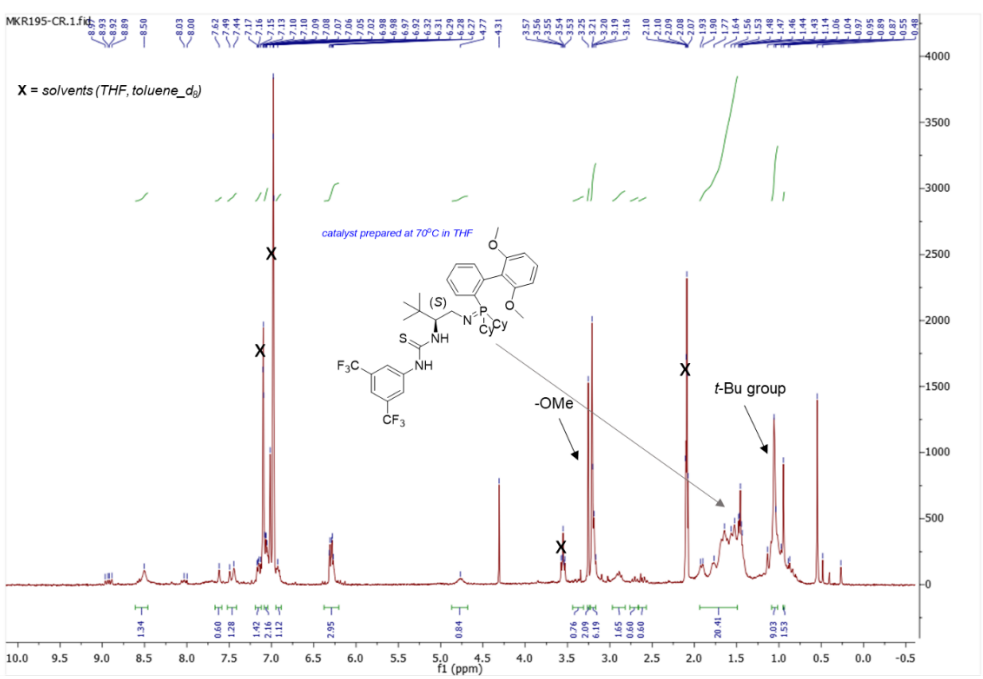

^{19}F NMR of BIMP catalyst 36a* (282.1 MHz, $C_6D_5CD_3$)

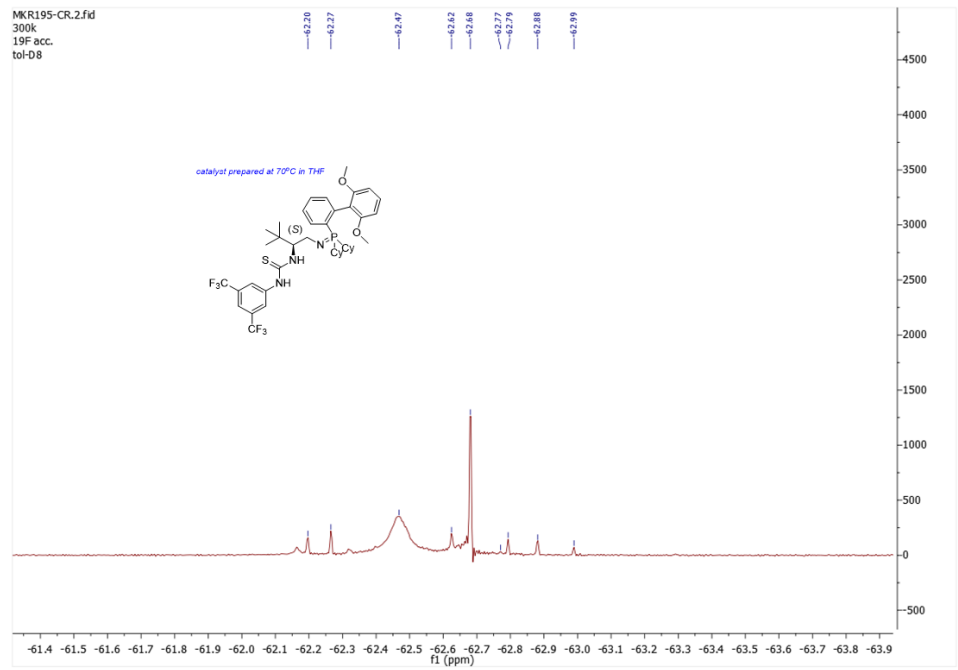

^{31}P NMR of BIMP catalyst 36a* (121.2 MHz, $C_6D_5CD_3$)

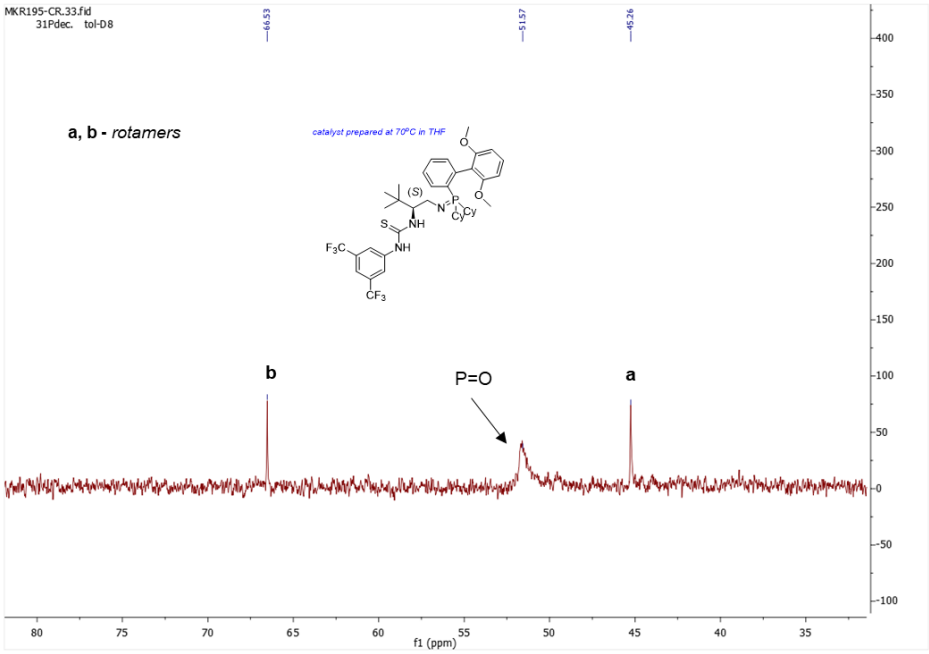

^{13}C NMR of BIMP catalyst 36a* (75 MHz, $CDCl_3$)

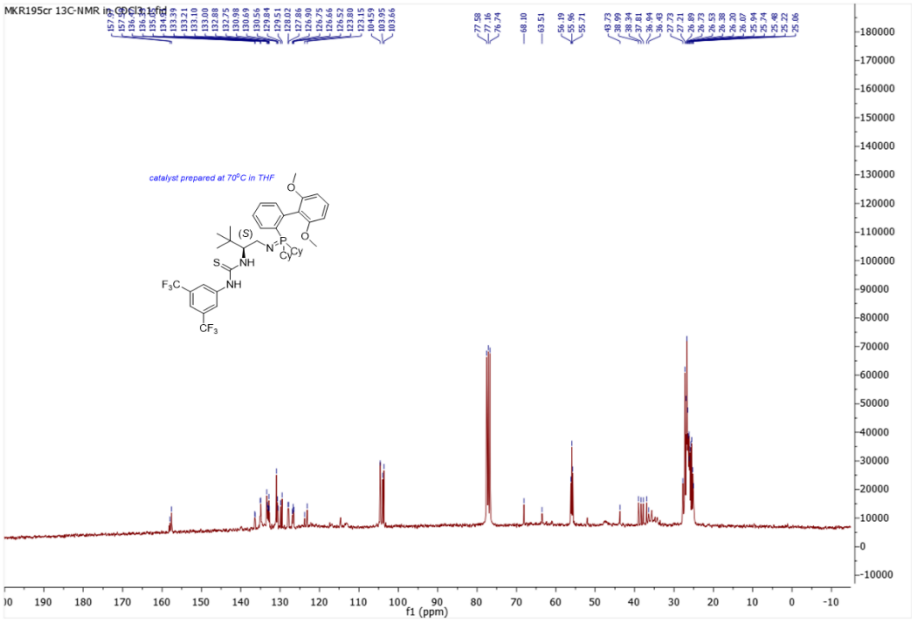

HR-MS of BIMP catalyst 36a*

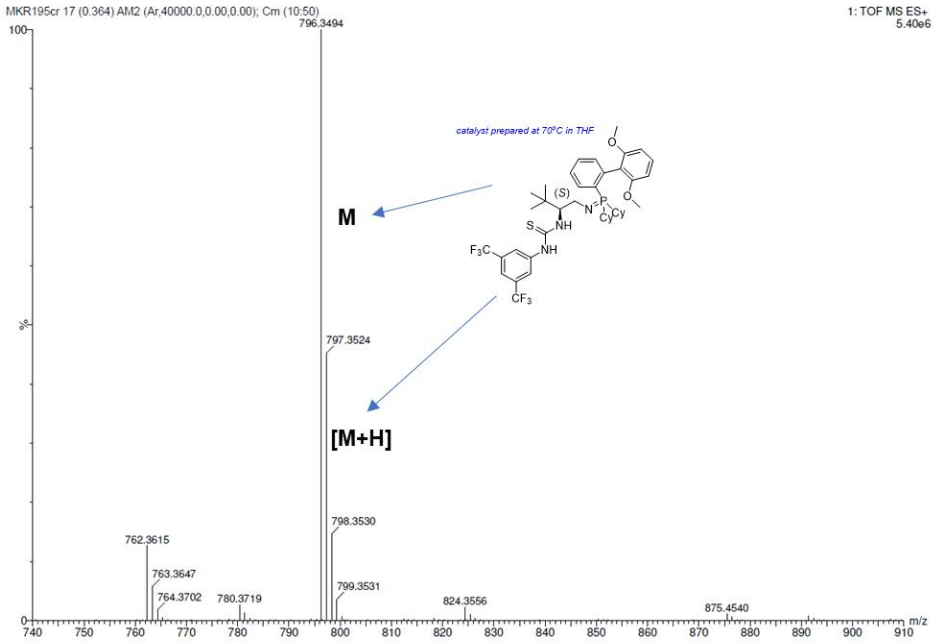

Elemental composition analysis of BIMP catalyst 36a*

Elemental Composition Report

Single Mass Analysis
Tolerance = 5.0 PPM / DBE: min = -5.0, max = 300.0
Element prediction: Off
Number of isotope peaks used for i-FIT = 7

Monoisotopic Mass, Even Electron Ions
1 formula(e) evaluated with 1 results within limits (all results (up to 1000) for each mass)
Elements Used:
C: 41-41 H: 52-53 N: 3-3 O: 2-2 Na: 0-1 S: 1-1 P: 1-1 F: 6-6

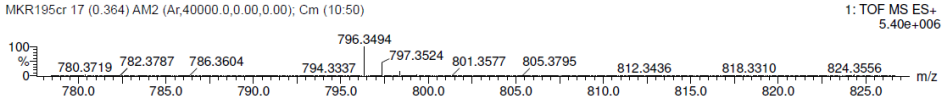

Minimum:				-5.0				
Maximum:		5.0	5.0	300.0				
Mass	Calc. Mass	mDa	PPM	DBE	i-FIT	Norm	Conf(%)	Formula
796.3494	796.3500	-0.6	-0.8	14.5	1612.0	n/a	n/a	C41 H53 N3 O2 S P F6

Synthesis of the BIMP phosphazide intermediate 36b* (room temperature in Et_2O):

In a two-necked flask was added 195 mg (0.47 mmol, 1.0 equiv.) of azide **24** and 193 mg (0.47 mmol, 1.0 equiv) of phosphine **SPhos** in 6 mL of dry Et_2O. The reaction mixture was monitored by TLC (*n*-hexane/ethyl acetate 7:3), ^{1}H NMR and ^{31}P NMR. Starting material disappeared after 66h stirring at room temperature.

Interestingly, although the consumption of the starting material was observed, the precatalyst **36b** showed very poor solubility in Et_2O and even in more polar solvents such as methanol. Physical appearance as well as spectral data was different from the catalyst **36a** (prepared at higher temperatures in THF). 400 mg of the product **36b** was isolated as amorphous milky solid (~79% yield).

In order to understand the behavior of s-*cis* / *s-trans* – phosphazide isomers and see if it is possible to convert one isomer to another, ^{1}H NMR, ^{19}F NMR and ^{31}P NMR analysis were performed on room temperature in deuterated chloroform as well at 50 ^{o}C in deuterated toluene. As expected, (see spectra below) at room temperature both isomers were visible by ^{19}F NMR and ^{31}P NMR (most likely s-*trans* isomer as a major, due to the high steric hindrance on phosphorus), while ^{19}F NMR and ^{31}P NMR spectra carried out at 50 ^{o}C showed the interconversion of the isomers and signals merging.

^{1}H NMR of phosphazide 36b* at room temperature (300 MHz, $CDCl_3$)

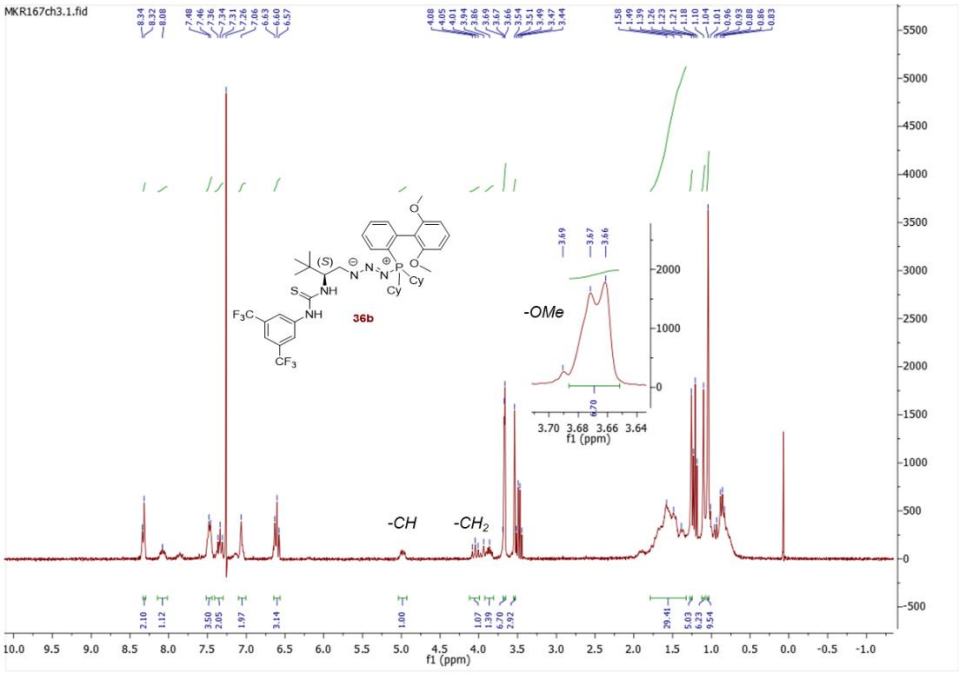

^{31}P NMR of phosphazide 36b* at room temperature (121.2 MHz, $CDCl_3$)

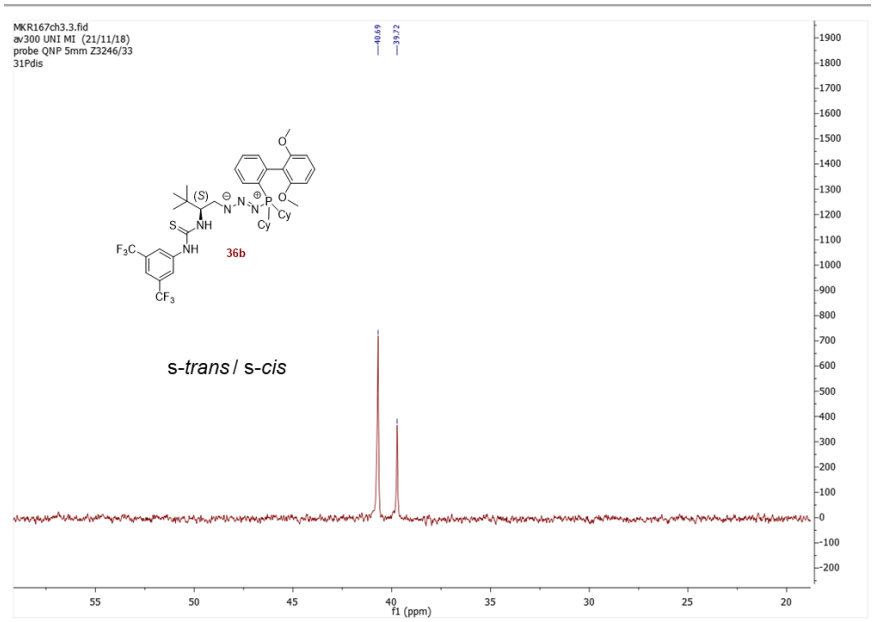

^{19}F NMR of phosphazide 36b* at room temperature (282.1 MHz, $CDCl_3$)

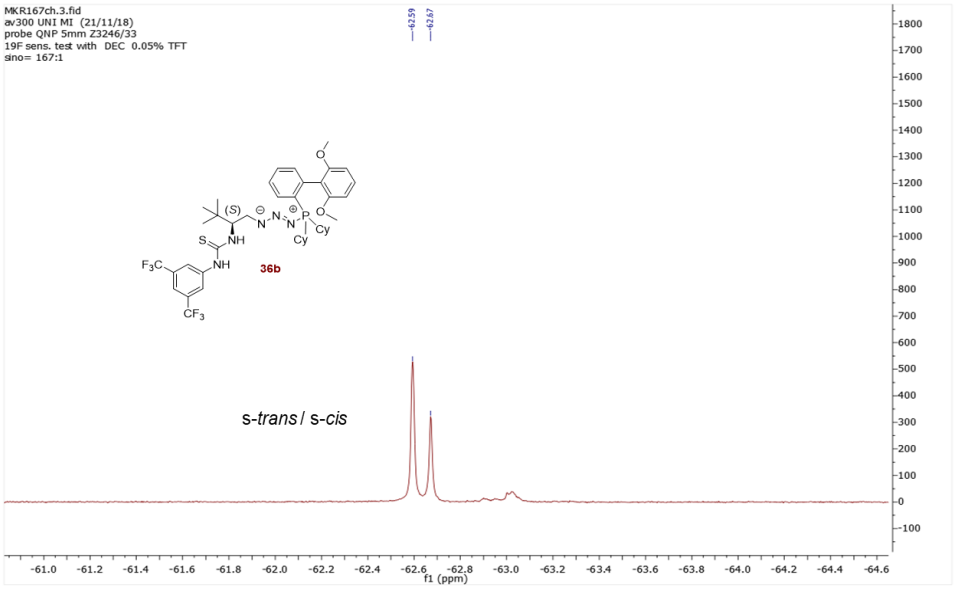

^{1}H NMR of phosphazide 36b* at 50 ºC (300 MHz, $C_6D_5CD_3$)

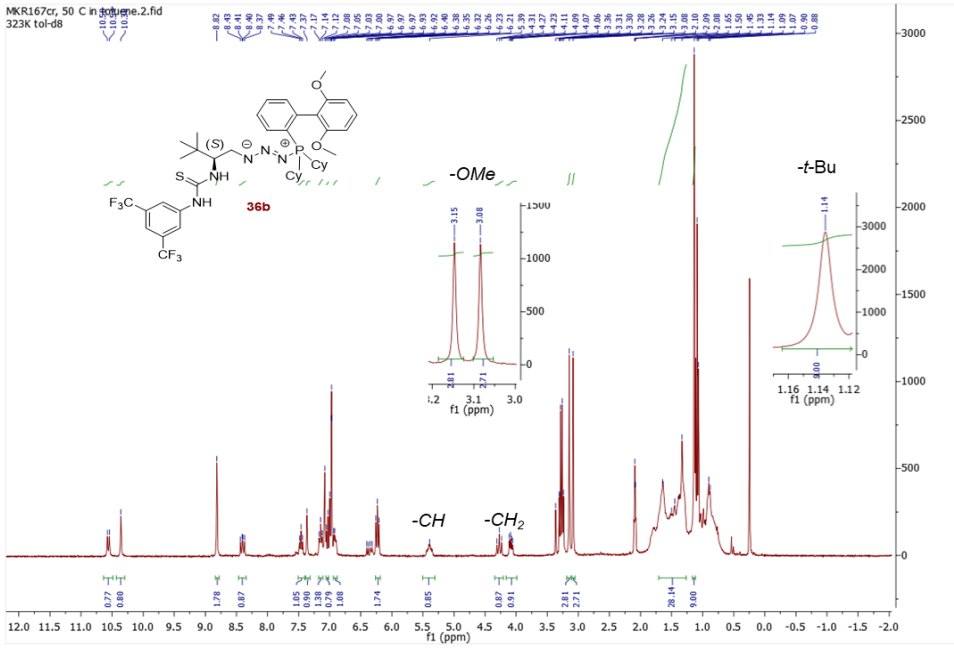

^{31}P NMR of phosphazide 36b* at 50 ºC (121.2 MHz, $C_6D_5CD_3$)

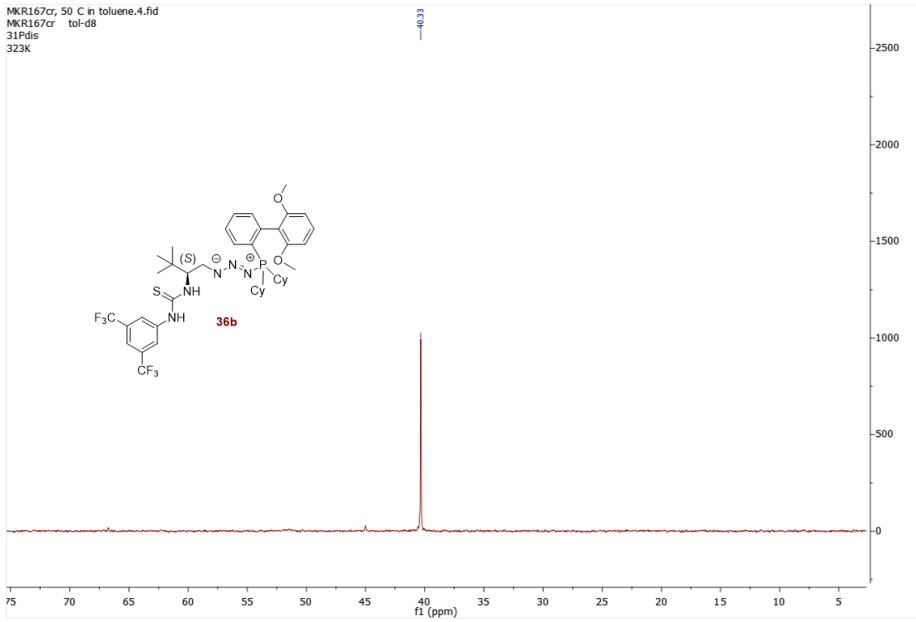

^{19}F NMR of phosphazide 36b* at 50 ºC (282.1 MHz, $C_6D_5CD_3$)

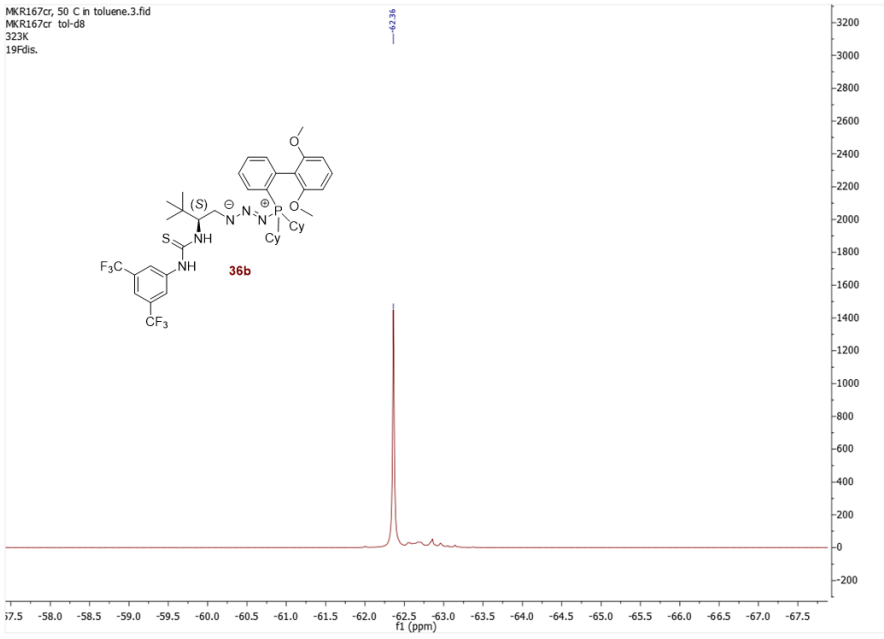

HR-MS of phosphazide 36b*

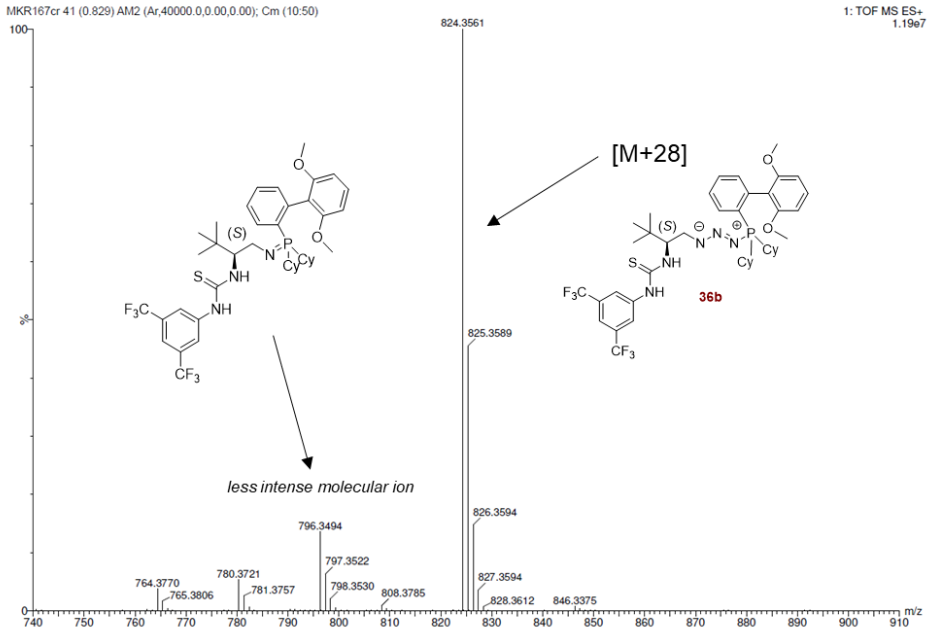

Elemental composition analysis of phosphazide 36b*

Elemental Composition Report

Single Mass Analysis
Tolerance = 5.0 PPM / DBE: min = -5.0, max = 300.0
Element prediction: Off
Number of isotope peaks used for i-FIT = 7

Monoisotopic Mass, Even Electron Ions
1 formula(e) evaluated with 1 results within limits (all results (up to 1000) for each mass)
Elements Used:
C: 41-41 H: 52-53 N: 3-3 O: 2-2 Na: 0-1 S: 1-1 P: 1-1 F: 6-6

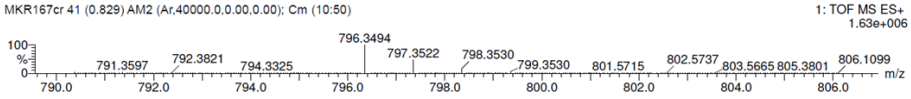

Minimum:				-5.0				
Maximum:		5.0	5.0	300.0				
Mass	Calc. Mass	mDa	PPM	DBE	i-FIT	Norm	Conf(%)	Formula
796.3494	796.3500	-0.6	-0.8	14.5	1748.3	n/a	n/a	C41 H53 N3 O2 S P F6

6.3.5 Synthesis of BIMP bearing two stereogenic centers and thiourea moiety

The synthesis of intermediates **37-41** as well as the catalyst **42** were prepared according to the Dixon's procedure.[74] The catalysts **42a** and **42b** are ***new compounds***.

General procedure for the synthesis of intermediates 38a/38b:

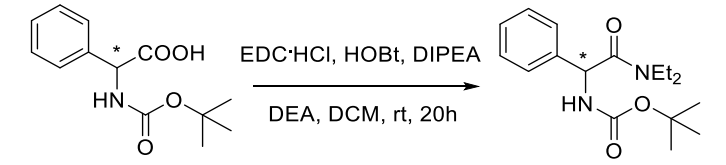

37a, *N*-Boc-D-phenylglycine (*R*)
37b, *N*-Boc-L-phenylglycine (*S*)

38a, 85% yield, (*R*)
38b, 84% yield, (*S*)

To a stirred solution of coupling reagent EDC hydrochloride (253 mg, 1.32 mmol, 1.1 equiv.) and 1- hydroxybenzotriazole hydrate, HOBt (178 mg, 1.32 mmol, 1.1 equiv.) in dry DCM (10 mL) under nitrogen atmosphere at room temperature was added *N*, *N*-diisopropylethylamine-DIPEA (0.3 mL, 1.8 mmol, 1.5 equiv.) and diethylamine-DEA (0.135 mL, 1.32 mmol, 1.1 equiv.) sequentially.

N-Boc-D-α-phenylglycine **37a** / *N*-Boc-L-α-phenylglycine **37b** (300 mg, 1.2 mmol, 1.0 equiv.) was added in one portion and the reaction mixture was stirred for 20 h. After the consumption of starting material (check by TLC in *n*-hexane/ethyl acetate 1:1), stained by $KMnO_4$), the reaction was diluted with Et_2O (20 mL), washed with 0.5 M HCl (2 x 20 mL) and the aqueous phase extracted with Et_2O (10 mL). The combined organic phases were washed with sat. aq. $NaHCO_3$ (20 mL) and brine (20 mL), dried (Na_2SO_4), filtered and concentrated in vacuo to afford the products **38a** (*R*) or **38b** (*S*) enantiomer as yellow solids in ~85% yield, which were used without further purification.

^{1}H NMR of 38a/38b (300 MHz, $CDCl_3$) d ppm: 0.92-0.97 (t, 3H), 1.08-1.13 (t, 3H), 1.41 (s, 9H), 3.07-3.19 (1H), 3.22-3.34 (2H), 3.44-3.54 (1H), 5.5-5.53 (d, 1H), 6.02-6.04 (d, 1H), 7.28-7.39 (m, 5H)

^{13}C NMR of 38a/38b (75 MHz, $CDCl_3$) d ppm: 12.63, 13.66, 28.37, 40.4, 41.6, 55.1, 79.53, 127.7, 128.1, 128.92, 138.64, 155.04, 169.09

Mass (ESI+) of 38a/38b: m/z=329 [M (306) + 23], fragment without Boc protecting group (m/z=207 [206+H])

General procedure for the synthesis of intermediates 39a/39b:

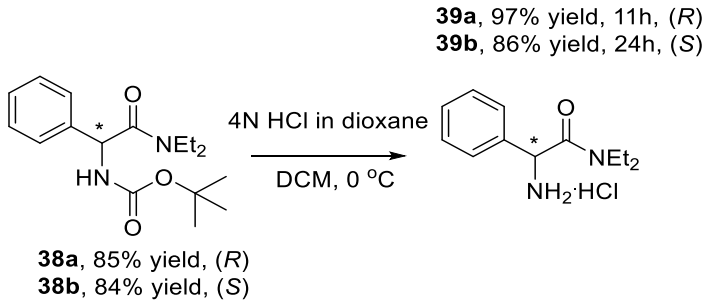

To a vigorously stirred solution of the **38a** (*R* enantiomer) or **38b** (*S* enantiomer) (300 mg, 0.97 mmol) in DCM (5 mL) under N_2 atmosphere at 0 °C was added 4 N HCl in 1,4-dioxane (2.33 mL, 9.3 mmol, 9.6 equiv.) over 10 min. The reaction mixture was stirred for 11h (in case of *R* enantiomer) or 24h (in case of *S* enantiomer) at 0 °C. The reactions were monitored by ^{1}H NMR in $CDCl_3$ (tracking the disappearance of Boc group). After the conversion of **38a/38b** to hydrochloride salt, the crudes were concentrated in vacuo to afford the product **39a** as light brown solid (230 mg, 97% yield) and product **39b** as light green solid (220 mg, 86% yield). The isolated salts were used without further purification.

^{1}H NMR of 39a/39b (300 MHz, $CDCl_3$) d ppm: 0.85-0.90 (t, 3H), 1.05.1.10 (t, 3H), 3.18 and 3.45 (m, 4H), 5.61 (d, 1H), 7.40 (m, 3H), 7.61 (m, 2H), 8.84 (bs, 2H)

^{13}C NMR of 39a/39b (75 MHz, $CDCl_3$) d ppm: 12.46, 13.25, 40.63, 41.81, 55.22, 129.14, 129.32, 129.69, 132.37, 166.49

Mass (ESI+) of 39a/39b: m/z=207 (R-NH_3^+ ion), m/z=229 [R-NH_2 + 23]

General procedure for the synthesis of isothiocyanates 40a/40b:

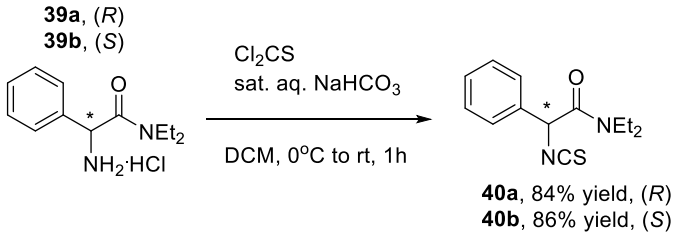

To a vigorously stirred solution of the hydrochloride salt **39a/39b** (0.816 mmol, 198 mg, 1.0 equiv.) in DCM (12 mL) under nitrogen atmosphere at 0 °C was added sat. aq. solution $NaHCO_3$ (12 mL), and the biphasic mixture was stirred for 20 min. Stirring was stopped and thiophosgene (0.09 mL, 1.22 mmol, 1.5 equiv.) was added to the organic layer. Immediately, vigorous stirring was restored, and the mixture allowed to warm to room temperature for 1h. The reaction mixture was monitored by TLC (*n*-hexane/ethyl acetate 1:1). After reaction completion, the organic phase was extracted with DCM (2 x 10 mL), washed with brine (10 mL), dried over Na_2SO_4, filtered, and concentrated in vacuo to afford the crude product **40a** as an orange solid (~84% yield, purity by ^{1}H NMR ~80%) or **40b** as a dark green oil (~86% yield, purity by ^{1}H NMR ~93%). The corresponding isothiocyanate **40a/40b** was used without further purification.

^{1}H NMR of 40a/40b (300 MHz, $CDCl_3$) d ppm: 0.96 (t, 3H)**,** 1.13 (t, 3H), 3.08-3.53 (m, 4H), 5.38 (s, 1H), 7.39-7.41 (m, 5H)

General procedure for the synthesis of azides 41a/41b:

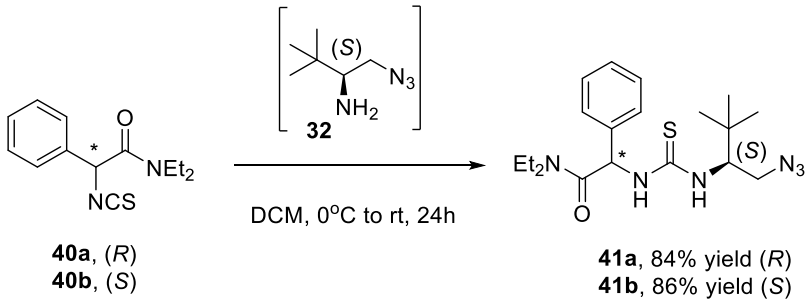

40a, (*R*)
40b, (*S*)

41a, 84% yield (*R*)
41b, 86% yield (*S*)

In a two necked flask connected with nitrogen line and cooled to 0 °C, the corresponding isothiocyanate **40a** or **40b** (114 mg, 0.46 mmol, 1.0 equiv.) was dissolved in 3 mL of dry DCM (0.18 M). Aminoazide **32** (80 mg, 0.56 mmol, 1.2 equiv.) was subsequently added in the solution of isothiocyanate, the reaction mixture was then warmed to room temperature and stirred overnight. The reaction mixture was monitored by TLC in *n*-hexane/ethyl acetate 1:1. After 24h, solvent was removed under reduced pressure and the crude was purified by silica gel column chromatography.

The products **41a/41b** were isolated with *n*-hexane/ethyl acetate 8:2 by column chromatography. **41a** and **41b** were obtained as dark red oils, (150 mg, 84% yield) and (154 mg, 86% yield), respectively.

^{1}H NMR of thiourea-azide 41 (300 MHz, $CDCl_3$)

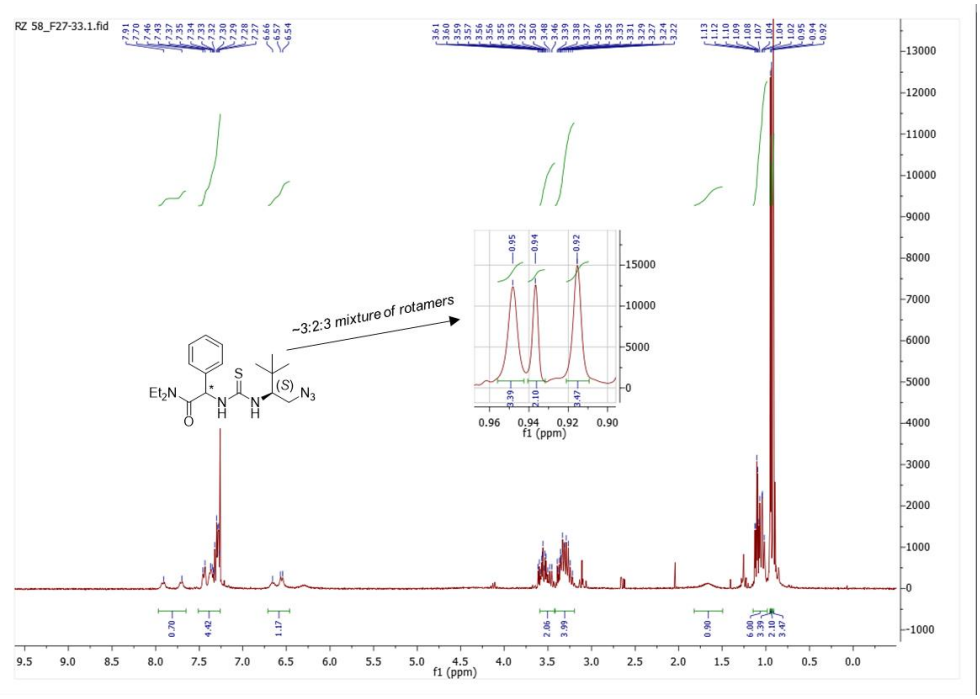

^{13}C NMR of thiourea-azide 41 (75 MHz, $CDCl_3$)

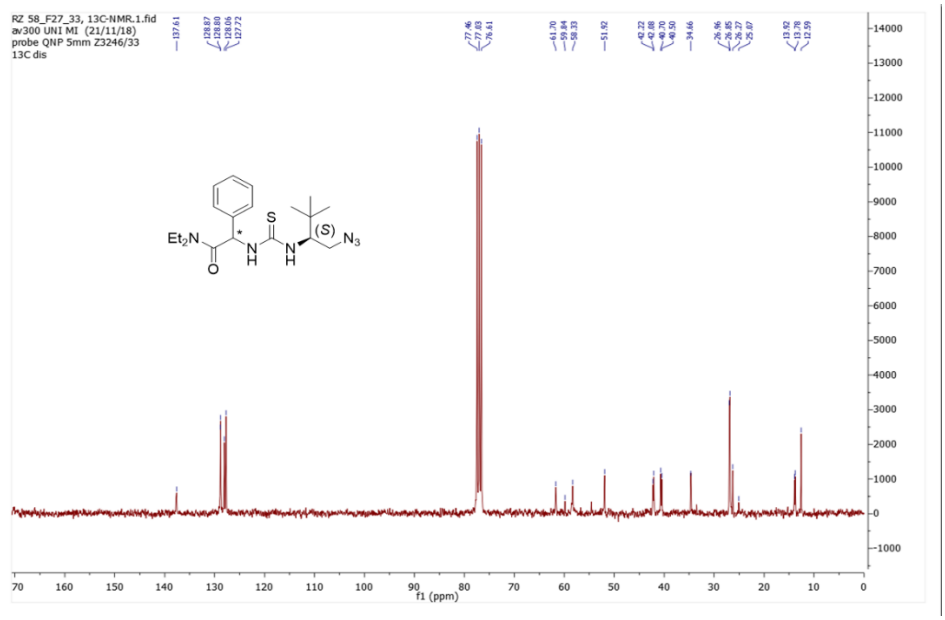

Mass (ESI+) of 41a/41b: visible ion m/z=414 [M+23]

General procedure for the synthesis of the catalysts 42a*/42b*:

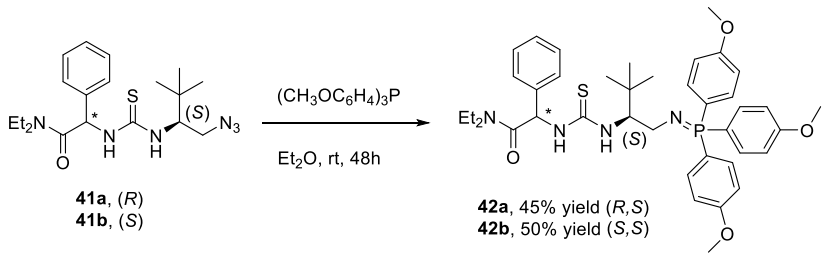

In the 5 mL glass vial with the septum (purged with nitrogen) was added 33 mg (0.084 mmol, 1.0 equiv.) of azide **41a** or **42b** and 30 mg (0.084 mmol, 1.0 equiv.) of tris(4-methoxyphenyl) phosphine in 0.4 mL of dry Et_2O. The reaction mixtures were stirred at room temperature for 48h. The reaction mixture was monitored by ^{1}H NMR and ^{31}P NMR, until the disappearance of starting material. After 48h, the residue of solvent was removed under the flow of nitrogen. The catalyst **42a** (*R,S* diastereomer) was isolated as a light-yellow solid (27 mg, 45% yield), while catalyst **42b** (*S,S* diastereomer) was obtained as a light orange solid (30 mg, 50% yield).

^{1}H NMR of BIMP catalyst 42* (300 MHz, $C_6D_5CD_3$)

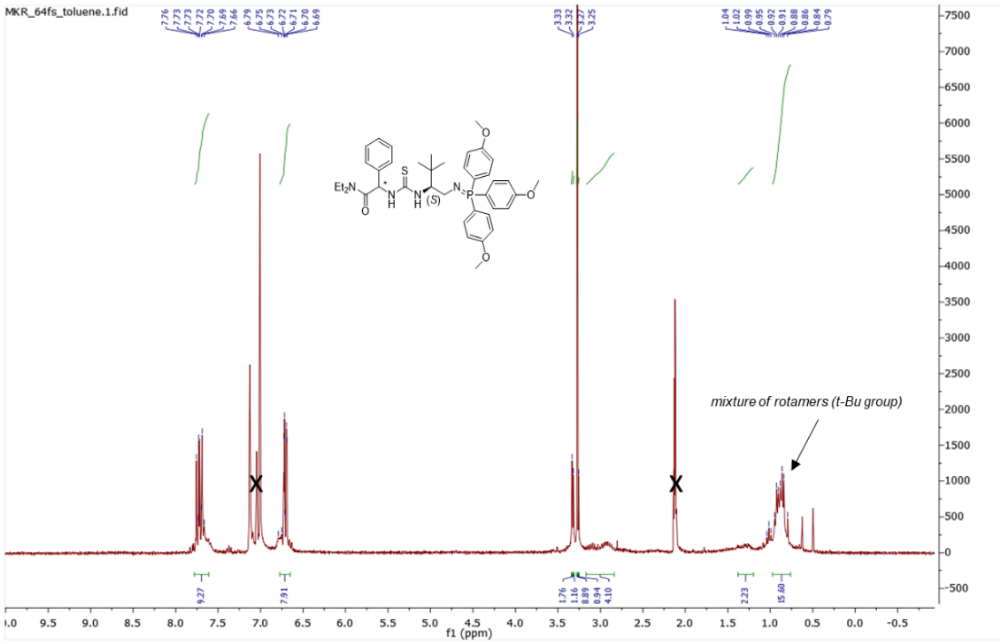

^{31}P NMR of BIMP catalyst 42* (121.2 MHz, $C_6D_5CD_3$)

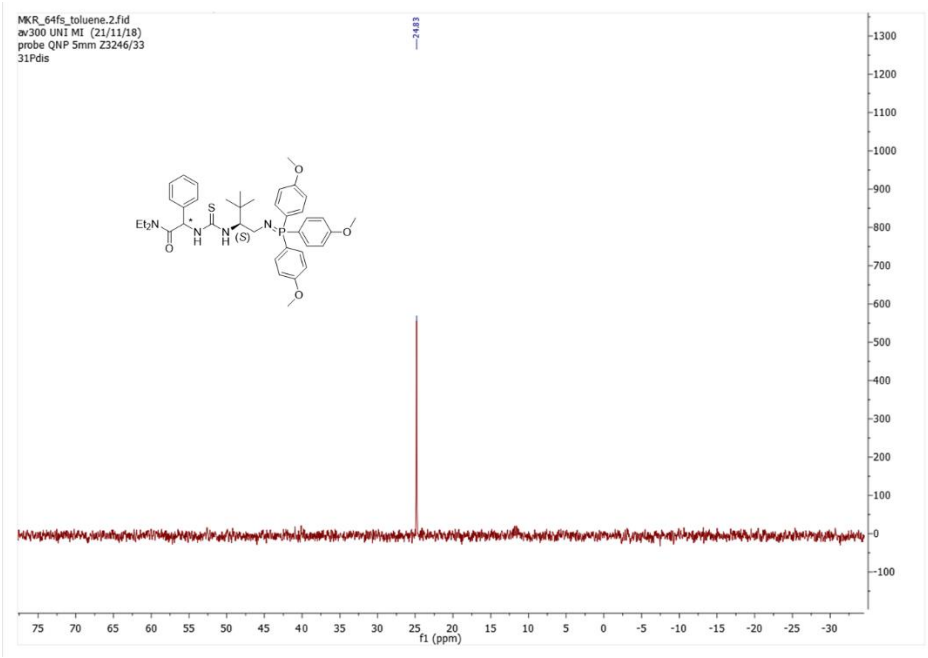

6.3.6 Synthesis of BIMP bearing two stereogenic centers and urea moiety

The intermediate urea-azide **44** is a ***new compound***.

General procedure for the synthesis of urea-azide 44*:

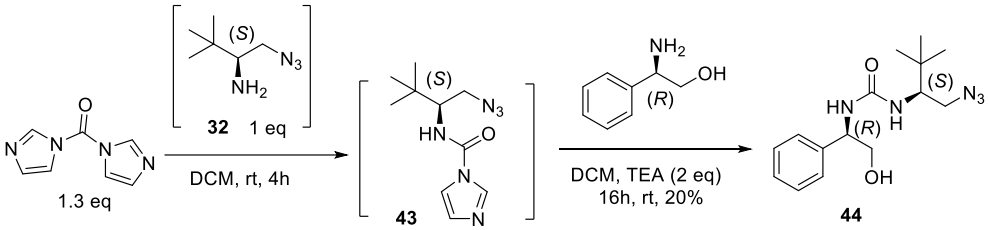

In a 25 mL two-necked flask 135 mg (1.0 equiv.) of carbonyldiimidazole (CDI) under the flow of nitrogen was dissolved in 3 mL of dry DCM. Aminoazide **32** (91 mg, 1.0 equiv.) was dissolved in another 2 mL of dry DCM and added dropwise in the solution of carbonyldiimidazole. The reaction mixture was stirred at room temperature for 4h. After the formation of intermediate **43** (check by TLC), 175 mg, 2.0 equiv. of (*R*)-2-phenylglycinol and 0.18 mL (2.0 equiv.) of freshly distilled TEA was added in the solution and stirred further at room temperature overnight. The intermediate **43** was consumed after 16h, solvent was removed, and the residue was dissolved in 20 mL of ethyl acetate. Organic layer was washed 5 times with water (5x20 mL), dried over Na_2SO_4, filtered and the solvent was removed under reduced pressure. In the residue was added 3 mL of dry Et_2O and stirred for 5 min, to remove impurities. The suspension was filtrated under vacuum and the product **44** was isolated as white solid (45 mg, ~20% yield, 80% pure by ^{1}H NMR). The product **44** contained around 20% of side product (formed symmetric urea of aminoazide **32** with CDI, see ^{13}C NMR spectra below).

^{1}H NMR of urea-azide 44* (300 MHz, $CDCl_3$)

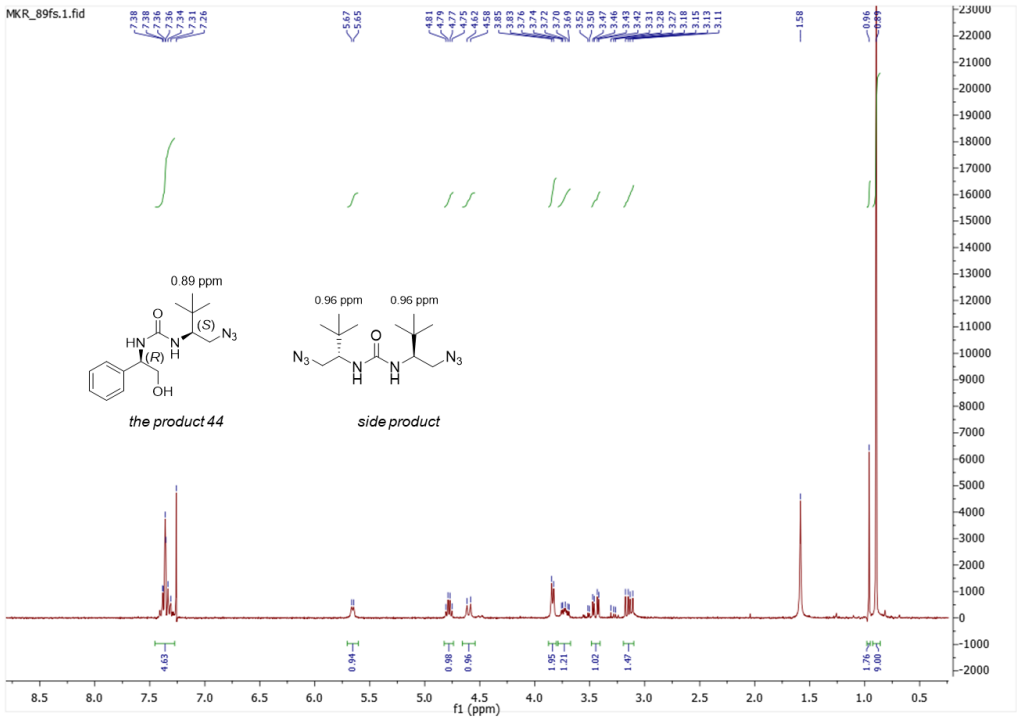

^{13}C NMR of urea-azide 44* (75 MHz, $CDCl_3$)

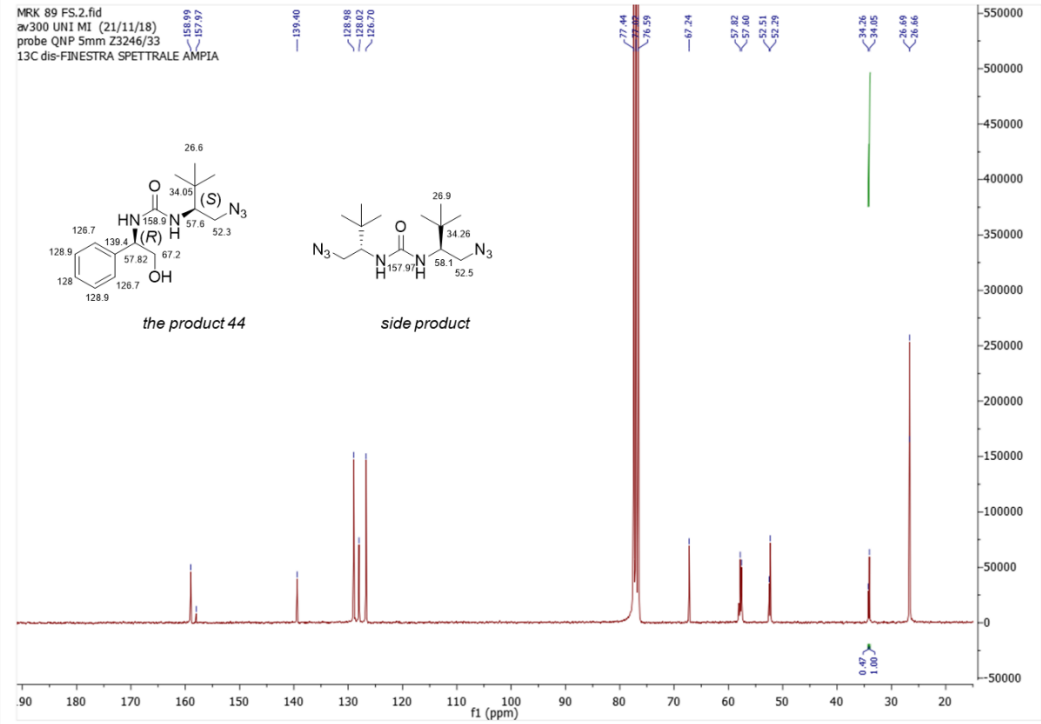

Mass (ESI+) of urea-azide 44*: visible molecular ion m/z=304.6

General procedure for the synthesis of BIMP 45*:

The bifunctional iminophosphorane organocatalyst **45** is a ***new compound*****.**

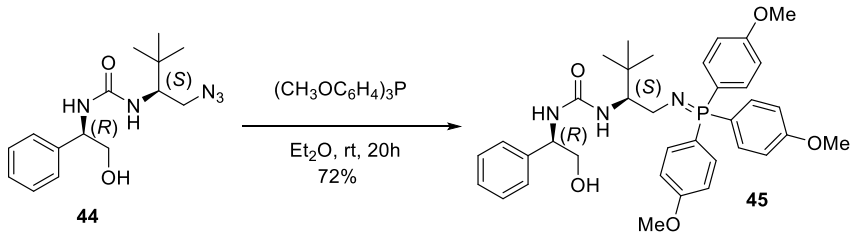

In a two-necked flask connected with nitrogen line was added 45 mg (0.147 mmol, ~1.0 equiv.) of azide **44** and 52 mg (0.147 mmol, 1.0 equiv.) of tris(4-methoxyphenyl) phosphine in 4 mL of dry Et_2O. The reaction mixture was stirred

at room temperature overnight. The consumption of starting material was followed by TLC (*n*-hexane/ethyl acetate 1:1), ^{1}H NMR and ^{31}P NMR. When the reaction is completed (disappearance of azide **44**), solvent was removed under the flow of nitrogen and the catalyst **45** was isolated as white solid containing around 30% unreacted phosphine (67 mg, ~70% yield). The BIMP catalyst **45** was used without further purification.

^{1}H NMR of BIMP catalyst 45* (300 MHz, $CDCl_3$)

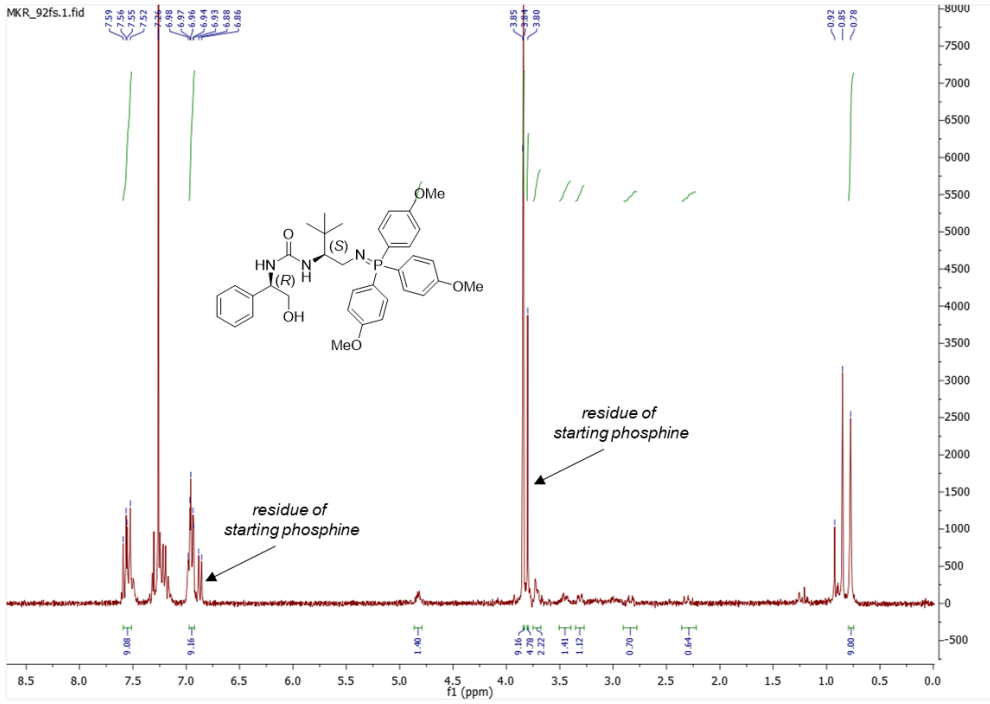

^{31}P NMR of BIMP catalyst 45* (121.2 MHz, $CDCl_3$)

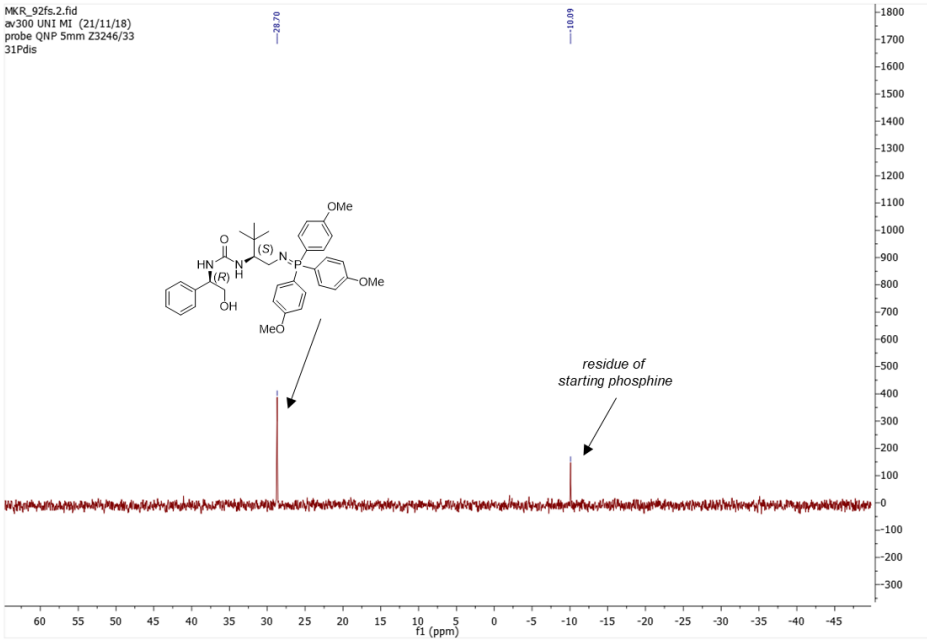

6.3.7 Synthesis of BIMP bearing one stereocenter on organoazide scaffold and stereogenic phosphorus

General procedure for the synthesis of BIMP catalysts 46* and 47*:

The bifunctional iminophosphorane organocatalysts **46** and **47** bearing stereogenic phosphorus are ***new compounds***.

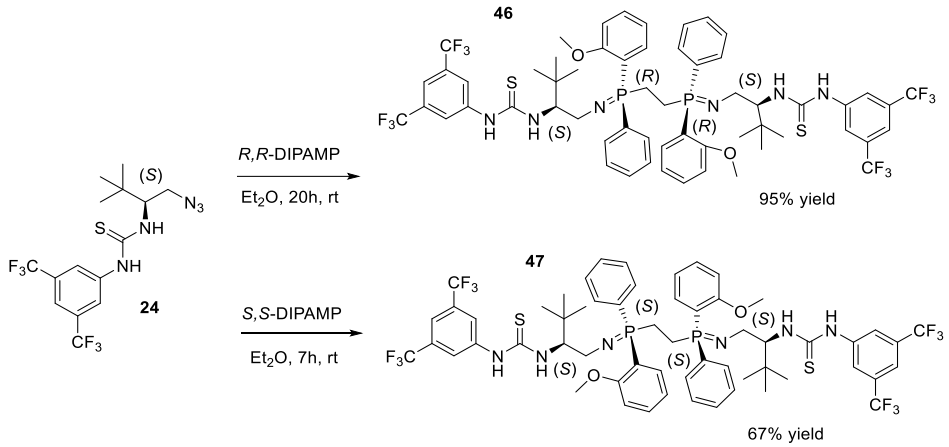

To perform the last step (formation of iminophosphorane via Staudinger reaction) for the catalysts **46/47** synthesis, in both cases the same thiourea-azide **24** was used. The synthesis of **24** was previously described in section 6.3.2.

In the two-necked flask was added 90.1 mg (0.218 mmol, 2.0 equiv.) of azide **24** and 50 mg (0.109 mmol, 1.0 equiv.) of **(*S,S*)-DIPAMP** or **(*R,R*)-DIPAMP** in 2 mL of dry Et_2O. The reaction mixture was stirred at room temperature, under N_2 conditions. Both reactions were followed by TLC (*n*-hexane/ethyl acetate 1:1) and ^{31}P NMR. In case of the catalyst **46**, starting material was consumed after 20h, and in case of catalyst **47** the reaction was done after 7h.

After removal of Et_2O, the residue was triturated with *n*-pentane (3x3 mL), filtered, the solid was collected and dried in vacuo additionally. The bisiminophosphoranes **46** and **47** were obtained as white solids in 95% and 67% yield, respectively. They were used without further purification.

^{1}H NMR of BIMP catalyst 46* at room temperature (300 MHz, $C_6D_5CD_3$)

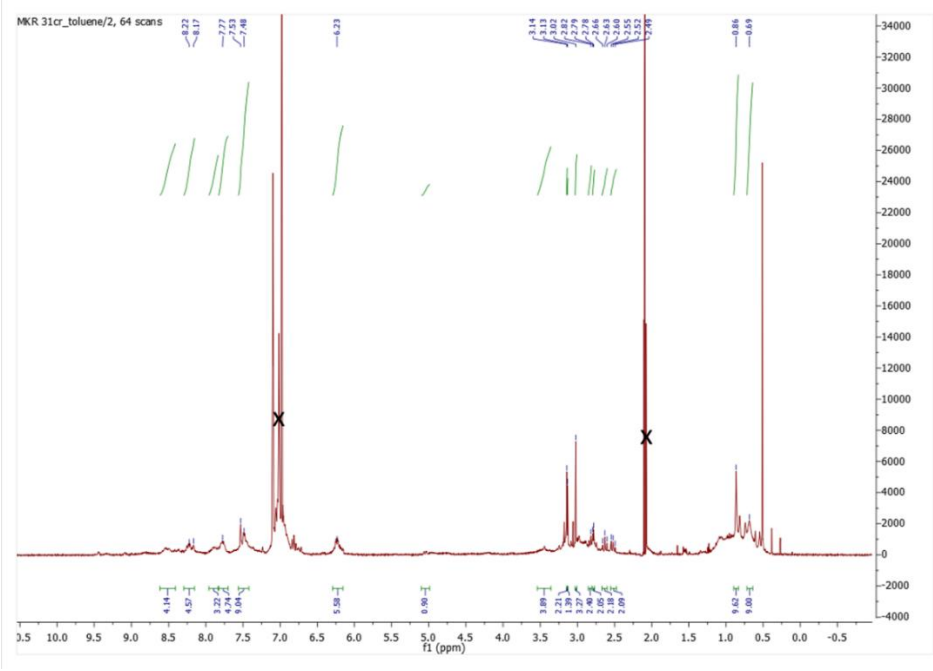

^{31}P NMR of BIMP catalyst 46* at room temperature (121.2 MHz, $C_6D_5CD_3$)

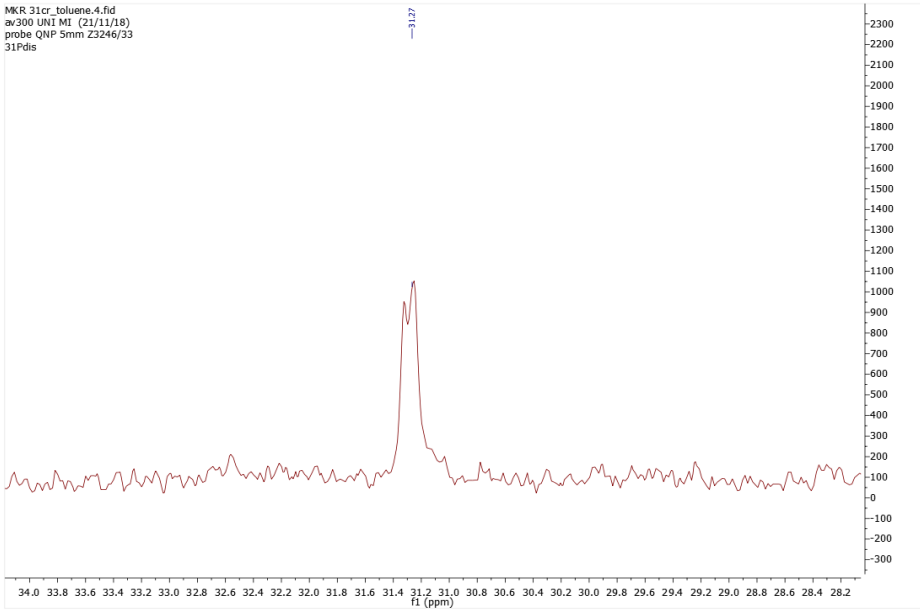

^{19}F NMR of BIMP catalyst 46* at room temperature (282.1 MHz, $C_6D_5CD_3$)

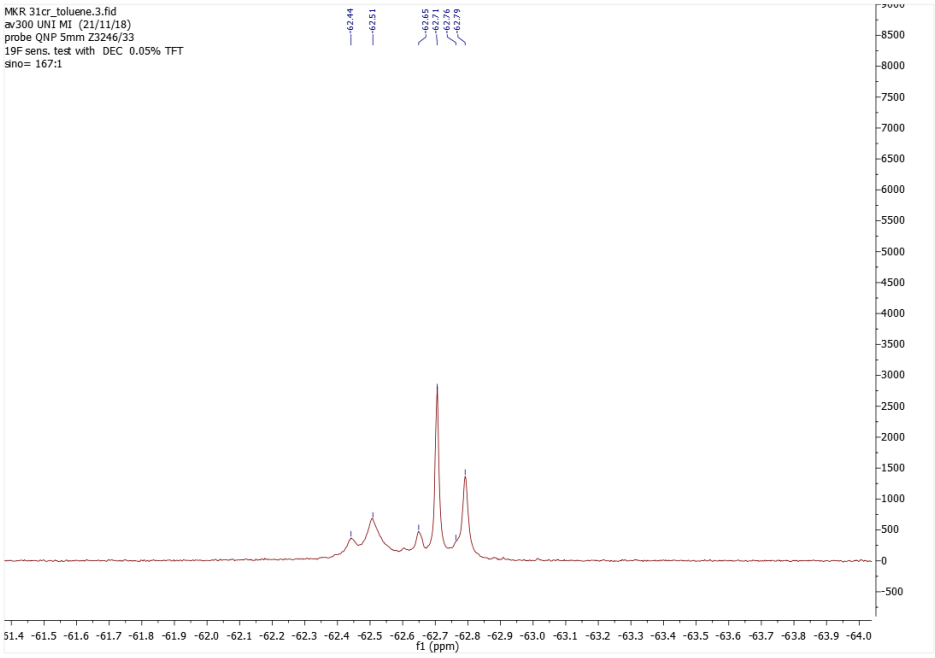

^{1}H NMR of BIMP catalyst 46* at 50 °C (300 MHz, $C_6D_5CD_3$)

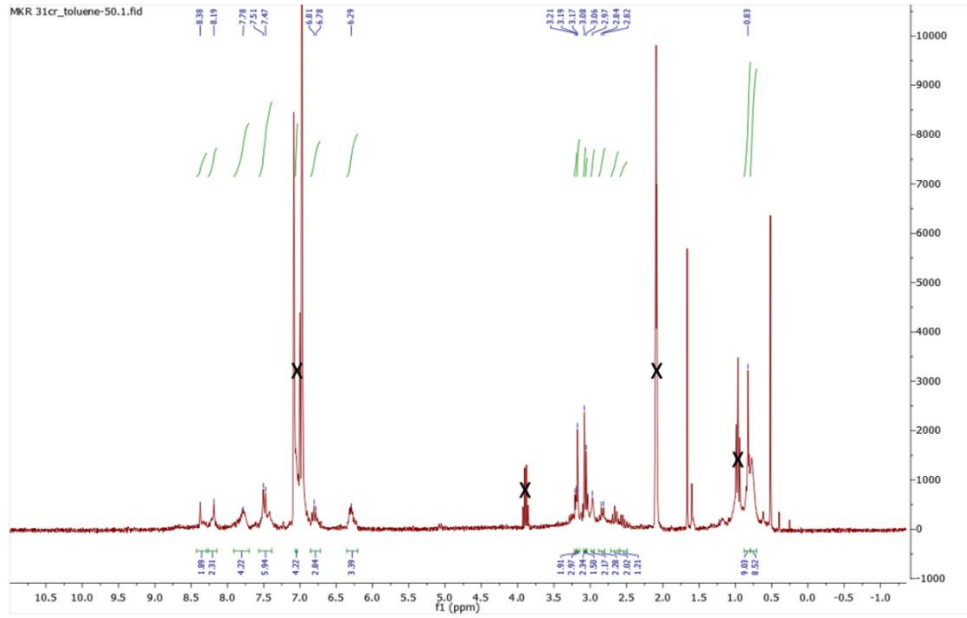

^{31}P NMR of BIMP catalyst 46* at 50 ºC (121.2 MHz, $C_6D_5CD_3$)

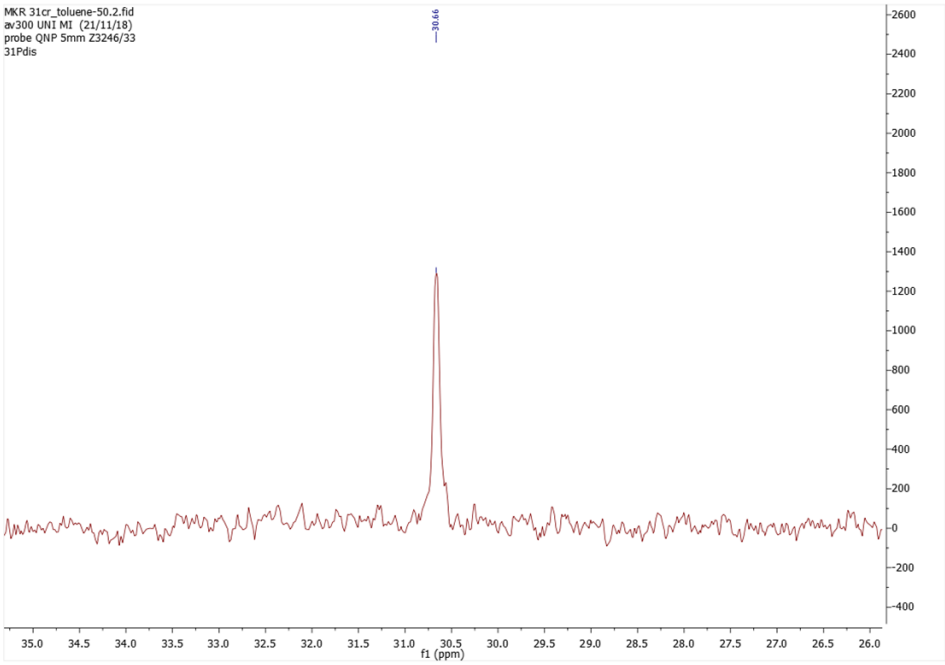

^{19}F NMR of BIMP catalyst 46* at 50 ºC (282.1 MHz, $C_6D_5CD_3$)

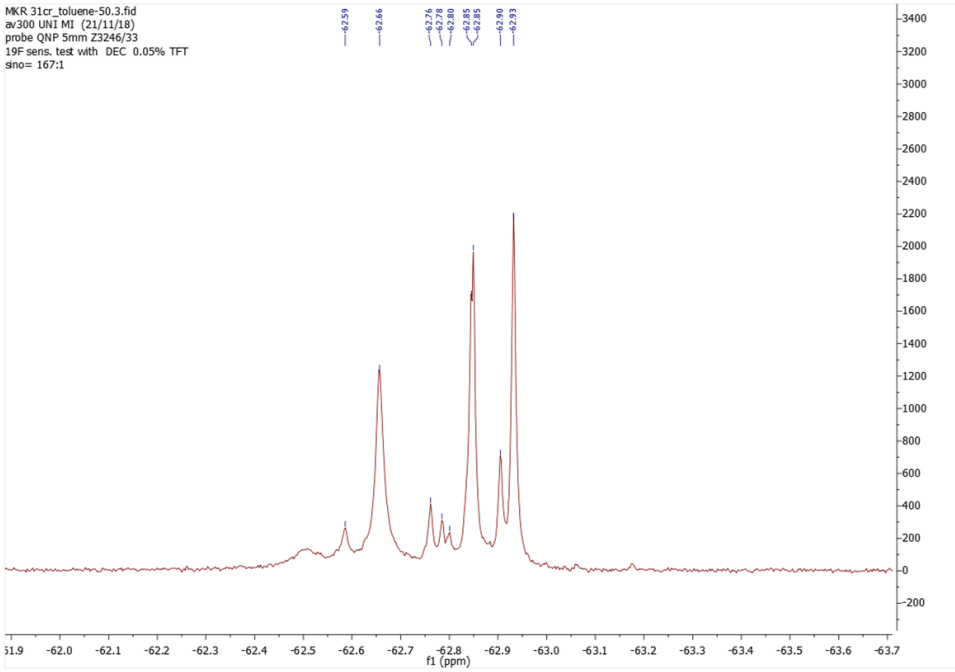

HR-MS of BIMP catalyst 46*

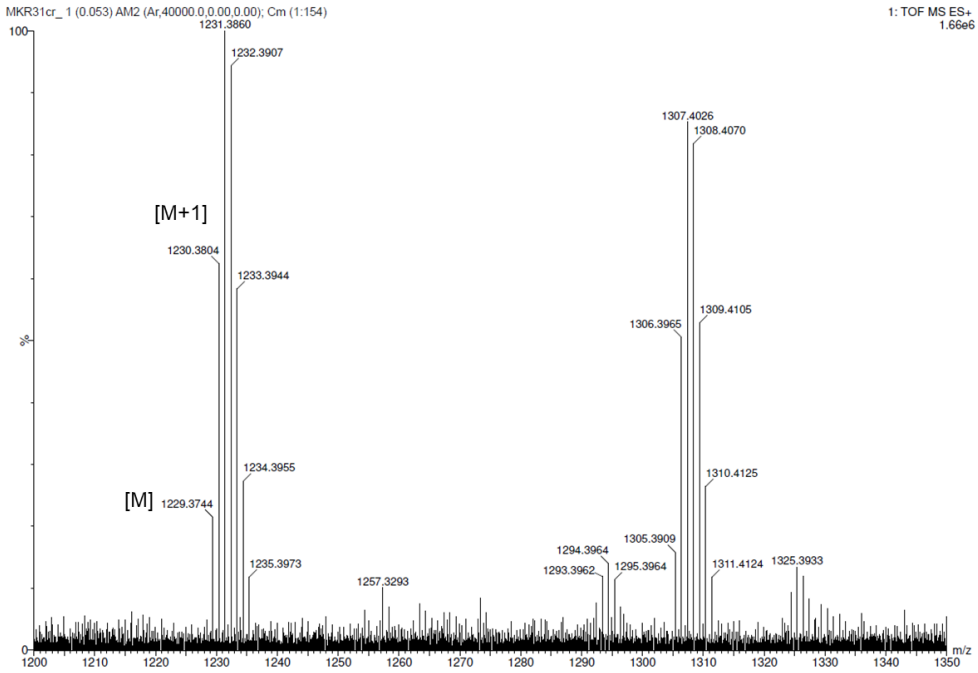

Elemental composition analysis of BIMP catalyst 46*

Elemental Composition Report

Single Mass Analysis
Tolerance = 5.0 PPM / DBE: min = -2.5, max = 200.0
Element prediction: Off
Number of isotope peaks used for i-FIT = 5

Monoisotopic Mass, Even Electron Ions
1 formula(e) evaluated with 1 results within limits (all results (up to 1000) for each mass)
Elements Used:
C: 58-58 H: 62-63 N: 6-6 O: 2-2 F: 12-12 P: 2-2 S: 2-2

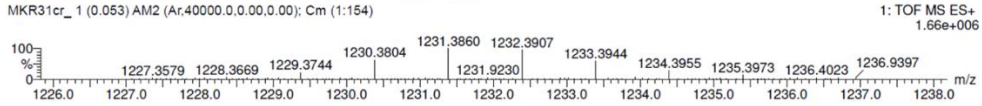

Minimum:				-2.5				
Maximum:		5.0	5.0	200.0				
Mass	Calc. Mass	mDa	PPM	DBE	i-FIT	Norm	Conf(%)	Formula
1229.3744	1229.3738	0.6	0.5	25.5	1208.2	n/a	n/a	C58 H63 N6 O2 F12 P2 S2

HR-MS of BIMP catalyst 47*

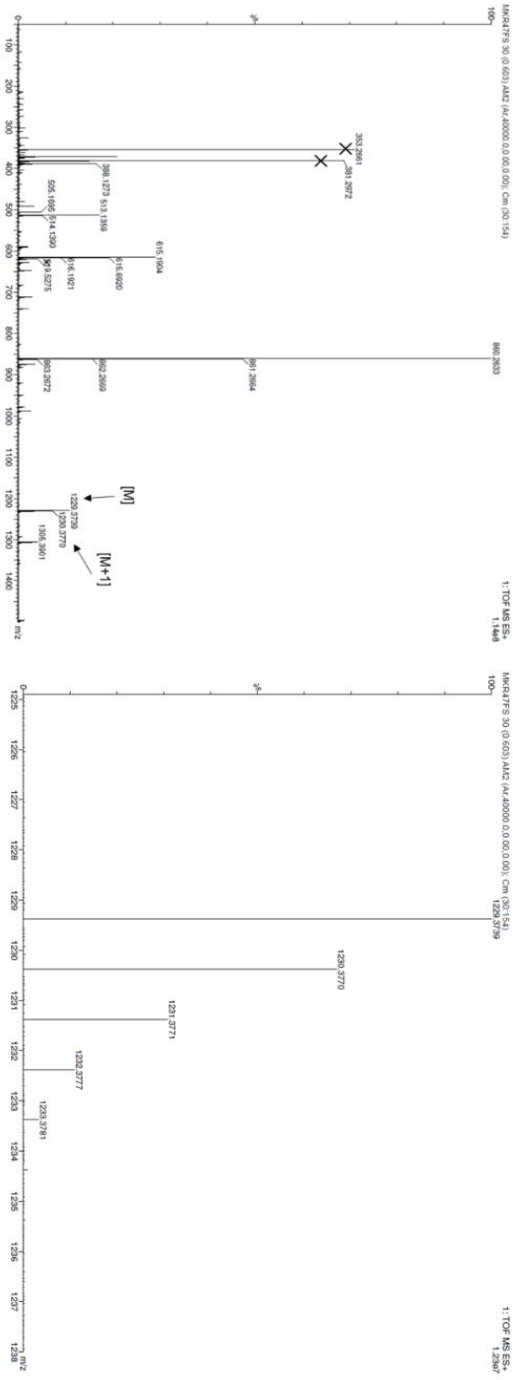

Elemental composition analysis of BIMP catalyst 47*

Elemental Composition Report

Single Mass Analysis
Tolerance = 5.0 PPM / DBE: min = -2.5, max = 200.0
Element prediction: Off
Number of isotope peaks used for i-FIT = 5

Monoisotopic Mass, Even Electron Ions
2 formula(e) evaluated with 1 results within limits (all results (up to 1000) for each mass)
Elements Used:
C: 58-58 H: 61-63 N: 6-6 O: 2-2 F: 12-12 Na: 0-2 P: 2-2 S: 2-2 K: 0-1

MKR47FS 30 (0.603) AM2 (Ar,40000.0,0.00,0.00); Cm (30:154) 1: TOF MS ES+ 1.23e+007

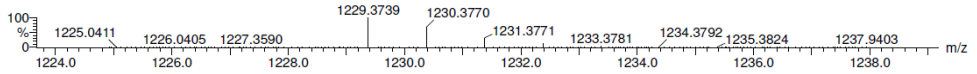

Minimum:				-2.5				
Maximum:		5.0	5.0	200.0				
Mass	Calc. Mass	mDa	PPM	DBE	i-FIT	Norm	Conf(%)	Formula
1229.3739	1229.3738	0.1	0.1	25.5	974.1	n/a	n/a	C58 H63 N6 O2 F12 P2 S2

6.4 Synthesis of *N*-Boc aryl trifluoromethyl ketimines

General procedure: *N*-Boc aryl trifluoromethyl ketimines **48-60** were synthesized according to procedure.[37]

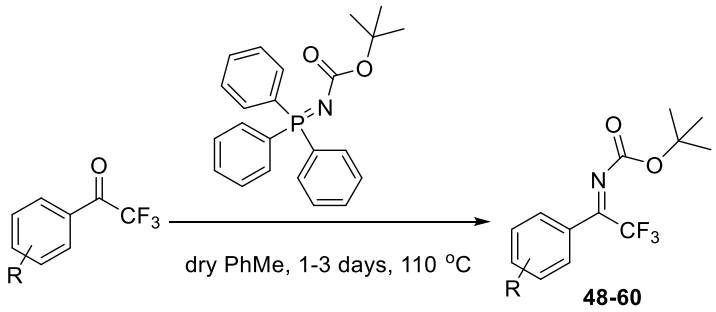

48-60

To a solution of 300 mg (1.0 equiv.) of the corresponding commercially available trifluoroacetophenone in toluene dried over molecular sieves (5 mL) was added 2.0 equiv. *N*-Boc-imino-(triphenyl)-phosphorane. The reaction mixture was heated and stirred usually overnight (or longer time depending on starting ketone) at 110 °C. It was monitored by TLC and/or ^{1}H NMR in $CDCl_3$. After the consumption of starting ketone, the reaction was stopped, cooled down to room temperature and toluene was removed on rotary evaporator. The residue was purified by silica gel column chromatography (eluent from *n*-hexane/ethyl acetate

98:2 to *n*-hexane/ethyl acetate 9:1, depending on the starting material) or it is washed with the eluent and filtered through a glass Büchner filtering funnel filled with a layer of silica. Fractions are collected, solvents were removed on rotary evaporator and ketimines are obtained with yield from 47% to 87%.

Ketimines **48, 49, 50, 51** are known compounds in the literature and they are in accordance with the published paper.[48] The ketimines **54** and **56** are mentioned in the article[37], with no spectra described.

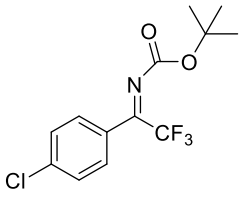

48
52% yield

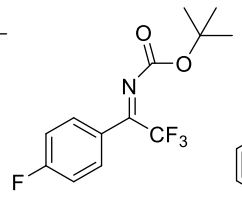

49
65% yield

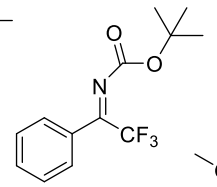

50
81% yield

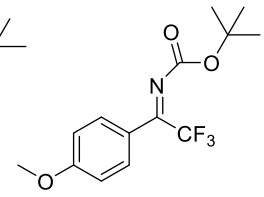

51
53% yield

tert-butyl (*Z*)-(2,2,2-trifluoro-1-(4-(trifluoromethyl)phenyl)ethylidene) carbamate (**52***):

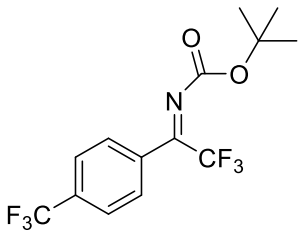

Reaction performed in high pressure tube (due to the volatility of starting ketone). Reaction time was 41h at 90 °C. The crude was purified by silica gel column chromatography (*n*-hexane/ethyl acetate 9:1), to afford imine in 85% yield, as colorless oil.

^{1}H NMR (300 MHz, $CDCl_3$) δ ppm: 1.40 (bs, 9H), 7.75 (bs, 4H)

^{19}F NMR (282.1 MHz, $CDCl_3$) δ ppm: -63.32 (major peak), -62.88 (minor peak)

tert-butyl (*Z*)-(1-(3,5-dichlorophenyl)-2,2,2-trifluoroethylidene) carbamate (**53***):

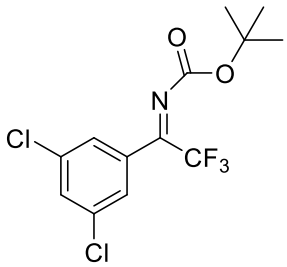

Reaction time was 32h at 110 °C. The crude was purified by trituration with *n*-hexane/ethyl acetate 95:5 (5x20 mL). White solid (triphenylphosphine oxide) was precipitated by stirring and it was filtered under the vacuum on glass frit filled with short layer of silica. The filtrates were combined and concentrated to afford imine in 80% yield, as colorless oil.

^{1}H NMR (300 MHz, $CDCl_3$) δ ppm: 1.46 (s, 9H), 7.55 (m, 2.5H)

^{19}F NMR (282.1 MHz, $CDCl_3$) δ ppm: -69.84 (major, the product), -69.03 (minor)

^{13}C NMR (75 MHz, $CDCl_3$) δ ppm: 27.97, 85.24, 126.57/126.70, 132.26, 135.98, 157.56 (CF_3 carbon and C=N carbon are not reported)

GC-MS: m/z = calc. for $C_{13}H_{12}Cl_2F_3NO_2$ = 341.02, found 241.1 [M - 100] (McLafferty rearrangement of the *t*-butyloxycarbonyl group)

tert-butyl (*Z*)-(1-(3,5-difluorophenyl)-2,2,2-trifluoroethylidene) carbamate (**54**):

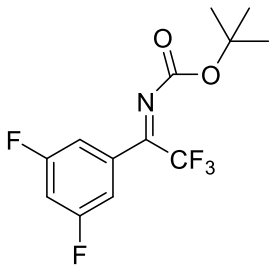

Reaction time was 32h at 110 °C. The crude was purified by trituration with *n*-hexane/ethyl acetate 95:5 (5x20 mL). White solid (triphenylphosphine oxide) was precipitated by stirring and it was filtered under the vacuum on glass frit filled with short layer of silica. The filtrates were combined and concentrated to afford imine in 78% yield, as colorless oil.

^{1}H NMR (300 MHz, $CDCl_3$) δ ppm: 1.46 (s, 9H), 7.02 (tt) and 7.21 (bs), <3H.

^{19}F NMR (282.1 MHz, $CDCl_3$) δ ppm: -70 (CF_3), -108.32, -108.57 (F)

^{13}C NMR (75 MHz, $CDCl_3$) δ ppm: 27.90, 85.03, 107.8, 111.55 and 111.91 (aromatic C in *orto* position), 118.54 (CF_3), 132.63, 157.58 (C=O), 161.33 and 164.7 (aromatic C in *meta* position, bonded to F, as doublets).

GC-MS: m/z = calc. for $C_{13}H_{12}F_5NO_2$ = 309.08, found 209.1 [M - 100] (McLafferty rearrangement of the *t*-butyloxycarbonyl group)

tert-butyl (*Z*)-(1-(3-chloro-5-fluorophenyl)-2,2,2-trifluoroethylidene) carbamate (**55***):

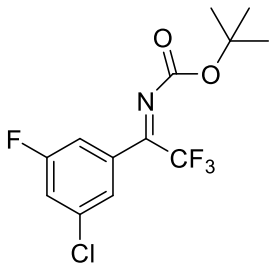

Reaction time was 24h at 110 °C. The crude was purified by trituration with *n*-hexane/ethyl acetate 95:5 (5x20 mL). White solid (triphenylphosphine oxide) was precipitated by stirring and it was filtered under the vacuum on glass frit filled with short layer of silica. The filtrates were combined and concentrated to afford imine in 62% yield, as pale-yellow oil.

^{1}H NMR (300 MHz, $CDCl_3$) δ ppm: 1.47 (s, 9H), 7.28 (t, 1H), 7.31 (t, 1H), 7.46 (bs, 1H)

^{19}F NMR (282.1 MHz, $CDCl_3$) δ ppm: -69.87 (CF_3), -109.34 (F)

tert-butyl (*Z*)-(1-(3-bromophenyl)-2,2,2-trifluoroethylidene) carbamate (**56**):

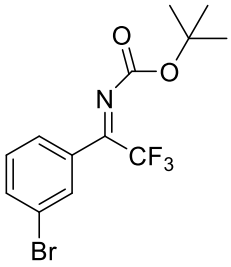

Reaction time was 32h at 110 °C. The crude was purified by silica gel column chromatography (*n*-hexane/ethyl acetate 9:1), to afford imine in 87% yield, as colorless oil.

^{1}H NMR (300 MHz, $CDCl_3$) δ ppm: 1.44 (s, 9H), 7.35 (t, 1H), 7.54 (bs, 1H), 7.68 (bs, 1H), 7.77 (bs, 1H)

^{19}F NMR (282.1 MHz, $CDCl_3$) δ ppm: -69.74

^{13}C NMR (75 MHz, $CDCl_3$) δ ppm: 27.95, 84.80, 122.8 (q, CF_3), 122.98, 126.67, 130.41, 131.05, 131.75, 132.99, 135.20, 157.94 (C=N carbon is not reported)

GC-MS: m/z = calc. for $C_{13}H_{13}BrF_3NO_2$= 351.01, found 251.4 [M - 100] (McLafferty rearrangement of the *t*-butyloxycarbonyl group)

tert-butyl (*Z*)-(2,2,2-trifluoro-1-(*m*-tolyl)ethylidene) carbamate (**57***):

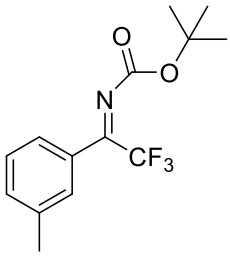

Reaction time was 16h at 110 °C. The crude was purified by silica gel column chromatography (*n*-hexane/ethyl acetate 9:1), to afford imine in 50% yield, as pale-yellow oil.

^{1}H NMR (300 MHz, $CDCl_3$) δ ppm: 1.40 (s, 9H), 2.39 (s, 3H), 7.33-7.53 (m, 4H)

^{19}F NMR (282.1 MHz, $CDCl_3$) δ ppm: -71.32

GC-MS: m/z = calc. for $C_{14}H_{16}F_3NO_2$ = 287.11, found 187.2 [M - 100] (McLafferty rearrangement of the *t*-butyloxycarbonyl group)

tert-butyl (*Z*)-(2,2,2-trifluoro-1-(4-propylphenyl)ethylidene) carbamate (**58***):

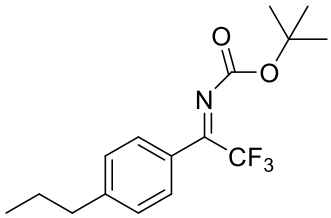

Reaction time was 52h at 110 °C. The crude was purified by silica gel column chromatography (*n*-hexane/ethyl acetate 98:2), to afford imine in 47% yield, as colorless oil.

^{1}H NMR (300 MHz, $CDCl_3$) δ ppm: 0.94 (t, 3H), 1.41 ppm (s, 9H), 1.66 (sext, 2H), 2.64 (t, 2H), 7.24 (s, 1H), 7.27 (s, 1H), 7.54 (d, 2H)

^{19}F NMR (282.1 MHz, $CDCl_3$) δ ppm: -71.36

^{13}C NMR (75 MHz, $CDCl_3$) δ ppm: 13.71, 24.25, 27.88, 37.99, 83.93, 127.50, 128.15, 128.88, 147.55, 158.60

GC-MS: m/z = calc. for $C_{16}H_{20}F_3NO_2$ = 315.14, found 215.25 [M - 100] (McLafferty rearrangement of the *t*-butyloxycarbonyl group)

tert-butyl (*Z*)-(2,2,2-trifluoro-1-(3-isopropylphenyl)ethylidene) carbamate (**59***):

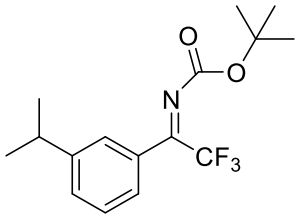

Reaction time was 3 days at 110 °C. The crude was purified by trituration with *n*-hexane/ethyl acetate 9:1 (5x20 mL). White solid (triphenylphosphine oxide) was precipitated by stirring and it was filtered under the vacuum on glass frit filled with short layer of silica. The filtrates were combined and concentrated to afford imine in 62% yield, as colorless oil.

^{1}H NMR (300 MHz, $CDCl_3$) δ ppm: 1.25 (s, 3H), 1.27 (s, 3H), 1.38 (s, 9H), 2.93 (sept, 1H), 7.39 (m, 4H)

^{19}F NMR (282.1 MHz, $CDCl_3$) δ ppm: -71.28

^{13}C NMR (75 MHz, $CDCl_3$) δ ppm: 23.73, 27.76, 34.10, 83.87, 125.35, 126.08, 128.61, 130.04 (as a doublet), 149.53, 158.38

GC-MS: m/z = calc. for $C_{16}H_{20}F_3NO_2$ = 315.14, found 215.25 [M - 100] (McLafferty rearrangement of the *t*-butyloxycarbonyl group)

tert-butyl (*Z*)-(1-(4-(*tert*-butyl)phenyl)-2,2,2-trifluoroethylidene) carbamate (**60***):

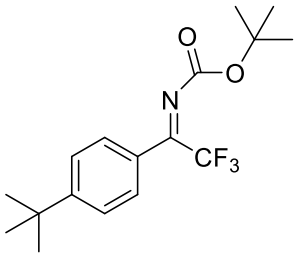

Reaction time was 3 days at 110 °C. The crude was purified by silica gel column chromatography (*n*-hexane/ethyl acetate 98:2), to afford imine in 47% yield, as colorless oil.

^{1}H NMR (300 MHz, $CDCl_3$) δ ppm: 1.33 (s, 9H), 1.41 (s, 9H), 7.46 (d, 2H), 7.56 (d, 2H)

^{19}F NMR (282.1 MHz, $CDCl_3$) δ ppm: -71.39

^{13}C NMR (75 MHz, $CDCl_3$) δ ppm: 27.89, 31.13, 35.14, 83.96, 124 (CF_3), 125.74, 127.26, 128.07, 155.92, 158.60

GC-MS: m/z = calc. for $C_{17}H_{22}F_3NO_2$ = 329.16, found 229.21 [M - 100] (McLafferty rearrangement of the *t*-butyloxycarbonyl group).

6.5 Asymmetric Aza-Henry reaction of *N*-Boc CF_3 ketimines promoted by **B**ifunctional **IM**inophos**P**horan**e** organocatalysts

6.5.1 Asymmetric addition of nitromethane to *N*-Boc CF_3 ketimines promoted by catalyst **36a**

General procedure for the synthesis of quaternary β-nitroamines - reaction scope with catalyst 36a:

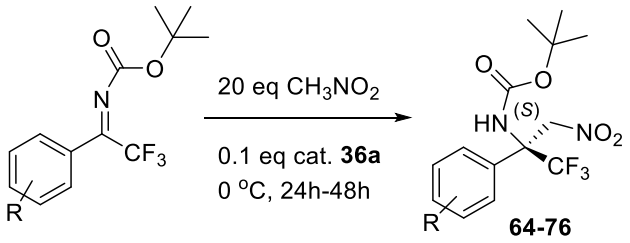

A 1.5 mL vial with septum connected with nitrogen inlet, was charged with 0.1 equiv. of iminophosphorane catalyst **36a** and 1.0 equiv. (50 mg) of *N*-Boc CF_3 ketimine (**48-60**). The reaction mixture was cooled down at 0 °C. After that, 20 equiv. of nitromethane was added, and the reaction mixture was stirred until the completion of the reaction. The reactions were monitored by TLC and ^{1}H NMR. After the reaction is done, nitromethane was removed under reduced pressure and the residue was purified by column chromatography on silica gel with *n*-hexane/ethyl acetate to afford the desired products **64-76**. Determination of ee% was done on chiral HPLC (Chiralpak AD column, eluent: *n*-hexane/isopropanol 95:5, flow rate 1 mL/min or Chiralcel OD-H, *n*-hexane/isopropanol 95:5, 0.8 mL/min).

Aza-Henry products **64, 65, 66, 67** are known compounds in the literature and spectral data can be found in the acticle.[48] Quaternary β-nitroamines **68-76** are ***new compounds.***

t-butyl (*S*)-(2-(4-chlorophenyl)-1,1,1-trifluoro-3-nitropropan-2-yl) carbamate, **64**:

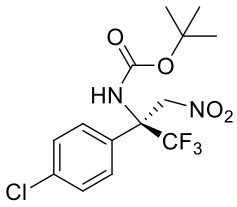

Reaction time was 24h at 0 °C. The product was isolated by silica gel column chromatography with *n*-hexane/ethyl acetate 95:5, as a pale-yellow oil, 78% yield. Determination of ee% was done on HPLC (Chiralpak AD column, eluent: *n*-hexane/isopropanol 95:5, flow rate 1 mL/min, t(major)=8.41 min, t(minor)=11.12 min, ~90% ee.

Determination of ee% for compound 64

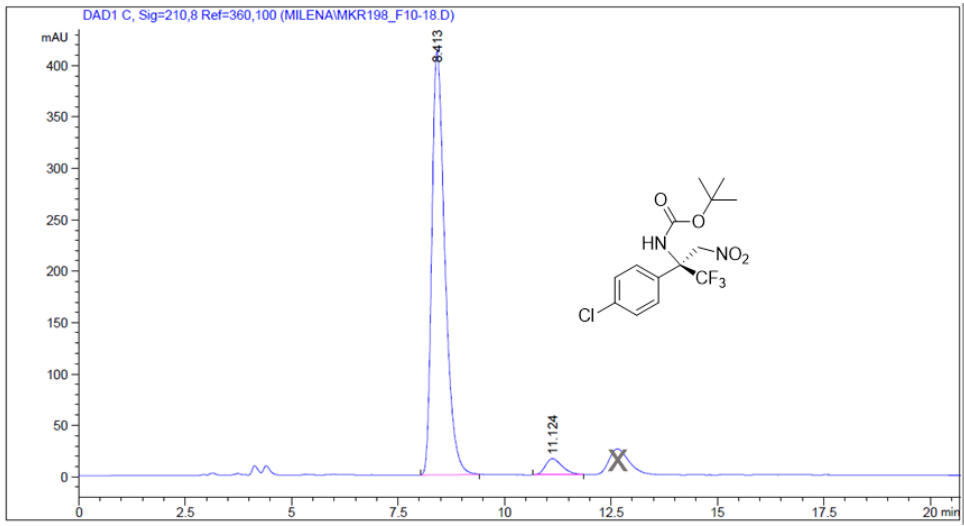

Peak #	RetTime [min]	Type	Width [min]	Area [mAU*s]	Height [mAU]	Area %
1	8.413	BB	0.3261	8835.59180	412.17361	95.3544
2	11.124	BB	0.4151	430.46368	15.64069	4.6456

t-butyl (*S*)-(1,1,1-trifluoro-2-(4-fluorophenyl)-3-nitropropan-2-yl) carbamate, **65**:

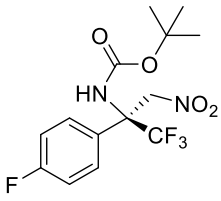

Reaction time was 48h at 0 °C. The product was isolated by silica gel column chromatography with *n*-hexane/ethyl acetate 9:1, as a colorless oil, 85% yield. Determination of ee% was done on HPLC (Chiralpak AD column, eluent: *n*-hexane/isopropanol 95:5, flow rate 1 mL/min, t(major)=8.95 min, t(minor)= 12.83 min, ~82% ee.

Determination of ee% for the compound 65

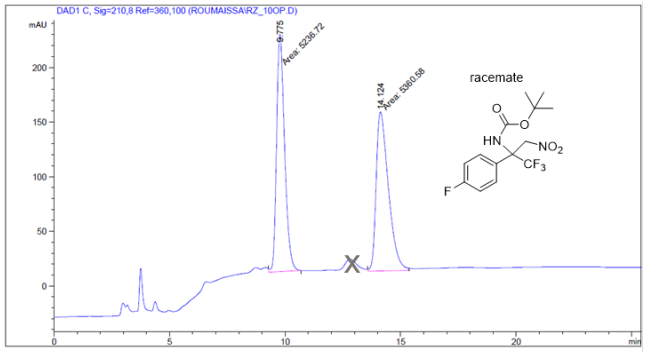

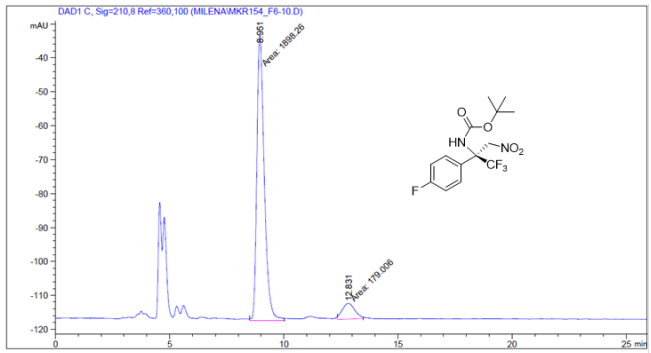

Peak #	RetTime [min]	Type	Width [min]	Area [mAU*s]	Height [mAU]	Area %
1	8.951	MM	0.3762	1898.26477	84.10024	91.3826
2	12.831	MM	0.6425	179.00598	4.64322	8.6174
Totals :				2077.27075	88.74346	

t-butyl (*S*)-(1,1,1-trifluoro-3-nitro-2-phenylpropan-2-yl) carbamate, **66**:

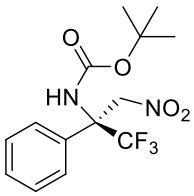

Reaction time was 26h at 0 °C. The product was isolated by silica gel column chromatography with *n*-hexane/ethyl acetate 95:5, as a colorless oil, 82% yield. Determination of ee% was done on HPLC (Chiralpak AD column, eluent: *n*-hexane/isopropanol 95:5, flow rate 1 mL/min, t(major)=9.57 min, t(minor)= 11.9 min, ~95% ee.

Determination of ee% for the compound 66

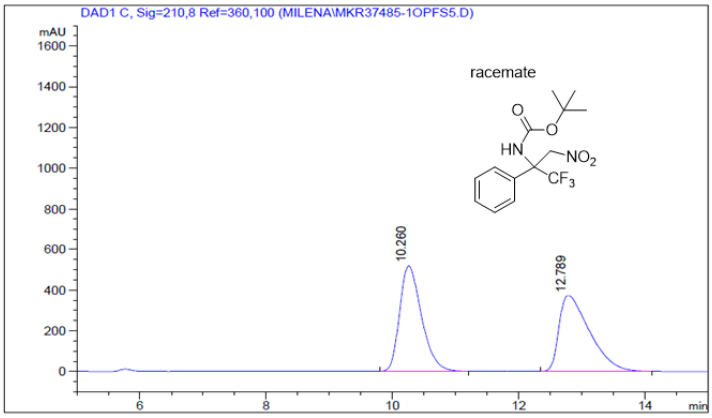

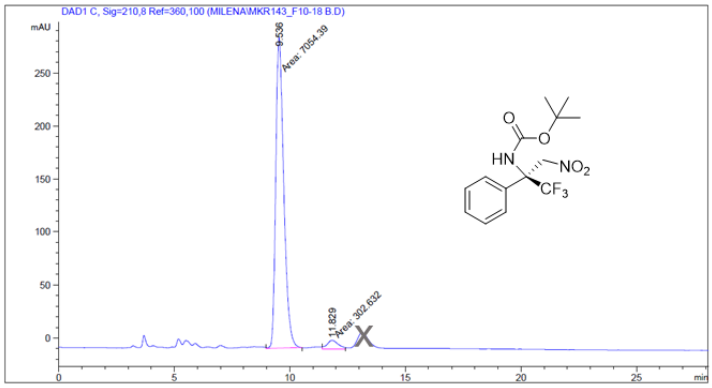

Peak #	RetTime [min]	Type	Width [min]	Area [mAU*s]	Height [mAU]	Area %
1	9.536	MM	0.4011	7054.38770	293.11954	95.8865
2	11.829	MM	0.5807	302.63181	8.68642	4.1135
Totals :				7357.01950	301.80596	

t-butyl (*S*)-(1,1,1-trifluoro-2-(4-methoxyphenyl)-3-nitropropan-2-yl) carbamate, **67:**

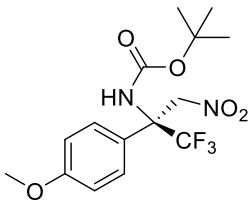

Reaction time was 48h at 0 °C. The product was isolated by silica gel column chromatography with *n*-hexane/ethyl acetate 98:2, as a colorless oil, 38% yield. Determination of ee% was done on HPLC (Chiralpak AD column, eluent: *n*-hexane/isopropanol 95:5, flow rate 1 mL/min, t(major)=10.95 min, t(minor)= 12.98 min, ~92% ee.

Determination of ee% for the compound 67

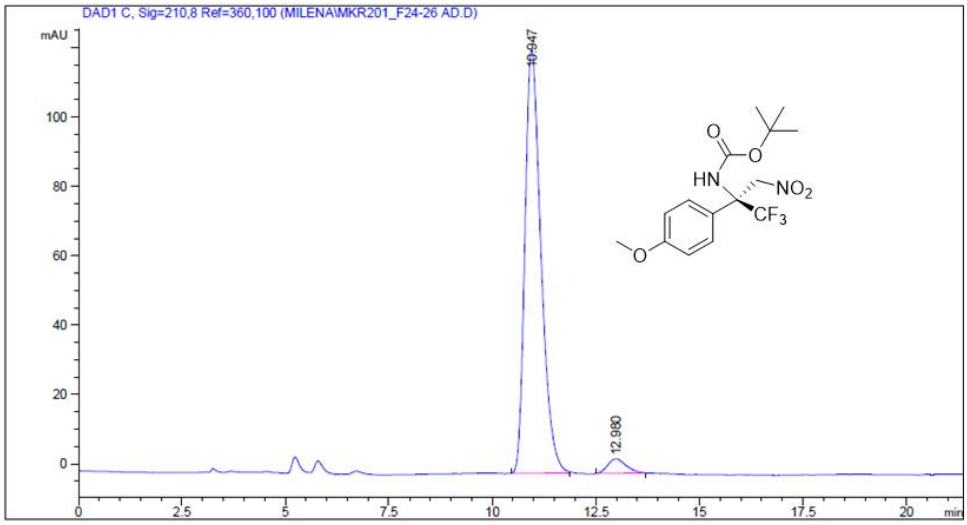

Peak #	RetTime [min]	Type	Width [min]	Area [mAU*s]	Height [mAU]	Area %
1	10.947	BB	0.4146	3297.95630	122.28411	96.1782
2	12.980	BB	0.3770	131.04813	4.21170	3.8218

t-butyl (*S*)-(2-(3,5-dichlorophenyl)-1,1,1-trifluoro-3-nitropropan-2-yl) carbamate, **68***:

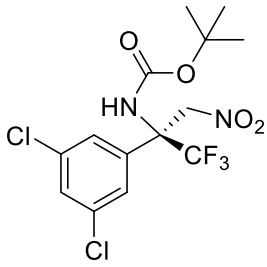

Reaction time was 48h at 0 °C. The product was isolated by silica gel column chromatography with *n*-hexane/ethyl acetate 98:2, as a colorless oil, 43% yield. Determination of ee% was done on HPLC (Chiralpak AD column, eluent: *n*-hexane/isopropanol 95:5, flow rate 1 mL/min, t(major)=6.72 min, t(minor)= 7.79 min, ~76% ee.

^{1}H NMR of compound 68* (300 MHz, $CDCl_3$)

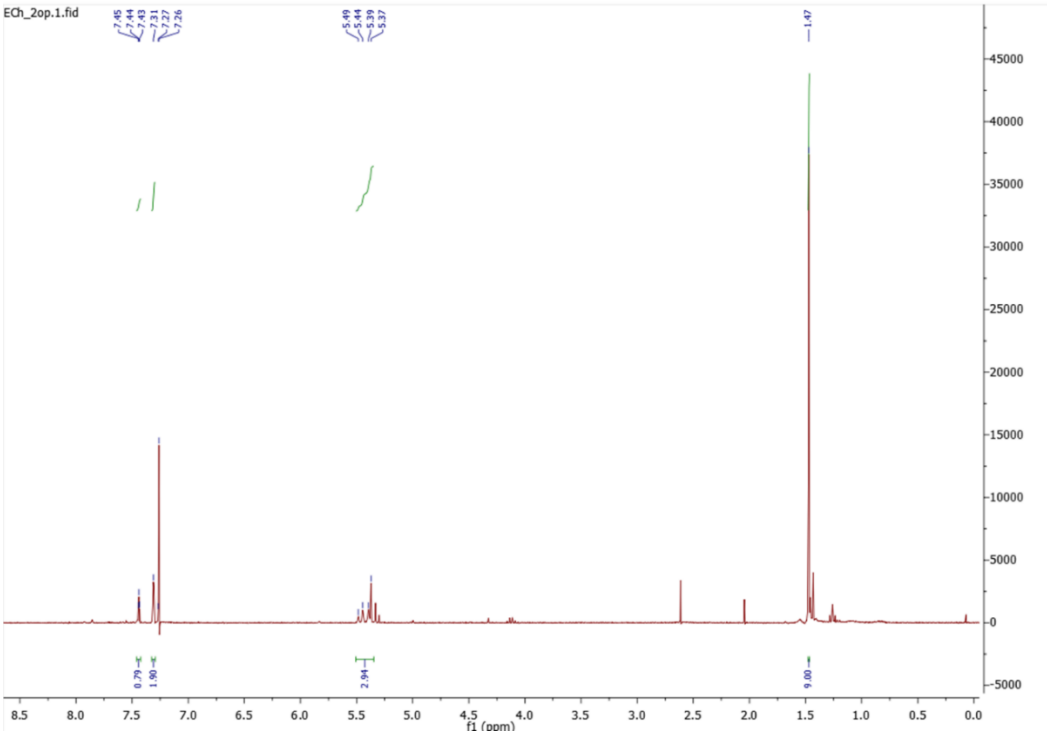

^{13}C NMR of compound 68* (75 MHz, $CDCl_3$)

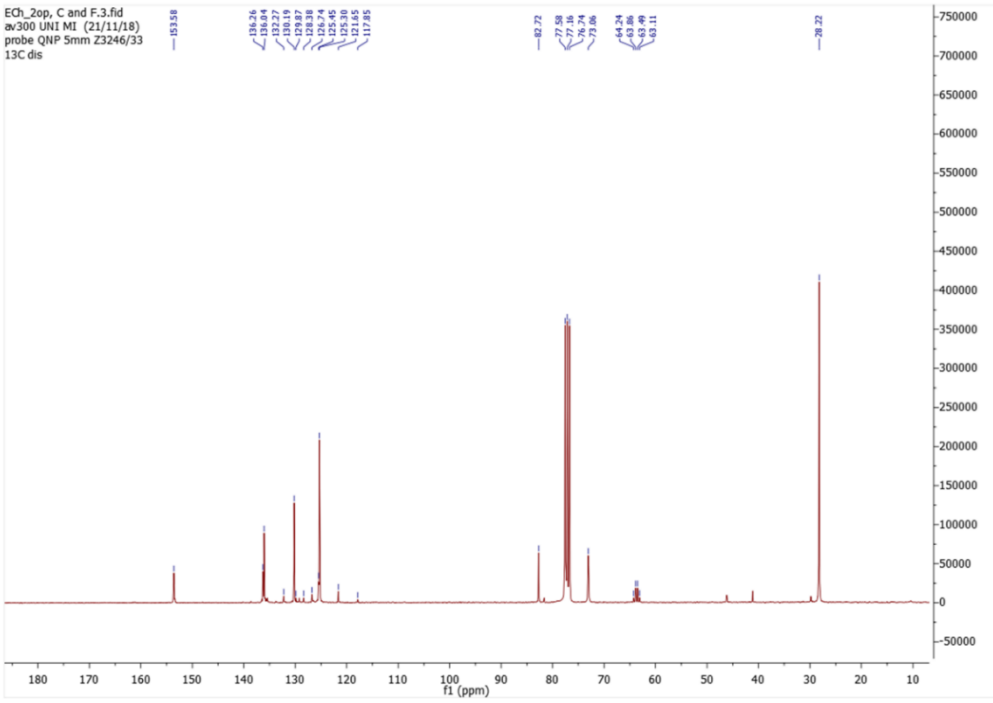

^{19}F NMR of compound 68* (282.1 MHz, $CDCl_3$)

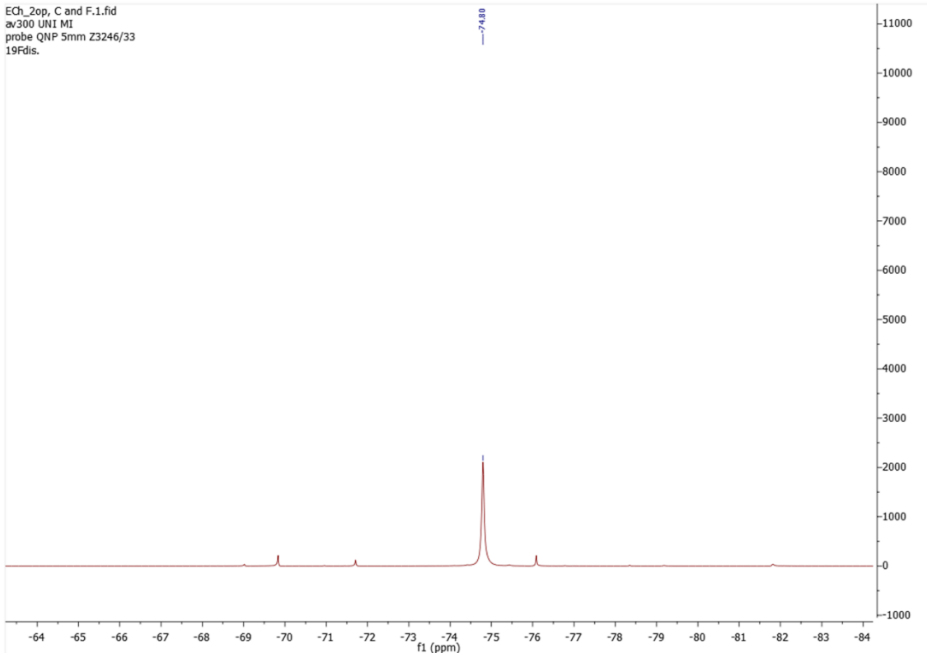

HR-MS of compound 68*

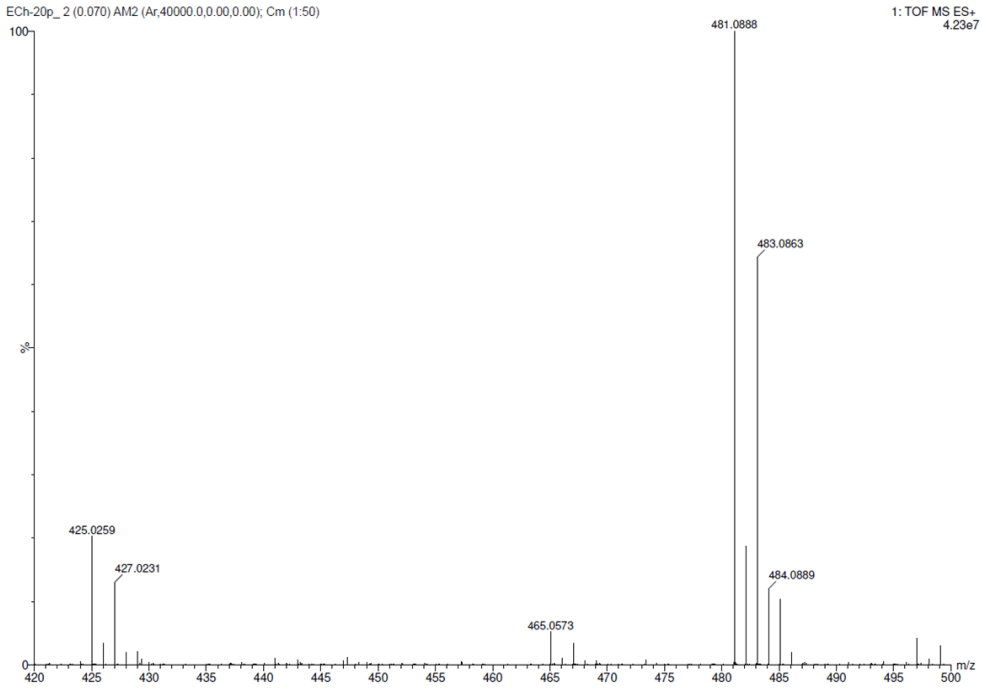

Elemental composition analysis of compound 68*

Elemental Composition Report

Single Mass Analysis
Tolerance = 5.0 PPM / DBE: min = -5.0, max = 300.0
Element prediction: Off
Number of isotope peaks used for i-FIT = 7

Monoisotopic Mass, Even Electron Ions
1 formula(e) evaluated with 1 results within limits (all results (up to 1000) for each mass)
Elements Used:
C: 14-14 H: 15-16 N: 2-2 O: 4-4 F: 3-3 Na: 0-1 Cl: 2-2

ECh-20p_ 2 (0.070) AM2 (Ar,40000.0,0.00,0.00); Cm (1:50)

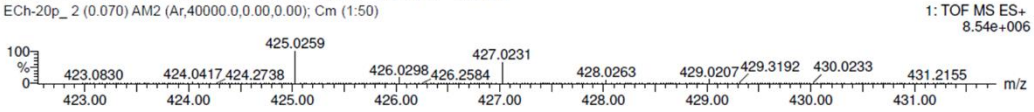

Minimum:				-5.0				
Maximum:		5.0	5.0	300.0				
Mass	Calc. Mass	mDa	PPM	DBE	i-FIT	Norm	Conf(%)	Formula
425.0259	425.0259	0.0	0.0	5.5	3281.3	n/a	n/a	C14 H15 N2 O4 F3 Na Cl2

Determination of ee% for compound 68*

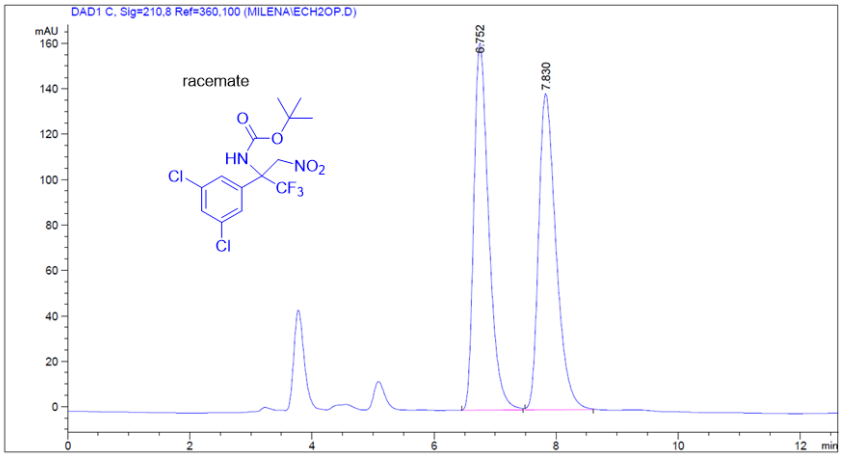

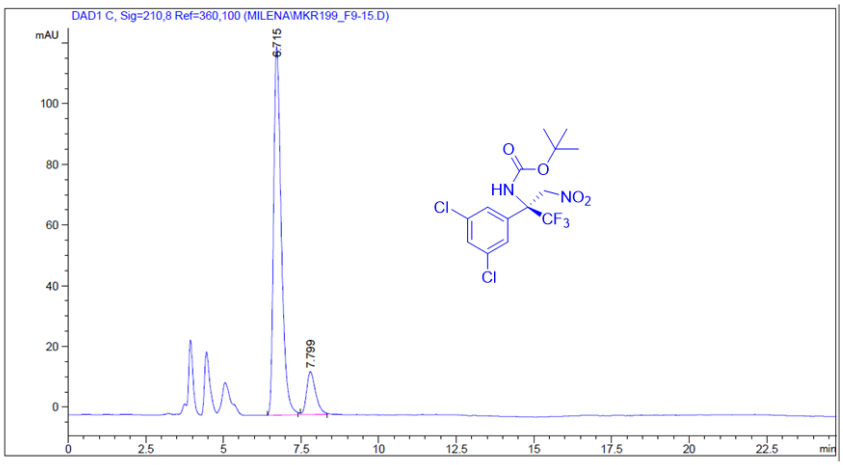

Peak #	RetTime [min]	Type	Width [min]	Area [mAU*s]	Height [mAU]	Area %
1	6.715	BB	0.2606	2085.82715	121.31470	87.9937
2	7.799	BB	0.2976	284.60175	14.09352	12.0063

t-butyl (*S*)-(2-(3,5-difluorophenyl)-1,1,1-trifluoro-3-nitropropan-2-yl) carbamate, **69***:

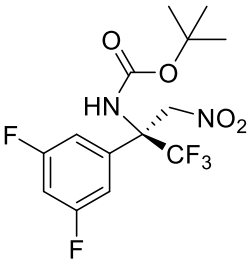

Reaction time was 48h at 0 °C. The product was isolated by silica gel column chromatography with *n*-hexane/ethyl acetate 98:2, as a colorless oil, 46% yield. Determination of ee% was done on chiral HPLC (Chiralpak AD column, eluent: *n*-hexane/isopropanol 95:5, flow rate 1 mL/min, t(major) = 6.56 min, t(minor) = 8.74 min, ~70% ee

^{1}H NMR of compound 69* (300 MHz, $CDCl_3$)

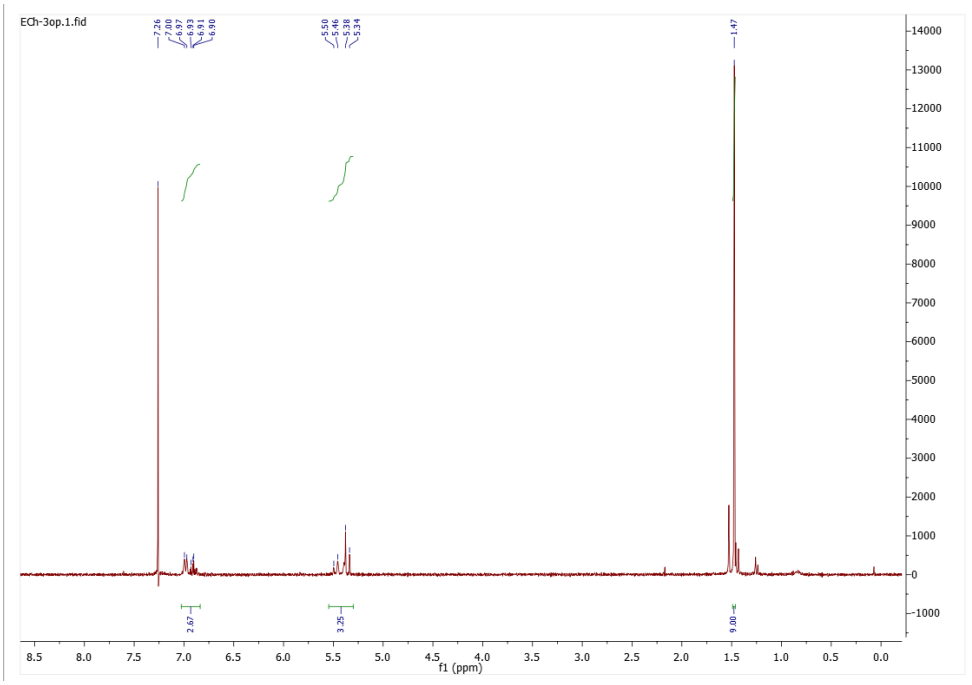

^{13}C NMR of compound 69* (75 MHz, $CDCl_3$)

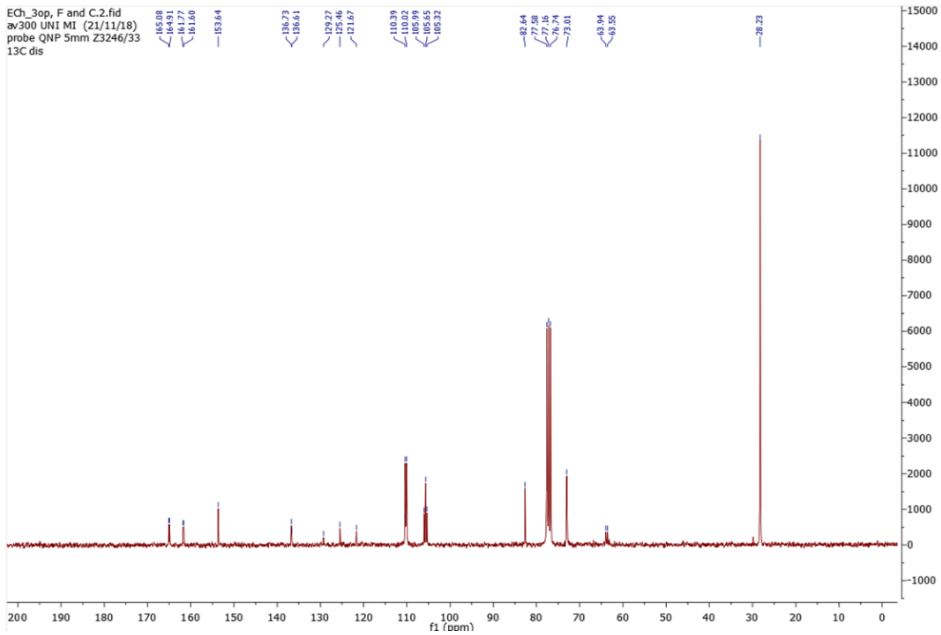

^{19}F NMR of compound 69* (282.1 MHz, $CDCl_3$)

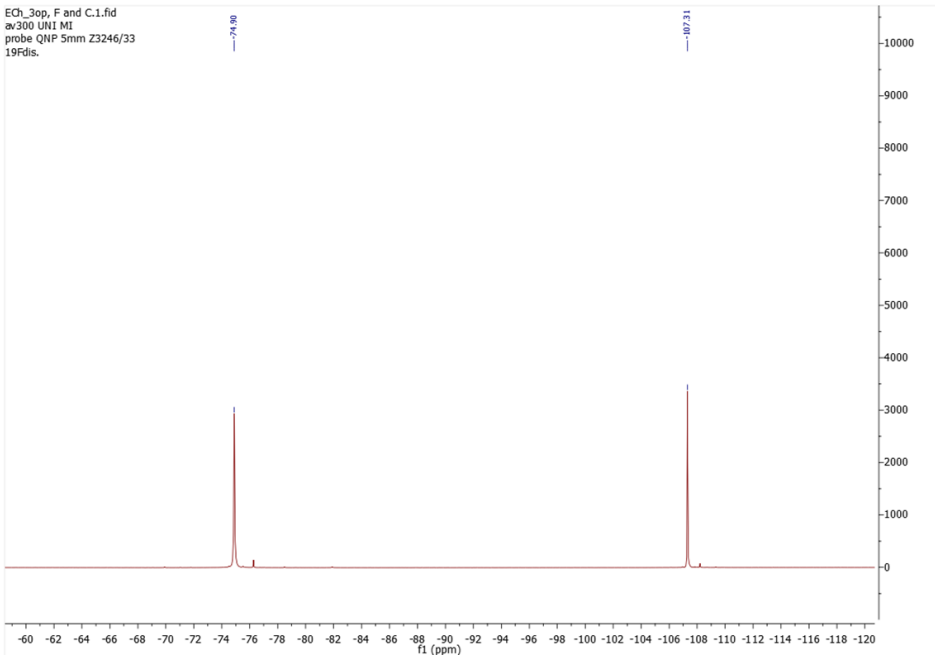

HR-MS of compound 69*

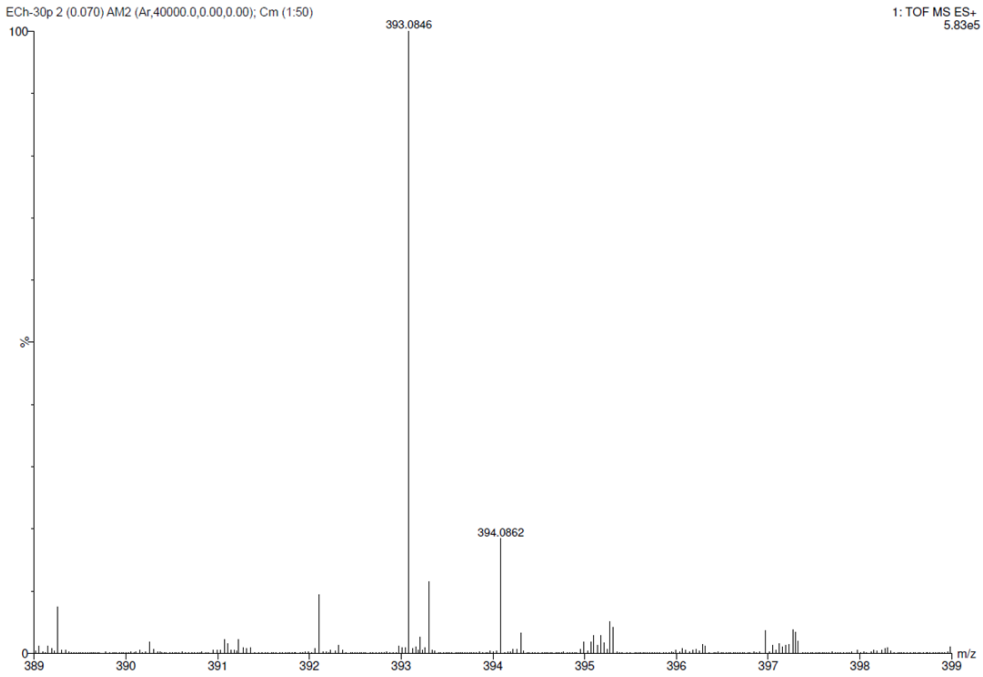

Elemental composition analysis of compound 69*

Elemental Composition Report

Single Mass Analysis
Tolerance = 5.0 PPM / DBE: min = -5.0, max = 300.0
Element prediction: Off
Number of isotope peaks used for i-FIT = 7

Monoisotopic Mass, Even Electron Ions
1 formula(e) evaluated with 1 results within limits (all results (up to 1000) for each mass)
Elements Used:
C: 14-14 H: 15-16 N: 2-2 O: 4-4 F: 5-5 Na: 0-1

ECh-30p 2 (0.070) AM2 (Ar,40000.0,0.00,0.00); Cm (1:50)

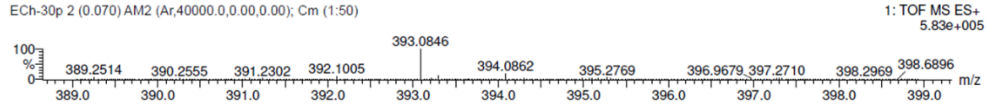

Minimum:				-5.0				
Maximum:		5.0	5.0	300.0				
Mass	Calc. Mass	mDa	PPM	DBE	i-FIT	Norm	Conf(%)	Formula
393.0846	393.0850	-0.4	-1.0	5.5	2642.0	n/a	n/a	C14 H15 N2 O4 F5 Na

Determination of ee% for compound 69*

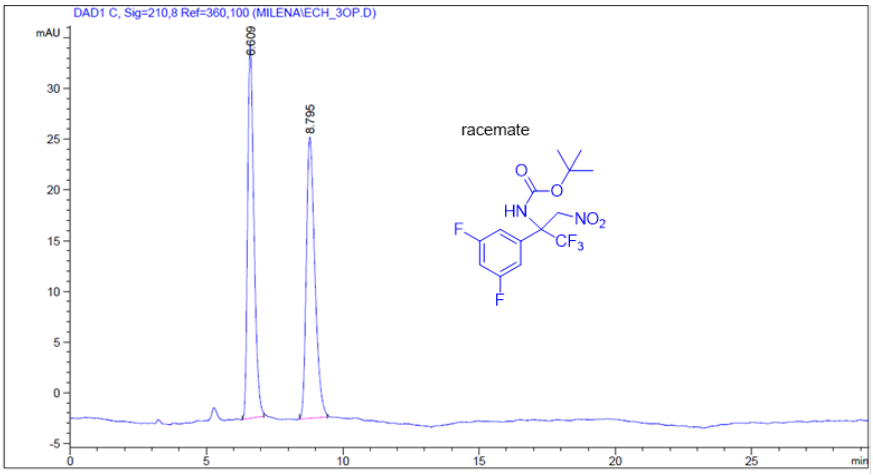

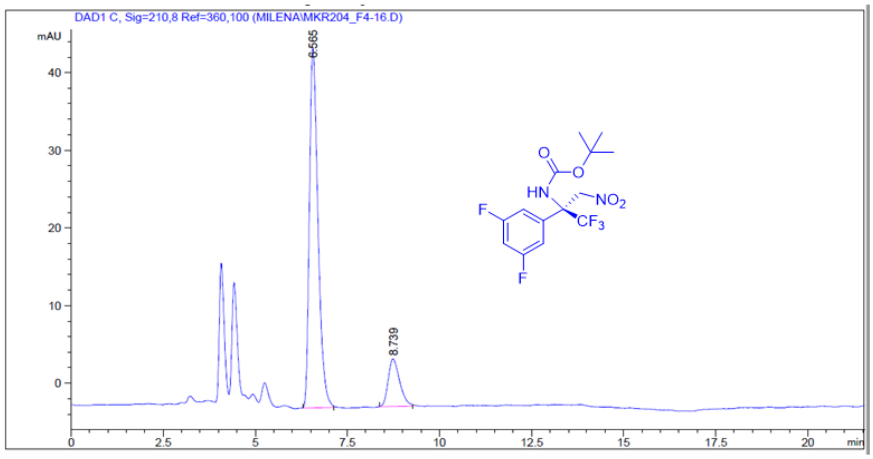

Peak #	RetTime [min]	Type	Width [min]	Area [mAU*s]	Height [mAU]	Area %
1	6.565	BB	0.2472	752.15491	46.37867	84.9452
2	8.739	BB	0.3252	133.30452	6.14341	15.0548

t-butyl (*S*)-(2-(3-chloro-5-fluorophenyl)-1,1,1-trifluoro-3-nitropropan-2-yl) carbamate, **70***:

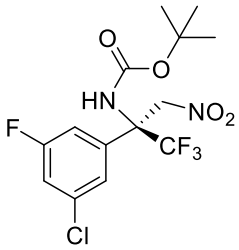

Reaction time was 48h at 0 °C. The product was isolated by silica gel column chromatography with *n*-hexane/ethyl acetate 98:2, as a colorless oil, 53% yield. Determination of ee% was done on chiral HPLC (Chiralpak AD column, eluent: *n*-hexane/isopropanol 95:5, flow rate 1 mL/min, t(major)=6.86 min, t(minor)= 8.59 min, ~80% ee.

^{1}H NMR of compound 70* (300 MHz, $CDCl_3$)

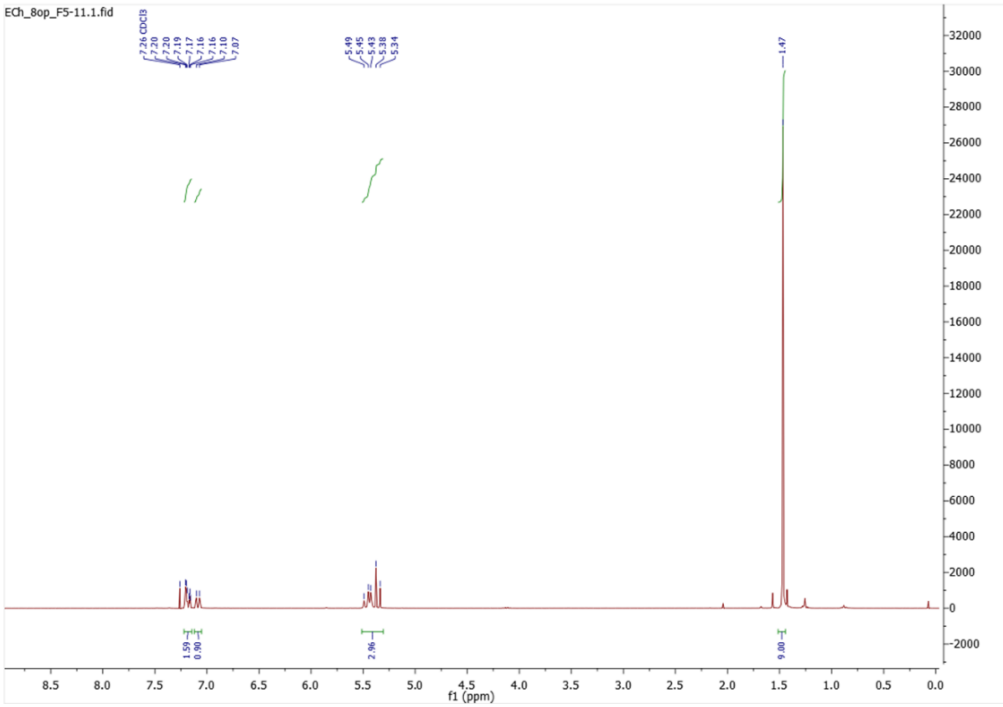

^{13}C NMR of compound 70* (75 MHz, $CDCl_3$)

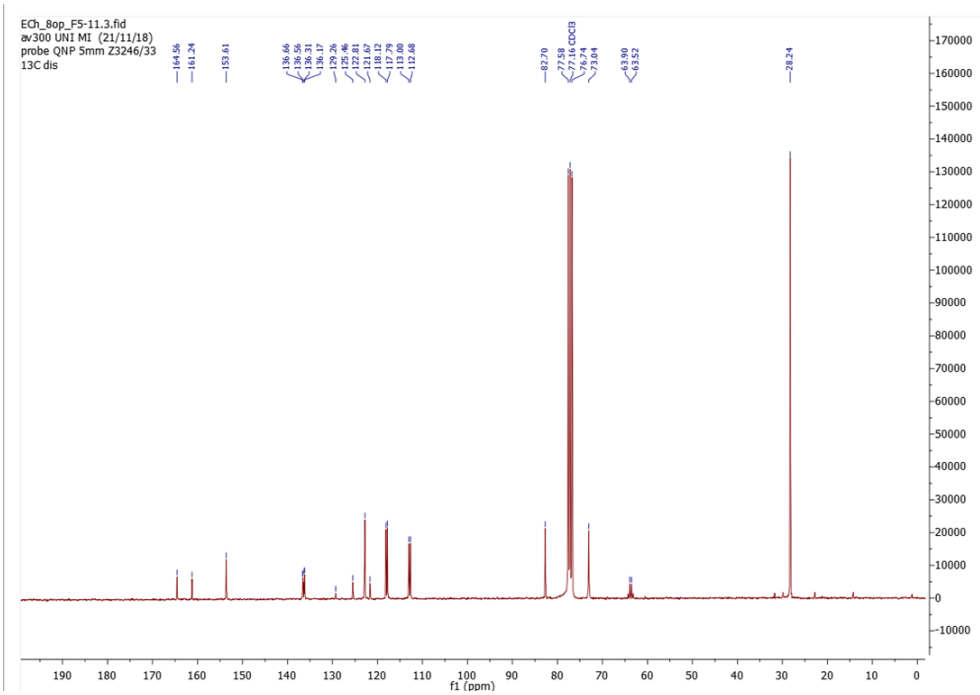

^{19}F NMR of compound 70* (282.1 MHz, $CDCl_3$)

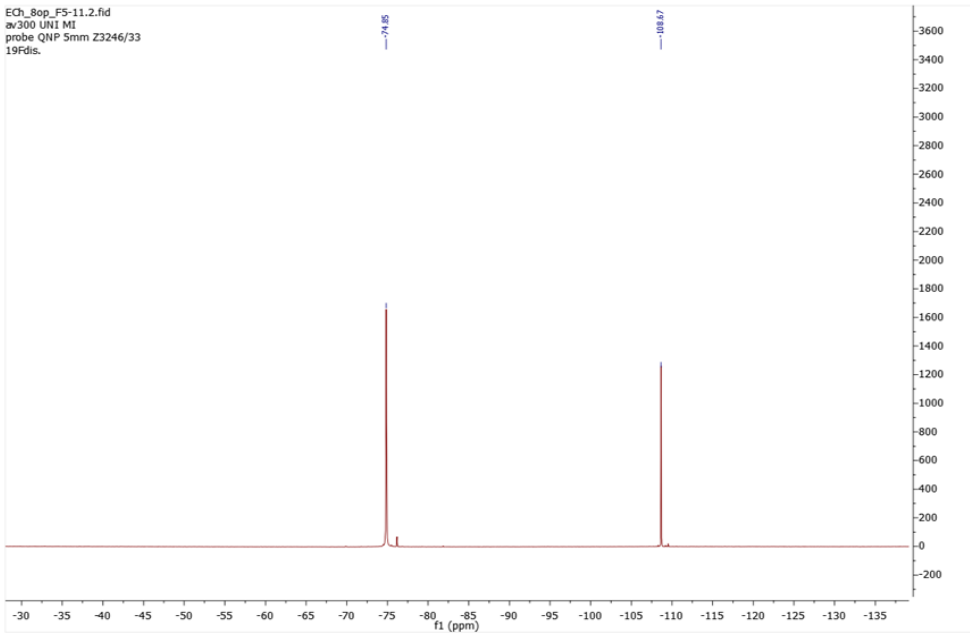

HR-MS of compound 70*

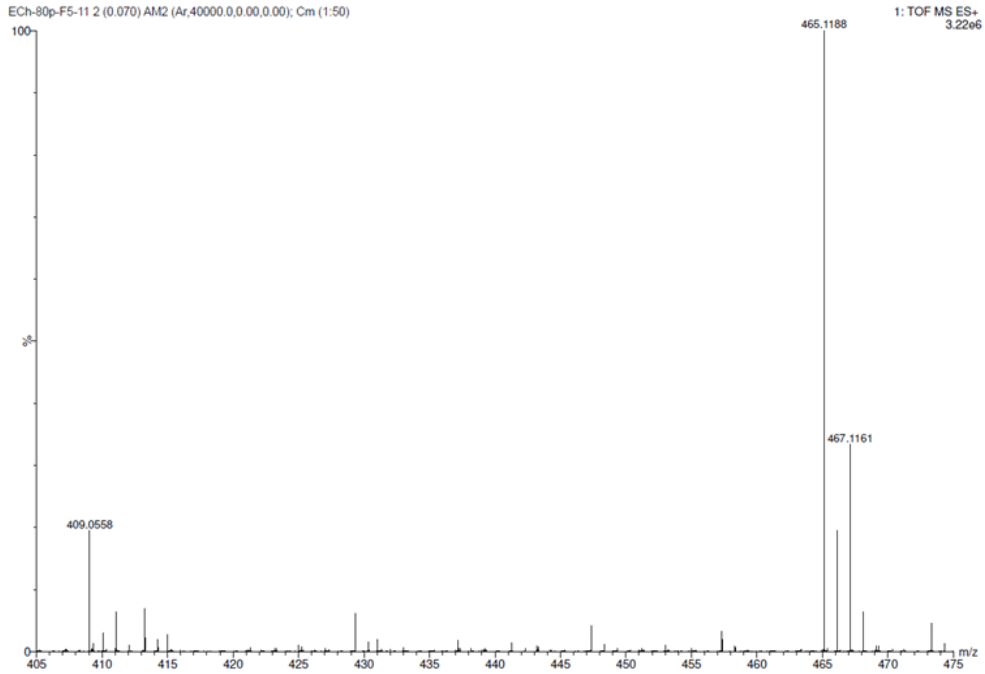

Elemental composition analysis of compound 70*

Elemental Composition Report

Single Mass Analysis
Tolerance = 5.0 PPM / DBE: min = -5.0, max = 300.0
Element prediction: Off
Number of isotope peaks used for i-FIT = 7

Monoisotopic Mass, Even Electron Ions
1 formula(e) evaluated with 1 results within limits (all results (up to 1000) for each mass)
Elements Used:
C: 14-14 H: 15-16 N: 2-2 O: 4-4 F: 4-4 Na: 0-1 Cl: 1-1

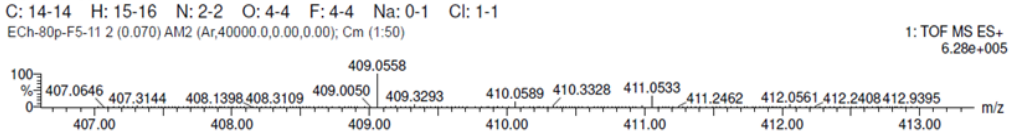

Minimum:				-5.0				
Maximum:		5.0	5.0	300.0				
Mass	Calc. Mass	mDa	PPM	DBE	i-FIT	Norm	Conf(%)	Formula
409.0558	409.0554	0.4	1.0	5.5	1696.3	n/a	n/a	C14 H15 N2 O4 F4 Na Cl

Determination of ee% for compound 70*

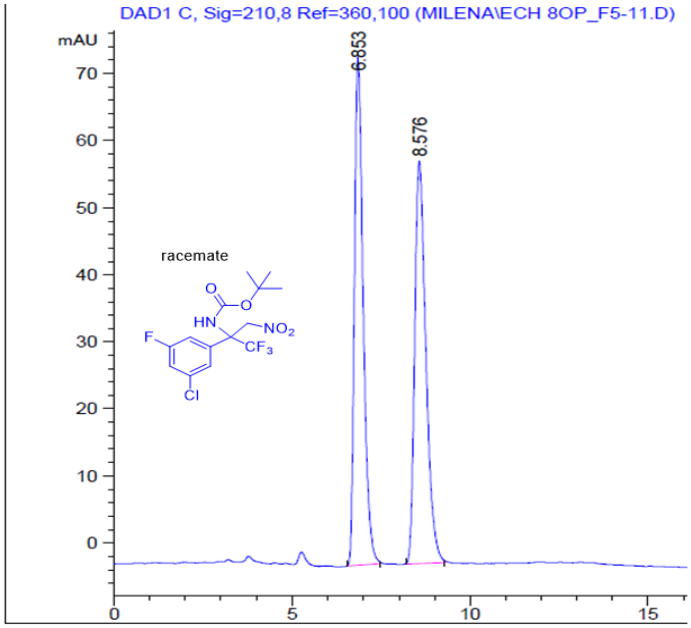

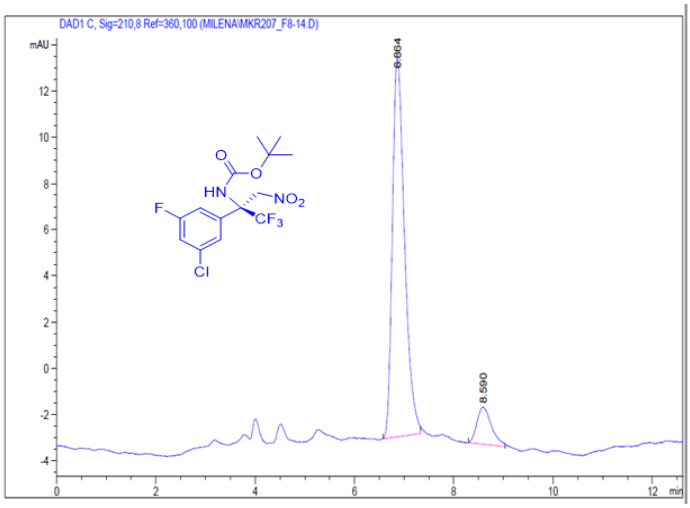

Peak #	RetTime [min]	Type	Width [min]	Area [mAU*s]	Height [mAU]	Area %
1	6.864	BB	0.2599	278.45642	16.41483	89.6027
2	8.590	BB	0.2639	32.31134	1.59809	10.3973

t-butyl (*S*)-(1,1,1-trifluoro-3-nitro-2-(m-tolyl)propan-2-yl) carbamate, **71***:

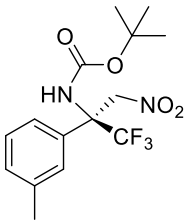

Reaction time was 48h at 0 °C. The product was isolated by silica gel column chromatography with *n*-hexane/ethyl acetate 98:2, as a colorless oil, 30% yield. Determination of ee% was done on chiral HPLC (Chiralpak AD column, eluent: *n*-hexane/isopropanol 95:5, flow rate 1 mL/min, t(major)=8.05 min, t(minor)= 8.91 min, 90% ee.

^{1}H NMR of compound 71* (300 MHz, $CDCl_3$)

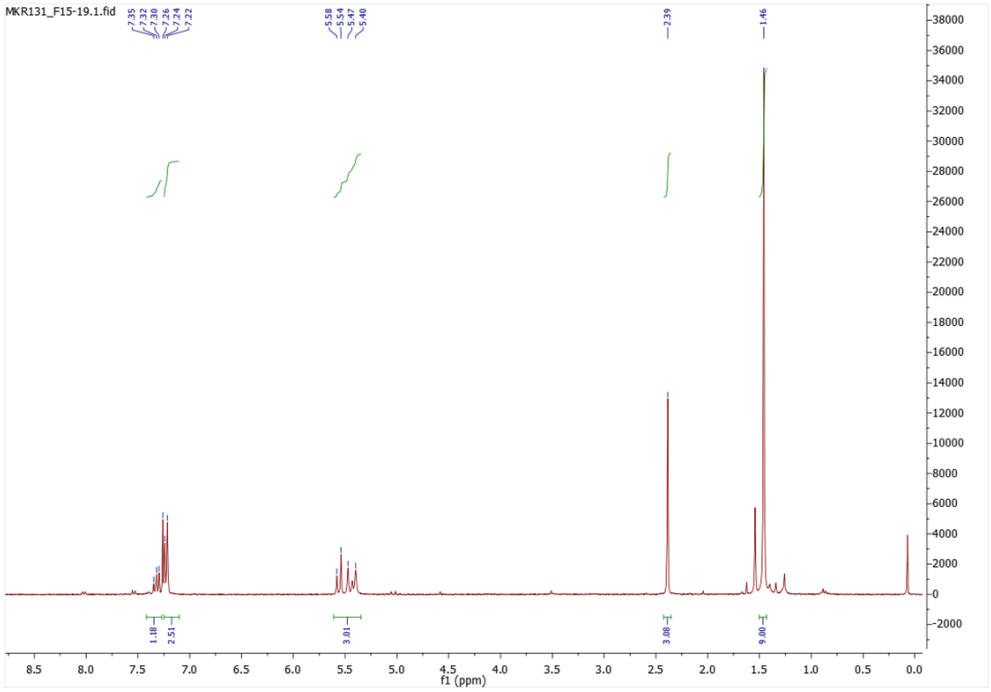

^{13}C NMR of compound 71* (75 MHz, $CDCl_3$)

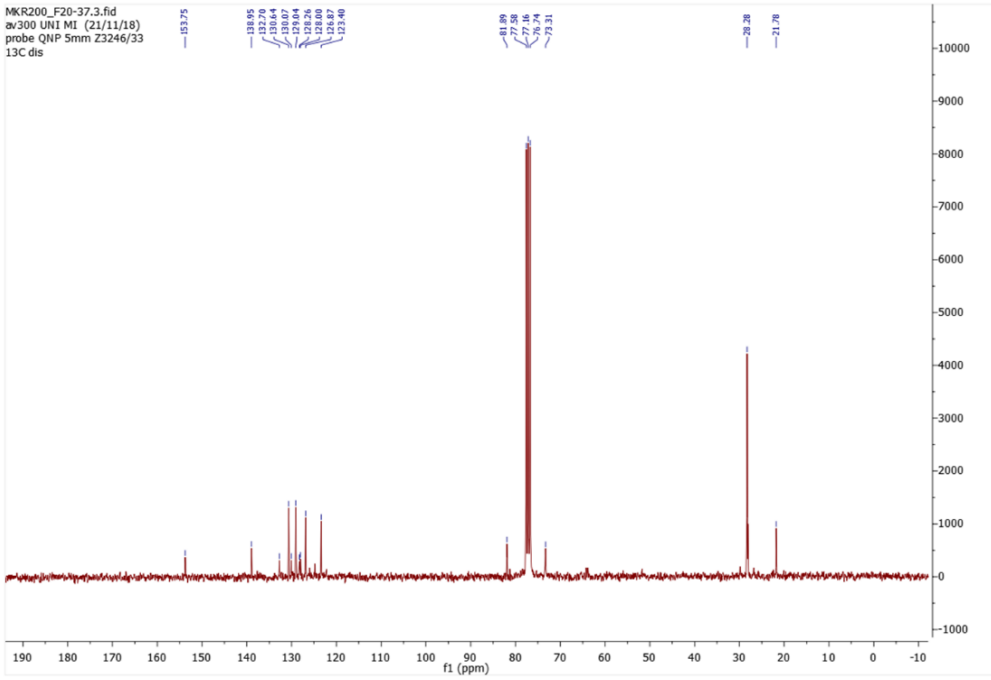

^{19}F NMR of compound 71* (282.1 MHz, $CDCl_3$)

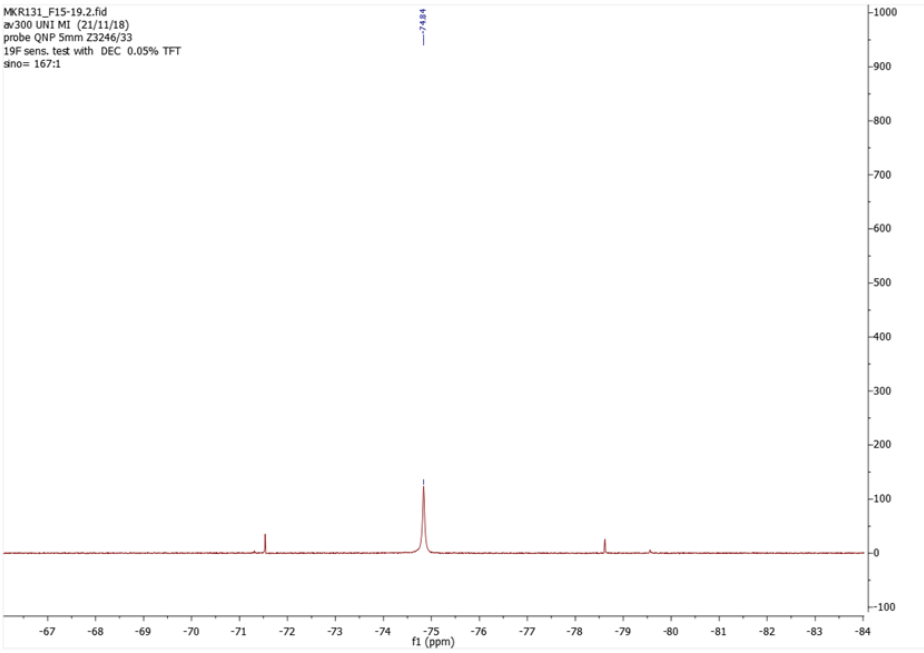

HR-MS of compound 71*

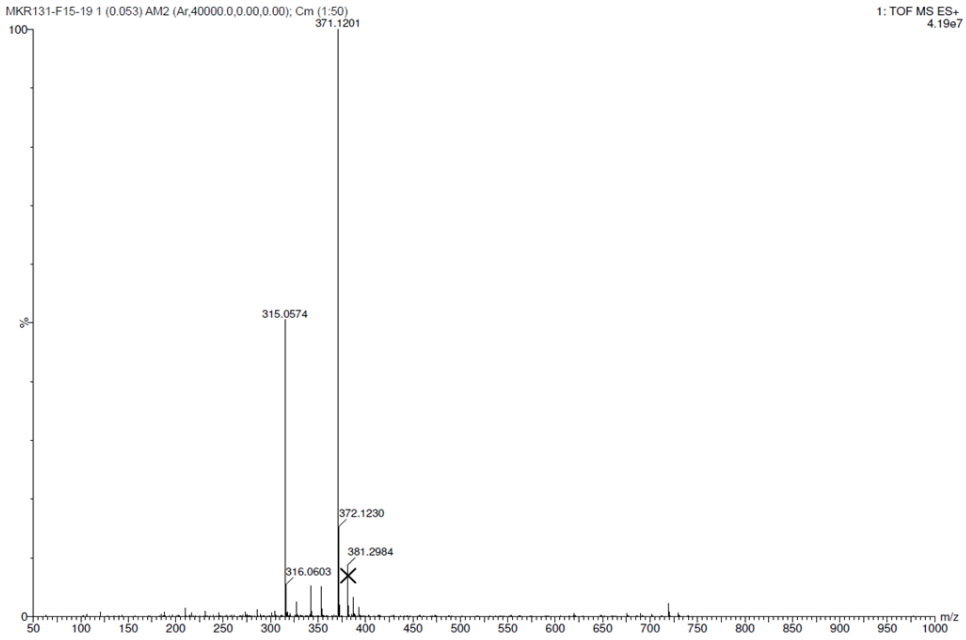

Elemental composition analysis of compound 71*

Elemental Composition Report

Single Mass Analysis
Tolerance = 5.0 PPM / DBE: min = -5.0, max = 300.0
Element prediction: Off
Number of isotope peaks used for i-FIT = 7

Monoisotopic Mass, Even Electron Ions
1 formula(e) evaluated with 1 results within limits (all results (up to 1000) for each mass)
Elements Used:
C: 15-15 H: 19-20 N: 2-2 O: 4-4 F: 3-3 Na: 0-1

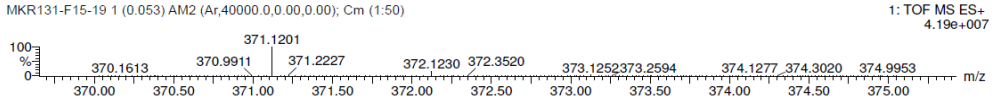

Minimum:				-5.0				
Maximum:		5.0	5.0	300.0				
Mass	Calc. Mass	mDa	PPM	DBE	i-FIT	Norm	Conf(%)	Formula
371.1201	371.1195	0.6	1.6	5.5	2486.4	n/a	n/a	C15 H19 N2 O4 F3 Na

Determination of ee% for compound 71*

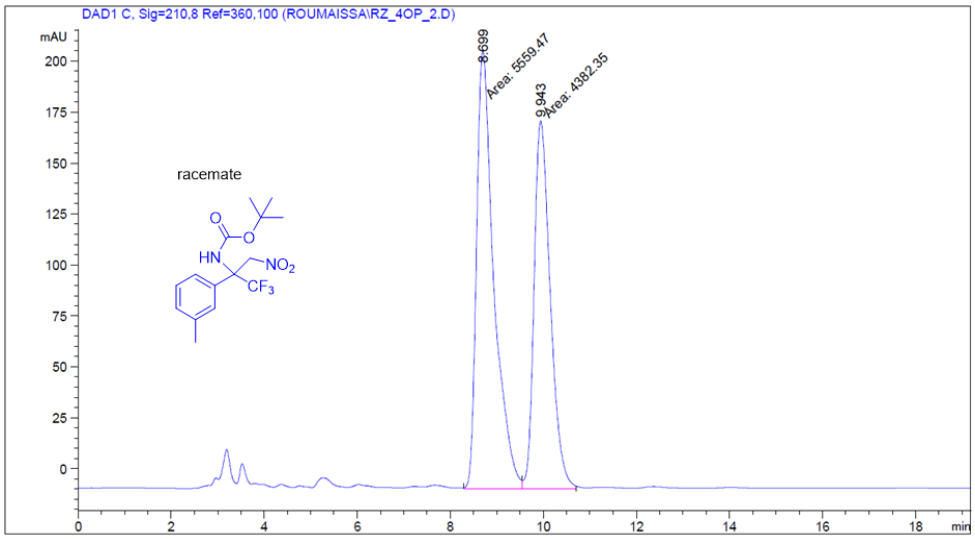

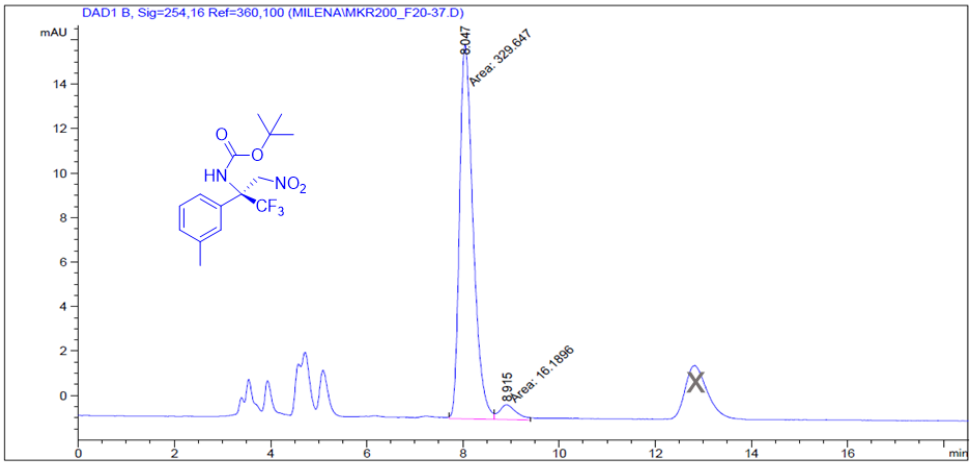

Peak #	RetTime [min]	Type	Width [min]	Area [mAU*s]	Height [mAU]	Area %
1	8.047	MF	0.3264	329.64716	16.83457	95.3187
2	8.915	FM	0.4073	16.18962	6.62434e-1	4.6813

t-butyl (*S*)-(2-(3-bromophenyl)-1,1,1-trifluoro-3-nitropropan-2-yl) carbamate, **72***:

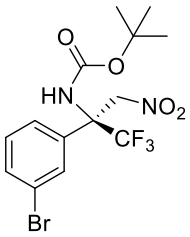

Reaction time was 48h at 0 °C. The product was isolated by silica gel column chromatography with *n*-hexane/ethyl acetate 95:5, as a colorless oil, 50% yield. Determination of ee% was done on chiral HPLC (Chiralpak AD column, eluent: *n*-hexane/isopropanol 95:5, flow rate 1 mL/min, t(minor)=12.94 min, t(major)= 13.99 min, ~88% ee.

^{1}H NMR of compound 72* (300 MHz, $CDCl_3$)

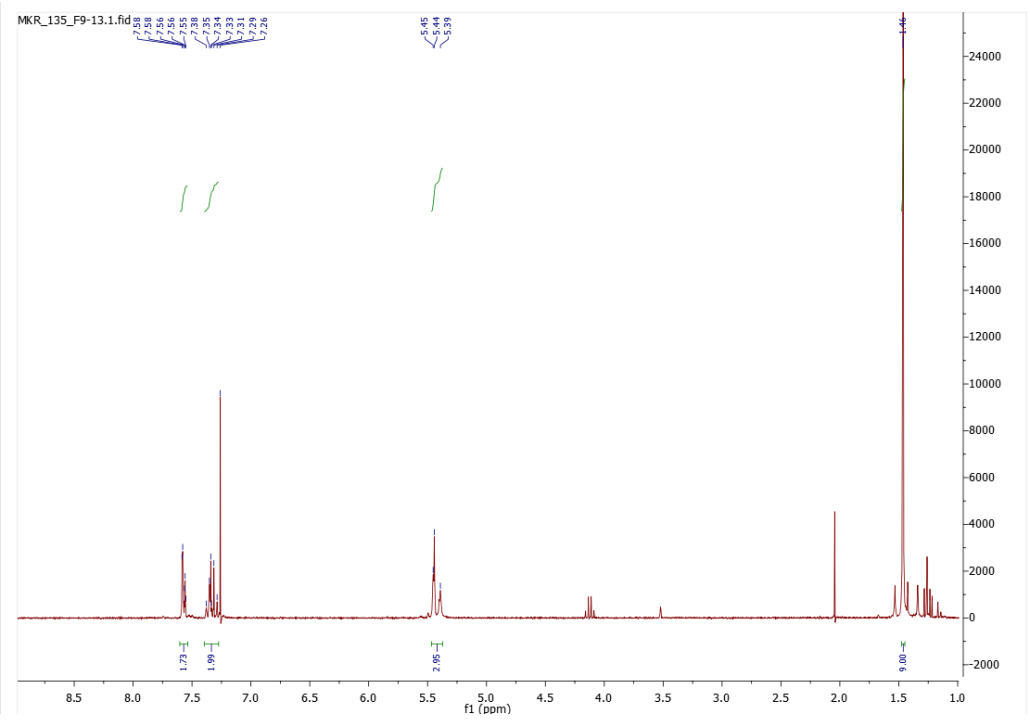

^{13}C NMR of compound 72* (75 MHz, $CDCl_3$)

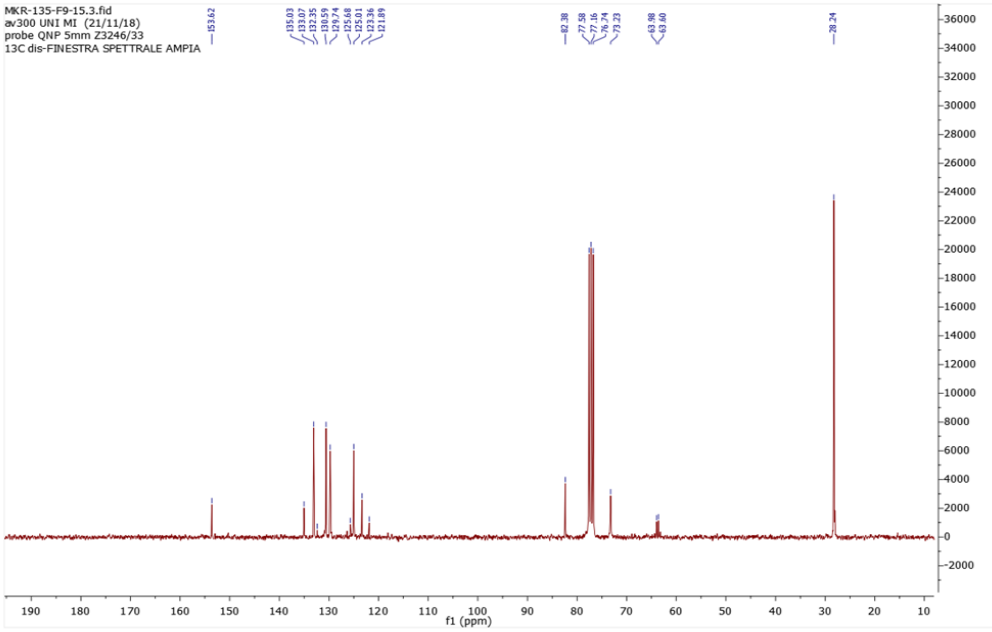

^{19}F NMR of compound 72* (282.1 MHz, $CDCl_3$)

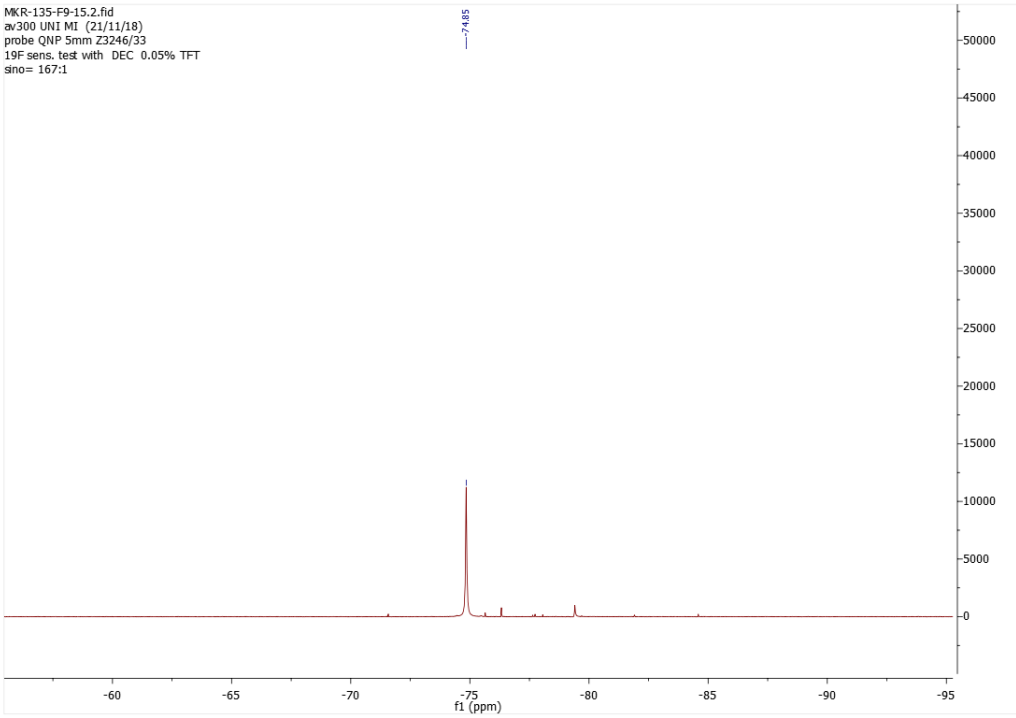

HR-MS of compound 72*

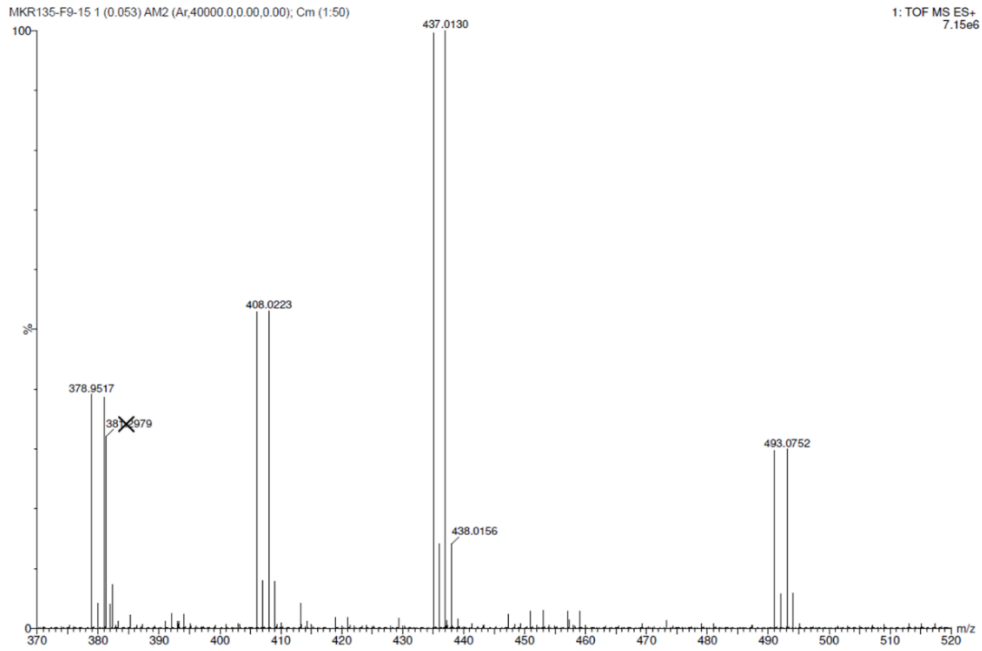

Elemental composition analysis of compound 72*

Elemental Composition Report

Single Mass Analysis
Tolerance = 5.0 PPM / DBE: min = -5.0, max = 300.0
Element prediction: Off
Number of isotope peaks used for i-FIT = 7

Monoisotopic Mass, Even Electron Ions
1 formula(e) evaluated with 1 results within limits (all results (up to 1000) for each mass)
Elements Used:
C: 14-14 H: 16-17 N: 2-2 O: 4-4 F: 3-3 Na: 0-1 Br: 1-1

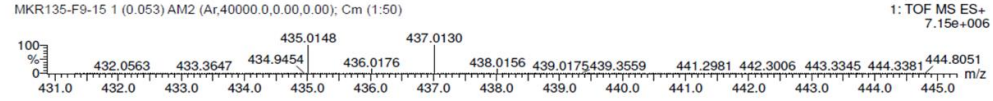

Minimum:				-5.0				
Maximum:		5.0	5.0	300.0				
Mass	Calc. Mass	mDa	PPM	DBE	i-FIT	Norm	Conf(%)	Formula
435.0148	435.0143	0.5	1.1	5.5	2902.0	n/a	n/a	C14 H16 N2 O4 F3 Na Br

Determination of ee% for compound 72*

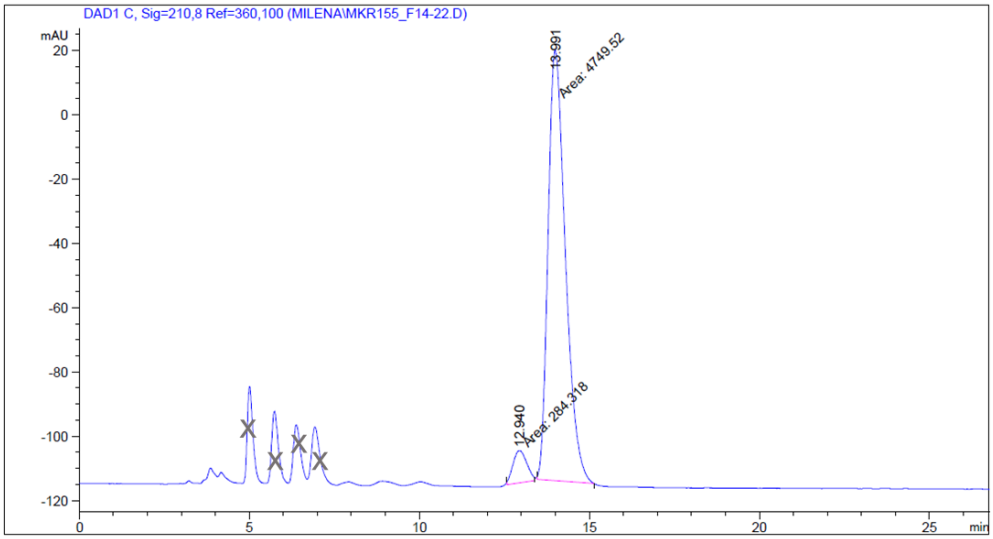

Peak #	RetTime [min]	Type	Width [min]	Area [mAU*s]	Height [mAU]	Area %
1	12.940	MM	0.4684	284.31839	10.11706	5.6481
2	13.991	MM	0.5914	4749.51660	133.83965	94.3519
Totals :				5033.83499	143.95671	

t-butyl (*S*)-(1,1,1-trifluoro-3-nitro-2-(4-(trifluoromethyl)phenyl)propan-2-yl) carbamate, **73***:

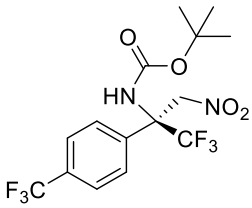

Reaction time was 48h at 0 °C. The product was isolated by silica gel column chromatography with *n*-hexane/ethyl acetate 95:5, as a pale-yellow oil, 35% yield. Determination of ee% was done on chiral HPLC (Chiralpak AD column, eluent: *n*-hexane/isopropanol 95:5, flow rate 1 mL/min, t(major)=6.90 min, t(minor)= 9.89 min, ~86% ee.

^{1}H NMR of compound 73* (300 MHz, $CDCl_3$)

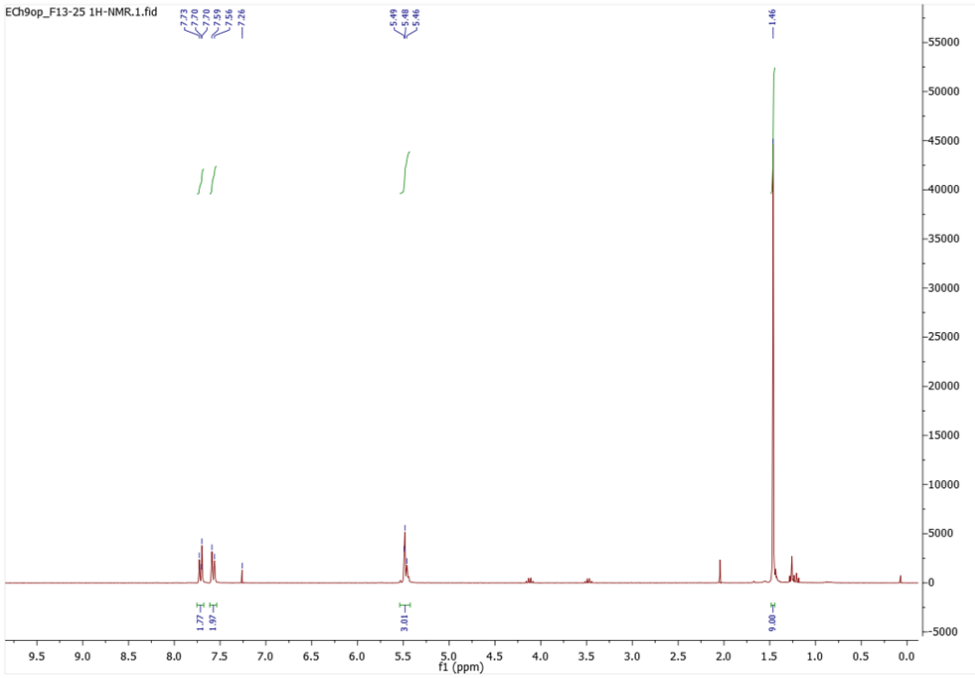

^{13}C NMR of compound 73* (75 MHz, $CDCl_3$)

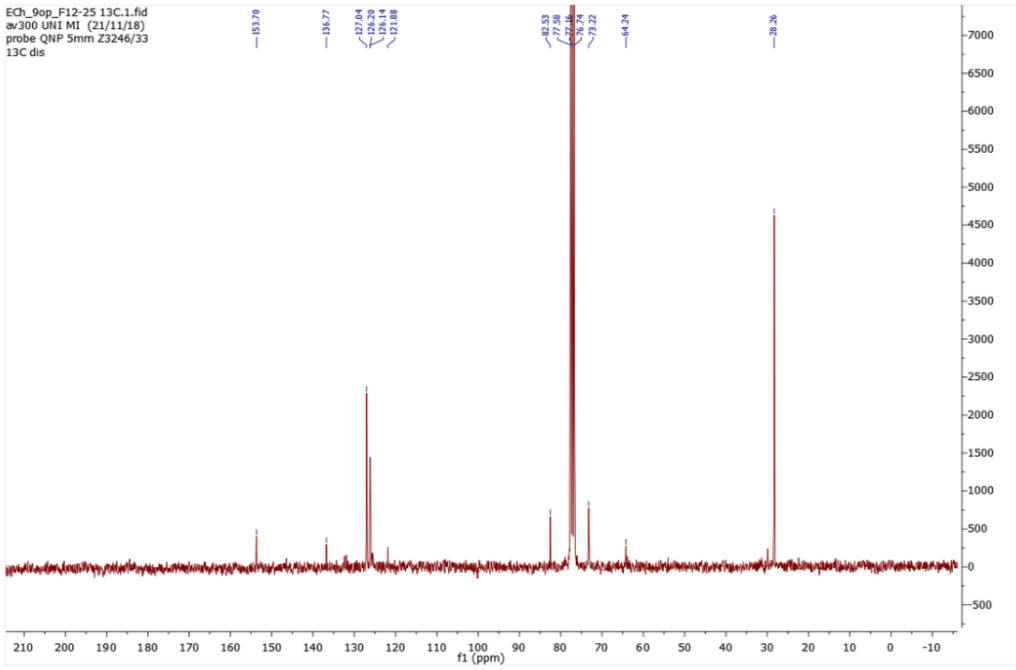

^{19}F NMR of compound 73* (282.1 MHz, $CDCl_3$)

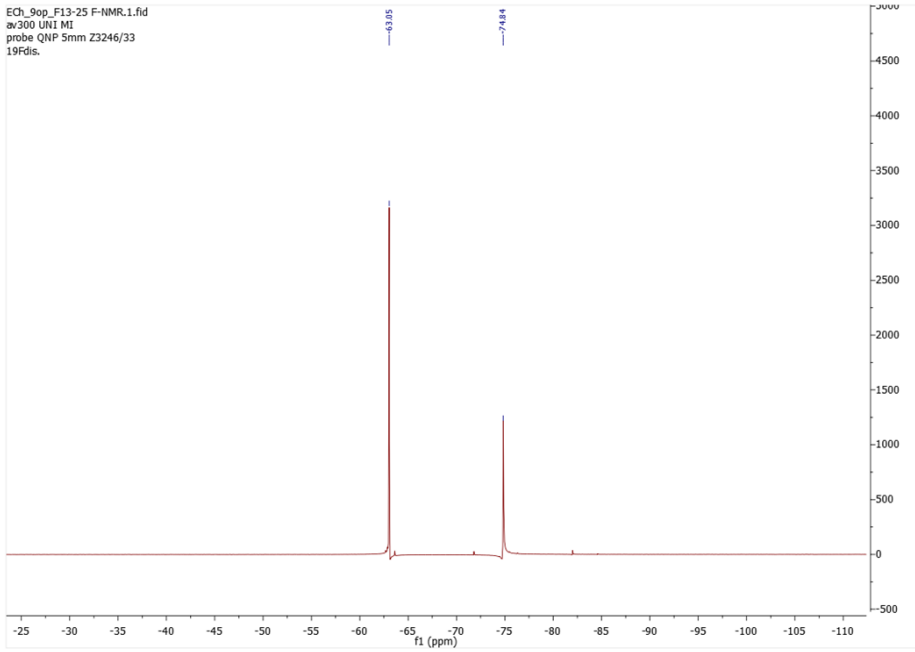

HR-MS of compound 73*

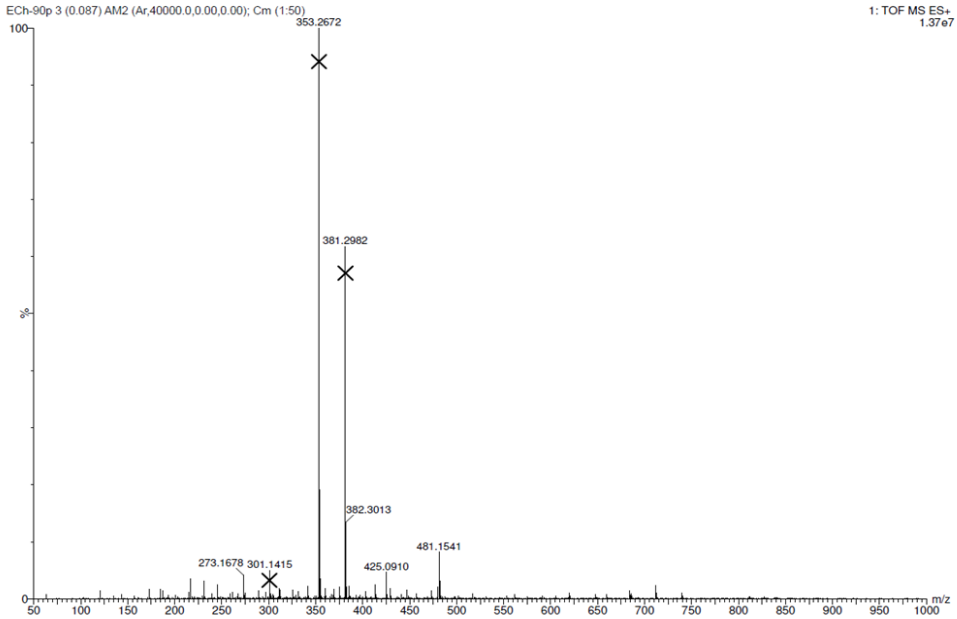

Elemental composition analysis of compound 73*

Elemental Composition Report

Single Mass Analysis
Tolerance = 5.0 PPM / DBE: min = -5.0, max = 300.0
Element prediction: Off
Number of isotope peaks used for i-FIT = 7

Monoisotopic Mass, Even Electron Ions
1 formula(e) evaluated with 1 results within limits (all results (up to 1000) for each mass)
Elements Used:
C: 15-15 H: 16-17 N: 2-2 O: 4-4 F: 6-6 Na: 0-1

ECh-90p 3 (0.087) AM2 (Ar,40000.0,0.00,0.00); Cm (1:50)

1: TOF MS ES+
6.35e+005

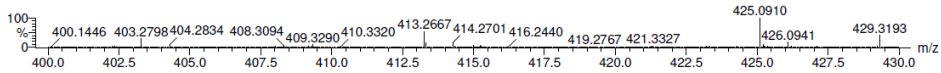

Minimum:				-5.0				
Maximum:		5.0	5.0	300.0				
Mass	Calc. Mass	mDa	PPM	DBE	i-FIT	Norm	Conf(%)	Formula
425.0910	425.0912	-0.2	-0.5	5.5	2169.8	n/a	n/a	C15 H16 N2 O4 F6 Na

Determination of ee% for compound 73*

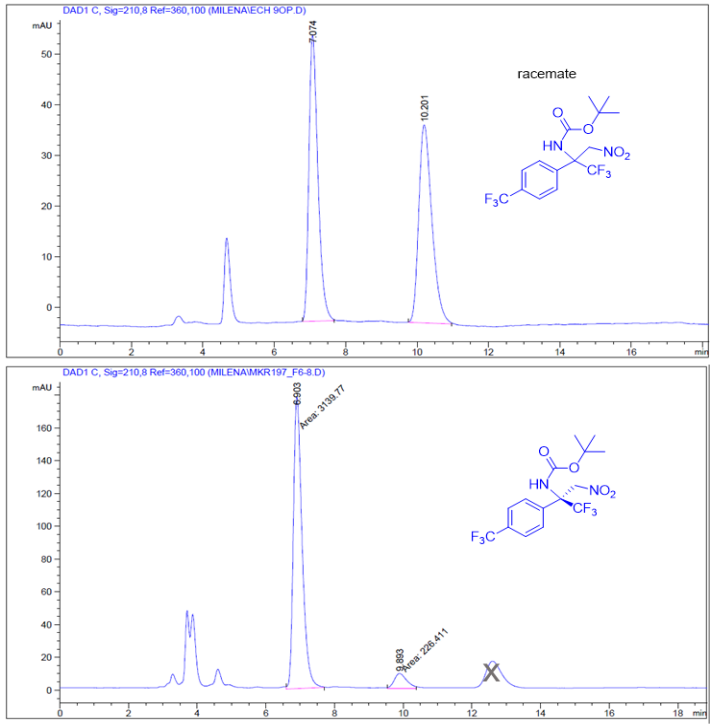

Peak #	RetTime [min]	Type	Width [min]	Area [mAU*s]	Height [mAU]	Area %
1	6.903	MM	0.2938	3139.77368	178.11678	93.2739
2	9.893	MM	0.4197	226.41133	8.99136	6.7261

t-butyl (*S*)-(2-(4-(*tert*-butyl)phenyl)-1,1,1-trifluoro-3-nitropropan-2-yl) carbamate, **74***:

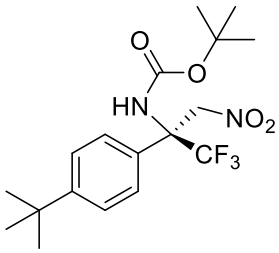

Reaction time was 63h at 0 °C. The product was isolated by silica gel column chromatography with *n*-hexane/ethyl acetate 98:2, as a colorless oil, 75% yield. Determination of ee% was done on chiral HPLC (Chiralcel OD-H, *n*-hexane/isopropanol 95:5, flow rate 0.8 mL/min), t(minor)=5.82 min, t(major)= 6.91 min, 92% ee.

^{1}H NMR of compound 74* (300 MHz, $CDCl_3$)

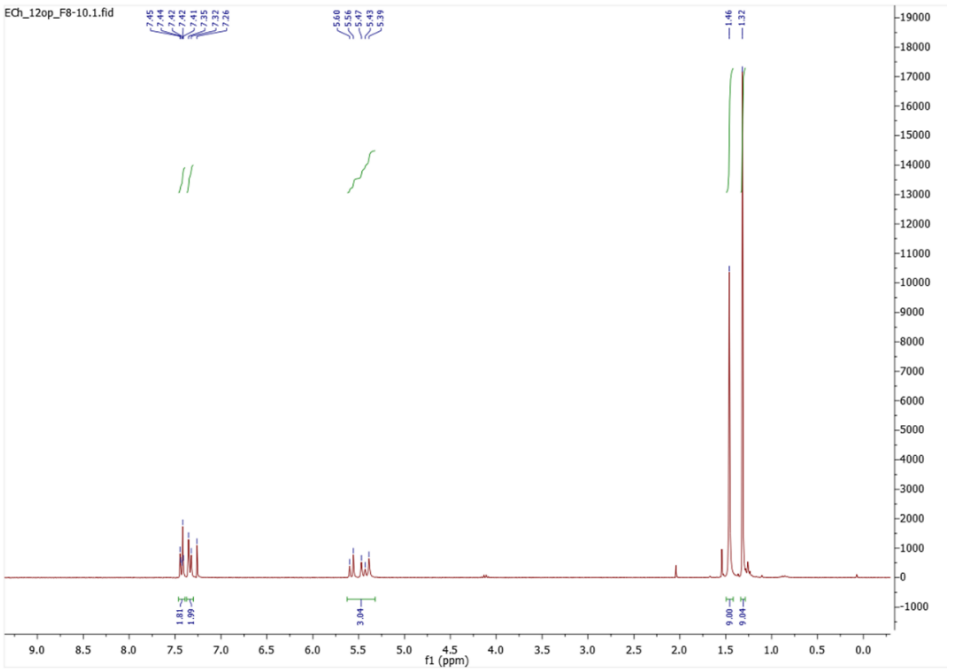

^{13}C NMR of compound 74* (75 MHz, $CDCl_3$)

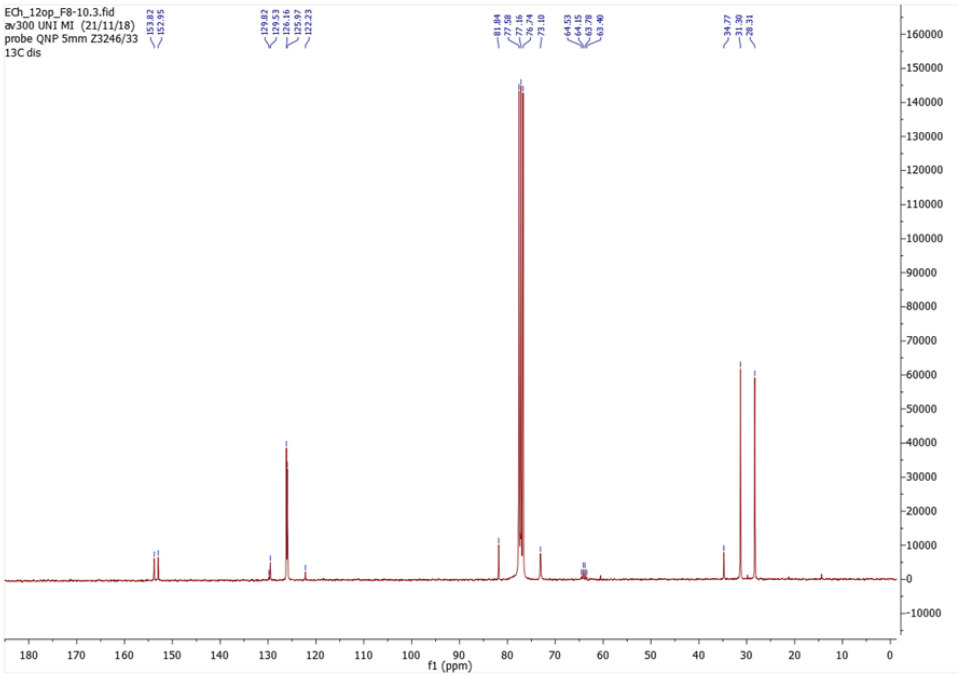

^{19}F NMR of compound 74* (282.1 MHz, $CDCl_3$)

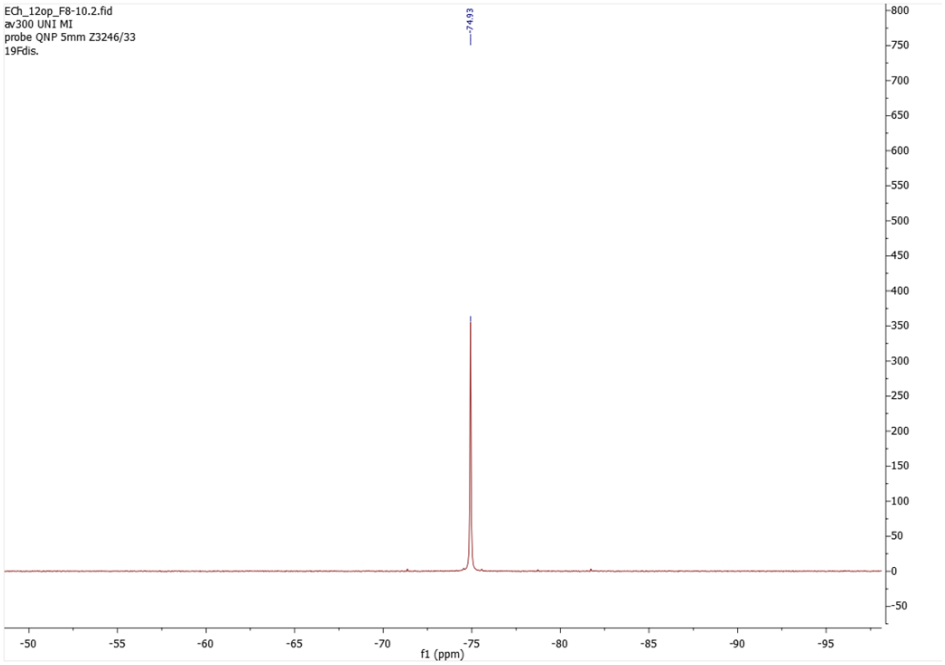

HR-MS of compound 74*

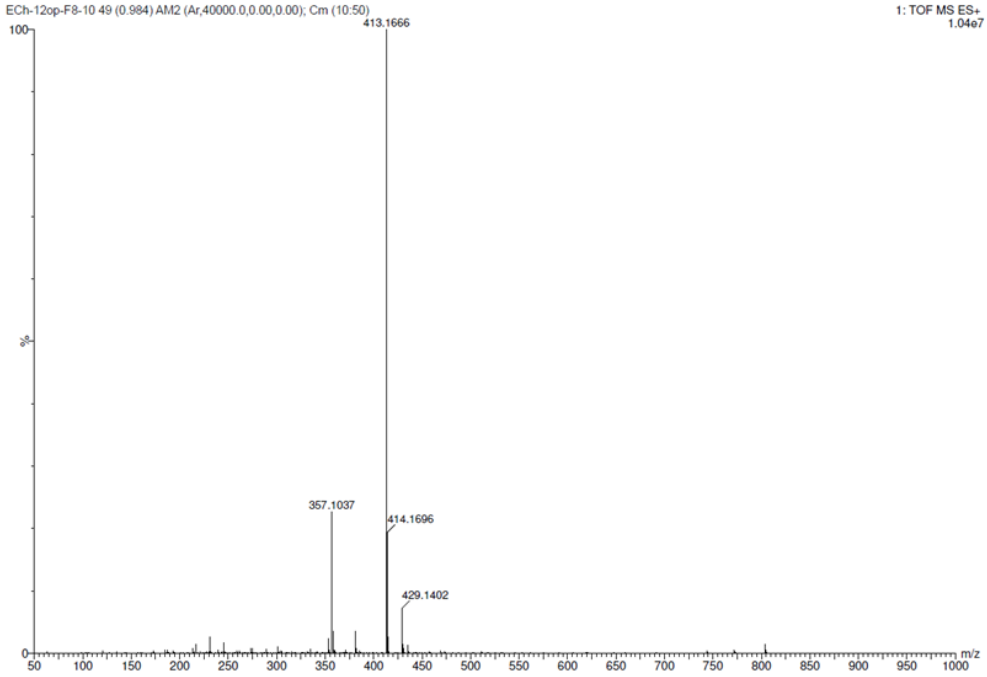

Elemental composition analysis of compound 74*

Elemental Composition Report

Single Mass Analysis
Tolerance = 5.0 PPM / DBE: min = -5.0, max = 300.0
Element prediction: Off
Number of isotope peaks used for i-FIT = 7

Monoisotopic Mass, Even Electron Ions
1 formula(e) evaluated with 1 results within limits (all results (up to 1000) for each mass)
Elements Used:
C: 18-18 H: 25-25 N: 2-2 O: 4-4 F: 3-3 Na: 0-1

ECh-12op-F8-10 49 (0.984) AM2 (Ar,40000.0,0.00,0.00); Cm (10:50)

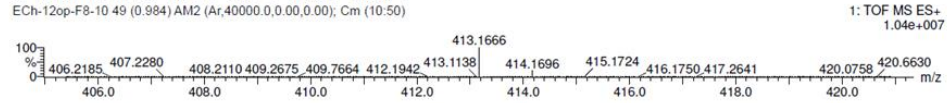

Minimum:				-5.0				
Maximum:		5.0	5.0	300.0				
Mass	Calc. Mass	mDa	PPM	DBE	i-FIT	Norm	Conf(%)	Formula
413.1666	413.1664	0.2	0.5	5.5	2824.3	n/a	n/a	C18 H25 N2 O4 F3 Na

Determination of ee% for compound 74*

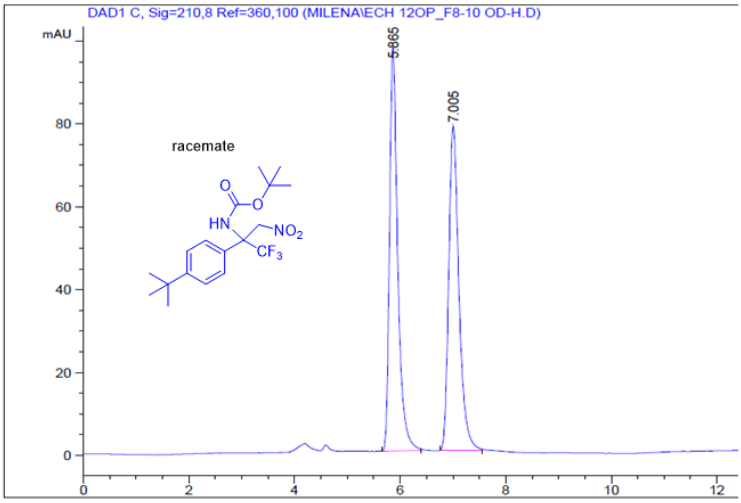

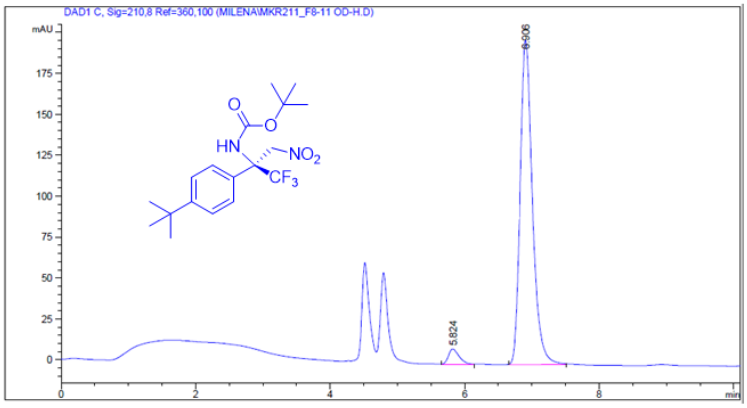

Peak #	RetTime [min]	Type	Width [min]	Area [mAU*s]	Height [mAU]	Area %
1	5.824	BB	0.1618	100.85136	9.35597	3.8702
2	6.906	BB	0.1935	2505.02539	198.17007	96.1298

t-butyl (*S*)-(1,1,1-trifluoro-3-nitro-2-(4-propylphenyl)propan-2-yl) carbamate, **75***:

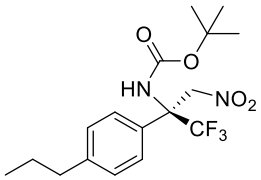

Reaction time was 48h at 0 °C. The product was isolated by silica gel column chromatography with *n*-hexane/ethyl acetate 98:2, as a colorless oil, 75% yield. Determination of ee% was done on chiral HPLC (Chiralcel OD-H, *n*-hexane/isopropanol 95:5, flow rate 0.8 mL/min), t(minor)=6.05 min, t(major)= 6.54 min, 95% ee.

^{1}H NMR of compound 75* (300 MHz, $CDCl_3$)

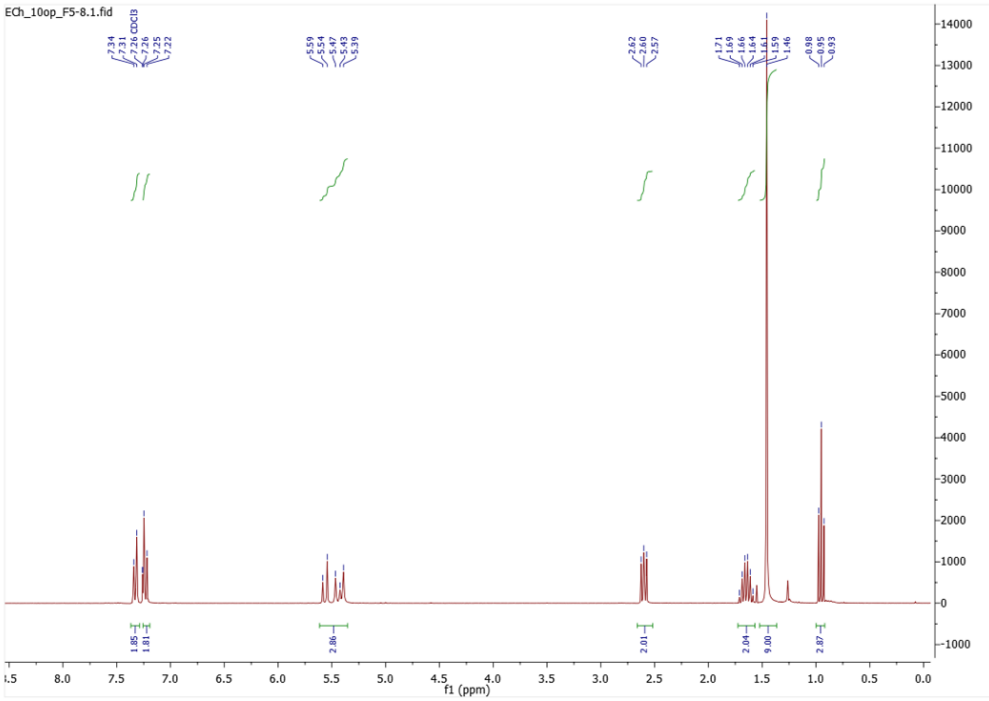

^{13}C NMR of compound 75* (75 MHz, $CDCl_3$)

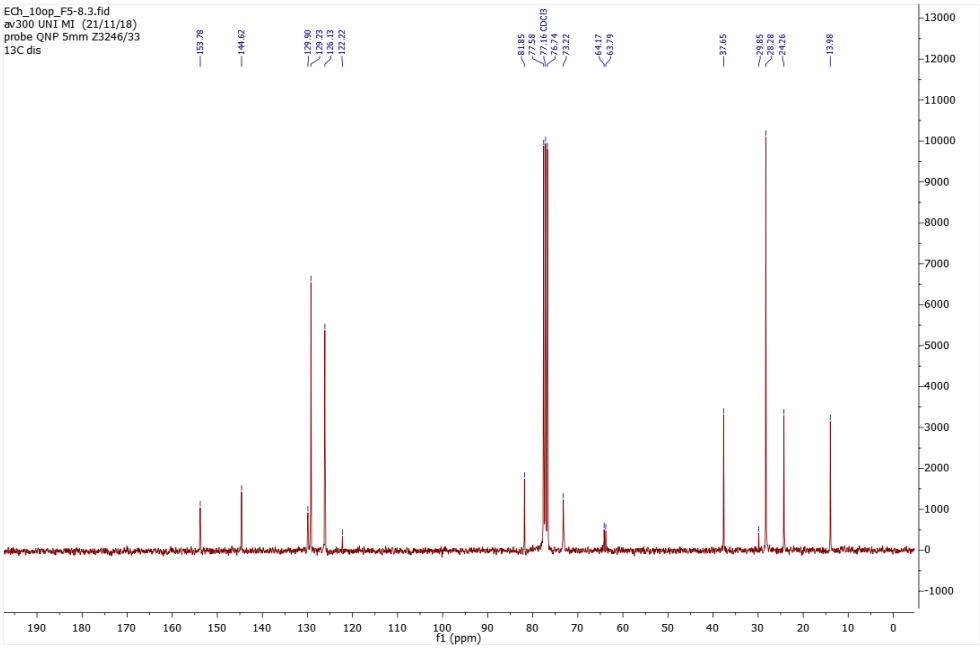

^{19}F NMR of compound 75* (282.1 MHz, $CDCl_3$)

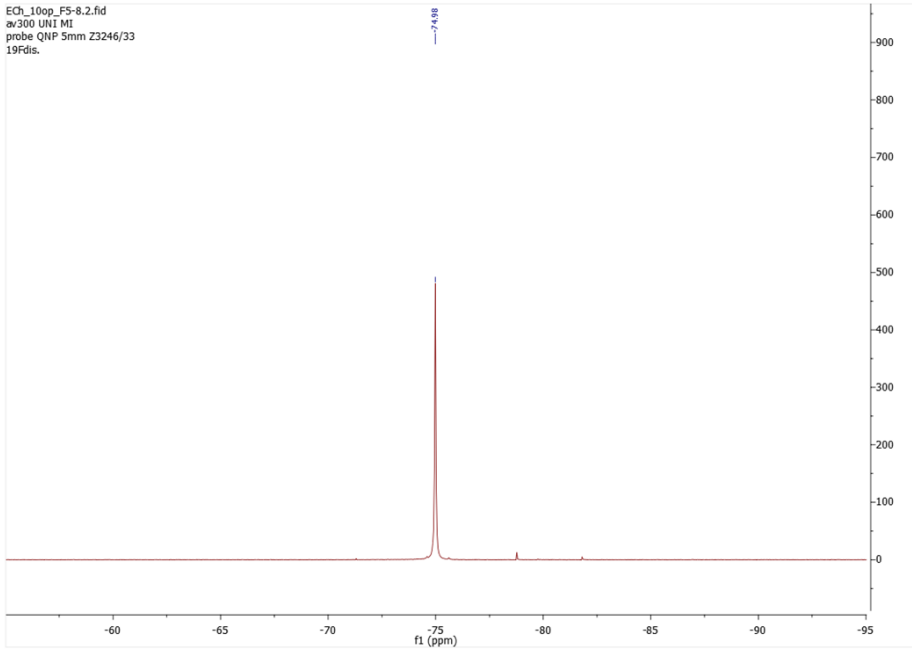

HR-MS of compound 75*

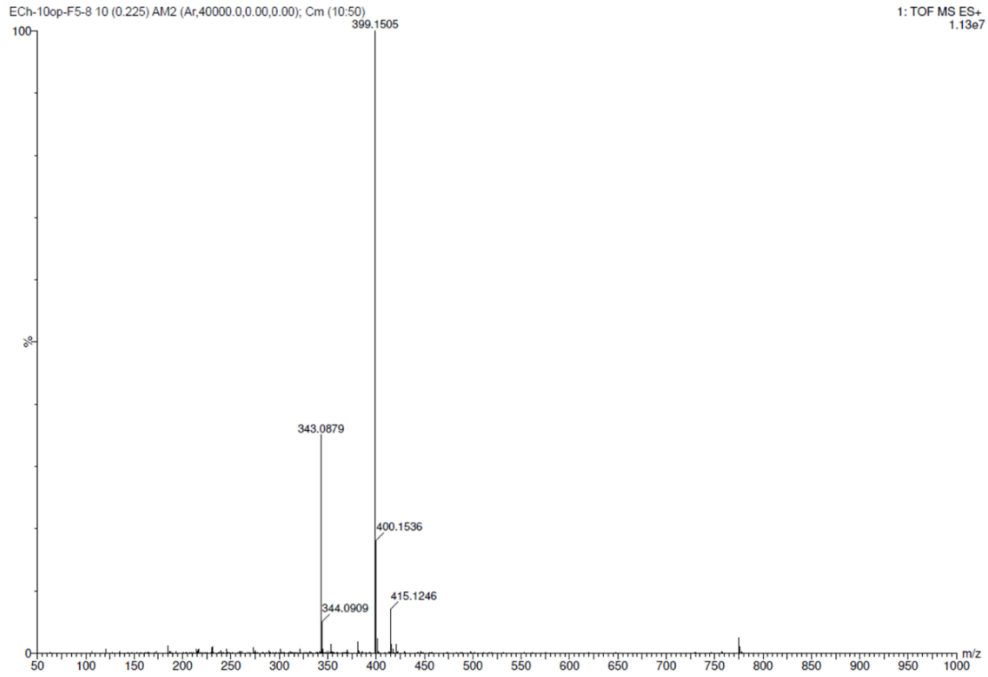

Elemental composition analysis of compound 75*

Elemental Composition Report

Single Mass Analysis
Tolerance = 5.0 PPM / DBE: min = -5.0, max = 300.0
Element prediction: Off
Number of isotope peaks used for i-FIT = 7

Monoisotopic Mass, Even Electron Ions
1 formula(e) evaluated with 1 results within limits (all results (up to 1000) for each mass)
Elements Used:
C: 17-17 H: 23-24 N: 2-2 O: 4-4 F: 3-3 Na: 0-1

ECh-10op-F5-8 10 (0.225) AM2 (Ar,40000.0,0.00,0.00); Cm (10:50)
1: TOF MS ES+
1.13e+007

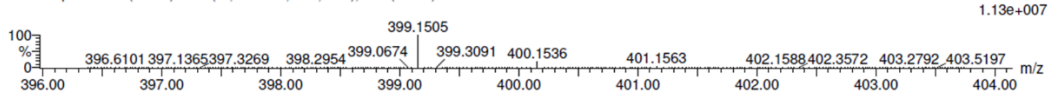

Minimum:				-5.0				
Maximum:		5.0	5.0	300.0				
Mass	Calc. Mass	mDa	PPM	DBE	i-FIT	Norm	Conf(%)	Formula
399.1505	399.1508	-0.3	-0.8	5.5	2154.6	n/a	n/a	C17 H23 N2 O4 F3 Na

Determination of ee% for compound 75*

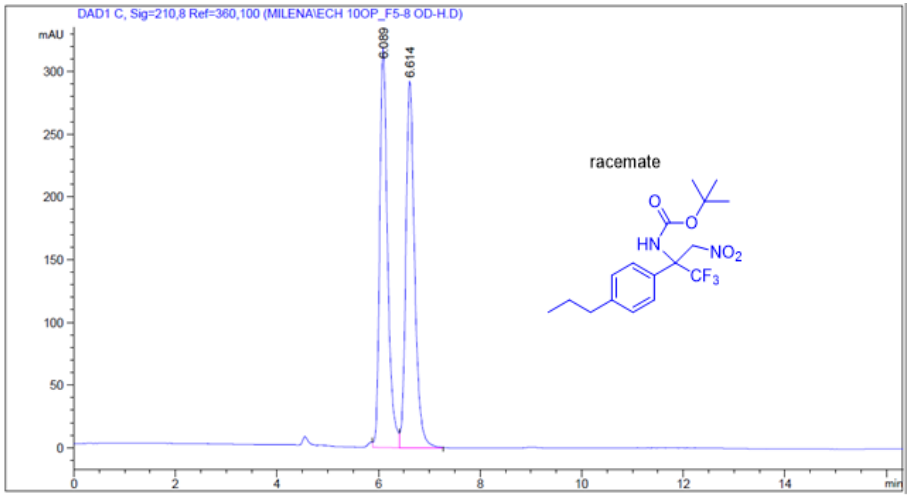

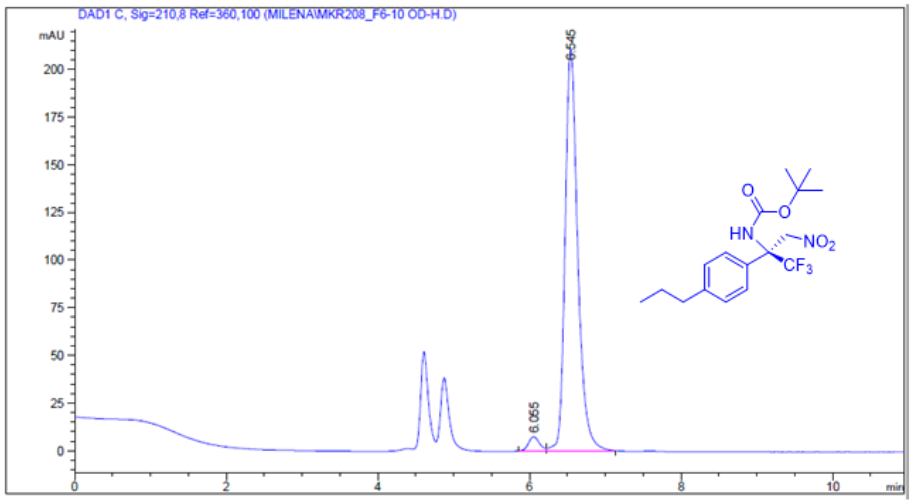

Peak #	RetTime [min]	Type	Width [min]	Area [mAU*s]	Height [mAU]	Area %
1	6.055	BV	0.1563	79.30680	7.68990	3.1241
2	6.545	VB	0.1759	2459.25366	211.17888	96.8759

t-butyl (*S*)-(1,1,1-trifluoro-2-(3-isopropylphenyl)-3-nitropropan-2-yl) carbamate, **76***:

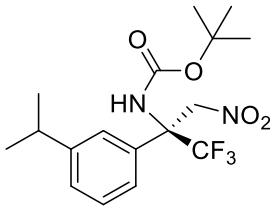

Reaction time was 48h at 0 °C. The product was isolated by silica gel column chromatography with *n*-hexane/ethyl acetate 98:2, as a colorless oil, 51% yield. Determination of ee% was done on chiral HPLC (Chiralcel OD-H, *n*-hexane/isopropanol 95:5, flow rate 0.8 mL/min), t(minor)=5.8 min, t(major)= 6.3 min, 95% ee.

^{1}H NMR of compound 76* (300 MHz, $CDCl_3$)

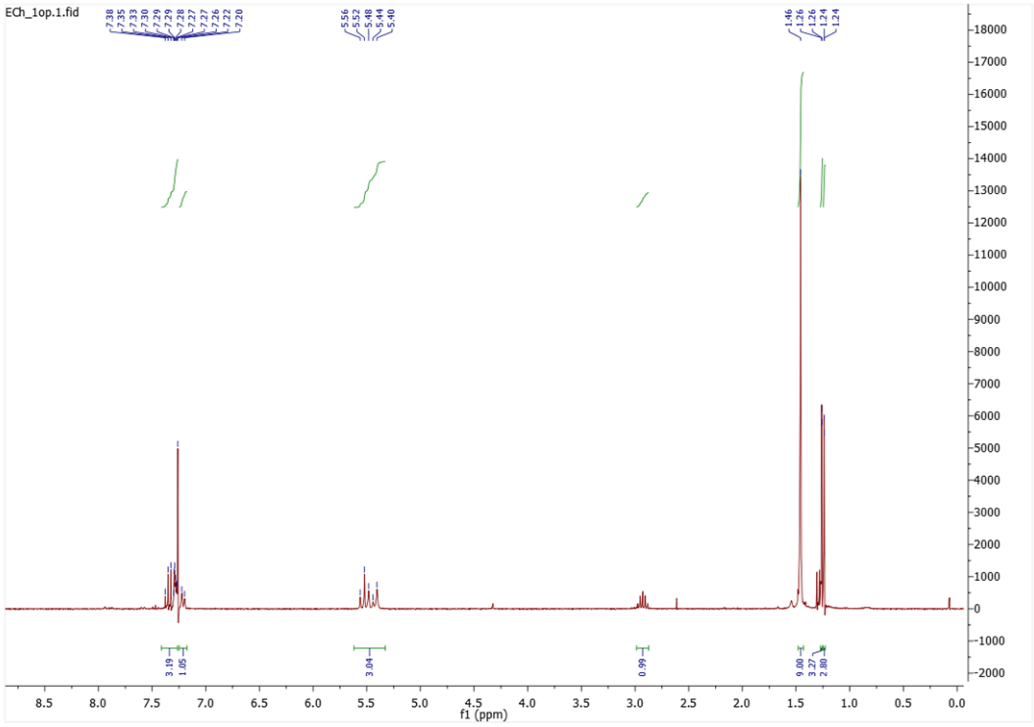

^{13}C NMR of compound 76* (75 MHz, $CDCl_3$)

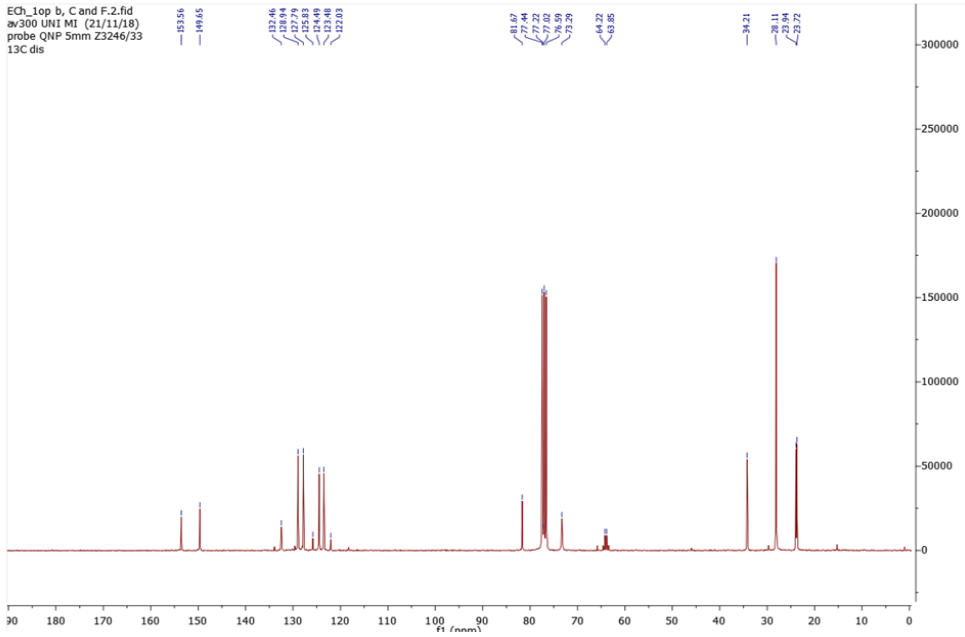

^{19}F NMR of compound 76* (282.1 MHz, $CDCl_3$)

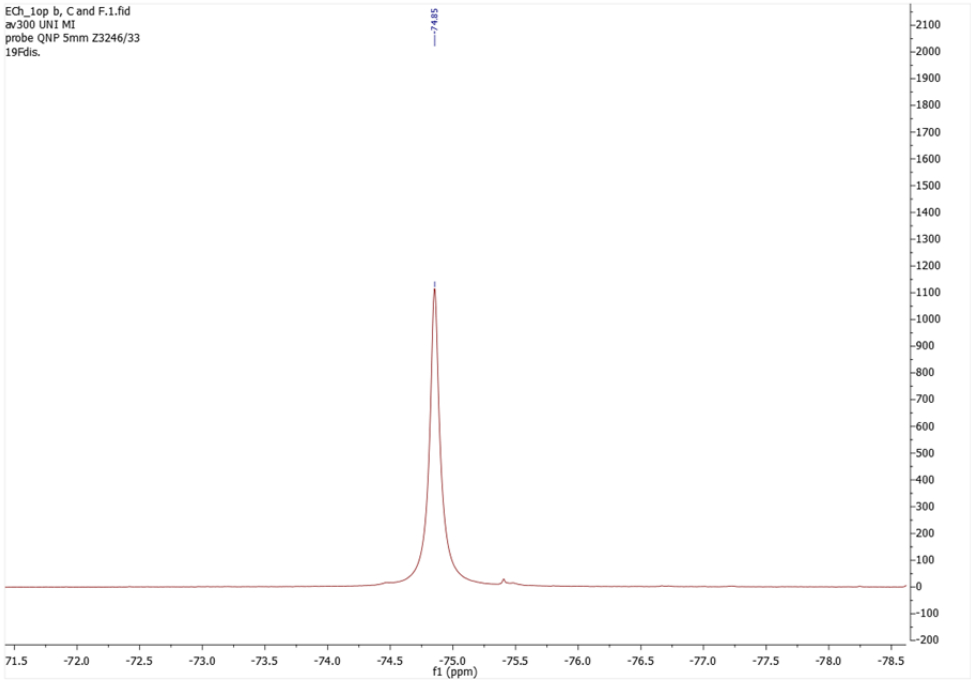

HR-MS of compound 76*

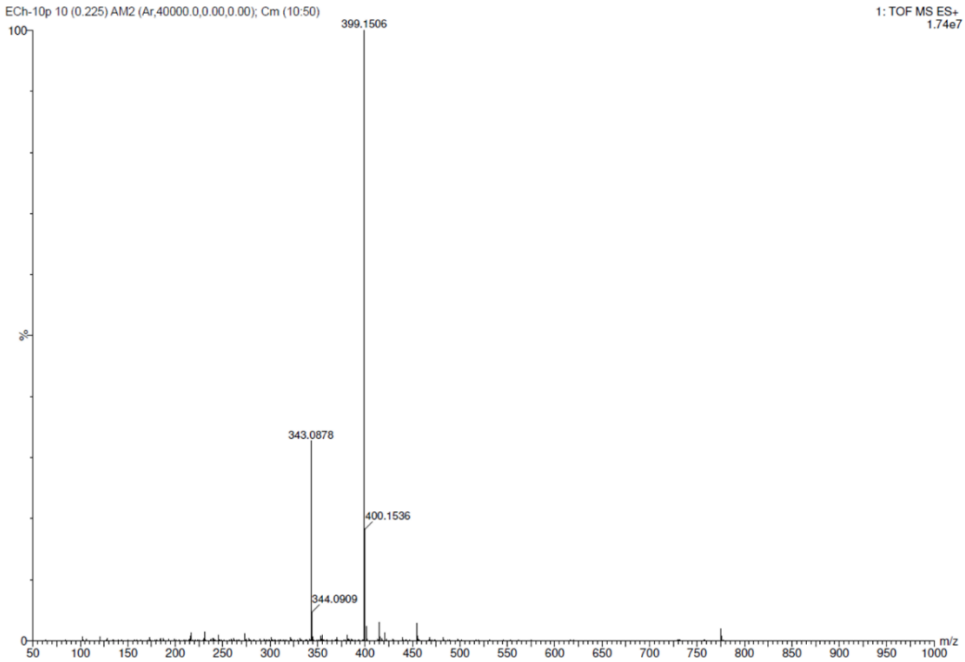

Elemental composition analysis of compound 76*

Elemental Composition Report

Single Mass Analysis
Tolerance = 5.0 PPM / DBE: min = -5.0, max = 300.0
Element prediction: Off
Number of isotope peaks used for i-FIT = 7

Monoisotopic Mass, Even Electron Ions
1 formula(e) evaluated with 1 results within limits (all results (up to 1000) for each mass)
Elements Used:
C: 17-17 H: 23-24 N: 2-2 O: 4-4 F: 3-3 Na: 0-1

ECh-10p 10 (0.225) AM2 (Ar,40000.0,0.00,0.00); Cm (10:50)

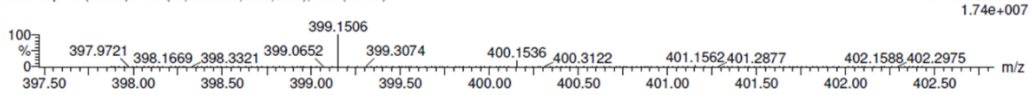

Minimum:				-5.0				
Maximum:		5.0	5.0	300.0				
Mass	Calc. Mass	mDa	PPM	DBE	i-FIT	Norm	Conf(%)	Formula
399.1506	399.1508	-0.2	-0.5	5.5	1606.3	n/a	n/a	C17 H23 N2 O4 F3 Na

Determination of ee% for compound 76*

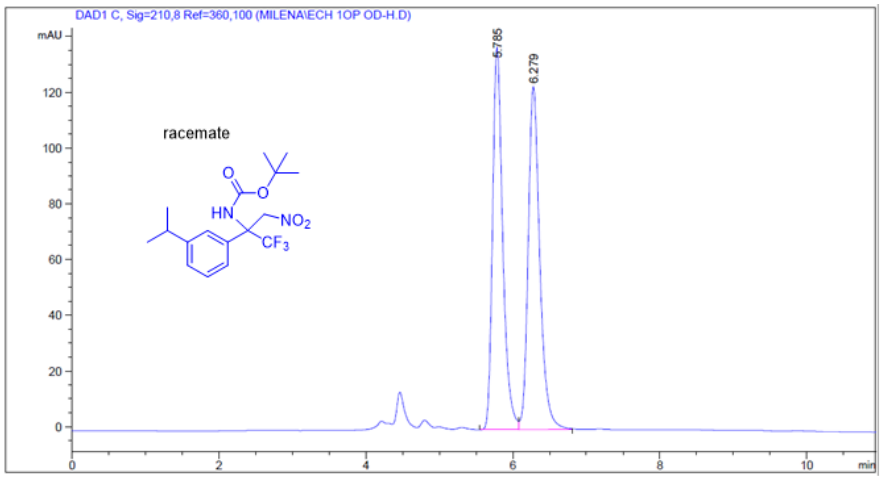

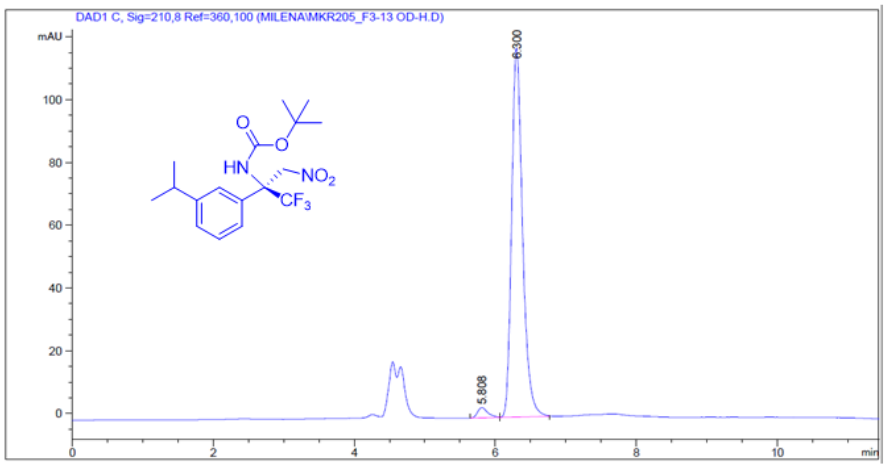

Peak #	RetTime [min]	Type	Width [min]	Area [mAU*s]	Height [mAU]	Area %
1	5.808	BV	0.1494	33.14052	3.29426	2.5460
2	6.300	VB	0.1641	1268.54358	117.39259	97.4540

6.5.2 Screening of BIMPs in aza-Henry reaction with model ketimines **48** or **50** - general procedure:

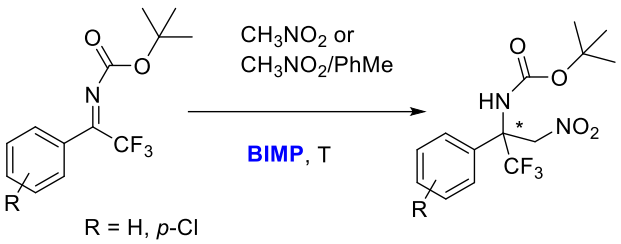

A 1.5 mL vial with septum connected with nitrogen inlet, was charged with 0.1 equiv. (table 3 and table 4) or 0.2 equiv. of BIMP catalyst (table 3, entry 20) and 1 equiv. (50 mg) of ketimine **48** or **50**. 20 equiv. of nitromethane (table 3 and 4) or mixture of nitromethane/toluene (table 3, entry 3) was added, and the reaction mixture was stirred at indicated temperature until the completion of the reaction. The reactions were monitored by TLC and ^{1}H NMR. After the reaction is done, nitromethane ($MeNO_2$) or nitromethane/toluene was removed under reduced pressure and the residue was purified by column chromatography on silica gel with *n*-hexane/ethyl acetate to afford the desired β-nitroamines. Determination of ee% was done on chiral HPLC (Chiralpak AD column, eluent: *n*-hexane/isopropanol 95:5, flow rate 1 mL/min). The detail about reaction conditions, yields and ee% values are reported in table 3 and 4, section 5.5.

Determination of ee% for aza-Henry products 48 and 50 with different BIMPs:

Aza-Henry reaction promoted by catalyst **25**

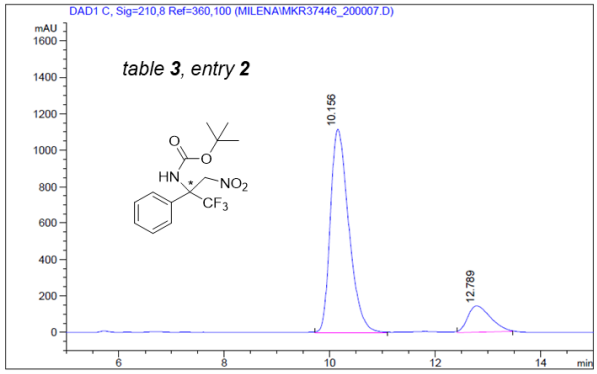

Signal 1: DAD1 C, Sig=210,8 Ref=360,100

Peak #	RT [min]	Type	Width [min]	Area	Area %	Name
1	10.156	MM	0.406	27233.713	86.139	
2	12.789	MM	0.503	4382.323	13.861	

Aza-Henry reaction promoted by catalyst **17**

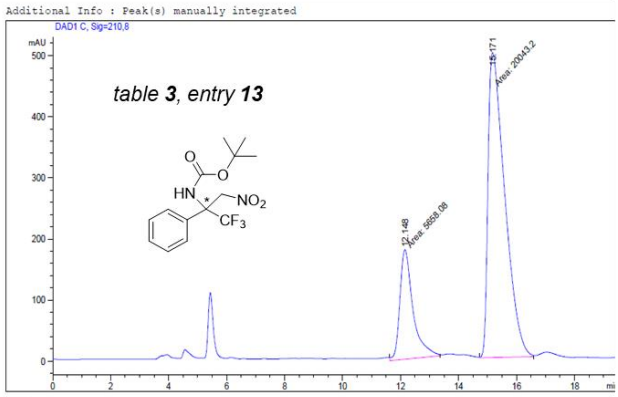

Peak #	RetTime [min]	Type	Width [min]	Area [mAU*s]	Height [mAU]	Area %
1	12.148	MM	0.5268	5658.08105	179.00389	22.0148
2	15.171	MM	0.6697	2.00432e4	498.84323	77.9852
Totals :				2.57013e4	677.84712	

Aza-Henry reaction promoted by catalyst **42a**

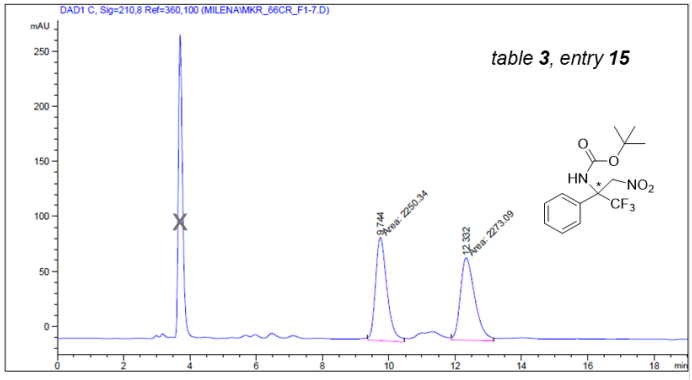

Peak #	RetTime [min]	Type	Width [min]	Area [mAU*s]	Height [mAU]	Area %
1	9.744	MM	0.4004	2250.33984	93.66335	49.7485
2	12.332	MM	0.5065	2273.08838	74.79371	50.2515
Totals :				4523.42822	168.45705	

Aza-Henry reaction promoted by catalyst **42b**

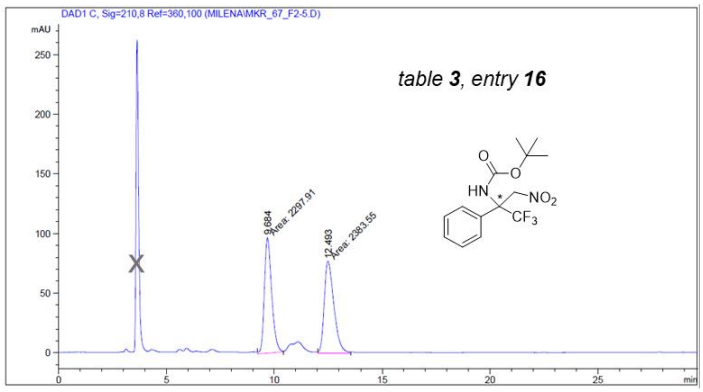

Peak #	RetTime [min]	Type	Width [min]	Area [mAU*s]	Height [mAU]	Area %
1	9.684	MM	0.3951	2297.91162	96.92691	49.0853
2	12.493	MM	0.5164	2383.55054	76.92194	50.9147
Totals :				4681.46216	173.84885	

Aza-Henry reaction promoted by catalyst **34**

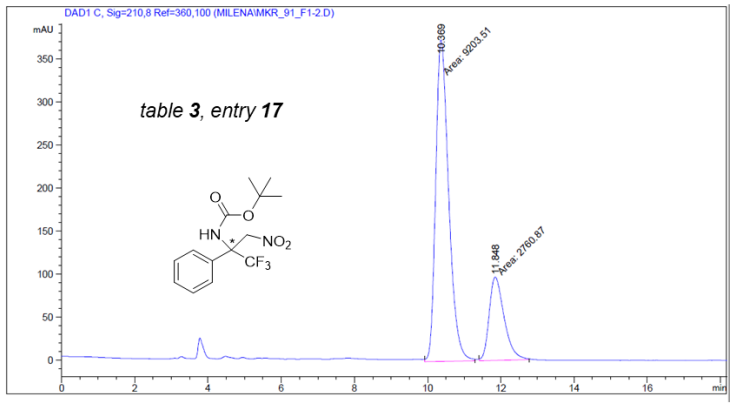

Peak #	RetTime [min]	Type	Width [min]	Area [mAU*s]	Height [mAU]	Area %
1	10.369	MM	0.4104	9203.50879	373.77548	76.9242
2	11.848	MM	0.4752	2760.87207	96.83169	23.0758

Aza-Henry reaction promoted by catalyst **29**

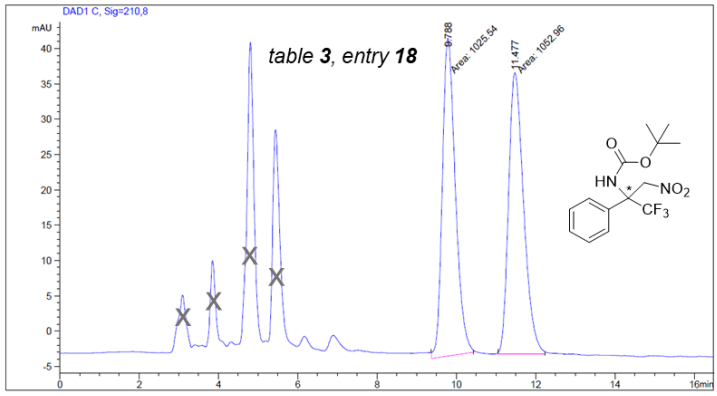

Peak #	RetTime [min]	Type	Width [min]	Area [mAU*s]	Height [mAU]	Area %
1	9.788	MM	0.3799	1025.53943	44.99496	49.3405
2	11.477	MM	0.4403	1052.95557	39.86164	50.6595

Aza-Henry reaction promoted by catalyst **27**

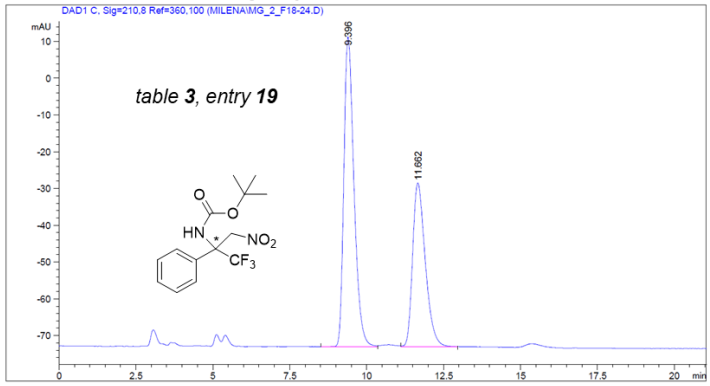

Peak #	RetTime [min]	Type	Width [min]	Area [mAU*s]	Height [mAU]	Area %
1	9.396	BV	0.3514	1931.91760	84.27702	60.1945
2	11.662	VB	0.4426	1277.53906	44.54738	39.8055

Aza-Henry reaction promoted by catalyst **45**

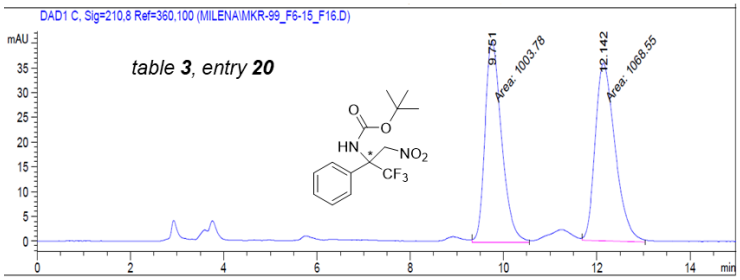

Peak #	RetTime [min]	Type	Width [min]	Area [mAU*s]	Height [mAU]	Area %
1	9.751	MM	0.4124	1003.77869	40.57106	48.4372
2	12.142	MM	0.4957	1068.55042	35.92856	51.5628
Totals :				2072.32910	76.49961	

Aza-Henry reaction promoted by catalyst **36b**

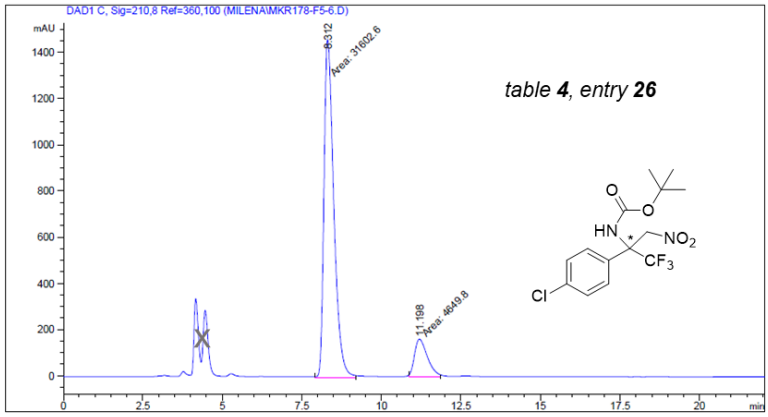

Peak #	RetTime [min]	Type	Width [min]	Area [mAU*s]	Height [mAU]	Area %
1	8.312	MM	0.3593	3.16026e4	1466.08850	87.1738
2	11.198	MM	0.4729	4649.80127	163.88666	12.8262

Aza-Henry reaction promoted by catalyst **35a**

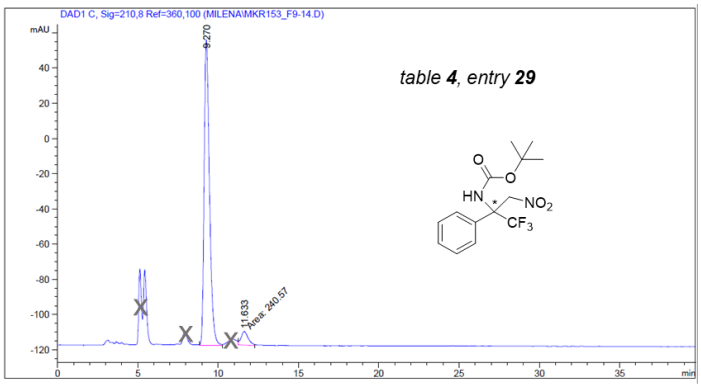

Peak #	RetTime [min]	Type	Width [min]	Area [mAU*s]	Height [mAU]	Area %
1	9.270	BV	0.3515	3971.60913	173.21063	94.2887
2	11.633	MM	0.5154	240.56963	7.77978	5.7113
Totals :				4212.17876	180.99041	

Aza-Henry reaction promoted by catalyst **35b**

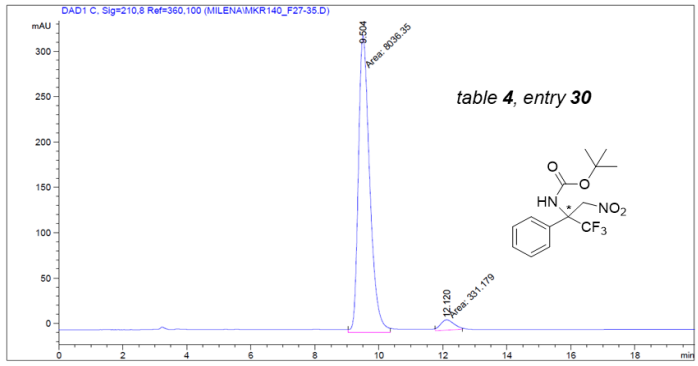

Peak #	RetTime [min]	Type	Width [min]	Area [mAU*s]	Height [mAU]	Area %
1	9.504	MM	0.4095	8036.35205	327.11377	96.0421
2	12.120	MM	0.4909	331.17865	11.24357	3.9579
Totals :				8367.53070	338.35734	

Aza-Henry reaction promoted by catalyst **47**

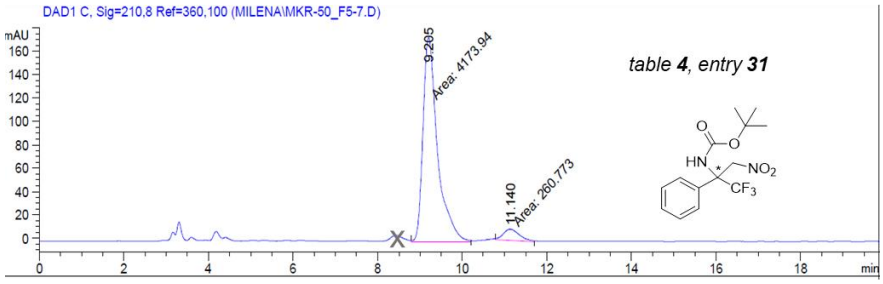

Peak #	RetTime [min]	Type	Width [min]	Area [mAU*s]	Height [mAU]	Area %
1	9.205	MM	0.3975	4173.94141	174.99263	94.1197
2	11.140	MM	0.4473	260.77310	9.71725	5.8803
Totals :				4434.71451	184.70988	

Aza-Henry reaction promoted by catalyst **46**

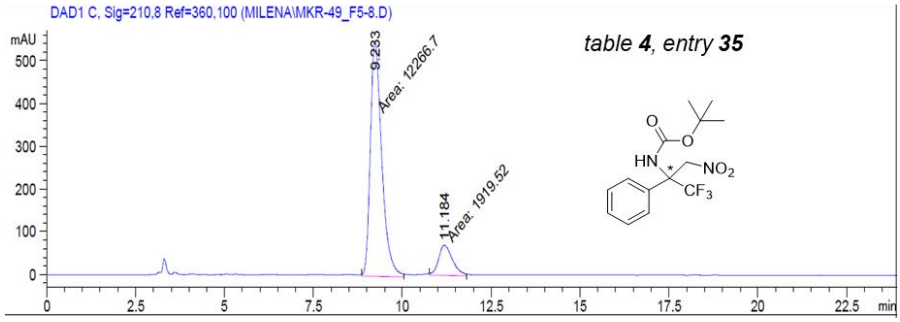

Peak #	RetTime [min]	Type	Width [min]	Area [mAU*s]	Height [mAU]	Area %
1	9.233	MM	0.3730	1.22667e4	548.08441	86.4691
2	11.184	MM	0.4544	1919.52222	70.40063	13.5309
Totals :				1.41862e4	618.48504	

6.6. Asymmetric Mannich reaction of malononitrile and oxidative decyanation

Mannich product **79*** is a ***new compound.***

General procedure for asymmetric Mannich reaction of malononitrile:

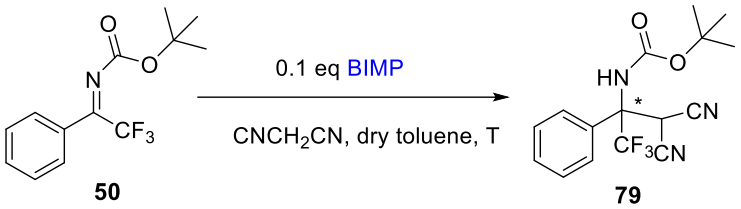

A 1.5 mL vial with septum connected with nitrogen inlet, was charged with 60 mg (1 equiv.) of ketimine **50** and 0.1 equiv. of iminophosphorane catalyst **25**, **36a** or **35b**. The reaction mixture was cooled down to indicated temperature (table 5, section 5.6), and 2 equiv. (table 5, entry 1 and 2) or 10 equiv. (table 5, entry 3) of malononitrile in 0.8 mL of dry toluene was added. The reaction mixture was monitored by TLC (*n*-hexane/ethyl acetate 5:1) and ^{1}H NMR. After starting material consumption, toluene was removed under reduced pressure and the crude was purified by silica gel column chromatography, eluent *n*-hexane/ethyl acetate 9:1, to afford the product **79** as a white solid, in 72-77% yield (table 5).

^{1}H NMR of compound 79* (300 MHz, $CDCl_3$)

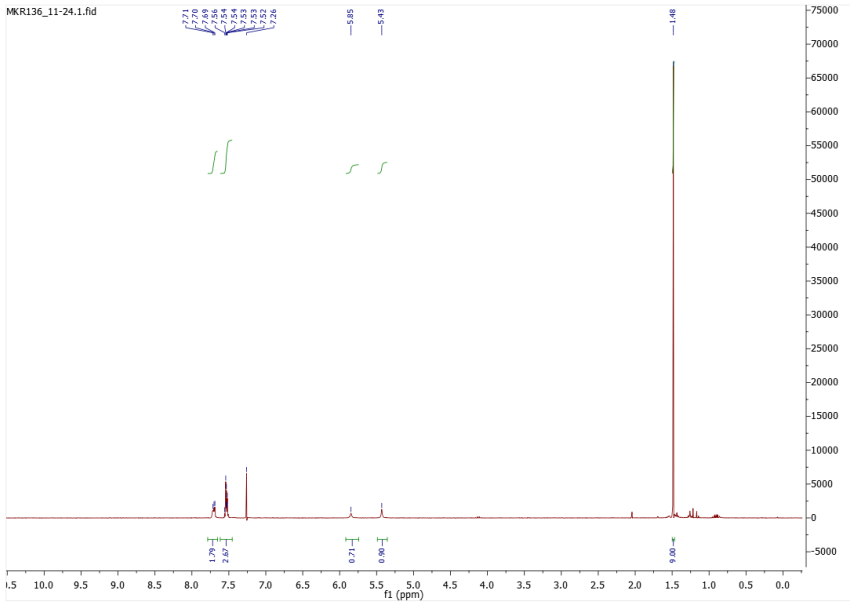

^{13}C NMR of compound 79* (75 MHz, $CDCl_3$)

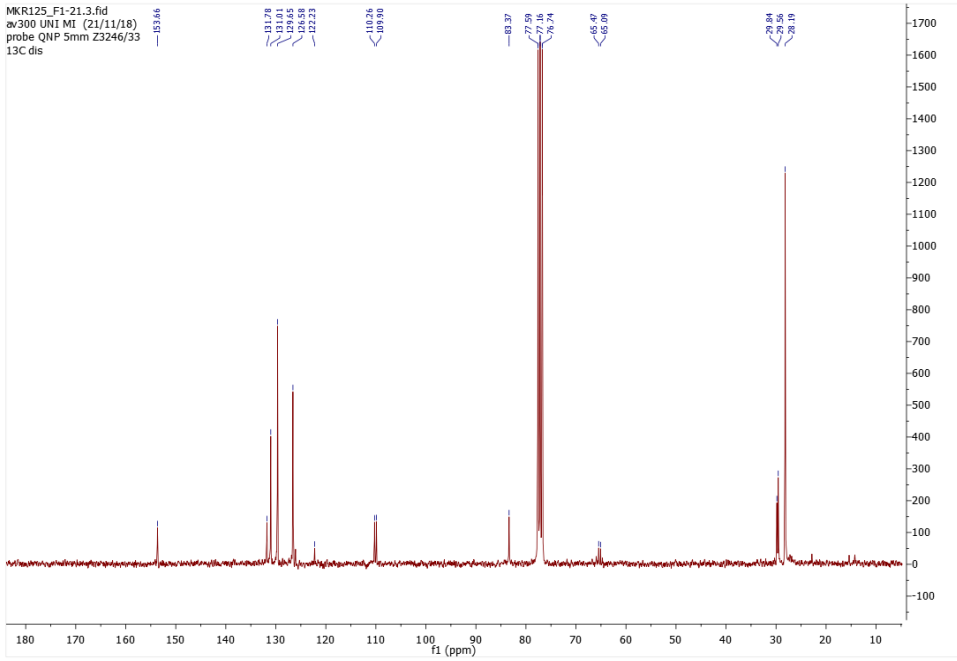

^{19}F NMR of compound 79* (282.1 MHz, $CDCl_3$)

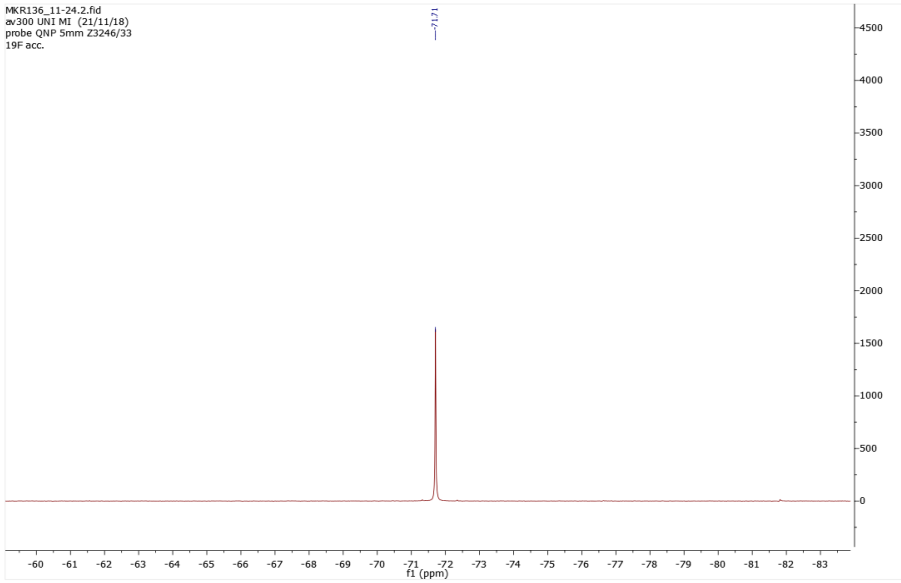

Mass (ESI+) for the compound 79*: m/z = calc. for $C_{16}H_{16}F_3N_3O_2$ = 339, found 362 [M + Na].

General procedure for oxidative decyanation of dicyano compound 79*:

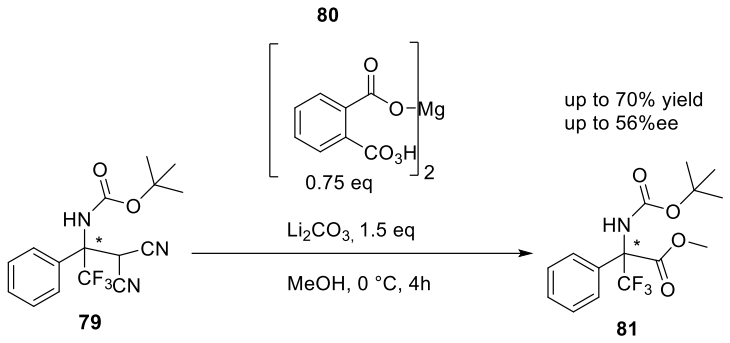

A 10 mL two-necked flask vial with nitrogen inlet, was charged with 50 mg (1 equiv., 0.147 mmol) dicyano compound **79** dissolved in 1.5 mL of MeOH at 0 °C. In the solution was added magnesium monoperoxyphthalate hexahydrate **80** (0.75 equiv., 0.110 mmol) and Li_2CO_3 (1.5 equiv., 0.22 mmol). The reaction mixture was stirred for 2 h at 0 °C. The reaction was stopped and quenched by water and extracted with DCM three times. The combined organic layers were dried over Na_2SO_4. After removal of Na_2SO_4 by filtration, solvent was removed under reduced pressure to afford quaternary amino ester **81** as a white solid (32 mg, 65% yield, entry 2, table 5). Determination of ee% was done on HPLC (Chiralpak AD column, eluent: *n*-hexane/isopropanol 95:5, flow rate 1 mL/min, t(major)=6.79 min, t(minor)= 9.48 min.

^{1}H NMR of 81 (300 MHz, $CDCl_3$) δ ppm: 1.41 (s, 9H), 3.83 (s, 3H), 5.62 (s, -NH), 7.43 (m, 5H)

^{13}C NMR of 81 (75 MHz, $CDCl_3$) δ ppm: 28.18, 53.51, 81.58 ppm, 126.75 ppm, 127.1 (CF_3, low intensity quartet), 128.39 (quaternary), 128.96, 129.56, 131.64 (quaternary aromatic), 153.66, 166.87.

^{19}F NMR of 81 (282.1 MHz, $CDCl_3$) δ ppm: -76.29 (major peak)

Mass (ESI+) of 81: m/z = calc. for $C_{15}H_{18}F_3NO_4$ = 333,3, found 356,4 [M + Na].

Determination of ee% for compound 81:

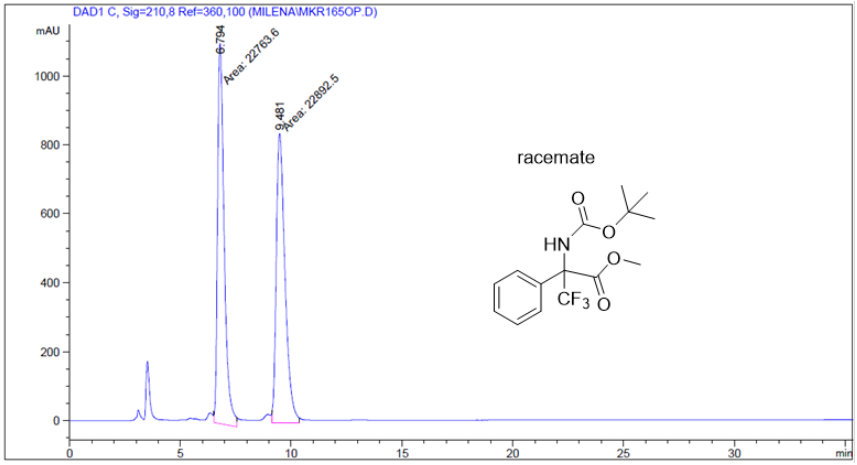

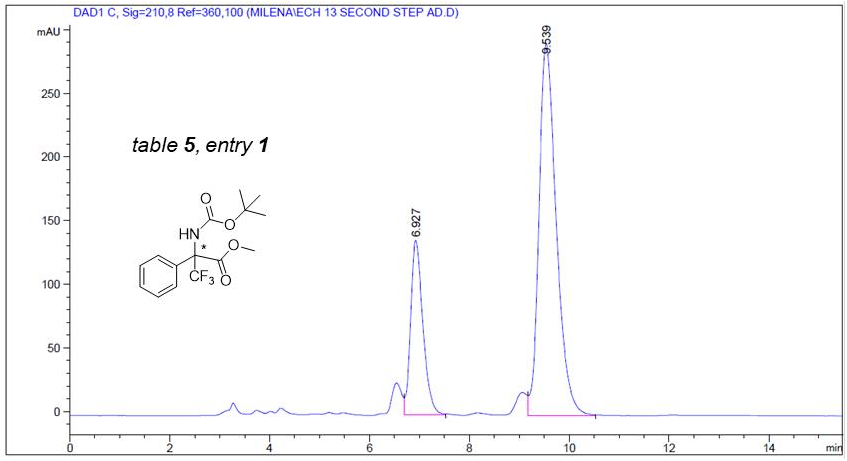

Peak #	RetTime [min]	Type	Width [min]	Area [mAU*s]	Height [mAU]	Area %
1	6.927	VB	0.2594	2347.60522	137.34274	25.0529
2	9.539	VB	0.3667	7022.99072	291.91614	74.9471

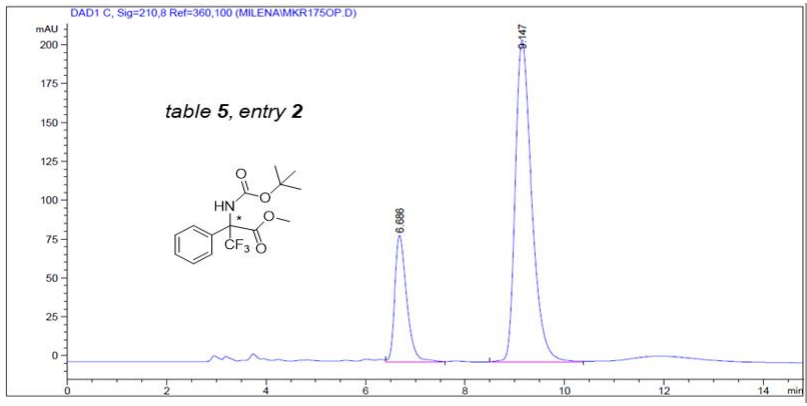

Peak #	RetTime [min]	Type	Width [min]	Area [mAU*s]	Height [mAU]	Area %
1	6.686	VV	0.2552	1360.65259	81.31734	22.1269
2	9.147	BB	0.3537	4788.67432	207.16536	77.8731
Totals :				6149.32690	288.48270	

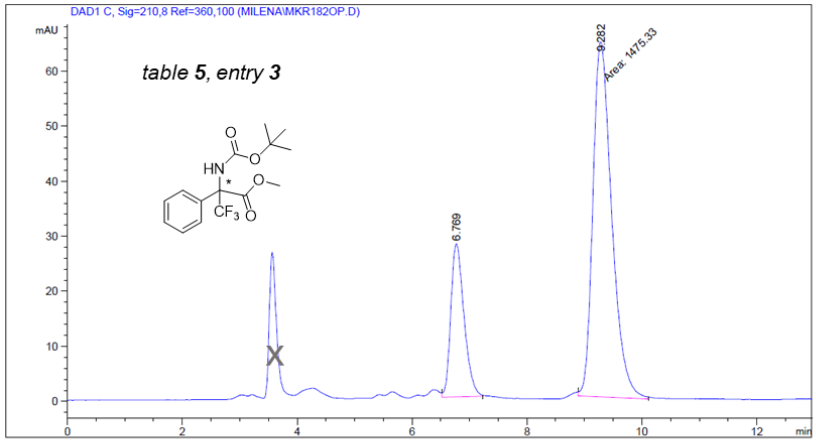

Peak #	RetTime [min]	Type	Width [min]	Area [mAU*s]	Height [mAU]	Area %
1	6.769	VB	0.2463	444.78751	27.84661	23.1647
2	9.282	MM	0.3813	1475.32556	64.48400	76.8353

Chapter 7. References

1. A. Perdih, M. S. Dolenc, *Curr. Org. Chem.*, **2011**, 15, 3750-3799
2. M.J. O'Donnell, *Tetrahedron*, **2019**, 75, 3667-3696
3. K. Maruoka, T. Ooi, T. Kano, *Chem. Commun*., **2007**, 15, 1487–1495
4. K. Maruoka, *Chem. Rec.*, **2010**,10, 254–259
5. K. Maruoka, T. Ooi, *Chem. Rev.* **2003**, 103, 3013-3028
6. T. Abellán, R. Chinchilla, N. Galindo, G. Guillena, C. Nájera, J. M. Sansano, *Eur. J. Org. Chem*. **2000**, 2689-2697
7. J.-A. Ma, *Angew. Chem. Int. Ed*. **2003**, 42, 4290 –4299
8. S. Shirakawa, K. Maruoka, *Angew. Chem. Int. Ed*. **2013**, 52, 4312 – 4348
9. T. Ooi, K. Maruoka, *Angew. Chem. Int. Ed*. **2007**, 46, 4222 – 4266
10. M. Kitamura, S. Shirakawa, Y. Arimura, X. Wang, K. Maruoka, *Chem. Asian J.* **2008**, 3, 1702 -1714
11. S.-S. Jew, B.-S. Jeong, J.-H. Lee, M.-S. Yoo, Y.-J. Lee, B.-S. Park, M. G. Kim, H.-G. Park, *J. Org. Chem*. **2003**, 68, 4514-4516
12. R. Chinchilla, C. Nájera, F.J. Ortega, *Eur. J. Org. Chem*. **2007**, 36, 6034–6038
13. M. J. O'Donnell, *Acc. Chem. Res.* **2004**, 37, 506-517
14. M. Kitamura, S. Shirakawa, K. Maruoka, *Angew. Chem. Int. Ed*. **2005**, 44, 1549 –1551
15. B. Lygo, D. J. Beaumont, *Chimia* **2007**, 61, 257-262
16. M. J. O'Donnell, S. Wu, *Tetrahedron Asymmetry* **1992**, 3, 591-594
17. B. Lygo, J. Crosby, J. A. Peterson, *Tetrahedron Lett.* **1999**, 40, 8671-8674
18. T. Ooi, M. Takeuchi, M. Kameda, K. Maruoka, *J. Am. Chem.Soc.* ***2000***,122, 5228-5229
19. M.J. O'Donnell, *Tetrahedron* **2019**, 75, 3667-3696
20. Y. Liu, N. Arumugam, A. I. Almansour, R. Suresh Kumar, K. Maruoka, *Chem. Rec*. **2017**, 17, 1059–1069
21. T. Ooi, M. Takeuchi, D. Ohara, K. Maruoka, *Synlett* **2001**, 7, 1185-1187
22. D.S. Timofeeva, A.R. Ofial, H. Mayr, *Tetrahedron* **2019**, 75, 459-463
23. Y. Kubota, S. Shirakawa, T. Inoue, K. Maruoka, *Tetrahedron Lett.* **2012**, 53, 3739–3741
24. Y. N. Belokon, K. A. Kochetkov, T. D. Churkina, N. S. Ikonnikov, S. Vyskocil, H. B. Kagan, *Tetrahedron Asymmetry* **1999**, 10, 1723–1728
25. H. Vogt, S. Bräse, *Org. Biomol. Chem*. **2007**, 5, 406–430
26. X.-L. Qiu, W.-D. Mengb, F.-L. Qing, *Tetrahedron* **2004**, 60, 6711–6745
27. W. Masamba, *Molecules* **2021,** 26, 1707, 1-23
28. R. Saladino, G. Botta, M. Crucianelli, *Mini Rev Med Chem*. **2012**, 12, 277-300
29. C. Cativiela, M. D. Díaz-de-Villegas, *Tetrahedron Asymmetry* **2007**, 18, 569–623
30. J. Martens, *ChemCatChem.* **2010**, 2, 379–381
31. P. Vachal, E. N. Jacobsen, *Org. Lett*. **2000**, 2, 867−870
32. M. Rueping, E. Sugiono, S. A. Moreth, *Adv. Synth. Catal*. **2007**, 349, 759–764

33. D. Enders, K. Gottfried, G. Raabe, *Adv. Synth. Catal*. **2010**, 352, 3147–3152
34. Y.-L. Liu, T.-D. Shi, F. Zhou, X.-L. Zhao, X. Wang, J. Zhou, *Org. Lett*. **2011**,13, 3826–3829
35. Y.-L. Liu, X.-P. Yin, J. Zhou, *Chin. J. Chem*. **2018**, 36, 321-328
36. Y.-L. Liu, J. Zhou, *Synthesis* **2015**, 47, 1210- 1226
37. M. Du, L. Yu, T. Du, Z. Li, Y. Luo, X. Meng, Z. Tian, C. Zheng, W. Cao, G. Zhao, *Chem.Commun*. **2020**, 56, 1581-1584
38. J. Moschner, V. Stulberg, R. Fernandes, S. H. J. Leppkes, B. Koksch, *Chem.Rev.* **2019**, 119, 10718-10801
39. H. Mei, J. Han, S. White, D. J. Graham, K. Izawa, T. Sato, S. Fustero, N. A. Meanwell, V. A. Soloshonok, *Eur. J. Chem*. **2020,** 26, 11349-11390
40. X.-X. Zhang, Y. Gao, X.-S. Hu, C.-B. Ji, Y.-L. Liu, J.-S. Yu, *Adv. Synth. Catal*. **2020,** 362, 4763-4793
41. G. Lupidi, A. Palmieri, M. Petrini, *Adv. Synth. Catal*. **2021**, 363, 3655-3692
42. A. M. F. Phillips, M. Fátima C. Guedes da Silva, A. J. L. Pombeiro, *Front. Chem*. **2020,** 8, 1-27
43. C. Tan, X. Liu, L. Wang, J. Wang, X. Feng, *Org. Lett*. **2008**,10, 5305–5308
44. H. Xie, Y. Zhang, S. Zhang, X. Chen, W. Wang, *Angew. Chem. Int. Ed*. **2011**, 50, 11773–11776
45. M. G. Núñez, A. J. M. Farley, D. J. Dixon, *J. Am. Chem. Soc.* **2013**, 135, 16348–16351
46. Y.-H. Wang, Y.-L. Liu, Z.-Y. Cao, J. Zhou, *Asian J. Org. Chem.* **2014**, 3, 429–432
47. Y. Fang, N. Lu, Z. Wei, J. Cao, D. Liang, Y. Lin, H. Duan, *Tetrahedron Lett*. **2018**, 59, 4371–4375
48. X. Wang, Y. Gao, Z. Wei, J. Cao, D. Liang, Y. Lin, H. Duan., *Org. Chem. Front*. **2019**, 6, 3269–3273
49. M. R. Chapman, M. H. T. Kwan, G. King, K. E. Jolley, M. Hussain, S. Hussain, I. E. Salama, C. G. Niño, L. A. Thompson, M. E. Bayana, A. D. Clayton, B. N. Nguyen, N. J. Turner, N. Kapur, A. J. Blacker, *Org. Process Res. Dev*. **2017**, 21, 9, 1294–1301
50. M. B. Plutschack, B. Pieber, K. Gilmore, P. H. Seeberger, *Chem. Rev*. **2017**, 117, 11796−11893
51. L. Malet-Sanz, F. Susanne, *J. Med. Chem*. **2012**, 55, 4062−4098
52. B. Gutmann, D. Cantillo, C. O. Kappe, *Angew. Chem. Int. Ed.* **2015**, 54, 6688–6728
53. C. A. Hone, C. O. Kappe, *Chemistry—Methods.* **2021**, 1, 454– 467
54. C. Wiles, P. Watts*, Eur. J. Org. Chem*. **2008**, 10, 1655–1671
55. N. Weeranoppanant, *React. Chem. Eng*. **2019**, 4, 235-243
56. M. J. Nieves-Remacha, M. Torres, M. Ruiz-Abad, J. A. Rincón, G. R. Cumming, P. Garcia-Losada, *React. Chem. Eng*. **2019**, 4, 334–345
57. Y. Mo, H. Lin, K. F. Jensen, *Chem. Eng. J*. **2018**, 335, 936–944
58. P. Borah, Y. Yamashita, S. Kobayashi, *Angew. Chem. Int. Ed.* **2017**, 56, 10330-10334

59. J. Jovanović, E. V. Rebrov, T. A. (Xander) Nijhuis, V. Hessel, J. C. Schouten, *Ind. Eng. Chem. Res.* **2010**, 49, 2681–2687
60. M. Ueno, H. Hisamoto, T. Kitamoriband, S. Kobayashi, *Chem. Commun.* **2003**, 3, 936–937
61. H. Okamoto, *Chem. Eng. Technol.* **2006**, 29, 504-506
62. J. R. Naber, S. L. Buchwald, *Angew. Chem*. **2010**, 122, 9659 –9664
63. E. Šinkovec, M. Krajnc, *Org.Process. Res. Dev*. **2011**, 15, 817–823
64. D. De Zani, M. Colombo, *J. Flow Chem.* **2012**, 2, 5–7
65. B. Reichart, C. O. Kappe, T. N. Glasnov, *Synlett.* **2013**, 24, 2393 – 2396
66. W. Cao, X. Liu, X. Feng, *Chin Chem Lett.* **2018**, 29,1201–1208
67. H. Krawczyk, M. Dzięgielewski, D. Deredas, A. Albrecht, Ł. Albrecht, *Chem. Eur. J.* **2015**, 21, 10268–10277
68. Y.-H. Wang, Z.-Y. Cao, Q.-H. Li, G.-Q. Lin, J. Zhou, P. Tian, *Angew. Chem. Int. Ed.* **2020**, 59, 8004-8014
69. A. Antenucci, S. Dughera, P. Renzi, *ChemSusChem*. **2021**, 14, 2785–2853
70. S. Dong, X. Feng, X. Liu, *Chem.Soc.Rev*. **2018**, 47, 8525-8540
71. B.-L. Zhao, J.-H. Li, D.-M. Du, *Chem. Rec.* **2017**, 17, 994–1018
72. K. Vazdar, D. Margetić, B. Kovačević, J. Sundermeyer, I. Leito, U. Jahn, *Acc.Chem.Res*. **2021**, 54, 3108−3123
73. M. Formica, D. Rozsar, G. Su, A. J. M. Farley, D. J. Dixon, *Acc. Chem. Res.*, **2020**, 53, 2235-2247
74. J. Yang, A. J. M. Farley, D. J. Dixon, *Chem. Sci.* **2017**, 8, 606-610
75. A. M. Goldys, M. G. Núñez, D. J. Dixon, *Org.Lett.* **2014**, 16, 6294−6297
76. C. J. Thomson, D. M. Barber, D. J. Dixon, *Angew. Chem. Int. Ed.* **2020**, 59, 5359-5364
77. A. J. M. Farley, C. Sandford, D. J. Dixon, *J. Am. Chem. Soc.* **2015**, 137, 15992-15995
78. J. C. Golec, E. M. Carter, J. W. Ward, W. G. Whittingham, L. Simón, R. S. Paton, D. J. Dixon, *Angew. Chem. Int. Ed.* **2020,** 59, 17417-17422
79. A. M. Goldys, M. G. Núñez, D. J. Dixon, *Org.Lett.* **2014**, 16, 6294−6297
80. A. J.M. Farley, P. Jakubec, A. M. Goldys, D. J. Dixon, *Tetrahedron.* **2018**, 74, 5206-5212
81. T. C. Cook, M. B. Andrus, D. H. Ess, *Org.Lett.* **2012**, 14, 5836- 5839
82. T. Kamachi, K. Yoshizawa, *Org.Lett.* **2014**, 16, 472-475
83. S. J. Zuend, M. P. Coughlin, M. P. Lalonde, E. N. Jacobsen, *Nature* **2009**, 467, 968-970
84. A. Genoni, M. Benaglia, E. Massolo, S. Rossi, *Chem. Commun*. **2013**, 49, 8365-8367
85. A. Henseler, M. Kato, K. Mori, T. Akiyama, *Ang. Chem. Int. Ed.* **2011**, 50, 8180-8183
86. G. Shang, Q. Yang, X. Zhang, *Angew. Chem. Int. Ed.* **2006**, 45, 6360–6362
87. G. Huang, J. Yang, X. Zhang, *Chem. Commun*. **2011**, 47, 5587–5589
88. J. M. Curto, J. S. Dickstein, S. Berritt, M. C. Kozlowski, *Org. Lett.* **2014**, 16, 1948−1951

89. K. Quinze, A. Laurent, P. Mison, *J. Fluor. Chem.* **1989**, 44, 233-265
90. E. J. Corey and Mark C. Noe, *Org. Synth.* **2003**, 80, 38-45
91. S. E. Denmark, R. C Weintraub, *Heterocycles.* **2011**, 82, 1527-1540
92. W. J. Nodes, K. Shankland, S. Rajkumar, A. J. A. Cobb, *Synlett.* **2010**, 20, 3011–3014
93. S.-s. Jew, M.-S. Yoo, B.-S. Jeong, Y. Park, H.-g. Park, *Org. Lett.* **2002**, 4, 4245-4248
94. S. Shirakawa, K. Yamamoto, K. Liu, K. Maruoka, *Org. Synth.* **2013**, 90, 121-129
95. R. L. Hartman, J. P. McMullen, K. F. Jensen, *Angew. Chem. Int. Ed.* **2011**, 50, 7502– 7519
96. https://www.freactor.com/index.html
97. M. J. McKennon, A. I. Meyers, *J. Org. Chem.* **1993**, 58, 3568-3571
98. A. Saitoh, K. Achiwa, K. Tanaka, T. Morimoto, *J. Org. Chem*. **2000**, 65, 4227-4240
99. S. Bräse, K. Banert, *Organic Azides: Syntheses and Applications*, © **2010** John Wiley & Sons, Ltd. ISBN: 978-0-470-51998-1
100. J.-M. Kim, Y. Bi, S. J. Paikoff, P. G. Schultz, *Tetrahedron Lett.* **1996**, 37, 5305-5308
101. E. D. Goddard-Borger, R. V. Stick *Org. Lett.* **2011**, 9, 3797-3800
102. A. Parra, R. Alfaro, L. Marzo, A. Moreno-Carrasco, J. L.G. Ruanoa, J. Alemán, *Chem. Commun.* **2012**, 48, 9759–9761
103. N. Lu, Y. Fang, Y. Gao, Z. Wei, J. Cao, D.Liang, Y. Lin, H. Duan, *J. Org. Chem.* **2018**, 83, 1486–1492
104. I. V. Kutovaya, O. I. Shmatova, V. M. Tkachuk, N. V. Melnichenko, M. V. Vovk, V. G. Nenajdenko, *Eur. J. Org. Chem.* **2015**, 30, 6749–6761
105. S. R. S. S. Kotti, C.Timmons, G. Li, *Chem Biol Drug Des*. **2006**, 67, 101–114
106. B. Westermann, *Angew. Chem. Int. Ed*. **2003**, 42, 151-153
107. D. Francis, A. Nelson, S. P. Marsden, *Chem. Eur. J.* **2020**, 26, 14861 – 14865
108. S. Kuwano, Y. Nishida, T. Suzuki, T. Arai, *Adv. Synth. Catal.* **2020**, 362, 1674–1678
109. Y. Liu, X. Yun, D. Z.-Negrerie, J. Huang, Y. Du, K. Zhao, *Synth.* **2011**,18, 2984–2994
110. A. M. F. Phillips, M. H. G. Prechtl, A. J. L. Pombeiro, *Catalysts.* **2021**, 11, 569
111. F. Mosa, C. Thirsk, M. Vaultier, G. Maw, A. Whiting, *Org. Synth.* **2008**, 85, 219-230
112. H. Staudinger. J. Meyer, *Helv. Chim. Acta*. **1919**, 2, 635
113. M. Alajarin, C. Conesa, H. S. Rzepa, *J. Chem. Soc., Perkin Trans.* 2. **1999**, 1811–1814
114. M. D. Velasco, P. Molina, P. M. Fresneda, M. A. Sanz, *Tetrahedron.* **2000**, 56, 4079-4084